Volume 32 No. 2 JNSChE 2017 ISSN 0794-6759

JOURNAL OF THE NIGERIAN SOCIETY OF CHEMICAL ENGINEERS

Published by,
THE NIGERIAN SOCIETY OF CHEMICAL ENGINEERS
National Secretariat: Infinite Grace House, Plot 4, Oyetubo Street,
Off Obafemi Awolowo Way, Ikeja, Lagos State, Nigeria.
E-mail: nationalhqtrs@nsche.org, nsche_headquarters@yahoo.com
Website: http:www.nsche.org.ng
Submission of Manuscript: nschejournal@yahoo.com

JOURNAL OF THE NIGERIAN SOCIETY OF CHEMICAL ENGINEERS

A Publication on the Science and Technology of Chemical Engineering

Subscription

a.	Individual Readers	N1,500.00
b.	Overseas Subscribers	US$30.00
c.	Institution, Libraries, etc	N2,500.00

NUCLEAR TECHNIQUES APPLICATIONS IN SOLID MINERALS ANALYSIS

Ojinnaka, C. A. S.[1], *Kuye, A.[1] and Akinola, A. A.[2]
[1] Centre for Nuclear Energy Studies, University of Port Harcourt, Port Harcourt, Nigeria
[2] Department of Chemical and Petroleum Engineering, University of Lagos, Lagos, Nigeria
*ayo.kuye@uniport.edu.ng

ABSTRACT

Nigeria is gifted with large deposits of solid minerals located in different parts of the country. However, the country has not fully exploited the minerals because of the lack of knowledge of the available technology to find and process them. While many nuclear and radiations technology techniques for many solid minerals processing and exploration exist, this paper aims to review the applicability of the Neutron Activation Analysis (NAA) and Proton Induced X-Ray Emission (PIXE) techniques in Nigeria for the reason that it is most common in the country. NAA has not only been used for coal exploration but also to obtain the elemental composition of coal found in Enugu and Okaba areas of Nigeria. The PIXE technique has been used to analyze mining waste and the technique has been successful in identifying trace materials and heavy metals. Evidence indicate that a wide range of radiation techniques and technologies offer great advantages to the mining industry, be it for exploration, optimization of processes, troubleshooting, assessment of mining sites or ensuring environmental protection. A Nigerian National Policy to promote the use of nuclear and radiation technologies in the solid mineral industry should be put in place.
Keywords: *Nuclear, Radiation, Neutron, Proton, Optimisation*

1. INTRODUCTION

Nigeria is endowed with large deposits of several solid minerals located in different parts of the country. The minerals that investors are interested in include coal, lignite, granite, bitumen, gold, coltan, limestone, lead, zinc, cassiterite, iron ore, limestone, clay, barite, columbite, marble, and tantalite (Adetunji *et al*. 2005; Akpan *et al*. 2011; FMSMD, 2016). Despite the abundance of the afore-mentioned minerals, the solid mineral industry only contributed approximately 0.33% to the gross domestic product of Nigeria in 2015. Some of the challenges facing the solid minerals sector are (FMSMD, 2016):

i) weak mechanism for gathering, disseminating and archiving critical geological data required by investors and policy makers
ii) insufficient infrastructure such as railroad, competitive financing systems, mine and asset security as well as policy uncertainty for operators

With the passage of the Nigerian Minerals and Mining Act (2007) and the Nigerian Mineral and Metals Policy (2008) as well as the recently approved roadmap for the growth and development of the Nigerian mining industry by the Federal Executive Council, it is hoped that these challenges would be appreciably addressed. However, the use of nuclear techniques in the solid minerals sector was not addressed by these policy documents despite the fact that the Nigeria Atomic Energy Commission Act (1976) empowers the Commission to prospect for and mine radioactive minerals.

The full economic value of the solid minerals resources can only be attained after they have passed through the exploration, mining and processing stages. Available techniques that have been used to analyze the products from each of these stages are quite extensive; they are based on chemical, physical and nuclear characteristics. The nuclear techniques that have been used include Atomic Absorption Spectrometer (AAS), Inductively Coupled Plasma-Atomic Emission Spectrometry (ICP-AES), Energy Dispersive X-ray Spectrometer Fluorescence (EDXRF), Scanning Electron Microscopy (SEM), Gamma-ray Spectrometry, X-Ray Fluorescence, Neutron Activation Analysis (NAA), Proton Induced X-ray Emission (PIXE) and Particle Induced Gamma Ray Emission (PIGE) (Smolka-Danielowska, 2006; Adedosu, *et al*., 2007; Funtua, *et al.,* 2012; Katrinak and Benson, 2014; Isaiah *et al*., 2015). Some of these techniques can be used during exploration while others are used to analyze the minerals. This paper aims to review the use of nuclear and radiations technology in the economic exploitation of the numerous solid minerals deposits that are available in Nigeria. Specifically, it focuses on NAA and PIXE since these techniques are readily accessible in the country.

2. NEUTRON ACTIVATION ANALYSIS (NAA)

NAA was first developed by G. Hevesy and H. Levi in 1936 when they used a neutron source (226Ra + Be) and a radiation detector (ionization chamber) and promptly recognized that the element Dy (dysprosium) in the sample became highly radioactive after exposure to the neutron source. They showed that the nuclear reaction may be used to determine the elements present in unknown samples by measuring the induced radioactivity. With the development of nuclear reactors later, providing neutron fluxes in order of $10^{16} m^{-2} \cdot s^{-1}$, the use of neutron activation analysis as a very sensitive

technique increased rapidly. Furthermore, the introduction of NaI(Tl) scintillation detectors of gamma-radiation and multichannel analysers as well as the introduction of semiconductor detectors made of germanium compensated by lithium (Ge(Li)) and high purity germanium (HPGe) detectors made neutron activation analysis much easier to use. Greenberg *et al.*, (2011), Hamidatou *et al.*, (2013) and Kubešová, (2016) have discussed extensively the history and development of NAA.

The sequence of events occurring during NAA is shown in Fig 1. A neutron interacts with a target nucleus by non-elastic collision, thus forming a highly excited compound nucleus. The compound nucleus has a short lifetime and can de-excite in different ways which usually involve emission of nuclear particles or gamma rays. Prompt Gamma NAA is based on the in-situ measurement of the latter. In most cases, the new nucleus is radioactive and will further evolve towards stability. Its nuclear decay is often accompanied by the emission of very characteristic gamma rays, "which can be considered as a fingerprint". A statistical correlation exists between the number of target nuclei and the amount of gammas in the activation spectrum recorded by a spectrometer (Pomme *et al.*, 1997). In practice, the first step in NAA is to irradiate the sample with neutrons in a nuclear reactor which then excites the sample to form a stable nucleus; in this transition state it emits prompt gamma rays. In some cases, the stable nucleus after absorbing neutrons may become a radioactive nucleus, if this happens a delayed gamma ray would be released with very high energy (see Fig. 1). The radioactive nuclei emit characteristic gamma rays, which can be measured to determine which element is present (Win, 2004). NAA can be used to detect the elements that are shaded in Fig 2.

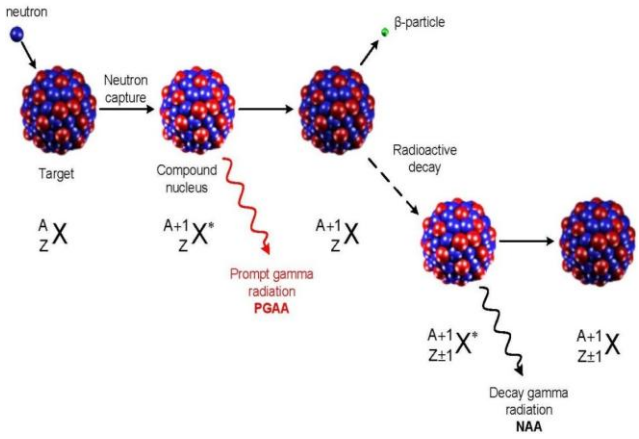

Fig 1: Schematic illustration of the physical phenomena involved in Neutron Activation Analysis (Hamidatou *et al.*, 2013).

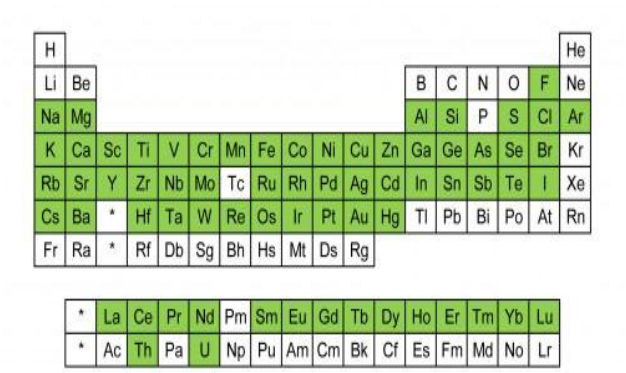

Fig 2: Shaded elements are detected by NAA (Kubešová, 2016).

NAA has several advantages and a few disadvantages. These are summarized below (De Corte, 1987; Avino *et al.* 2007; Win, 2004; Kogo *et al.*, 2009; Gwarzo *et al.*, 2014; Win, 2004; IAEA, 2001; Kučera and Řanda, 2001; Kubešová, 2016):

Advantages:

1. Wide possibilities of applications for different types of samples
2. Low detection limits down to 10^{-6} mg·kg^{-1}
3. The relative freedom from interference and matrix effects.
4. The possibility of non-destructive analysis
5. The high specificity based on characteristics of induced radionuclides.
6. A completely independent nuclear principle, in contrast to electron nature of most of other analytical methods.
7. The method is theoretically simple and well understood, which makes it possible to evaluate and model sources of uncertainty of results.
8. The neutron energy and neutron flux density can be chosen to certain extents, which allows obtaining of the best results using simple optimization means, such as selective activation.
9. The isotopic basis, which makes it possible to use analytically independent routes of determination of many elements and to cross-check the results, obtained using so called internal self-verification principle.

Disadvantages:

1. The need of a nuclear reactor
2. The use of highly radioactive materials and the resulting consequences
3. The feasibility of determination of traces of some toxicologically important elements, such P, Cu, Ga, Ge, Gd, Y, Nb, Mo, Pr, Mn, Dy, Er, Hg and Pb is limited, because they do not form radionuclides with suitable properties
4. Samples for NAA should preferably be dried (or freeze-dried), because the presence of water radiolysis occurs on irradiation in a nuclear

reactor. This may increase pressure in the sample container and may cause explosion during handling.

5. The time of analysis can be quite long; up to about six weeks for elements, which produce long-lived radionuclides.
6. NAA is not available as a simple apparatus with software, which can easily be operated in any analytical laboratory.

For the solid minerals, NAA, especially INAA, has always played an important role in characterizing raw mineral materials, such as ore bodies and other valuable raw materials. The main task of NAA was not only to determine the elements of interest, but also to study various inter-element correlations, such as those of rare earth elements, which help in elucidating of origin and formation of geological structures. Nigeria has a Miniature Neutron Source Reactor which is designated as NIRR-1. NIRR-1 is the first Nigeria research reactor and its first criticality was achieved on 03 February 2004. It is specifically designed for use in NAA and limited radioisotope production (Jonah *et al.*, 2007). NIRR-1 has a tank-in-pool structural configuration and a nominal thermal power rating of 31 kW. It is located at Centre for Energy Research and Training (CERT), Ahmadu Bello University, Zaria. A number of authors have used NIRR-1 for NAA of solid minerals.

Isaiah *et al.* (2015) analyzed Nigerian coals from Enugu and Okaba using NAA and found that seventeen elements were detected from Enugu coal while sixteen were present in Okaba coal with a total of twenty two elements detected from either the Enugu or Okaba coals. The elements found in both Enugu and Okaba were Al, Ti, K, Na, V, Mn Ba, La, Th, Hf, Fe, and Cr while that found in only Enugu were Lu, Ta, Rb, Eu and Co and elements found in Okaba are Sc, Br, Yb, and U. For coal an energy source, the major elements of interest are carbon, oxygen, hydrogen, nitrogen and sulphur. However, as can be seen from Fig 2, NAA cannot be used to detect these elements; Isaiah *et al.* (2015) results confirmed this. Ewa (2004) also used NAA determined element abundances (Al, As, Ba, Br, Ca, Ce, Cs, Dy, Eu, Fe, Ga, Gd, Hf, K, La, Lu, Mg, Mn, Na, O, Rb, Sb, Sc, Sm, Sr, Ta, Tb, Th, Ti, U, V, Yb, Zn and Zr) of prepared and run-of mine coals from eight principal mines (Onyeama, Ogbete, Enugu, Gombe, Asaba-Ugwashi, Okaba, Afikpo and Lafia) in Nigeria. Ogugbuaja, and James (1995) also used NAA to analyse Nigerian bituminous coal and ash. Funtua *et al.*, (2012) evaluation of the composition of some geo-standard reference materials (Fly ash 1633b, SO-2, SARM-1, SARM-52, W-2, DNC-1, BIR-1, AGV-1, IAEA SL-3, and IAEA Soil-7) using NAA and their results indicated an insignificant maximum deviation error of 0.304 to 0.393% in all the geo-standard reference materials.

3. PROTON INDUCED X-RAY EMISSION (PIXE)

PIXE is based on the fact that irradiation of a material with proton or other charged particles of a few megaelectron volts per nucleon gives emission of characteristic X-rays of the present elements. PIXE analysis consists of two parts. The first is to identify the atomic species in the target from the energies of the characteristic peaks in the X-ray emission spectrum and the second part is to determine the amount of a particular element present in the target from the intensity of its characteristic X-ray emission spectrum. This normally requires knowledge of the ionisation cross-sections, fluorescence yields and absorption coefficients. Depth profile analysis may be performed if the PIXE is combined with other methods like Rutherford Back Scattering (RBS) and/or sample etching techniques (Govil, 2001).

The basic principle of PIXE analysis is shown in Fig 3. If an atom is ionized on an inner shell, its energy state is less stable than that of a simple ion. First, before any chemical reaction, it should lose energy. The energy loss usually takes place by the emission of a photon. These photons are called characteristic X-rays because they characterize the elements emitting them (Nagy, 2009). The incident ions themselves may undergo further elastic or inelastic scattering during the collision. The excited target atom seeks to regain a stable energy state by reverting to its original electron configuration. In doing so, the electronic transition, which takes place, may be accompanied by emission of electromagnetic radiation in the form of X-rays characteristic of the excited atom. The emission consists of K, L, M,... lines produced by electron transitions to the K, L, M,... shells of the target atom (Govil, 2001). These X-rays are usually detected by using a solid-state detector such as a Si(Li) detector and the spectrum obtained results in qualitative and quantitative information on the elements of interest (Alfassi and Peisach, 1991).

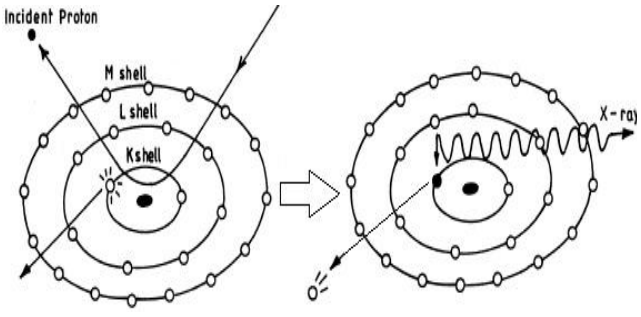

Fig 3 Basic Principle of PIXE analysis

Elements that can be detected using the PIXE are: Ca, Si, Mg, Mn, Al, Fe, K, Ti, V, S, Rb, Sr, Y, Zr, Nb, Mo, Tc, Ru, Rh, Pd, Ag, Cd, In, Sn, Sb, Te, I, Cs, Ba, La, Hf, Ta, W, Re, Os, Ir, Pt, Au, Hg, Pb, Bi, P, Sr, Cl, Zn, Na, Cr, Co, Cu, Ni, Ge, Ga, As, Se, Br, Ce, Pr, Nd, Pm, Sm, Eu, Gd, Tb, Dy, Ho, Er, Tm, Yb, Lu, Th and U

(Deconninck, 1976; Ene *et al.*, 2009; Akpan *et al.*, 2011). Some of the advantages and disadvantages of PIXE are the followings.

Advantages:

1. PIXE is able to detect between 10 – 20 element, making it a multi-element detector
2. It takes the PIXE about 17 minutes to complete a single analysis, making it a fast analyzer
3. In most case, sample does not need preparation
4. Just a little amount of sample is required during sampling and detection
5. It cost very little to run a sample using the PIXE
6. PIXE is non-destructive during analysis
7. It is easy to focus on very small sample area of less than $1mm^2$

Disadvantages:

1. During irradiation, volatile compounds could be lost
2. PIXE functions better in a well-equipped accelerator facility
3. Samples containing liquid must be dried before irradiating to avoid explosion

PIXE needs a collimated beam of positively charged particles. This can be produced by a radioactive alpha source or by particle accelerators. The Centre for Energy Research and Development (CERD), Obafemi Awolowo University, Ile-Ife, Nigeria has a 1.7MeV Tandem accelerator that can be used to produce proton beams. A number of authors have used this facility to PIXE analysis of solid minerals. Akpan *et al.* (2011) carried out PIXE analysis of Yandev and Odukpani limestone deposits using proton beams produced by Ion Beam Analysis (IBA) facility at the CERD, They concluded that all waste from industries mining the limestones (especilally the one from Yandev deposit) should be closely monitored since it was found to contain some rare earth elements (Ti, S, Rb, P, Mn, Sr, Cl and Zn). Wilberforce (2015) analyzed four different tubers and the soil where they were grown within Enyigba lead-zinc derelict for heavy metals using PIXE technique. The results revealed that heavy metals in soil decreased in the order Pb > Zn > Cu > Mn > Cd > Ni > As > Cr. PIXE was used by Abdullahi (2012) to characterize fourteen geological samples collected from North-Western Nigeria to determine concentration of zirconium (Zr) and other trace elements. The result obtained indicated that zirconium is of commercial deposit at some of the regions. Alongside zirconium, Fe, Cu, Rb, Cd, Ba, Ce, W, Bi, and Sn were determined. Also element Fe and Cu concentrations appears to be deposited in commercial quantities. Abdullahi and Funtua (2012) used PIXE to characterize Lead and other elements in fourteen samples of gold ores from North Western Nigeria. Olabanji, (1991), on the other hand, used PIXE with the protons produced from another accelerator in Lund to measure the concentrations of the major, minor and trace elements in Nigerian coal samples. The results show that Nigerian coals have a low (0.82–0.99)% sulfur content.

4. CONCLUSIONS

Two of the available nuclear techniques (NAA and PIXE) for analyzing solid minerals have been presented. NAA has many advantages and few disadvantages. Luckily, Nigeria has a nuclear reactor which is required for NAA. PIXE is a multi-element detector and a fast analyzer. PIXE also requires a proton or particle generator such as an accelerator which is available in Nigeria. Available evidence indicate these facilities can be used to analyze solid minerals such as coal, gold, phosphate, bitumen, zirconium, copper, cadmium and other trace elements in the country. Both NAA and PIXE are non-destructive during analysis and require that the sample be irradiated before being analyzed. Despite the numerous applications that have been enumerated in this work, there is no clear Nigerian National Policy on the use of nuclear and radiation technology in the solid mineral industry and we recommend that one should be put in place by Federal Government.

REFERENCES

Abdullahi, B., (2012), The Determination of Zirconium from North-Western Nigeria using PIXE Technique, *International Journal of Science and Technology*, 2(9), 613-617

Abdullahi, B. and Funtua, I. I., (2012), Characterization of Lead Poisoning Gold Ores from North Western Nigeria Using PIXE Technique, *IUP Journal of Physics*, 5(1), 33-41.

Adedosu, T., Adedosu, H., and Adebiyi, F., (2007), Geochemical and Mineralogical Significance of Trace Metals in Benue Trough Coal, Nigeria, *Journal of Applied Sciences*, *7*(20).

Adetunji, A. R., Siyanbola, W. O., Funtua, I. I., Olusunle, S. O. O., Afonja, A. A., & Adewoye, O. O., (2005), Assessment of Beneficiation Routes of Tantalite Ores from Key Locations in Nigeria, *Journal of Minerals and Materials Characterization and Engineering*, 4(02), 85.

Akpan, I. O., Amodu, A. E., & Akpan, A. E., (2011), An Assessment of the Major Elemental Composition and Concentration in Limestones Samples from Yandev and Odukpani Areas of Nigeria Using Nuclear Techniques, *Journal of Environmental Science and Technology*, 4(3), 332-339.

Alfassi, Z. B. and Peisach, M., (Eds.), (1991), *Elemental Analysis by Particle Accelerators*, CRC Press, Boca Raton

Avino, P., Capannesi, G., and Rosada, A., (2007), Instrumental Neutron Activation Analysis, A Powerful

Instrument in Determining Environmental Pollution: Theory and applications. *Prevention Today*, 3(2), 13-36

De Corte, F., (1987), *The k0-Standardization Method, A Move to the Optimization of Neutron Activation Analysis*, University of Gent, Belgium.

Ewa, I. O. B., (2004), Data evaluation of Trace Elements Determined in Nigerian Coal Using Cluster Procedures, *Applied Radiation and Isotopes*, 60(5), 751-758

Federal Ministry of Solid Minerals Development (FMSMD), (2016), Roadmap for the Growth and Development of the Nigerian Mining Industry: on the Road to Shared Mining Prosperity, Federal Ministry of Solid Minerals Development, Abuja

Funtua, I., Oladipo, M., Njinga, R., Jonah, S., Yusuf, I., and Ahmed, Y., (2012), Evaluation for Accuracy and Applicability of Instrumental Neutron Activation Analysis of Geological Material on Nigeria Nuclear Research Reactor-1 (NIRR-1), *International Journal of Applied Science and Technology*, *2*(1).

Govil I. M., (2001), Proton Induced X-ray Emission – A Tool for Non-Destructive Trace Element Analysis, *Current Science*, 80(12), 1542-1549

Greenberg, R. R., Bode, P., & Fernandes, E. A. D. N., (2011), Neutron Activation Analysis: A Primary Method of Measurement, Spectrochimica Acta Part B: *Atomic Spectroscopy*, 66(3), 193-241

Guerra, M. F., & Calligaro, T., (2004), Gold Traces to Trace Gold, *Journal of Archaeological science*, 31(9), 1199-1208.

Gwarzo, U. S, Gimba, C. E., Adeyemo, D. J and Paul, E. D., (2014), Neutron Activation Analysis (NAA) of Senna occidentalis Linn. *Journal of Natural Sciences Research*, *4*(11), 22 – 28.

Hamidatou, L., Slamene, H., Akhal, T., and Zouranen, B., (2013), Concepts, Instrumentation and Techniques of Neutron Activation Analysis, In: F. Kharfi, Ed., *Imaging and Radio-analytical Techniques in Interdisciplinary Research— Fundamentals and Cutting Edge Applications*, InTech, Rijeka, , pp. 141-178. http://dx.doi.org/10.5772/53686

International Atomic Energy Agency (IAEA), (2001), Use of Research Reactors for Neutron Activation Analysis, IAEA-TECDOC-1215, IAEA Vienna.

Isaiah, A., Sonloye, S., and Ewa, I. O. B., (2015), Instrumental Neutron Activation Analysis (INAA) Of High Ranking Nigerian Coals From Enugu and Okaba, *International Journal of Scientific Research And Innovative Technology*, *Vol. 2* (No. 1). 60 – 69.

Jonah, S. A., Balogun, G. I., Obi, A. I., Ahmed, Y. A., Nkom, B., Mati, A. A., Yusuf, I. and Training, A.B.U., (2007), *Operational Experience and Programmes for Optimal Utilization of the Nigeria Research Reactor-1*, In Proceedings of International Conference on Research Reactors: Safe Management and Effective Utilization (pp. 5-9).

Katrinak, K. A., and Benson, S. A., (2014), *Trace Metal Content of Coal and Ash as Determined Using Scanning Electron Microscopy with Wavelength-Dispersive Spectrometry*, [Online] Available: http://large.stanford.edu/publications/coal/references/docs/katrinak.pdf (October 11, 2014)

Kogo, B. E., Gajere, E. N., Ogunmola, J. K., and Ogbole, J. O. (2009). Neutron Activation Analysis of Soil Samples from Different Parts of Abuja Metropolis. *Middle-East Journal of Scientific Research*, 4(4), 254-262

Kubešová, M., (2016), *Introduction to NAA | Neutron Activation Analysis*. Retrieved 23 August 2016, from http://www.naa-online.net/theory/introduction/

Kučera J. and Řanda Z., (2001), *The Present Role of Neutron and Photon Activation Analysis in Determination of Trace Elements*, 3rd Symposium on Nuclear Chemistry, Halifax, NS, Canada, June 11–14.

Ogugbuaja, V. O. and James, W.D., (1995), INAA Multi Elemental Analysis of Nigerian Bituminous Coal and Coal Ash, *Journal of Radioanalytical and Nuclear Chemistry* 19(1), 181-187

Okoh, S., Adeyemo, D., Onoja, R., and Arabi, S. (2013), Determination of Some Trace Elements in Leather, *International Journal of Applied Science and Technology*, *3*(1).

Olabanji, S.O. (1991). Nigerian Coal Analysis by PIXE and RBS Techniques, *Journal of Radioanalytical and Nuclear Chemistry*, 149(1): 41–49

Pomme, S., F. Hardeman, P. Robouch, N. Etxebarria and G. Arana (1997) Neutron Activation Analysis with k_0-standardisation: General Formalism and Procedure, Nuclear Spectrometry Radiation Protection Department, SCK-CEN, BLG-7G0

Smolka-Danielowska, D., (2006), Heavy Metals in Fly Ash from a Coal-Fired Power Station in Poland, *Polish Journal of Environmental Studies*,15(6), 943-946

Wilberforce, J. O. O., (2015), Heavy Metal Accumulation in Tubers Grown in a Lead-zinc Derelict Mine and their Significance to Health and Phytoremediation. *American Chemical Science Journal*, 8(3), 1-9.

Win, D. T. (2004): Neutron Activation Analysis (NAA), *Assumption University Journal of Technology*. 8(1): 8-14.

CENTRALIZED ROBUST MULTIVARIABLE CONTROLLER DESIGN USING OPTIMIZATION

***Taiwo, O.[1], Adeyemo, S.[1], Bamimore, A.[1], Sorinolu, A.[1] and King, R.[2]**

[1]Process Systems Engineering Laboratory, Obafemi Awolowo University, Ile-Ife, Nigeria
(E-mails:femtaiwo@yahoo.com, adeyesam@yahoo.com, ayobamimoreonline@yahoo.com)
[2]Measurement and Control Group, Institute of Process and Plant Technology, Sekr, P2-1, Technical University of Berlin,Hardenberger Str.36a D-1063, Germany

ABSTRACT

The paper deals with the determination of controller parameters for multivariable systems by means of parameter optimization. In order to reduce the computational burden, the starting point in the optimization is determined through information provided by the feedback controller parameterized using the multivariable internal model controller (IMC) computed from the plant's p/q moment approximant and the original plant's multi-loop controller parameter magnitudes. Thereafter, controller parameter optimization proceeds to completion using the MATLAB optimization toolbox which is widely available. A potency of this technique is that all performance specifications and stipulated constraints are easily accommodated in the problem formulation thus facilitating complete problem solution in one go. The technique has been found to be effective for all plants considered so far and generally produces closed loop systems with favorable characteristics when compared to systems designed by similar methods.

Keywords: Centralized controller, robust stability and performance, optimization, moment approximant

1. INTRODUCTION

Effective methods for designing simple controllers for multivariable plants which guarantee good performance and satisfy stipulated constraints is still a topic of on-going research. One reason for this is that the plants usually have distinctive complex characteristics and each must usually be separately analyzed. Parameter optimization has been used in many situations for feedback control system design. One such method is the method of inequalities (Zakian and Al-Naib, 1973 , Taiwo, 1980, Whidborne et al., 1995, Balachandran et al., 1997 and Zakian, 2005). This method works by solving a set of inequalities and has been found to work in many situations, although it is yet to be used to design centralized controllers for complex systems involving 4*4 or higher transfer function matrices. Recently, Escobar and Trierweler (2013) designed PID controllers for large process plants by an optimization technique based on frequency response approximation. Their results are compared to those of the work reported here. Other methods of optimizing the performance of the closed loop systems are based on genetic algorithms and simulated annealing. Although such methods have the property of global convergence, they are usually computationally intensive and their applications to large multivariable plants are scanty. This paper proposes a new technique for centralized multivariable controller design. Here, the initial controller parameters in the optimization are specified by using data from the feedback controller parameterized using the p/q moment approximant of the plant model and the magnitudes of the multi-loop controller parameters giving good closed loop performance for the system involving the original plant. The optimization then proceeds and is deemed to have been completed when the nominal and robust performance of the feedback system meets the control objectives. In all cases so far considered, the centralized proportional plus integral (PI) controller has proved adequate, giving favourable performance in most situations. A merit of this method is that MATLAB optimization toolbox, which is widely available, has been used. Another advantage of this method is that various constraints such as bounds on structured singular values, internal variable magnitudes or their rates of change can be directly handled during optimization. The paper is arranged as follows. In section 2, the new method is described. Applications of the new method to large multivariable systems is considered in section 3. A discussion of the results and conclusions from the work are considered in section 4.

2. DESCRIPTION OF THE NEW METHOD

The new method computes the centralized feedback controller of simple structures (typically PI, proportional plus integral controller) using parameter optimization. In order to reduce computational burden, it is recommended that a good starting point for optimization be used. This is done by studying information from the feedback controller parameterized using the IMC controller computed for, typically, the 0/1 moment approximant of the plant as well as the magnitudes of

the parameters of the multi-loop PI feed-back controller designed for the original plant.

Computation of p/q moment approximant

If it is desired to use the new method to design a simple feedback controller for the plant then its p/q moment approximant should be computed. This is undertaken as follows: Expand the plant model G(s) (assumed asymptotically stable) in infinite series:

$$\mathbf{G(s)} = \sum_{i=0}^{\infty} G_i s^i \qquad \mathbf{(1)}$$

Here, without loss of generality, we elect to express its reduced model R(s) in the right matrix fraction form:

$$\mathbf{R(s)} = \left(\sum_{i=0}^{p} V_i s^i\right)\left(\sum_{i=0}^{q} T_i s^i\right)^{-1}, \quad (T_q = I) \qquad \mathbf{(2)}$$

R(s) is a p/q moment approximant at s=0 if R(s) is asymptotically stable and

$$\sum_{i=0}^{q-1} G_{\mu-i} T_i = -G_{\mu-q} \quad (q \le \mu \le p+q) \qquad \mathbf{(3)}$$

$$V_\mu = \sum_{i=0}^{\mu} G_{\mu-i} T_i \quad (0 \le \mu \le p) \qquad \mathbf{(4)}$$

In (3) and (4), $G_\mu = 0$, $\mu < 0$. A unique solution exists and

$$\mathbf{R(s) = G(s) + 0(s^{p+q+1})} \qquad \mathbf{(5)}$$

where the notation means that the power series expansion on both sides exist and agree up to terms of degree (p+q) inclusive. However, if expansion about s=0 does not furnish a stable p/q moment approximant, Taiwo and Krebs (1995) have shown how, generically, a stable approximant may be obtained by resorting to matching moments about more than the single point s=0. All the controllers designed in this work were based on parameterizing a classical feedback controller from the IMC controller computed from the 0/1 moment approximant of the original complex plant. Consequently, for space economy, we limit discussion to this case in the sequel.

Assume that the PI controller is desired, then the 0/1 reduced model R(s) given by

$$\mathbf{R(s) = V_o(Is + T_o)^{-1}} \qquad \mathbf{(6)}$$

will be computed. In order to obtain the IMC controller $\bar{Q}$, invert (6), giving,

$$\mathbf{\bar{Q} = R^{-1} = (Is + T_o)V_o^{-1}} \qquad \mathbf{(7)}$$

also, $Q = \bar{Q}f$ where f is the filter given by

$$\mathbf{f = 1/(\lambda s + 1)} \qquad \mathbf{(8)}$$

The conventional feedback controller $C_o(s)$ is given by

$$\mathbf{C_o(s) = \bar{Q}f(I - fI)^{-1}} \qquad \mathbf{(9)}$$

For illustration purposes, suppose G(s) is 3*3 and $\bar{Q}f = (q_{ij})/(\lambda s + 1)$, (9) simplifies to

$$\mathbf{C_o(s) = \frac{1}{\lambda s}\begin{bmatrix} q_{11} & q_{12} & q_{13} \\ q_{21} & q_{22} & q_{23} \\ q_{31} & q_{32} & q_{33} \end{bmatrix}} \qquad \mathbf{(10)}$$

where $q_{ij} = \hat{V}_{oij} s + \hat{G}_{oij}$ **(11)**

and $\hat{V}_{oij}$, $\hat{G}_{oij}$ respectively denotes the (i,j)th element of V_o^{-1} and G_o^{-1}.

The next issue is the choice of λ. One way to determine a preliminary value is to compute the multi-loop controllers for the original plant. The order of magnitude observed here should be used to estimate the starting value of λ in order to optimize the parameters of the feedback controller, C(s). Usually it is advisable to start with a λ which gives a closed loop stable system. A detailed exposition of this procedure will be given in the next Section. If it is desired to use a PID controller, then either a ½ or 0/2 moment approximant would be used for controller parameterization.

3. ILLUSTRATIVE EXAMPLES

3.1 Example 1: Depropanizer column

The process is a depropanizer column used to separate propane from the feed that comes from a de-ethanizer column (Wang, 2003) and its transfer function is given by

$$G(s) = \begin{pmatrix} \frac{-0.26978e^{-27s}}{97.5s+1} & \frac{1.978e^{-53.5s}}{118.5s+1} & \frac{0.07724e^{-56s}}{97.5s+1} \\ \frac{0.4881e^{-117s}}{56s+1} & \frac{-5.26e^{-26.5s}}{58.5s+1} & \frac{0.19996e^{-35s}}{51s+1} \\ \frac{0.6e^{-16.5s}}{40.5s+1} & \frac{5.5e^{-15.5s}}{19.5s+1} & \frac{-0.5e^{-17s}}{18s+1} \end{pmatrix} \qquad (12)$$

The following steps should be taken in designing a controller for the plant G(s):

Step 1: Assuming a centralized controller having PI elements is to be designed, then an 0/1 approximant of (12) should be computed and the controller C(s) should be calculated. In this example, V_0^{-1} and G_0^{-1} are given respectively as

$$V_0^{-1} = \begin{bmatrix} 567.308936 & 371.82068 & 161.84048 \\ 102.65397 & 31.06735 & 17.22488 \\ 1756.6934 & 738.70682 & 285.76937 \end{bmatrix} \qquad (13)$$

$$G_0^{-1} = \begin{bmatrix} 2.01784 & 1.86435 & 1.057307 \\ 0.480027 & 0.116762 & 0.12085 \\ 7.7017 & 3.5216 & 0.59812 \end{bmatrix} \qquad (14)$$

Step 2 is to estimate the value of λ. The computation of a multiloop PI controller for the plant will assist here. The relative gain array is given by

$$\text{RGA} = \begin{bmatrix} -0.5444 & 0.9495 & 0.595 \\ 0.91 & -0.6142 & 0.704 \\ 0.634 & 0.6647 & -0.299 \end{bmatrix} \qquad (15)$$

By simultaneously computing the Niederlinski index, it was found that the best control structure is as follows: $u_2 \rightarrow y_1$, $u_3 \rightarrow y_2$, and $u_1 \rightarrow y_3$, where u_i and y_i are

respectively the controlled and manipulated variables. On computing the controller dictated by this structure, it was found that the values of the proportional and integral gains in (13) and (14) would have the same order of magnitude as those of the multi-loop controller elements if $\lambda \approx 1000$. Consequently, λ=1000 was used in (10). Hence with starting value

$$C_o(s) = \frac{1}{1000}\left(V_o^{-1} + {G_o^{-1}}/{s}\right) \qquad (16)$$

and the performance index chosen as the integral of the absolute error (IAE) for step responses to unit step changes in the reference at time zero and simultaneous disturbance inputs of size 0.1 at time 2000, MATLAB optimization toolbox function *fmin* was used to compute

$$C(s) = \begin{bmatrix} 0.6316 & 1.2807 & 0.2981 \\ 0.2757 & -0.5333 & 0.1389 \\ 3.4248 & -4.7539 & -0.1580 \end{bmatrix} + \frac{1}{s}\begin{bmatrix} 0.0040 & 0.0181 & 0.0051 \\ 0.0026 & -0.005 & 0.0022 \\ 0.0313 & -0.0205 & -0.0391 \end{bmatrix} \qquad (17)$$

Although the IAE associated with this controller is acceptable, the value of a robust performance metric, the structured singular value is greater than unity. Further computation was therefore done and the computed set of parameters (17) were used as starting point with a constraint that $\mu_{RP} < 1$, where μ_{RP} denotes structured singular value for robust performance. Here the MATLAB optimization toolbox function *fmincon* was used. The final controller computed is

$$C(s) = \begin{bmatrix} 0.7351 & 1.0706 & 0.5431 \\ 0.2776 & -0.4192 & -0.0131 \\ 3.5645 & -3.6019 & -1.6202 \end{bmatrix} + \frac{1}{s}\begin{bmatrix} 0.0047 & 0.0119 & 0.0134 \\ 0.0025 & -0.0029 & -0.0003 \\ 0.0308 & -0.0079 & -0.0528 \end{bmatrix} \qquad (18)$$

Note that to determine the robustness of the designed controllers the input uncertainty weight used by Garrido et al. (2012), $W_u = \frac{0.009s+0.15}{0.0045s+1}$ which permits up to 15% uncertainty at low frequencies and 200% uncertainty at high frequencies attaining 100% uncertainty at a frequency of about 15 rad/min, was used. The performance weight was also chosen as in Garrido et al. (2012), namely, $W_p = \frac{s/2.75+0.00075}{s}$.

The responses of the closed loop system with the controller are displayed in fig.1. The characteristics of the feedback systems are compared with those of the closed loop system designed by Garrido et al. (2012) (fig.2) in Table I. It is found that the overall characteristics of the system designed in this work are superior to those of Garrido et al. (2012). Note in this work that μ_{RS} and μ_{NP} respectively denotes structured singular value for robust stability and nominal performance.

Table 1: Performance and robustness indices for the depropanizer

	Proposed	Garrido et al.
IAE for a step in y_1	396.1	888.9
IAE for a step in y_2	307.2	811.8
IAE for a step in y_3	194.7	701.4
TOTAL IAE	898.0	2402.0
μ_{RP}	0.9735	0.7262
μ_{RS}	0.1504	0.0399
μ_{NP}	0.8131	0.6443

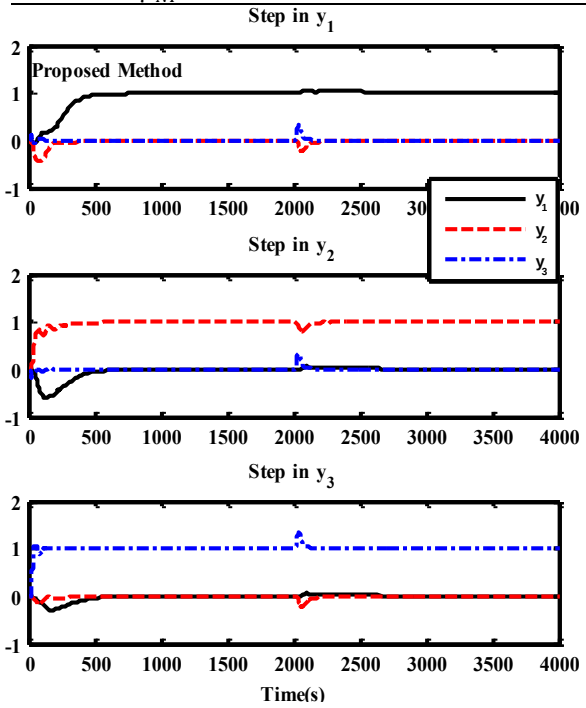

Fig.1: Depropanizer closed-loop response, this work

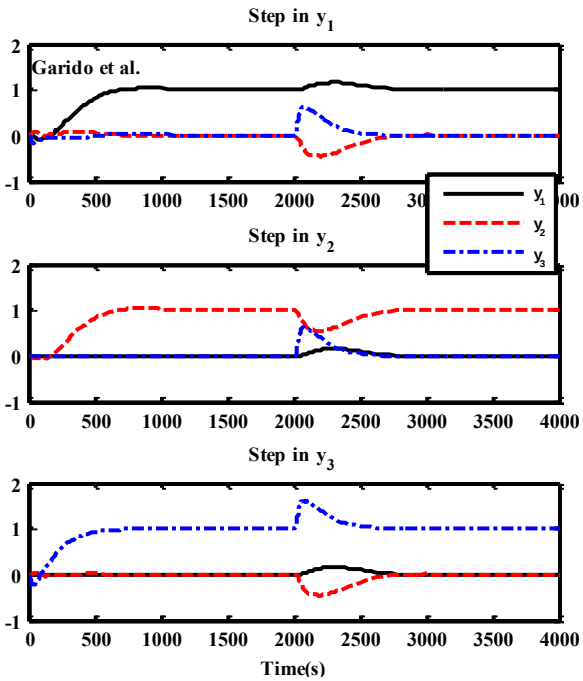

Fig.2: Depropanizer closed-loop response, Garrido et al.

3.2 Example 2: Heat integrated distillation column

Ding and Luyben (1990) presented the transfer function model for a Low-Purity heat integrated distillation column as

$$\begin{bmatrix} XB_1 \\ XD_2 \\ XS_2 \\ XB_2 \end{bmatrix} = \begin{bmatrix} g_{11} & g_{12} & g_{13} & g_{14} \\ g_{21} & g_{22} & g_{23} & g_{24} \\ g_{31} & g_{32} & g_{33} & g_{34} \\ g_{41} & g_{42} & g_{43} & g_{44} \end{bmatrix} \begin{bmatrix} Q_1 \\ R_2 \\ S_2 \\ Q_2 \end{bmatrix} + \begin{bmatrix} g_{d_{11}} & g_{d_{12}} \\ g_{d_{21}} & g_{d_{22}} \\ g_{d_{31}} & g_{d_{32}} \\ g_{d_{41}} & g_{d_{42}} \end{bmatrix} \begin{bmatrix} Z_1 \\ Z_2 \end{bmatrix}$$

where, $\mathbf{g_{11} = \frac{-7.39e^{-s}}{(11s+1)(s+1)}}$, $\mathbf{g_{12} = g_{13} = g_{14} = 0}$

$g_{21} = \frac{-0.11(200s+1)e^{-5s}}{(20s+1)^3}$, $g_{22} = \frac{10.1e^{-s}}{(28s+1)(4s+1)}$

$g_{23} = \frac{1.18e^{-11s}}{(31s+1)(6s+1)}$, $g_{24} = \frac{-18.3e^{-s}}{(28s+1)(5s+1)}$

$g_{31} = \frac{1.9e^{-2s}}{(4s+1)^2}$, $g_{32} = \frac{1.7(200s+1)e^{-1.4s}}{(108s+1)(s+1)^2}$, $g_{33} = \frac{-3.15e^{-s}}{(3s+1)(0.3s+1)}$, $g_{34} = \frac{-1.27(188s+1)e^{-s}}{(68s+1)(s+1)}$

$g_{41} = \frac{4.9e^{-1.6s}}{(40s+1)(3s+1)}$, $g_{42} = \frac{-8.21e^{-2.5s}}{(24s+1)(3s+1)}$

$g_{43} = \frac{12e^{-s}}{(29s+1)(3s+1)}$, $g_{44} = \frac{-19.4e^{-s}}{(26s+1)(3s+1)}$

$g_{d_{11}} = g_{d_{12}} = 0$

$g_{d_{21}} = \frac{2.42e^{-5s}}{(3s+1)(26s+1)^2}$, $g_{d_{22}} = \frac{-2.47e^{-5s}}{(3s+1)(22s+1)^2}$

$g_{d_{31}} = \frac{0.592e^{-5s}}{(7s+1)^2}$, $g_{d_{32}} = \frac{1.83e^{-6s}}{(25s+1)(2s+1)}$

$g_{d_{41}} = \frac{-1.51e^{-19s}}{(45s+1)(5s+1)^2}$, $g_{d_{42}} = \frac{-4.52e^{-8s}}{(50s+1)(7s+1)^2}$

Steps 1 and 2 are similar to those in the previous example except that RGA indicates a diagonal structure $D(s) = \text{diag}(d_{11}, d_{22}, d_{33}, d_{44})$, which was tuned to give $d_{11} = -0.259 - 0.0226/s$, $d_{22} = 0.248 + 0.008/s$ $d_{33} = -0.217 - 0.069/s$, $d_{44} = 0.142 + 0.005/s$. Hence in choosing $C0(s)$, the values of these diagonal parameters were retained while every other element in V_0^{-1} and G_0^{-1} was divided by 10. In other words, $\lambda \cong 10$ was used for this example. Additionally, note that all the elements in row and column 1 of V_0^{-1} and G_0^{-1} apart from element (1,1) were zero. Upon applying the optimization toolbox in MATLAB, the eventual controller giving a system with acceptable servo and regulator characteristics is given by

$$C(s) = \begin{bmatrix} -0.3374 & 0 & 0 & 0 \\ 0 & 0.2854 & -0.0860 & 0.3356 \\ 0 & 0.3014 & -0.2001 & 0.2616 \\ 0 & -0.0237 & -0.0122 & 0.1962 \end{bmatrix}$$

$$+\frac{1}{s}\begin{bmatrix} -0.0285 & 0 & 0 & 0 \\ 0 & 0.0108 & 0.0825 & 0.0032 \\ 0 & 0.0072 & -0.0145 & 0.0096 \\ 0 & 0.0008 & 0.0442 & 0.0023 \end{bmatrix} \quad (19)$$

The adequacy of this controller in following reference changes and rejecting disturbance changes of 5% in Z_1 and Z_2 can be verified from figures 3 and 5 respectively. This is compared with controller $C_1(s)$, with PID elements, in Escobar and Trierweiler (2013) as shown in figs.4 and 5. The other attractive characteristics of the closed loop system are tabulated in Tables II and III. The uncertainty weight used for robustness analysis was chosen as $W_u = \frac{s+0.15}{0.5s+1}$.This permits up to 15% uncertainty at low frequency and 200% at high frequency attaining 100% uncertainty at a frequency of about 1rad/min. The performance weight was chosen as $W_p = \frac{s/2.25+0.04}{s}$. Here, we have specified peak sensitivity, M_s=2.25 (with an implication that $GM \geq 1.8$ and $PM \geq 25.68^0$) and zero steady state error. Note that the Escobar and Trierweiler controller lacks performance robustness.

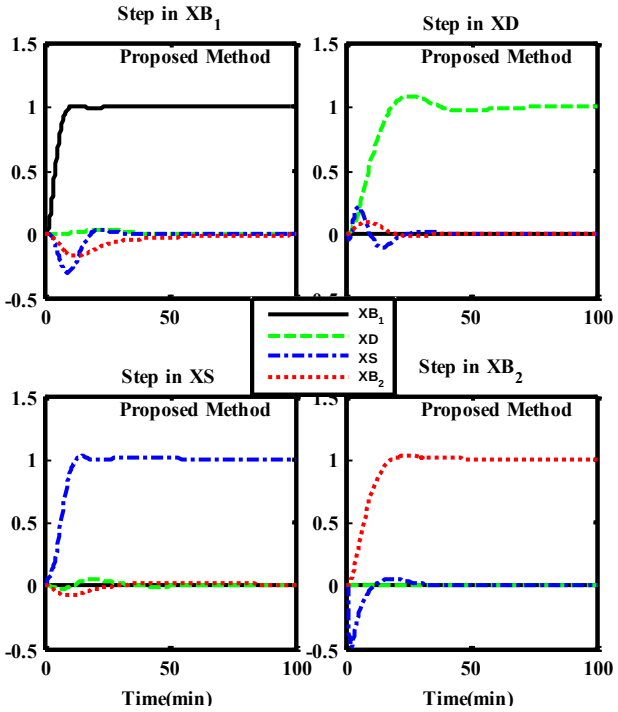

Fig.3: Servo performance for the Ding and Luyben column

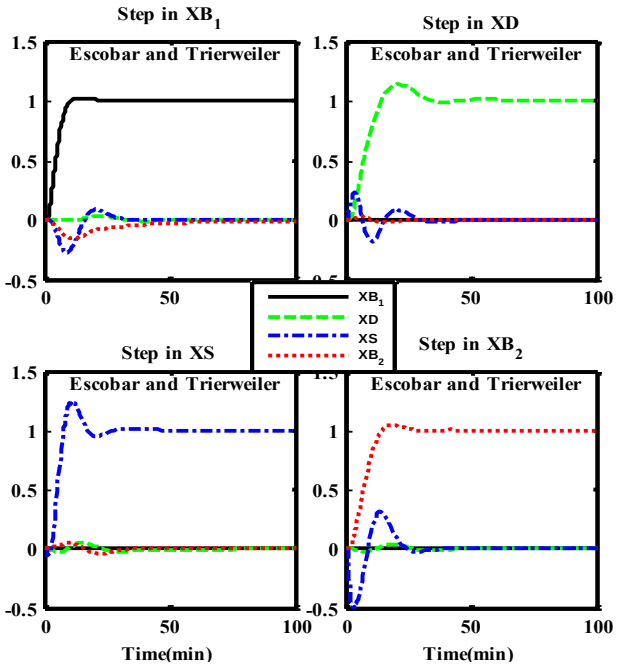

Fig.4: Servo performance for the Ding and Luyben column

Table III:Regulatory performance indices

	Proposed	Escobar & Trierweller
Total IAE for a step in Z_1	47.33	31.50
Total IAE for a step in Z_2	55.16	36.38

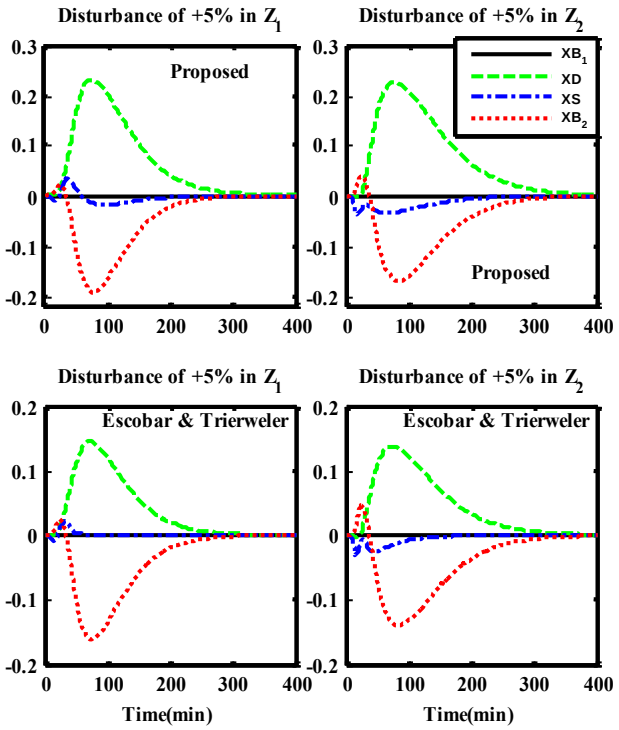

Fig.5: Regulatory performance for the Ding and Luyben column (z_1 and z_2 of size 5%).

Table II: Performance and robustness indices for the Ding and Luyben column

	Proposed	Escobar & Trierweler
IAE for a step in XB_1	13.24	12.99
IAE for a step in XD	14.94	12.65
IAE for a step in XS	10.24	9.67
IAE for a step in XB_4	11.26	13.90
TOTAL IAE	49.68	49.21
μ_{RP}	0.9648	1.8016
μ_{RS}	0.2144	0.2034
μ_{NP}	0.8749	1.1305

3.3 Example 3: Alatiqi distillation column

The Alatiqi column system used here is taken from Garrrido et al. (2012). It is a 4 by 4 system modelled by the transfer function matrix:

$$\mathbf{G} = \begin{bmatrix} \mathbf{g_{11}} & \mathbf{g_{12}} & \mathbf{g_{13}} & \mathbf{g_{14}} \\ \mathbf{g_{21}} & \mathbf{g_{22}} & \mathbf{g_{23}} & \mathbf{g_{24}} \\ \mathbf{g_{31}} & \mathbf{g_{32}} & \mathbf{g_{33}} & \mathbf{g_{34}} \\ \mathbf{g_{41}} & \mathbf{g_{42}} & \mathbf{g_{43}} & \mathbf{g_{44}} \end{bmatrix}, \textbf{ where}$$

$$g_{11} = \frac{2.22e^{-2.5s}}{(36s+1)(25s+1)}, g_{12} = \frac{-2.94(7.9s+1)e^{-0.05s}}{(23.7s+1)^2}$$

$$g_{13} = \frac{0.017e^{-0.2s}}{(31.6s+1)(7s+1)}, g_{14} = \frac{-0.64e^{-20s}}{(29s+1)^2}, g_{21} = \frac{-2.33e^{-5s}}{(35s+1)^2},$$

$$g_{22} = \frac{3.46e^{-1.01s}}{32s+1}, g_{23} = \frac{-0.51e^{-7.5s}}{(32s+1)^2}, g_{24} = \frac{1.68e^{-2s}}{(28s+1)^2}$$

$$g_{31} = \frac{-1.06e^{-22s}}{(17s+1)^2}, g_{32} = \frac{3.511e^{-13s}}{(12s+1)^2}, g_{33} = \frac{4.41e^{-1.01s}}{16.2s+1},$$

$$g_{34} = \frac{-5.38e^{-0.5s}}{17s+1}, g_{41} = \frac{5.73e^{-2.5s}}{(8s+1)(50s+1)}, g_{42} = \frac{4.32(25s+1)e^{-0.01s}}{(50s+1)(5s+1)}$$

$$g_{43} = \frac{-1.25e^{-2.8s}}{(43.6s+1)(9s+1)}, g_{44} = \frac{4.78e^{-1.15s}}{(48s+1)(5s+1)}$$

Steps 1 and 2 are similar to those of the preceding examples. A good starting point in this case was found by retaining the exact value of the diagonal controller for the multiloop structure. For the off-diagonal elements of the centralized controller, a value of λ of approximately 18 or greater was used, yielding

$$C_o(s) = \begin{bmatrix} 0.5200 & 0.7000 & -0.1500 & -0.3500 \\ -0.6000 & 0.4500 & -0.06500 & -0.1500 \\ 1.1500 & -0.37500 & 0.6000 & 0.5500 \\ 0.7500 & -0.3650 & -0.1500 & 0.5300 \end{bmatrix}$$

$$+\frac{1}{s}\begin{bmatrix} 0.0100 & 0.0500 & 0.0040 & -0.0050 \\ 0.0100 & 0.0300 & 0.0015 & -0.0050 \\ 0.1000 & -0.0450 & 0.0350 & 0.0150 \\ 0.0800 & 0.0450 & 0.0100 & 0.0100 \end{bmatrix} \quad (20)$$

Upon using the *fmin* function, the controller in (21) was computed which gives a system with satisfactory nominal and robust performance.

$$C(s) = \begin{bmatrix} 0.8050 & 1.3115 & 0.1698 & -0.9105 \\ -0.1109 & 0.4034 & 0.0415 & 0.0936 \\ 1.5406 & 0.0430 & 1.8670 & 1.5954 \\ 1.3153 & 0.2395 & -0.0700 & 1.4410 \end{bmatrix}$$

$$+\frac{1}{s}\begin{bmatrix} 0.0098 & 0.0521 & -0.0002 & -0.0119 \\ -0.0117 & 0.0266 & 0.0002 & -0.0137 \\ 0.0384 & 0.0553 & 0.1393 & 0.0221 \\ 0.0341 & 0.0538 & 0.0082 & 0.0302 \end{bmatrix} \quad (21)$$

The responses of the system with this controller are given in fig.(6) and some of the dynamic properties are listed in Table IV. Again, it is observed that the system obtained in this work is superior to the one in Garrido et al. (2012) displayed in fig.7. One observation is that we have used a more realistic uncertainty weight here rather than the one given by Garrido et al (2012). This is because among other considerations, we believe that uncertainty usually increases with frequency rather than the contrary impression given in their uncertainty weight. It is worth noting that our computed controller meets the required constraint $\mu_{RP}<1$ even when their original weight is used. The new uncertainty weight used for the robust analysis is given by $W_u = 0.15\frac{5s+1}{0.5s+1}$. However, the same performance weight as theirs is used, namely, $W_p = \frac{s/2.6+0.001}{s}$.

Table IV: Performance and robustness indices for the Alatiqi column

	Proposed	Garrido et al.
IAE for a step in y_1	59.95	47.62
IAE for a step in y_2	51.16	77.44
IAE for a step in y_3	8.67	14.32
IAE for a step in y_4	28.55	32.56
TOTAL IAE	148.3	172.0
μ_{RP}	0.9728	3.4457
μ_{RS}	0.2615	0.2890
μ_{NP}	0.7486	1.6601

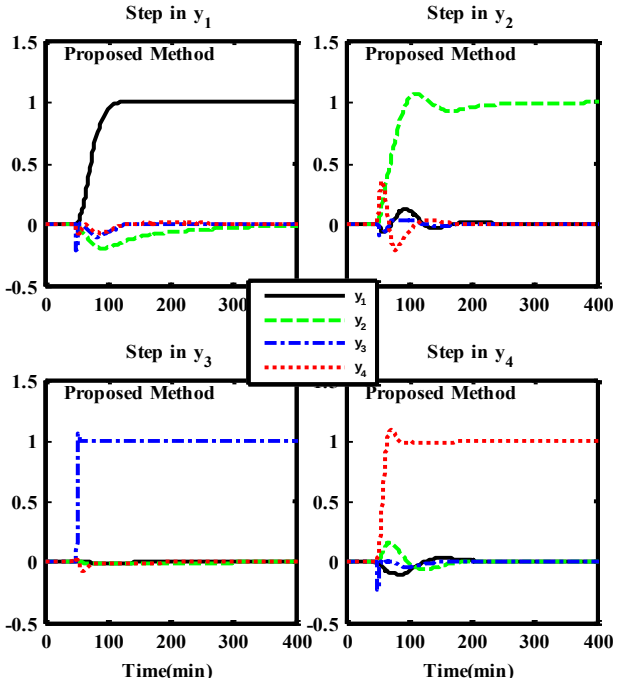

Fig.6:Servo responses for the Alatiqi column

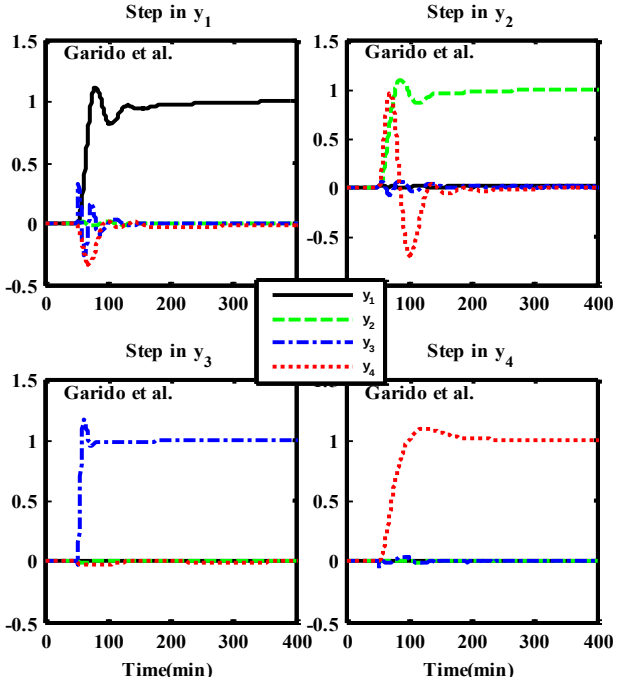

Fig.7: Servo responses for the Alatiqi column

4. DISCUSSION AND CONCLUSIONS

Simple centralized controllers have been computed for three benchmark process systems. It is gratifying that in all cases, PI elements suffice in producing closed-loop systems meeting desired performance and constraints. A novel technique for estimating the starting values of the controller parameters ensures that the starting closed-loop system is stable as well as substantially reduce computational burden. It also helps in determining the signs of the controller elements. Although optimization can be done in the Simulink environment, results in this work were obtained using the MATLAB environment and I_{MN} approximants (Zakian, 1975) (M=14, N=22) was used to compute system responses during optimization. The final results were confirmed by simulation using Simulink.

The design of simple feedback controllers through an initial IMC parameterization using a moment approximant is novel and has worked effectively for all the plants considered so far with many of the plants being matrices of orders 3 or 4. These are the highest transfer function matrix dimensions of plants we found in the current literature.

During controller parameter optimization, several performance indices were tried. It was found that either the integral of the squared error criterion or the integral of the absolute error criterion worked well for most examples. The integral of time multiplied by the absolute error criterion produced closed loop systems with relatively small settling times but large overshoots and large transient interactions.

ACKNOWLEDGMENT

The first author acknowledges the donation of the software packages used in this work by the Alexander von Humboldt Foundation, Germany.

An abridged version of this work which was presented at the 2014 NSChemE Conference won the Best Paper Presentation Award under Pinnacle Holdings Award category.

REFERENCES

Balachandran, R. and Chidambaram, M. (1997). Decentralized control of crude unit distillation towers, *Comput. Chem. Eng*., 21, 783-786.

Escobar, M. and Trierweiler, J.O. (2013). Multivariable PID controller desing for chemical processes by frequency response approximation. *Chem. Eng. Sci*., (88):1-15.

Garrido, J., Vazquez, F. and Morilla, F. (2012). Centralized multivariable control by simplified decoupling. *Journal of process control*, (22):1044-1062.

MATLAB optimization tool box, *mathwoks*.

Taiwo, O. (1980) Application of the method of inequalities to the multivariable control of binary distillation columns, *Chem. Eng. Scie*., (35):847-858.

Taiwo, O. and Krebs, V. (1995) Multivariable system simplification using moment matching and optimization. *IEE Proc. Control Theory Application*, Vol.142 pp103-110.

Wang, Q.W.(2003) Decoupling control, lecture notes in control and information sciences,vol.285, springer-verlag.

Whidborne, J.F., Murad, G., Gu, D.W., and Postlewaite (1995) Robust control of an unknown plant, the IFAC '93 benchmark, *Int. J. Control*, (61):589-640.

Zakian, V. and Al-Naib, U.M.T. (1973). Design of dynamical and control systems by the method of inequalities, *Proc. IEE*, vol.120, pp1421-142.

Zakian, V.(1975). Properties of I_{MN} and J_{MN} approximants and applications to numerical inversion of Laplace transforms and initial value problems. *J. Math. Anal. Appl.*, 50, 191-222.

Zakian, V. (2005). Control Systems Design: A new Framework. *Springer*, London.

PREPARATION AND APPLICATION OF KF/EGGSHELL CATALYST IN TRANSESTERIFICATION OF NEEM OIL: OVAT APPROACH

***Ajayi, O.A.[1] Oladipo, S.A.[1], Ogunyemi, S.S.[1], Nurudeen, Y.[2], Atta, Y.A.[3],**
[1]Department of Chemical Engineering, Ahmadu Bello University, Zaria
[2] Department of Chemical Engineering, Bayero University, Kano
[3] National Research Institute for Chemical Technology, Zaria
*corresponding author: aoajayi@abu.edu.ng and segeaj@gmail.com

ABSTRACT

A solid base KF/Eggshell catalyst was prepared by wet impregnation method and applied for biodiesel production from high FFA neem oil. The XRF and XRD analyses confirmed the presence of CaO in the eggshell and crystalline phases of the desired catalyst. The 79 nm sized crystallites of the best catalyst having hexagonal shapes determined by SEM images were systemically arranged to give a BET specific surface area of 128 m^2/g, pore size 3.24nm and pore volume0.045 cm^3/g. The parameters affecting the preparation of the catalyst were investigated using OVAT approach. The best synthesis conditions were found to be 900^{0}C eggshell calcination temperature for 2h, 30 wt. % KF dosage, and 600^{0}C KF/Eggshell post-impregnation calcination temperature for 3h. The catalyst was applied in a single stage transesterification of neem oil having FFA of 4.2% to produce 94.8% yield of biodiesel. The biodiesel produced was confirmed using FTIR and GC-MS and comparable to the ASTM commercial standard. The reusability test shows that the catalyst was active recording high yield of 90% even after the fifth run and more efficient than KF/commercial CaO. Accordingly, eggshell can serve as a very good source of CaO for catalysing biodiesel formation.

Keywords: *Biodiesel, Transesterification, Waste Eggshell, Neem oil,*

1. INTRODUCTION

In recent time, continuous crude oil price crash in the international market and discovery of more shale oil reserves have stirred a strong debate on the competitive advantage of biodiesel as compared to fossil diesel based on production cost. Also, environmental benignity and renewability of biodiesel remain unbeatable. The Nigerian biofuel and incentive policy stipulated usage of B20 biodiesel blend in automobiles by the year 2020, while currently countries like United States of America, Brazil, Indonesia, Malaysia, France and Germany uses biodiesel (Libai *et al.*, 2010). Biodiesel is conventionally produced via transesterification of vegetable oils and animal fats with methanol in presence of homogeneous alkali (Encinar *et al.*, 2002), acid (Rashid *et al.*, 2008),chemical catalytic conversion (Verhé*et al.*,2011) and enzyme catalysts (Xu *et al.*, 2005). Homogeneous catalyzed transesterification yields catalyst-contaminated biodiesel and glycerol, and generate huge quantity of effluents during product purification stage (Venkat Reddy *et al.*, 2006). Heterogeneous catalysts could provide a viable solution to the product purification problems associated with homogeneous catalysts. Alkali-earth metal oxides (CaO, MgO, SrO and BaO), transition metal oxides (ZrO, TiO and ZnO) and zeolite have been reported to successfully catalyzed various vegetable oils producing biodiesel yields according to the specific surface area and basic strength of the catalysts (Zabeti*et al.*, 2009; Suppes *et al.*, 2001).

Chicken eggshells are renewable resources containing $CaCO_3$ in varying amounts, calcination of these eggshells above 700^{0}C producesheterogeneous CaO-catalyst for biodiesel production (Wei *et al.*, 2009). According to the report of the United State Department of Agriculture (USDA, 2013), Nigeria ranks as the largest chicken egg producer with a progressive trend from 500,000 metric tons egg production in 2005 to 650,000 metric tons in 2013, as depicted in Figure 1. These figures ensure adequate and continuous availability of eggshell wastes from which CaO can be obtained when treated, as untreated waste eggshells are usually disposed in landfill and its degradation often leads to pollution.

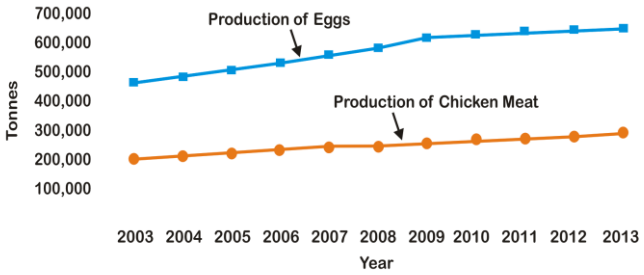

Figure 1: Nigerian poultry industry growth trend (Source: USDA, 2013)

CaO is the most promising and frequently applied metal oxide catalyst for biodiesel production, due to its cheap price, relatively high basic strength and less environmental impacts (Madhu*et al.*, 2017). Pure metal oxide like CaO usually possess a less catalytic activity in comparison with mixed metal oxides (Lee and Taufiq-Yap, 2014; Hodnett, 2000 and Centi *et al.*, 2001). Apparently, large number of mixed oxides such as KF/CaO–Fe_3O_4 (Hu *et al.*, 2011), KF/ZnO (Xie *et al.*, 2006) and KF/Ca–Mg–Al (Gao *et al.*, 2009) have been

reported for the transesterification reactions. Basic heterogeneous catalysts performed more actively, react faster and are less corrosive in comparison with acidic heterogeneous catalyst (Helwani *et al.,* 2009), but they are unfavourable for feedstocks with high FFAs and moisture content leading to saponification and hydration respectively (Wei *et al.,* 2009; Gao *et al.,* 2010). To mitigate this problem, two-step method is most commonly used (Wei *et al.,* 2009). The first step is the FFA esterification reaction, this reaction is commonly carried out using homogenous acid catalyst (Wei *et al.,* 2009). The second step is transesterification reaction mostly using base catalysts (Wei *et al.,* 2009). However, the two-step method increases system complexity and the cost of production (Wei *et al.,* 2009). Thus, synthesis of a heterogeneous catalyst from adequately available and cheap spent eggshell impregnated with potassium fluoride (KF) for a single stage transesterification process can be an ideal cost-effective process for biodiesel production from vegetable oils having high FFA (Wen *et al.,* 2010 and Liu *et al.,*2012).

Accordingly, the paper sets out to synthesis, characterized and optimize the synthetic and operational conditions using OVAT for a catalyst from spent eggshell for a single stage transesterification of neem oil.

2. EXPERIMENTAL

2.1 Materials

3.5kg spent eggshells were collected at Frizlers restaurant in Ahmadu Bello University main campus, Zaria, and wet beneficiated. The neem oil was provided by National Research Institute for Chemical Technology, Zaria, Nigeria. The oil had FFA of 4.2%. It contains 0.02% (wt) water and its molecular weight was 870gmol^{-1}. Analytical grade anhydrous methanol used was purchased from Zayo Chemicals Limited, Jos. Nigeria. The Commercial CaO and KF used were analytical reagents purchased at Hadis Chemicals Limited, Zaria, Nigeria.

2.2 Method

The collected waste eggshells were parboiled, satisfactorily washed and dried overnight in hot air oven at 105^{0}C. The dried eggshells were crushed, ball milled and then sieved using a 63µm mesh sized sieve. The powdered eggshell obtained was calcined in a muffle furnace under static air condition at 900^{0}C at holding time of 2hr (Viriya-Empikul *et al.,* 2012 and Singh *et al.,*2012). The highly active CaO species derived from eggshell calcined at varied holding times and commercial CaO were hydrated at 60^{0}C, dehydrated at 140^{0}C and recalcined at 600^{0}C for 3h to convert the hydroxide formed to a highly porous oxide.

2.2.1 Catalyst Synthesis: wet impregnation of KF/Eggshell

10g each of the dehydrated-activated-CaO eggshell based catalysts was mixed with previously prepared aqueous solution of potassium fluoride (KF) with dosage (in wt%) of 20 to 40. The resulting slurries were dried at 105^{0}C overnight in an oven and was subsequently calcined at temperatures ranging between 200^{0}C and 600^{0}C at holding times of 2 to 4hrs. These as-prepared catalysts were applied in a transesterification process to investigate their efficacies.

2.2.2 Transesterification: catalyst efficacy tests

The procured neem oil was pre-treated and analysed for physicochemical properties. The transesterification reaction parameters used in this study for the purpose of testing the efficacy of the catalysts were derived from the report of Libai *et al.,*(2011) with some modifications. In this study, 5wt. % catalyst weight was used for a reaction time of 1.5h with oil-methanol ratio and reaction temperature of 1:12 and 65^{0}C, respectively. Typically, a 250ml 3-neck flat bottom flask was charged with 23g of the pre-treated neem oil and 5 different catalysts prepared in section 2.2.1, while the reaction condition employed are as mentioned earlier. The medium was stirred at 500r.p.m and refluxed with a water-cooled condenser, placed on a calibrated magnetic stirrer. At the stipulated reaction time, the product was cooled down and allowed to separate into three distinct layers after staying for 24hrs in a separating funnel. The topmost layer consisted majorly of the methyl ester, middle-dissolved methanol and bottom-unreacted triglycerides. It was decanted, washed with distilled water and the residual methanol was separated by distillation at 75^{0}C. The biodiesel yield was determined as ratio of the weight of decanted topmost oil layer to the weight of neem oil used in the reaction. The catalyst having the highest yield of biodiesel was chosen as the best and subjected to further upgrade.

2.2.3 Comparative and Reusability Tests

Four different types of catalysts were prepared based on the selected favourable conditions, namely; KF/eggshell, KF/Commercial CaO, Eggshell and Commercial CaO were applied in transesterification reaction. The as-synthesized KF/eggshell based catalyst was repeatedly used in the transesterification reaction. After each complete cycle of transesterification, the catalyst was centrifuged from the mixture, washed with methanol, dried and weighed before applying them in another cycle. The biodiesel yield and catalyst weight after each run were determined and noted.

2.2.4 Characterization Technique

The chemical composition of the eggshell was determined by XRF spectrometry using Shidmadzu EDX-720 spectrometer. The morphology and specific composition for each stage of the transformation of the eggshell were observed under Scanning Electron Microscopy with Energy Dispersive X-ray Spectroscopy

(SEM-EDX) using Hitachi S-4500 field emission SEM with a Quartz PCI XOne SSD X-ray analyzer. The crystalline phase of each stage of the transformation of eggshell into the desired catalysts was studied using the Shidmadzu XRD-6000 Diffractometer. The XRD patterns were identified and analyzed by comparing their diffraction lines and intensities using the Joint Committee on Powder Diffraction Standards (JCPDS). The Quantachrome Nova 4200e BET machine was employed to determine the specific surface area, pore diameter and volume of the catalyst produced under optimal conditions using the N_2 adsorption-desorption technique. The FTIR analyses on the catalyst performed using the Agilent machine. The fresh biodiesel produced from the best condition was analysed qualitatively using FTIR and GC-MS.

3. RESULTS AND DISCUSSION

3.3.1 Eggshell and Catalysts

The result of XRF analysis of the beneficiated eggshell suggests, shown in Table 1, that the choice of eggshell as a raw material in this study is justified by the rich content in calcium needed basically for the catalysis. Hunton (2005) reported that the chicken eggshell is 97% calcium carbonate crystals, which are stabilized by a protein matrix, he also mentioned that an amount as low as 78% has been reported. The variance in the values of the main component, i.e CaO seen in Table 1 with the literature (Eletta *et al.*, 2016 and Amal and Manusamy, 2015) might be attributed to difference in the chicken feeding culture and/or location.

Table 1: Chemical composition (wt. %) of eggshell

Composition	CaO	SO_3	Na_2O	Al_2O_3	Fe_2O_3	CeO_2	BaO	SiO_2	TiO	MgO	P_2O_5
Present work	98.04	0.21	0.08	0.28	0.08	0.03	0.06	0.36	0.02	nd	nd
Eletta et al (2016)	89.85		0.21	0.32	0.03	nd	nd	0.1	nd	0.01	0.26
Amal and Manusamy, 2015	76.99	0.33	0.11	nd	0.02	nd	nd	nd	nd	0.93	0.42

nd = not determined

The result of thermal transition, crystalline phase and morphology of samples are detailed here. The most intense peak observed occur at $2\theta = 29.32^0$ in Figure 2 (a) having crystalline plane of (104) and other minor peaks were noted at 35.95^0(110), 39.37^0(113), 43.08^0(202), according to JCPDS card number; 01-085-1108 for calcium carbonate. It should be noted that the results displayed in Figures 2 and 3 as well as the BET data were for the starting material and best catalyst in transesterification reaction.

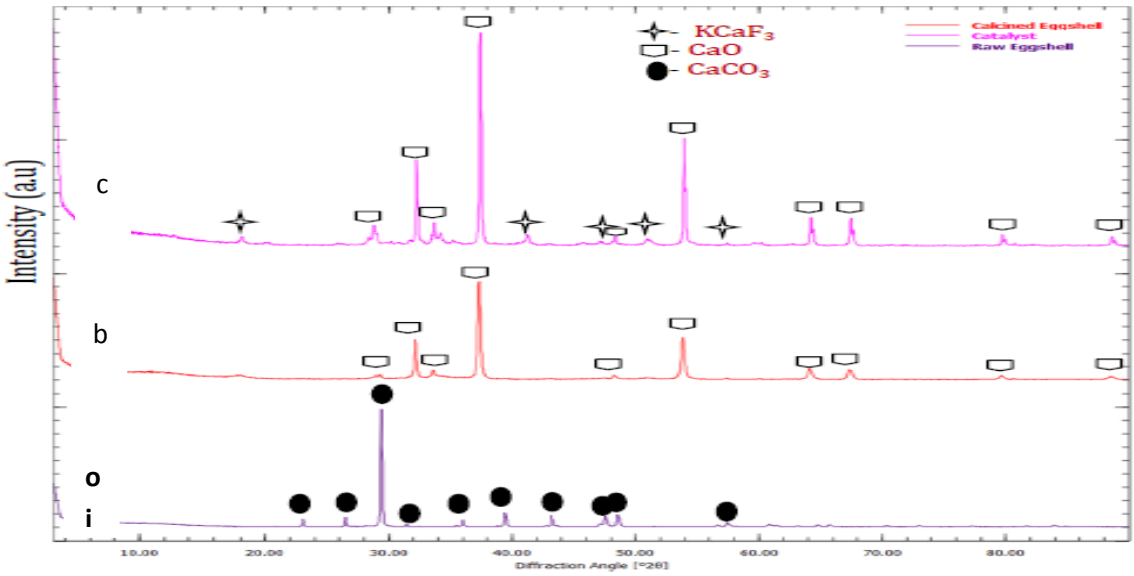

Figure 2: XRD patterns for raw eggshell, calcined eggshell and KF/eggshell catalyst

This is in agreement with the XRF result in Table 1 which showed that beneficiated raw eggshell is majorly composed of $CaCO_3$. Thermal treatment of the calcite at the optimum operating condition assisted in the transformation of the $CaCO_3$ into CaO as depicted by Figure 2 (b). The peaks prominent for lime were observed at $2\theta = 32.03^0$(111), 37.26^0(200), 53.71^0(220), which corresponds with the JCPDS card number- fm-3m: 01-077-2376 for face-centred cubic lime lattice. The peaks corresponding to the $KCaF_3$ were consistent with

the standard pattern reported in JCPDS file (3-567) for $KCaF_3$ crystal, having intense peaks of the magnetite observed at $2\theta = 30.04^0(220)$, $43.08^0(400)$ as depicted in figure 2(c)contained in the file number (79-0417). According to XRD analysis, the crystallinity (%), size (nm) and shape for beneficiated eggshell, calcined eggshell, catalyst and magnetic catalyst, respectively, are 94, 100, hexagonal; 92, 84, cubic; 87, 79, hexagonal and 98, 108, orthorhombic.

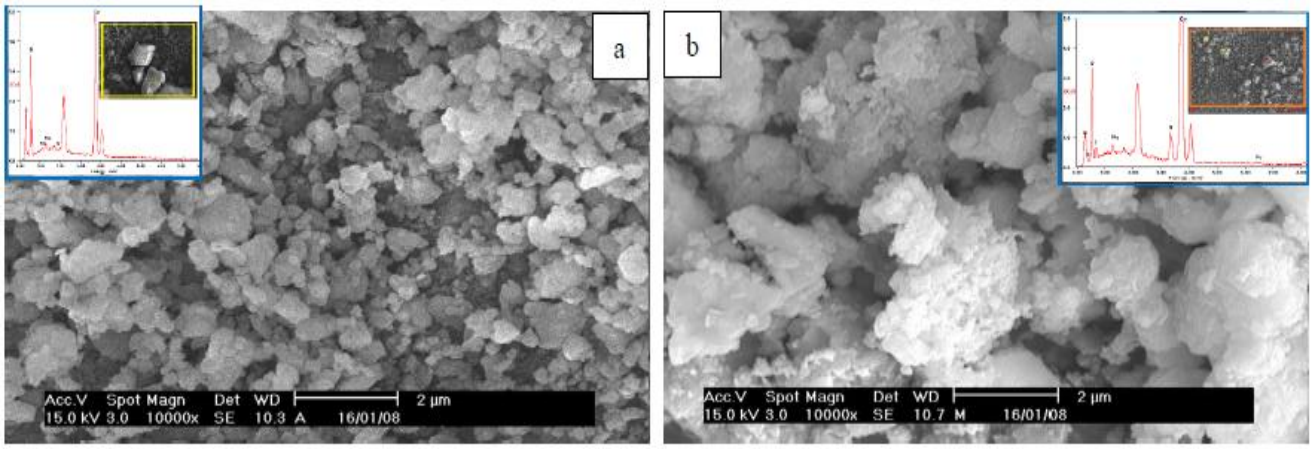

Figure 3: SEM for beneficiated eggshell and magnetite KF/Eggshell catalysts

Figure 3(a) is the SEM image of the beneficiated eggshell, shows irregular agglomerates of rod-like particles of eggshell indicative of a low specific surface area, which is similar to report Khemthong*et al.,* (2012) and Niju*et al.,* (2014). Figure 3(b) is the SEM micrograph of the magnetic catalyst, shows an irregularly shaped structure, but having some closely parked agglomerates probably resulting from the magnetic nature of the catalyst. This feature may possibly be an advantage in catalyst activity and recoverability. The EDS gave an indication of the introduction of magnetite in the final catalyst and its result for the beneficiated eggshell was found to corroborate the XRF result.

The hydration-dehydration technique after initial calcination was reported by (Yoosuk *et al.,* 2010) to play an important role in improving the specific surface of CaO catalyst. The specific surface area, pore size and pore volume of the catalyst were determined to be $128m^2/g$, 3.24 nm and 0.046 cm^3/g, respectively, an indication of its mesoporosity.

3.3.2 Transesterification reaction

Figure 4 shows the combined effects of post-impregnation calcination time (PICtime) and KF dosage at post-impregnation calcination temperature (PICtemp) of 600^0C. The biodiesel yield was observed to increase with increase in PICtemp and KF dosage but climaxed at KF dosage of 30wt%. Further increase in the dosage led to drop in biodiesel yield, which suggest that the excess KF have negatively affected the activity of the catalyst resulting in the promotion of reverse reaction (Singh *et al.,* 2012). The increase in biodiesel yield was spontaneous as the value spike from 70.3% for PICtemp of 200^0C to 91.8% at PICtemp of 600^0C. Accordingly, the PICtemp of 600^0C and KF 30wt% were chosen as the best point for these parameters of investigation. This suggest that the dosage and temperature are favourable for the synthesis of an active highly porous catalyst with good surface area.

The produced KF/eggshell catalyst produced from post-impregnation calcination temperature of 200^0C to 600^0C and PICtime of 2 to 4hrs using 30wt% KF was tested in the transesterification reaction and the biodiesel yield obtained are depicted in Figure 5. The result in figure 4 shows that holding time does not have significant effect on biodiesel yield as the increase in its value is less than 2% for holding time up to 4hrs, irrespective of the post-impregnation temperature. On the contrary, the temperature of thermal treatment had a positive effect on the biodiesel yield. For holding time of 2hr, the yield increases from 69.2% at 200^0C to 89.5% at 600^0C, an improvement was noticed when the holding time was increased to 4hrs, recording 70.3% and 91.8% at 200^0C and 600^0C, respectively. This is an indication that the reaction between CaO and KF was highly favoured at higher temperature, leading to highly active catalyst producing high biodiesel yield (Wen *et al.,* 2010).

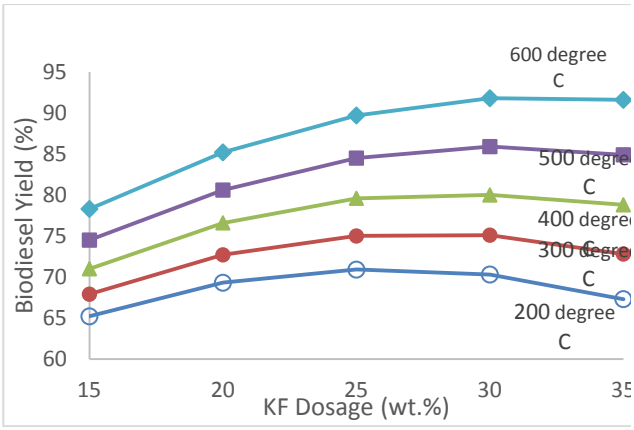

Figure 4: Biodiesel yield obtained at PICTime of 3hrs understudying PICTemperature and KF dosage

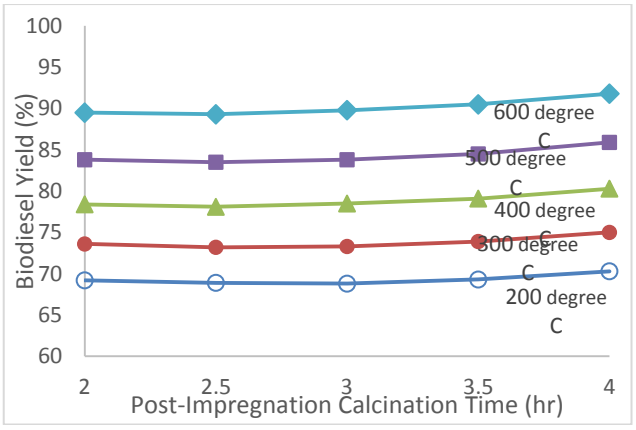

Figure 5: Biodiesel yield obtained at KF-30wt% understudying PICTemperature and PICTime.

Figure 6 shows the effect of KF dosage and PICTime at fixed PICTemperature of 600^{0}C of biodiesel yield. It was found to increase with increase in both parameters, suspected to have resulted from formation of the desired catalyst at this temperature and appropriate dosage of KF. The biodiesel yield increased from 75.9% for KF dosage of 15% at PICTime of 2hrs to 89.2% for KF dosage of 30% and same PICTime. Increasing the PICTime to 4hrs, biodiesel yield of 78% and 91.2% were respectively, obtained for KF dosage of 15 and 30%. It should be mentioned here that, the biodiesel yield obtained for KF dosage of 30 and 35wt % were observed to be close in terms of value, which implies that further increase in KF dosage does not favour biodiesel yield.

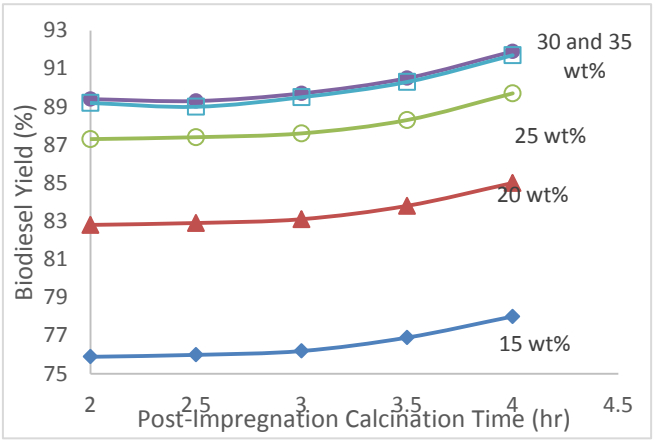

A KF dosage of 30wt%, PICTemperature of 600^{0}C and PICTime of 3hrs were observed to be a favourable condition for the formation of an active KF/eggshell based biodiesel catalyst. Accordingly, the proposed transesterification reaction mechanism for KF/eggshell based catalyst is presented in Figure 7.

Figure 6: Biodiesel yield obtained at KF-30wt% understudying PICTemperature and PICTime.

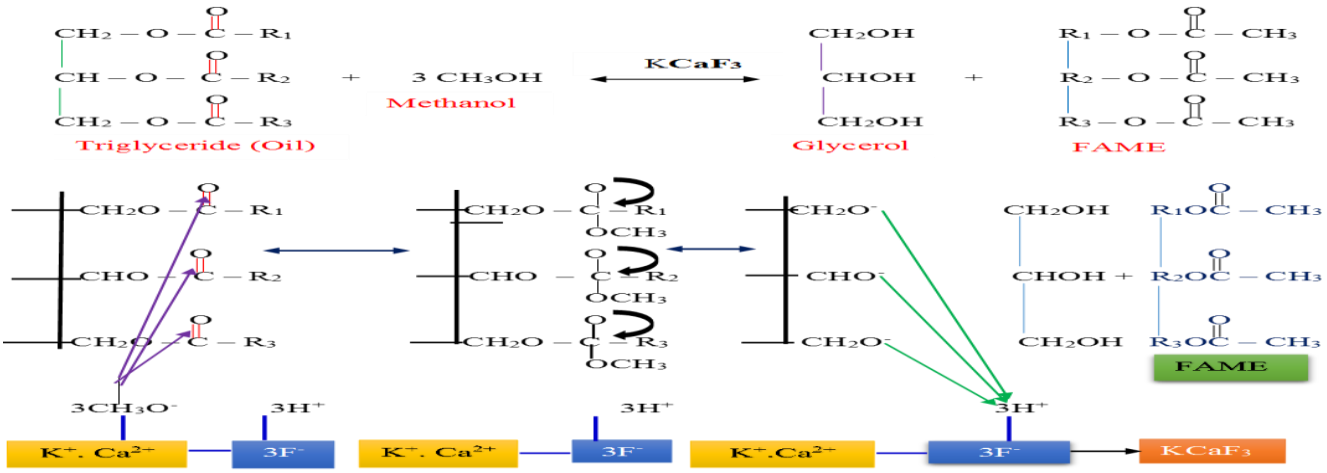

Figure 7: Proposed transesterification reaction mechanism in the presence of KF/eggshell catalyst.

3.3.3 Comparative and Reusability Test

Figure 8 showed the biodiesel yield produced from four different catalyst. It worth mentioning that the eggshell based CaO was more active than its commercial counterpart, for the former recorded 68.6%, while the commercial had only 60.8%.

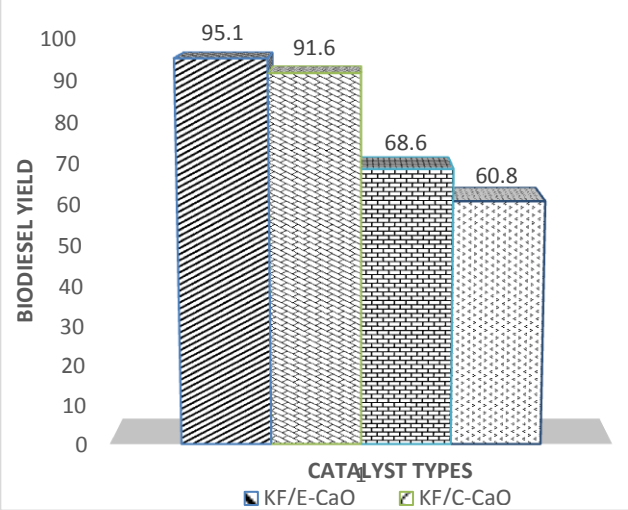

Figure 8: Comparative transesterification yield study.

It is suggestive that the eggshell based CaO have less resistance to thermal activation compare with the commercial one, that might have gone through several processes during its production. The KF/eggshell catalyst was also found to be more reactive than the KF/C-CaO, producing biodiesel yield of 95.1% compared with 90.1% from the other. The reason for this might be partly what was stated earlier and/or inability of the KF to interact properly with a more rigid structure of the commercial CaO.

The reusability study conducted showed that the catalyst can be economically used for more than four runs with biodiesel yield of 79% at the fifth run, as depicted in Figure 9. The test was further conducted for yet other runs and it was observed that as the weight of the recovered catalyst drop, the yield dropped in same trend. This suggests that the quantity of catalyst viz-a-viz the needed active were reduced hence less biodiesel formation, resulting from leakage of K and Ca to water and methanol (Liu *et al.*, 2012).

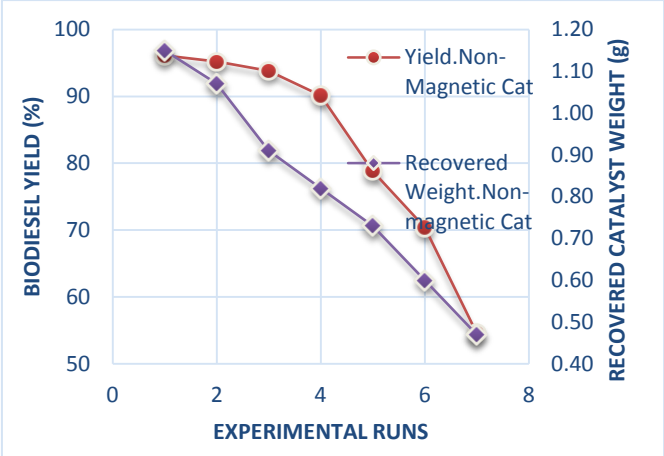

Figure 9: Catalyst reusability study.

3.3.4 Biodiesel Characterization

Figure 10 depicting the FTIR for biodiesel produced, showed a slight absorption in the 3600-3300 cm^{-1} range indicating a very little presence of moisture this is also complimented by the "water and sediment" result in Table 2.

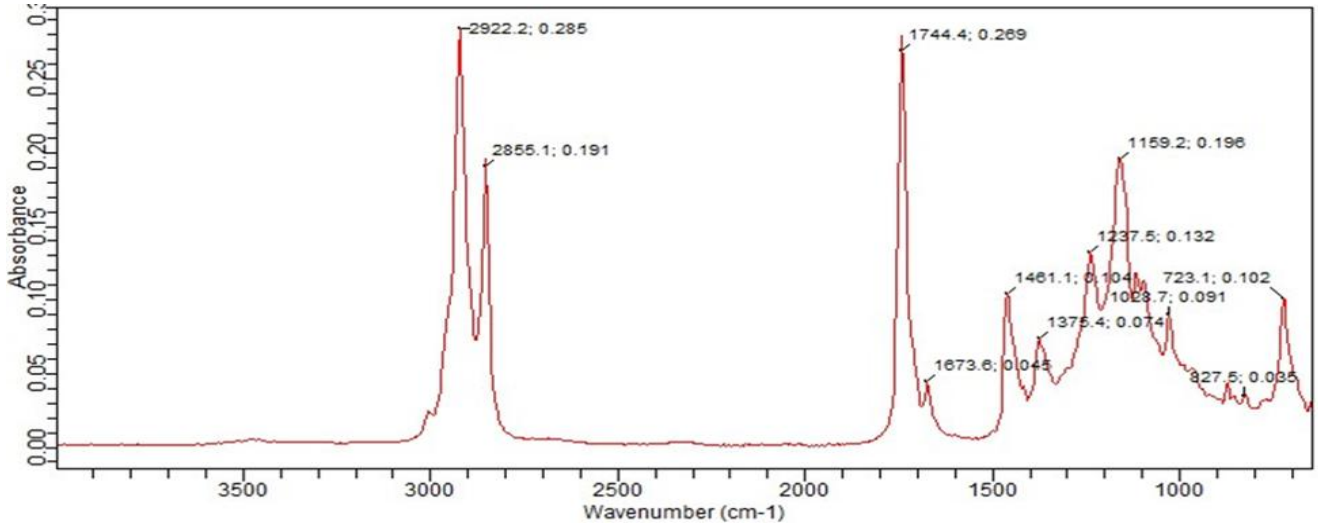

Figure 10: FTIR spectra of biodiesel fuel produced over the KF/Eggshell catalyst

This also suggests absence of unreacted alcohol in the fuel produced, resulting from the distillation of the fuel after the transesterification process. The slightly sharp peaks in the 1147 – 1122cm^{-1} indicates low presence of unsaturated compounds in the fuel produced. This is evident in the observed reduction of the iodine value of the fuel which is probably due to transformation during the transesterification process. There is a very strong ester absorption in the range 1750 – 1730cm^{-1} depicted by a very sharp peak suggesting, almost complete

conversion of triglycerides to methyl esters (Tanwar*et al.*, 2013)

Table 2: Physicochemical Properties of Neem Oil and Biodiesel

Properties	Neem Oil Measured value	Biodiesel (B100) Measured value	ASTM Standard B100	Test Methods
Density at 40^0C (g/cm^3)	0.92	0.89	0.86 – 0.89	ASTM D1298
Iodine value (mg I/100g oil)	71.4	42.5	-	ASTM D5554
Viscosity at 40^0C (mm^2/s)	26.09	4.78	1.9 – 6.0	ASTM D445
Acid value (mg KOH/g)	8.36	0.264	0 – 0.5	ASTM D664
Flash point ^{0}C	-	137	93 -170	D93
Cloud point ^{0}C	-	10	(-3) - 12	Refrigeration
Pour point ^{0}C	-	4	(-15) - 10	Refrigeration
Water & sediment (% vol)	-	0.02	0 – 0.05	ASTM D2709
Molecular weight (g/mol)	870	-	-	(Xu *et al.*, 2006)
Colour	Dark brown	Light brown	-	-

The major shift from direct use of vegetable oil in diesel engines to transesterified oil is because of its high viscosity; this fuel property affects the flow and atomization characteristics of a liquid fuel. A 4.78 mm^2/sec kinematic viscosity of the produced neem oil biodiesel can ensure a superior injection and atomization performance with added advantage of lubrication for the moving engine parts. High flash point temperatures for fuels ensure safe handling and storage. All the properties investigated in Table 2 were observed to fall within the ASTM standard.

Figure 11 shows the GC for fatty acid methyl esters, which contains about 34 methyl ester compounds. Eleven ester compounds out of the 15 observed were matched to the standard**.** Molecules of glycerine that is present in the biodiesel may be due to insufficient purification after production. Squalene and octacosane are inherent compounds found in vegetable oils, squalene; an unsaturated alkene compound was observed to be present in a minute quantity. This was also confirmed by both the iodine value and FTIR peak. The relatively low amount of this compound, is beneficial to the oxidative stability of the biodiesel fuel. The ester content of the produced was found to be 96.82%, which compares favourably with the standard stipulated by ASTM is 96.5%.

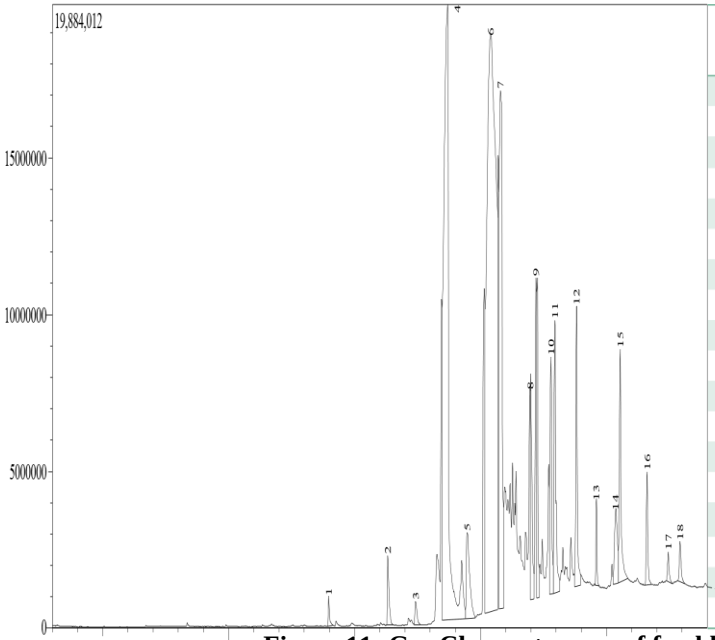

Peak No	IUPAC Name	Molecular weight g/mole	RT (min)
1	Methyl Tridecanoate	228	14.0
2	Methyl Myristate	242	16.3
3	Methyl Pentadecanoate	256	17.4
4	Methyl Palmitate	270	18.7
5	Methyl Margarate	284	19.5
6	Methyl Oleate	296	20.4
7	Methyl Stearate	298	20.8
8	Methyl Eicosatrienoate	320	22.0
9	Methyl Eicosadienoate	322	22.3
10	Methyl 11-eicosanoate	324	22.8
11	Methyl Arachidate	326	23.0
12	Methyl Heneicosanoate	340	23.8
13	Methyl Behenate	354	24.6
14*	Glycerin 1-monooleate	356	25.4
15	Methyl Lignocerate	382	25.5
16*	n-Octacosane	394	26.6
17*	Squalene	410	27.5
18	Methyl Melissate	466	27.9

Figure 11: Gas Chromatogram of freshly prepared neem oil biodiesel

4.0 CONCLUSION

Chicken eggshell wastes are cheaply available rich source of $CaCO_3$ from which CaO can be synthesized as a catalyst for biodiesel production. The best temperature for calcination of chicken eggshell for the production of usable CaO-catalyst in biodiesel production was

established to be 900^0C for a period of 2h.The impregnation of KF in the calcined eggshell consequentially led to the formation of $KCaF_3$ crystals with probable higher basic strength than CaO. The KF/Eggshell synthesized after impregnation are more acid tolerant than CaO, hence usable in the transesterification of neem having FFA of 4.2%.
30 wt.% of KF was found to be the best amount needed for the impregnation, calcination of KF/Eggshell at 600^0 for 2h were also found to be the optimal conditions for the preparation of the acid tolerant catalyst
The KF/Eggshell catalyst prepared at optimal conditions was found to be highly crystalline and porous with large hexagonal-like surface area. These structural properties together with the basic strength of the catalyst were believed to be responsible for its high catalytic activity. The catalyst was found to be reusable up to four and five turnovers respectively producing biodiesel of about 90% yield.

5.0 REFERENCES

Amal S.M. Bashir and Y. Manusamy (2015). Characterization of Raw Egg Shell Powder (ESP) as A Good Bio-filler. *Journal of Engineering Research And Technology*, Volume 2, Issue 1, 56-60

ASTM, D. (2002). *6751-02, Standard Specification for Biodiesel Fuel (B100) Blend Stock for Distillate Fuels*. Designation D-6751-02, American Society for Testing and Materials: West Conshohocken, PA.

Centi, G., Cavani, F., & Trifirò, F. (2012). *Selective oxidation by heterogeneous catalysis*. Springer Science & Business Media.

Eletta, O.A.A., O.A. Ajayi, Ogunleye, O.O. and I.C. Akpan (2016). Adsorption of cyanide from aqueous solution using calcinated eggshells: Equilibrium and optimisation studies. *Journal of Environmental Chemical Engineering* 4 (2016) 1367–1375

Encinar, J. M., Gonzalez, J. F., Rodriguez, J. J., & Tejedor, A. (2002). Biodiesel fuels from vegetable oils: transesterification of Cynara c ardunculus L. oils with ethanol. *Energy & fuels*, *16*(2), 443-450.

Gao, L., Teng, G., Lv, J., & Xiao, G. (2009). Biodiesel synthesis catalyzed by the KF/Ca− Mg− Al hydrotalcite base catalyst. *Energy & Fuels*, *24*(1), 646-651.

Helwani, Z., Othman, M. R., Aziz, N., Kim, J., & Fernando, W. J. N. (2009). Solid heterogeneous catalysts for transesterification of triglycerides with methanol: a review. *Applied Catalysis A: General*, *363*(1), 1-10.

Hu, S., Guan, Y., Wang, Y., & Han, H. (2011). Nano-magnetic catalyst KF/CaO–Fe_3O_4 for biodiesel production. *Applied energy*.

Hunton, P. (2005). Research on eggshell structure and quality: an historical overview. *Revista Brasileira de Ciência Avícola*, *7*(2), 67-71.

Kaur, M., & Ali, A. (2014). Potassium fluoride impregnated CaO/NiO: An efficient heterogeneous catalyst for transesterification of waste cottonseed oil. *European Journal of Lipid Science and Technology*, *116*(1), 80-88.

Khemthong, P., Luadthong, C., Nualpaeng, W., Changsuwan, P., Tongprem, P., Viriya-Empikul, N., & Faungnawakij, K. (2012). Industrial eggshell wastes as the heterogeneous catalysts for microwave-assisted biodiesel production. *Catalysis Today*, *190*(1), 112-116.

Lee, H.V and Y.H. Taufiq-Yap (2014). Optimization study of binary metal oxides catalysed transesterification system for biodiesel production. Journal of Process Safety and Environmental Protection, *Official Journal of European Federation of Chemical Engineering*, Part B.

Liban, W., Wang, Y., Lu, D., Hu, S and Han, H (2010). Preparation of KF/CaO nanocatalyst and its application from Chinese tallow seed oil. *Fuel*, vol.89, Issue 9, 2267-2271

Liu, H., Su, L., Y, Shao and L. Zou (2012). Biodiesel production catalysed by cinder supported CaO/KF particle catalyst. *Fuel*, vol. 97, 651-657

Madhu, D., Arora, R., Sahani, S., Singh, V., and Sharma, Y.C (2017). Synthesis of High-Quality Biodiesel Using Feedstock and Catalyst Derived from Fish Wastes. *Journal of Agricultural and Food Chemistry* 65(10):2100-2109. doi: 10.1021/acs.jafc.6b05608.

Nakatani, N., Takamori, H., Takeda, K., & Sakugawa, H. (2009). Transesterification of soybean oil using combusted oyster shell waste as a catalyst. *Bioresource Technology*, *100*(3), 1510-1513.

Niju, S., Meera, K. M., Begum, S., & Anantharaman, N. (2014). Modification of egg shell and its application in biodiesel production. *Journal of Saudi Chemical Society*, *18*(5), 702-706.

Verhé, R., C. Echim, W. De Greyt, C. Stevens (2011). Production of biodiesel via chemical catalytic conversion. In R. Luque. J. Campelo, J. Clark (Eds.), *Handbook of Biofuels Production: processes and technologies* (pp.97- 127) Sawston, Cambridge: Woodhead

Rashid, U., Anwar, F., Moser, B. R., & Ashraf, S. (2008). Production of sunflower oil methyl esters by

optimized alkali-catalyzed methanolysis. *Biomass and Bioenergy*, *32*(12), 1202-1205.

Singh, B., Birla, A., Upadhyay, S.N, Yaakob, Z and Y.C. Sharma (2012). Synthesis of biodiesel using potassium fluoride supported by hydrotalcite and process optimization by Box- Behnken design. *Biomass Conversion and Biorefinery*, vol. 2, issue 4, 317-325

Suppes, G. J., Bockwinkel, K., Lucas, S., Botts, J. B., Mason, M. H., & Heppert, J. A. (2001). Calcium carbonate catalyzed alcoholysis of fats and oils. *Journal of the American Oil Chemists' Society*, *78*(2), 139-146.

Tanwar, D., Ajayta, D. S., & Mathur, Y. P. (2013). Production and characterization of neem oil methyl ester. In *International Journal of Engineering Research and Technology* (Vol. 2, No. 5 (May-2013)). ESRSA Publications.

United States Department of Agriculture (USDA). 2013. International Egg and Poultry Report.http://www.thefarmsite.com/reports/contents/IntlPoultryandEgg19Feb2013.pdf [accessed March 25, 2016]

Venkat Reddy, C. R., Oshel, R., & Verkade, J. G. (2006). Room-temperature conversion of soybean oil and poultry fat to biodiesel catalyzed by nanocrystalline calcium oxides. *Energy & Fuels*, *20*(3), 1310-1314.

Viriya-Empikul, N., Krasae, P., Puttasawat, B., Yoosuk, B., Chollacoop, N., & Faungnawakij, K. (2010). Waste shells of mollusk and egg as biodiesel production catalysts. *Bioresource technology*, *101*(10), 3765-3767.

Wei, Z., Xu, C., & Li, B. (2009). Application of waste eggshell as low-cost solid catalyst for biodiesel production. *Bioresource technology*, *100*(11), 2883-2885.

Wen, L., Wang, Y., Lu, D., Hu, S., & Han, H. (2010). Preparation of KF/CaO nanocatalyst and its application in biodiesel production from Chinese tallow seed oil. *Fuel*, *89*(9), 2267-2271.

Xie, W and X. Huang (2006). Synthesis of biodiesel from soybean oil using heterogeneous KF/ZnO catalyst. *Catalysis Letters*, vol. 107, Issue 1-2, 53-59

Xu, H., Miao, X., & Wu, Q. (2006). High quality biodiesel production from a microalga Chlorella protothecoides by heterotrophic growth in fermenters. *Journal of biotechnology*, *126*(4), 499-507.

Xu, Y., Du, W and Liu, D (2005). Study of the kinetics of enzymatic interesterification of triglycerides for biodiesel production with methyl acetate as the acyl acceptor. Journal of Molecular Catalysis B: *Enzymatic*, *vol. 32, Issues* 5-6, 241-245

Yoosuk, B., Udomsap, P., Puttasawat, B., & Krasae, P. (2010). Improving transesterification acitvity of CaO with hydration technique. *Bioresource technology*, *101*(10), 3784-3786.

Zabeti, M., Daud, W. M. A. W., & Aroua, M. K. (2009). Activity of solid catalysts for biodiesel production: a review. *Fuel Processing Technology*,*90*(6), 770-777.

UTILISING CLEAN COAL TECHNOLOGIES FOR MEETING NIGERIA'S ENERGY NEEDS

Denloye, A. O. and *Akinola, A. A.
Chemical and Petroleum Engineering Department
University of Lagos, Lagos, Nigeria
akinjideakinola@gmail.com

ABSTRACT

Coal is expected to remain one of the dominant fuels in global electricity power generation as a result of its low cost, high reliability and high availability. In Nigeria, however, coal is yet to make a significant contribution to Nigeria's energy needs because of the numerous challenges associated with coal electricity power generation. One of the challenges is that the use of coal to generate electric power produces toxic gases which are hazardous to human health and the environment; it is also perceived as dirty to the environment. This paper focuses on the roles clean coal technologies can play in the sustainable exploitation of Nigeria's coal reserves and how it can be effectively utilized to meet Nigeria's energy needs. The Nigerian situation on electricity is reviewed, and the Nigerian national policy on coal utilization is evaluated. Recommendations on methods for implementing some aspects of the Nigerian national coal policy are made. Many clean coal technologies that can help overcome the challenges of electric power generation were also reviewed. It is concluded that the core of the Nigerian national policy on coal should be the promotion of clean coal technology for electricity production. Clean coal technologies can reduce the hazardous gaseous emissions generated by the thermal decomposition of the fuel. By developing clean coal technologies, Nigeria will be able to use her considerable coal resources better and reduce the emissions of harmful substances associated with coal mining, thereby make a significant contribution to Nigeria's energy needs.

1.0 INTRODUCTION

1.1 Origin of Coal

Coal is a brownish-black sedimentary rock usually occurring in rock strata in layers or veins called coal beds or coal seams. Coal is the solid end-product of millions of years of decomposition of organic materials. Over millions of years, accumulated plant and animal matter is covered by sediment and stored within the earth's crust, gradually being transformed into hard black solids by the sheer weight of the earth's surface. Coal, like other fossil fuel supplies, takes millions of years to create but releases its stored energy within only a few moments when burned. Different types of coal exist, and they all have different uses. However, the most significant uses of coal are in electricity generation, steel production, cement manufacturing and as a liquid fuel. (WCA, 2016)

1.2 Types of Coal

Coal is a complex resource and can vary in composition even within the same deposit. There are four different types or ranking levels of coal, lignite, sub-bituminous coal, bituminous coal, and anthracite. Each type with differences in energy output as a result of increased pressurization, heat, and time. The four types of coal are discussed extensively in literature (Parr, 1922; World Coal Institute, 2005).

1.3 Reserves of Coal

Over 984 billion tonnes of proven coal reserves are estimated worldwide (World Coal Institute, 2005). The implication is that there are enough coal reserves to last us for over 190 years. Coal can be found on every continent in over 70 countries, with the biggest reserves in the USA, Russia, China and India (World Coal Institute, 2005). Nigeria ranks low in worldwide coal production, with less than 10 thousand tons of coal production yearly (Statistical Review of World Energy 2015). Nigerian Coal Corporation (NCC) estimated Nigeria's coal reserves to be at least 2 billion tons, with approximately 190 million metric tons as proven (Odesola *et al.*, 2013). Although coal was the first energy resource to be exploited by Nigeria, Coal production has dropped to insignificant levels from its high of almost 1 million tonnes in 1959 Fig. 1 (Odesola *et al.*, 2013).

Nigeria is endowed with abundant sub-bituminous coal resources distributed in about 22 coal fields spread over the country. Fig. 2 presents the map showing the location of the coals in the sedimentary basins of Nigeria

(Nyakuma, 2015; Obaje, 2009). Coal seams occur in three main stratigraphic levels (Ogunsola, 2008):

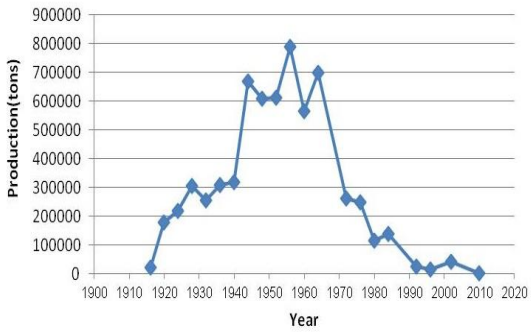

Fig. 1: Nigerian Coal Production Since 1909 (Odesola *et al.*, 2013)

1. The brown coals (lignite) of Ogwashi-Asaba Formation of Miocene to Pliocene ages,
2. The upper and lower sub-bituminous coal measures of Maastrichtian age and
3. The bituminous coals of the Awgu shales of Coniacian age.

Table 1: Nigeria's Coal Mines (M2M Workshop – Nigeria, 2005)

Mines	Coal Type	Estimated Reserves (Million Tons)	Proven Reserves (Million Tons)	Depth of Coal (m)
Okapara	Sub-Bituminous	100	24	180
Onyeama	Sub-Bituminous	150	40	N/A
Ihioma	Lignite	40	N/A	20-80
Ogboyoga	Sub-Bituminous	427	107	20-100
Ogwashi Azagba /Obomkpa	Lignite	250	63	15-100
Ezimo	Sub-Bituminous	135	56	30-45

Table 2: Ultimate Analyses of Coals from Selected Nigerian Coal Fields (Nyakuma, 2015)

Property	Garin Maiganga Coal Mines	Shankodi-Jangwa Coal Seam	Afuze Coalfields
Carbon	61.69%	71.46%	72.46%
Hydrogen	4.42%	6.40%	6.07%
Nitrogen	1.07%	1.37%	1.63%
Sulphur	0.39%	2.03%	1.41%
Oxygen	32.16%	18.76%	18.43%
Heating Value	23.7MJ/Kg	27.34 MJ/Kg	30.52 MJ/Kg

Table 3: Proximate Analyses of Coals from Selected Nigerian Coal Fields (Nyakuma, 2015)

Property	Garin Maiganga Coal Mines	Shankodi-Jangwa Coal Seam	Afuze Coalfields
Moisture	5.28%	5.14%	1.97%
Volatile Matter	51.16%	40.73%	45.80%
Ash	21.05%	14.94%	30.99%
Fixed Carbon	22.52%	39.18%	21.24%
Mineral Matter	22.95%	17.25%	34.24%

Table 1 provides an overview of estimates and proven reserves in some coal mines in Nigeria. More comprehensive information is given in the Nigeria-Summary of Coal Industry document (M2M Workshop – Nigeria, 2005).

The coals in the coal mines are low in sulfur and ash content, making them attractive for use as a source of fuel for electric power generation. Table 2 presents the ultimate analyses of coal from Afuze coalfields in Afuze, Edo state; Shankodi-Jangwa coal seam in Obi, Nasarawa state; and the Garin Maiganga coal mines in Akko, Gombe state of Nigeria (Nyakuma, 2015). Proximate analyses of the coal from the three selected coal fields are also presented in Table 3 (Nyakuma, 2015). The low moisture content of the coal in all three fields indicates the maturity of coal found in Nigeria

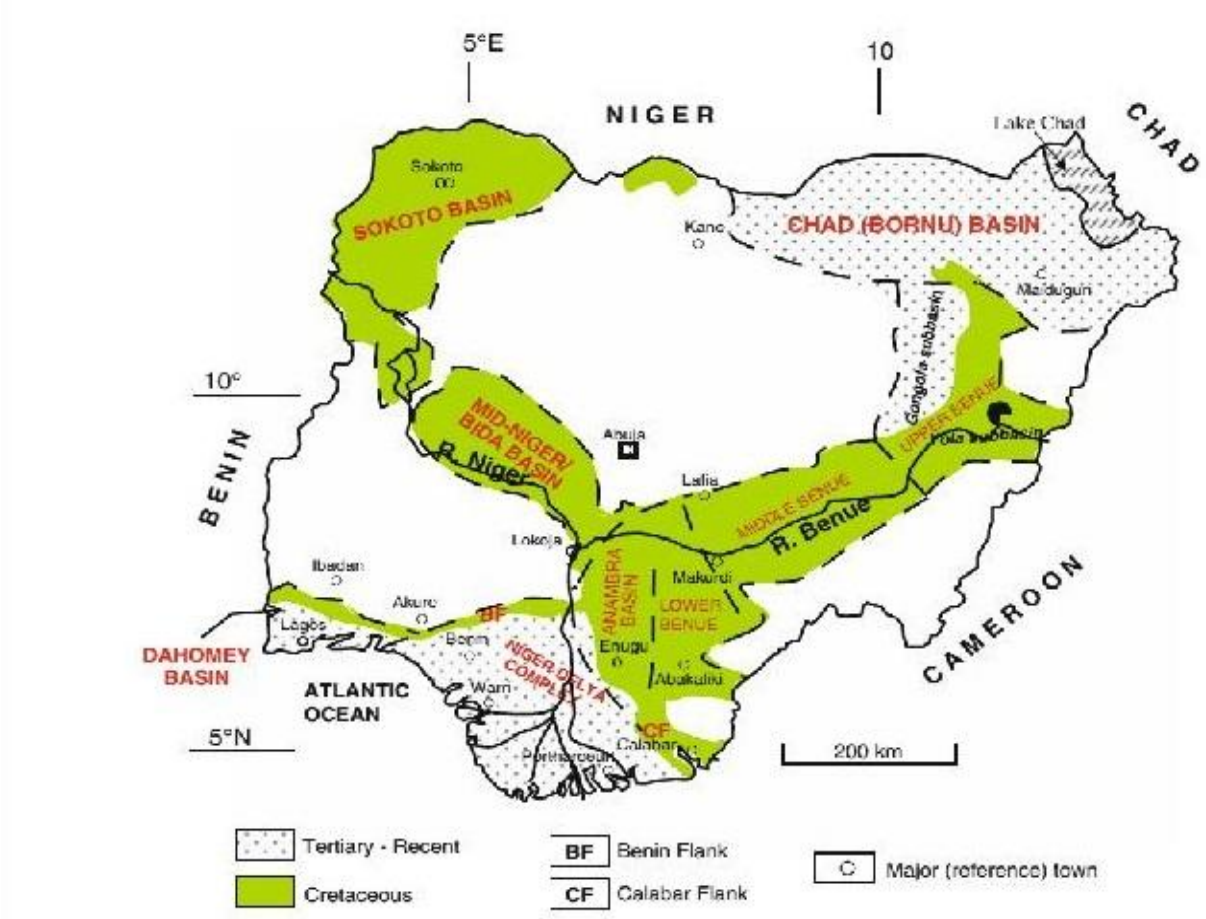

Fig. 2: Nigeria's Sedimentary Coal Basins And Deposits (Obaje, 2009)

2.0 ELECTRICITY FROM COAL

2.1 Coal and Electricity

In this day and age, electricity is an essential part of our lives and economy. Coal plays a vital role in electric power generation worldwide. Coal-fired electric power plants currently fuel 41% (Fig. 3) of global electricity (WCA, 2016). In some countries, coal fuel produces a high percentage of electric power generated. Table 4 presents the percentage of coal used for electric power generation in different countries.

Table 4: Coal in Electricity Generation (IEA, 2010)

South Africa 93%	Poland 92%	PR China 79%
Australia 77%	Kazakhstan 70%	India 69%
Israel 63%	Czech Rep 60%	Morocco 55%
Greece 52%	USA 49%	Germany 46%

Table 4 indicates that coal is an important electric energy source for many countries, such as South Africa, Poland, People Republic of China, etc. The importance of coal to electricity generation worldwide is set to continue. Sasol Limited, an integrated energy, and chemical company, operates commercial clean coal gasification plants in Secunda, Mpumalanga, South Africa, and in Sasolburg, Free State province of South Africa to generate electricity (Sichinga and Buchanan, 2005). Sub-Bituminous grade coal is used in these plants. Nigerian coal being sub-bituminous can use this same technology in generating electric power.

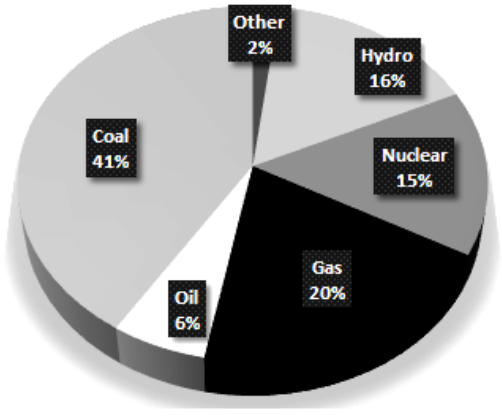

Fig. 3: Total World Electricity Generation by Fuel (WCA, 2016)

2.2 Conversion of Coal to Electricity

The process of converting coal to electricity involves the milling of the coal to a fine powder, and its combustion in a boiler to generate steam to drive turbines (IEA, 2010). A diagram of the process is shown in Fig. 4 below.

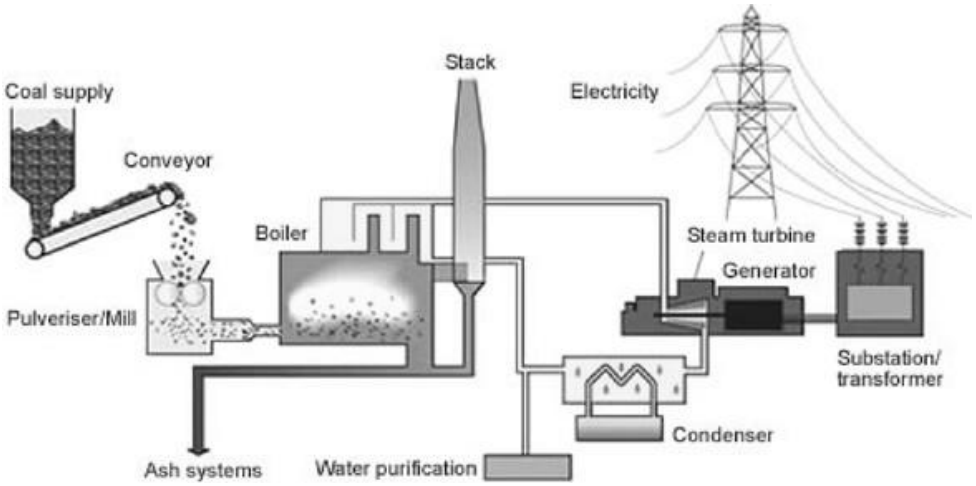

Fig. 4: Conversion of Coal to Electricity (Conventional PCC) (Moazzem *et al*., 2012)

The combustion process in the boiler generates gaseous emissions by the thermal decomposition of the coal. These gases include sulphur dioxide SO_2, nitrogen oxides (NO_2), carbon dioxide (CO_2), mercury, and other chemical by-products that vary depending on the type of the coal being used (Moretti and Jones, 2012). These emissions have been established to have a negative impact on the environment and human health, contributing to acid rain, lung cancer, and cardiovascular diseases.

2.3 Generation and Distribution of Electricity in Nigeria

Nigeria's electric power generation and grid distribution capability is currently in the range of 3,500 to 4,500 megawatts (MW) (MMSD, 2010). This is far short of that required to support the current population and to keep the economy growing. Current estimates of National electricity demand are in the range of 20,000 to 25,000 MW. Power is currently produced from several gas-fired and hydropower generating facilities. Power from the electricity distribution grid is supplemented by numerous small, costly diesel powered generators in the country's cities, towns, and villages. The electricity supply in Nigeria is characterized by frequent power failures and load shedding, resulting in economic losses through lost production, damaged equipment and the need for expensive stand-by power. The Country has an over reliance on its current non-coal generating facilities while its vast coal reserves remain unutilized.

Privatization of the energy sector has already been initiated through the Electric Power Sector Reform Act of 2005 (NERC, 2005). The former Nigerian National Electricity Power Authority (NEPA) has been unbundled into generation, transmission and distribution companies that have become privatized. Meanwhile, several Independent Power Producers (IPPs) are already in operation. The exploitation of coal for electricity generation and the production of coal briquettes for domestic and industrial heating will bring a number of benefits including the following:

i. Increased and more reliable electricity supply,
ii. Lower cost electrical energy,
iii. Expanded industrialization of the economy,
iv. Increased employment and human resources development,
v. Increased capacity utilization of existing industries and
vi. Increased national income through taxes

3.0 NATIONAL ENERGY POLICY ON COAL

Clean Coal Technologies are environmentally superior and more operationally efficient than technologies in common use today. Improved operating efficiencies of new power generation technologies from the Clean Coal Technology programs are 30-40% higher than conventional coal plants. This translates to nearly the same percentage reduction in carbon dioxide emissions.

A cornerstone of the National Policy on Coal is the promotion of clean coal for electricity production. The following objectives of the National Energy Policy seek

to promote the utilization of clean coal. These include: (Lukman, 2003)

i. Promotion of production of coal for export.
ii. Promotion of effective utilization of coal for complementing the nation's energy needs and as an industrial feedstock.
iii. Attracting increased investment into, and promote indigenous participation in the coal industry.
iv. Utilizing coal to meet the critical national need of providing a viable alternative to fuel wood in order to conserve our forests.
v. Minimizing environmental pollution arising from the utilization of coal.

To achieve these stated objectives, the National Policy has adopted the following strategies: (Lukman, 2003)

i. Intensifying the drive for coal exploration and production activities.
ii. Providing adequate incentives to indigenous and foreign entrepreneurs so as to attract investments in coal exploration and production.
iii. Providing adequate incentives for the large scale production of **coal stoves** at affordable prices.
iv. Providing adequate incentives to indigenous and foreign entrepreneurs for the establishment of coal-based industries.
v. Developing adequate infrastructure for handling and transportation of coal within and out of the country.
vi. Organizing awareness programs for the use of smokeless coal briquettes as an alternative to fuel wood.
vii. Encouraging R & D in the production, processing and utilization of coal.
viii. Introducing clean coal technologies into coal utilization.
ix. Re-introducing the use of coal for power generation
x. Focus on Clean Coal Technologies to provide cleaner electric power at less cost.

4.0 CLEAN COAL TECHNOLOGIES

Clean coal technology is a term used to describe the combination of different technologies to generate electricity from coal with minimal environmental impacts. In practice 'clean coal' technology means a range of technologies which includes the preparation of coal (i.e. washing), its combustion, and the clean-up of waste gases (e.g. CO_2, SO_2, NOx) as well as the better maintenance and management of facilities and the use of more sophisticated control and monitoring systems (Watson and Oldham, 1999). In the past, the methods used for cleaning coal included chemically washing impurities from coal, gasification, flue gas treatment, carbon capture, and storage technologies; to capture CO_2 from flue gas and dewatering low calorific coals to increase their energy conversion rates, and thus the efficiency of electricity generation. However, modern methods have been developed, and they include Efficiency improvement/Advanced Combustion Technologies, Integrated Carbon Capture and Sequestration Technology (CSS), Underground Coal Gasification, Oxy-fuel Combustion Carbon Capture Technology and Integrated Gasification Combined Cycle Process.

4.1 Advanced Combustion Technologies

Advanced Combustion Technologies are developed to incorporate new techniques and components with the old infrastructure to make power generation from coal cleaner, efficient and effective while reducing costs of production. These combustion technologies are amenable to CO_2 sequestration (by producing high pressure and/or high CO_2 flue gas concentration (Beèr, 2000). Some of these technologies are Low Emission Boiler Systems (LEBS) (Moretti and Jones, 2012), Indirectly Fired Power System (IFPS), and Fluidized Bed Combustion (Philibert and Podkanski, 2005).

4.1.1 Low Emission Boiler Systems (LEBS)

Low Emission Boiler Systems are the future of coal-fired power plants. These plants rates of emissions of SOx, NOx, and particulates are much lower than those of the other coal-fired power plants, and the net efficiency of these systems is also higher than that of coal-fired utility plants. Fly ash and scrubber solids waste streams are produced from these systems which make them very clean and efficient in nature. The ash is easily transformed into a non-leachable slag, which can be used for blasting or roofing granules. The slag byproduct can be used for making cement and other building materials. This gives the Low Emission boiler system a dual role that help saves energy and cost (Moretti and Jones, 2012).

4.1.2 Indirectly Fired Power System (IFPS)

Indirectly Fired Power System uses an indirectly fired gas turbine combined cycle, where heat energy is supplied to the gas turbine through series of high-temperature heat exchangers (Zhu, 2015). In the indirectly fired cycle, the products obtained during

combustion are shielded from the gas turbine, and a higher thermal efficiency is also produced. Indirectly Fired Power System use compressed air, and other fuels such as natural gas can be used to increase the temperature in the air furnace to that of the gas turbine inlet. Indirectly Fired Power System reduces the emission of SO_2 and NO_X significantly. This combustion technique is very promising however, reducing carbon emissions to its lowest for a coal fired boiler, and producing electricity that will cost at a cheaper rate than today's power plants.

4.1.3 Fluidized Bed Combustion

Fluidized Bed Combustion systems provide an alternative form of using coal to generate electricity with minimal carbon emissions. Two types of Fluidized Bed Combustion are available: the atmospheric system and the pressurized system. In the atmospheric system, dolomite is used as a sorbent to capture sulfur and its compounds from coal combustion. A stream of air is used to suspend the sorbent and change it into a fluid-like substance. The pressurized bed combustion (Fig. 5) operates in the same way as the atmospheric system except that it runs at a higher pressure, which creates a gas stream at temperatures that can drive a steam turbine (Watson and Oldham, 1999).

In Japan, research and development of pressurized fluidized-bed combined electricity power generation technology was conducted at J-POWER's Wakamatsu Coal Utilization Research Center (now known as Wakamatsu Research Institute) using a 71 MWe-PFBC Plant (JCOAL, 2007). The test plant was the first plant in the world to adopt a full-scale ceramic tube filter (CTF) capable of collecting dust from high-temperature, high-pressure gas at a high-performance level. Results of PFBC technology development were (1) Gross efficiency of 43% was achieved by increasing efficiency through combined power generation utilizing pressurized fluidized-bed combustion and (2) SO_x level of approximately 5 ppm through in-bed desulfurization; NO_x level of approximately 100 ppm through low-temperature combustion (approximately 860^oC), and dust of less than 1mg/Nm^3 by CTF.

4.2 Integrated Gasification Combined Cycle (IGCC)

In integrated gasification combined cycle (IGCC) systems, steam and hot pressurized air or oxygen is mixed with coal in a reaction that forces carbon molecules to be separated (Subbarao, 2010). The produced syngas, which comprises carbon monoxide and hydrogen, is then cleaned and burned in a gas turbine to generate electricity. The heat energy from the gas turbine can also be used to power another steam turbine. Integrated Gasification Combined Cycle power plants generally produce two forms of energy and that makes the plants to have a potentially high fuel efficiency. In addition to that, if an improvement is made on the technology to allow rechanneling of waste heat back to the process steam, there will certainly be an increase in the conversion efficiency. The IGCC is relatively efficient and the byproducts generated from coal gasification have series of domestic and industrial uses.

A practical example of the IGCC plant is the Duke Energy's Edwardsport Generating Station in Knox County, Ind., United States. The plant started operation commercially in June 2013. The plant is one of the world's cleanest coal-fired power systems and is the first to use integrated gasification combined cycle (IGCC) system on a large scale. The 618MW advanced IGCC plant substantially reduces the acid gases emission and environmental impact of burning coal to generate electricity in a coal-fired power plant (Sourcewatch, 2106).

The Duke Energy's Edwardsport IGCC power plant gasifies Bituminous coal, strips out acid gases and other impurities, and then burns the produced cleaner gas to generate electricity (Sourcewatch, 2106). The IGCC power plant produces 10 times as much power as the former coal-fired power plant at Edwardsport, yet with about 70 percent fewer emissions of sulfur dioxide, nitrogen oxide and particulates combined together. The efficiency of the IGCC power plant also significantly reduces its carbon emissions per megawatt-hour by nearly half. As Nigerian power plant could be built using the IGCC technology as the grade of coal used in the Duke Energy's Edwardsport Generating Station is similar to the of Nigerian coal.

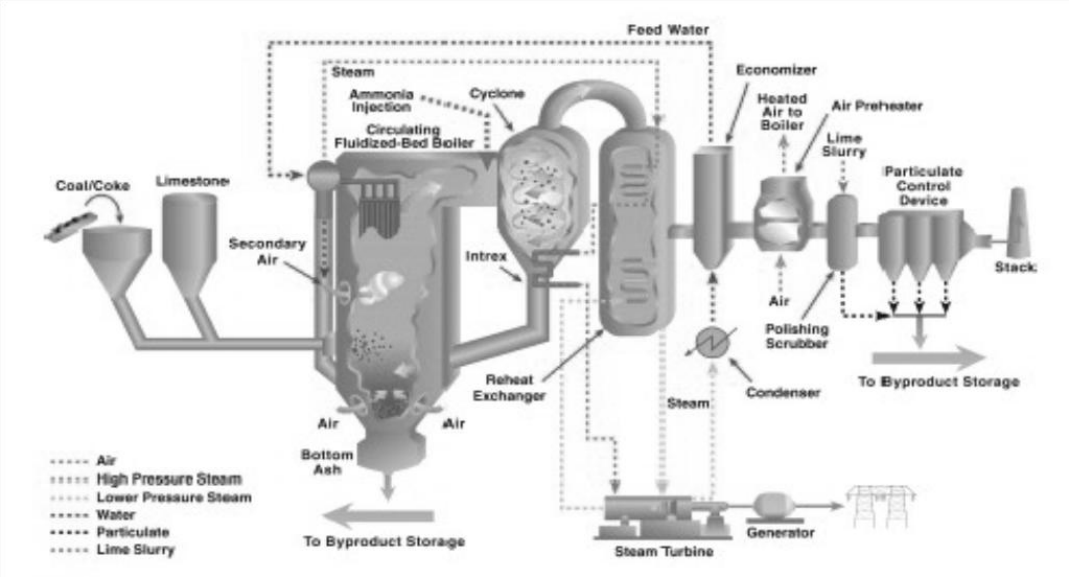

Fig. 5: Basic CFB Plant (Source JEA, 2003)

4.3 Integrated Carbon Capture and Sequestration Technology (CSS)

Carbon Capture and Sequestration (CCS) is a system that captures carbon dioxide from any available source, compresses it into a dense liquid-like substance, injects and permanently stores the CO_2 underground (Folger, 2013). Coal-fired plants in addition to power generation, generally release carbon dioxide into the atmosphere, which pollutes the environment. A better option is to sequester the carbon dioxide and prevent or slow its emission into the air. To achieve this, however, the CO_2 must first be captured (Beèr, 2000).

Integrated Carbon Capture and Sequestration Technology is a post-combustion capture process that captures carbon dioxide from the byproduct of combustion using sorbents, solvents or membrane separation to remove the produced CO_2 from the byproduct. The captured CO_2 can be pipelined and used for enhanced oil recovery in depleting oil fields during crude oil production. The Carbon Capture and Sequestration Technology, (Beèr, 2000) consist of three major steps:

i. Capture: The produced CO_2 from byproducts of combustion processes is separated from the other gases.
ii. Transport: The captured carbon dioxide is then compressed and transported through pipelines, ships or other methods to a suitable site where it can be used or stored.
iii. Storage: The carbon dioxide is injected into deep rock formations for secondary oil recovery to increase the pressure available within the formation and the remaining stored permanently.

A practical example of Integrated Carbon Capture and Sequestration Technology is the Boundary Dam CSS Project. The project transformed the old Boundary Dam Power Station near Estevan, Saskatchewan, Canada into a reliable, long-term producer of up to 115 megawatts (MW) of baseload electricity, capable of reducing acid gas emissions significantly (Monea, 2013). The carbon dioxide produced is also captured. The captured CO_2 is sold and also transmitted through a pipeline to depleted oil fields in southern Saskatchewan for secondary oil recovery while the unused carbon dioxide is stored. In addition to capturing carbon dioxide, the CSS plant also captures and sells other byproducts during power generation. The sulphur dioxide in the byproduct is also captured and converted to useful sulphuric acid for industrial purposes. Fly ash, another byproduct is captured as well and used in the production of ready-mix concrete, pre-cast structures, and concrete products.

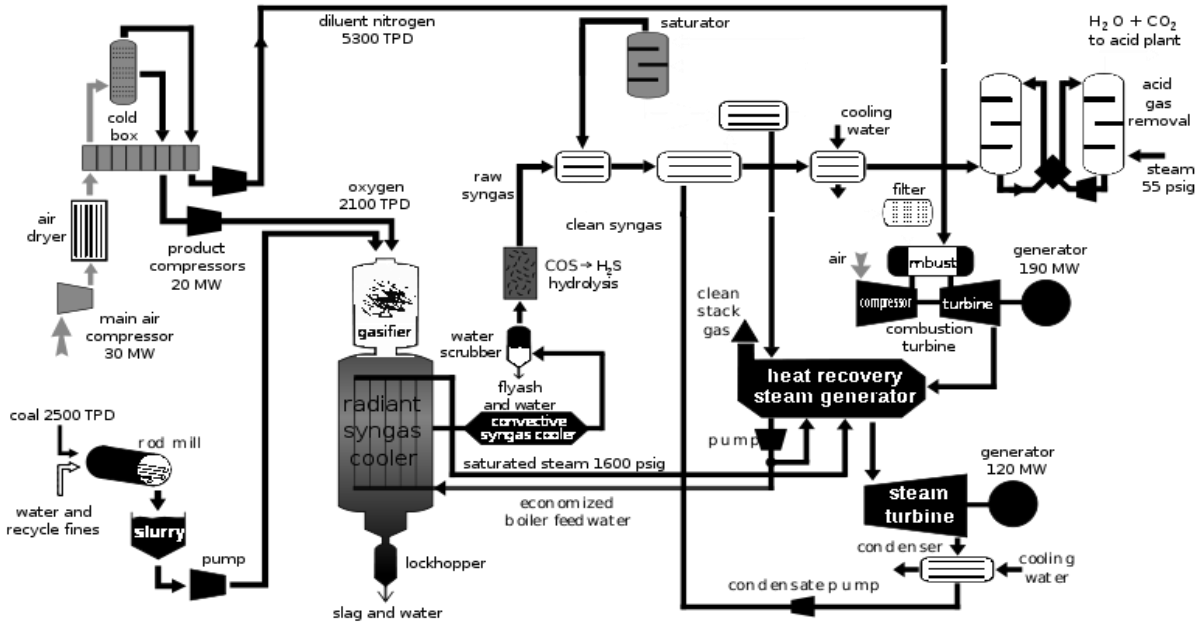

Fig. 6: Schematic of Integrated Coal Gasification Combined Cycle Unit (Crook, 2006)

4.4 Underground Coal Gasification

Underground Coal Gasification is a process of harvesting coal which is purer than the cleanest of current coal technologies. In this process, coal is gasified without mining. Two wells with a distance of twenty to fifty meters apart are drilled into the coal seam. Then, air is introduced through a pump into the injection well, while burning charcoal is placed into the production well. As the production well burns, it draws air from the bottom of the injection well and through the coal seam. This process makes the production well to burn and form a tunnel in the direction of the injection well. When the tunnel reaches the injection well, fire explodes and consumes every area surrounding the two wells and the tunnel. The resulting gas is captured and harvested (Watson and Oldham, 1999).

There are four basic problems associated with the UCG that have streamlined its development and delayed exploitation of its theoretical benefits: (Ali et al., 2012)

1. It is not economical when compared to standard methods for coal harvesting
2. The combustible gas generated is diluted with nitrogen due to air that is pumped into the coal seam for combustion
3. There is possibility of coal seam to collapse
4. And the UCG process can significantly contaminate underground water.

However, availability of cheaper oxygen will improve the viability of UCG. If oxygen is pumped into the injection wells instead of air, the resultant gas is not diluted with nitrogen, thereby increasing the productivity of UCG.

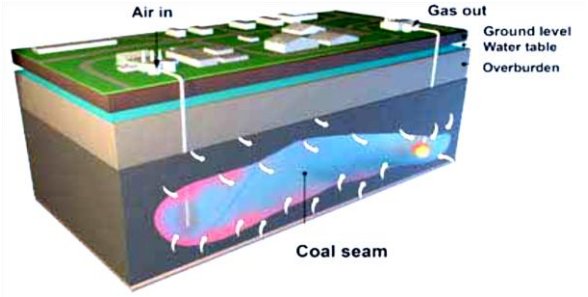

Fig. 7: Schematic of Underground Coal Gasification (Walter, 2007)

4.5 Oxy-fuel Combustion Carbon Capture Technology

In this process, oxygen needed for combustion is separated from air prior to combustion and the fuel is combusted in oxygen diluted with recycled flue-gas instead of using air. This oxygen-rich, nitrogen-free atmosphere results in final flue-gases consisting mainly of CO_2 and H_2O (water), so producing a more concentrated CO_2 stream for easier purification (Beèr, 2000).

This oxygen-rich, nitrogen-free atmosphere results in final flue-gases consisting mainly of CO_2 and H_2O (water), so producing a more concentrated CO_2 stream for easier purification. The Oxy-fuel Combustion technology has significant advantages over traditional air-fired plants.

Among these advantages are:

i. The mass and volume of the flue gas are significantly reduced.
ii. Because the flue gas volume is reduced, less heat is lost during combustion.
iii. The size of the flue gas treatment equipment is also significantly reduced.
iv. The flue gas is primarily CO_2 suitable for sequestration and storage.
v. Most of the flue gases are condensable; this makes compression separation possible.

Heat of condensation can be captured and reused rather than lost in the flue gas.
Oxy-fuel is an alternative to removing CO_2 from the flue gas from a conventional air-fired fossil fuel plant. However, an oxygen concentrator might be able to help, as it simply removes nitrogen from air.

5.0 CONCLUSIONS

Coal is expected to continue to be an important fuel for electric power generation due to its low cost and abundance. Conventional coal power generation is a major contributor to global greenhouse gas emissions through the production of acid gases and is increasingly being regulated. However, clean coal technologies that improve the environmental performance of coal electric power generation are expected to enable coal to remain an attractive fuel option well into the future. Different clean coal technologies that increase the efficiency of coal power plants and reduce emissions are being developed to meet these challenges. As a result of these advances and increasing emissions regulation around the world, the use and development of technologies that reduce SO_2, NOx, and particulate emissions have increased over the past decade. Concurrently, combustion technologies including super critical (SC), ultra-super critical (UC) pulverized coal combustion (PCC), and circulating and pressurized fluidized bed combustion (FBC) technologies are increasing the power conversion efficiencies of coal power plants. These advanced technologies have enabled simultaneous improvements in emissions and economics of coal-fired generation.

The greatest opportunity for the Nigerian coal industry lies in the deployment of the following three clean coal technologies which are Integrated Carbon Capture and Sequestration Technology, Oxy-fuel Combustion Carbon Capture Technology and Integrated Gasification Combined Cycle Process. These technologies capture carbon dioxide and other gaseous pollutants from coal power conversion processes and store it in either underground or in offshore geological formations; virtually eliminating greenhouse gas emissions from coal combustion.

The technologies are currently being used to solve global energy challenges and meet the vastly increasing energy demands. The selectivity of any of these technologies is based on the suitability of the system to be deployed and how it can be utilized effectively and efficiently to solve National energy challenges. Clean Coal Technologies can undoubtedly provide the platform to solve the energy challenges in Nigeria while minimizing the emission of harmful gaseous byproducts. This will enable Nigeria to utilize her vast coal resources to produce abundant electricity that will meet the energy needs of the nation.

REFERENCES

Ali, S. M., Pattanayak, P. and Shubhra, (2012), Underground Coal Gasification Techniques, Problems and its Solutions, *International Journal of Engineering and Innovative Technology (IJEIT)*, Volume 2, Issue 3, Pages 129 – 134.

Beèr, J. M., (2000), Combustion Technology Developments in Power Generation in Response to Environmental Challenges, *Progress in Energy and Combustion Science*, Volume 26, Issue 4, Pages 301–327.

CMM Global Overview, (2006), *Coal-bed Methane Outreach Program*, Report by the U.S. Environmental Protection Agency, United States, Pages 2 – 8.

Crook, J., (2006), Back to the Future, *IET Power Engineer*, June/July 2006, Issue 3, pp. 26-29
Folger, P., (2013), *Carbon Capture and Sequestration (CCS): A Primer*, Congressional Research Service.

Philibert C. and Podkanski J., (2005), *Case Study 4: Clean Coal Technologies*, Paper Presented for the International Energy Agency, for discussion at a seminar with non-Annex I countries, "Working Together to Respond to Climate Change", held by the Annex I Expert Group in March 2005.

International Energy Agency (IEA), (2010), *Power Generation from Coal*, IEA Publications, 9 rue de la Fédération, 75739 Paris cedex 15 Printed in France by Corlet, October 2010w.

International Energy Agency (IEA), (2010), Retrieved from http://www.iea.org/ August 01, 2010.

JEA, (2003), *Clean Coal Technology, the JEA Large-Scale CFB Combustion Demonstration Project*, Topical Report Number 22, a report on a project conducted jointly under a Cooperative Agreement between The U.S. Department of Energy/NETL and JEA, March.

Japan Coal Energy Center (JCOAL), (2007), *Clean Coal Technologies in Japan - Technology Innovation in the Coal Industry*, Meiji Yasuda Seimei Mita Building 9F, 3-14-10 Mita, Minato-ku, Tokyo 108-0073 Japan.

Lukman, R. (Presidential Adviser on Petroleum & Energy), (2003), *National Energy Policy*, The Presidency Energy Commission of Nigeria, April 2003.

M2M Workshop – Nigeria, (2005), Nigeria's Country Report on Coal Mine Methane Recovery and Use, presented at the *Methane to Markets Regional Workshop*, December 2, 2005, http://methanetomarkets.org/documents/events_coal_20060525_nigeria.pdf.

Ministry of Mines and Steel Development (MMSD), (2010), Coal – Exploration and Power Generating Opportunities in Nigeria.

Moazzem, S., Rasul, M. G., & Khan, M. M. K., (2012), *A Review on Technologies for Reducing CO_2 Emission from Coal Fired Power Plants*, INTECH Open Access Publisher.

Monea, M. J., (2013), SASKPOWER CCS, Boundary Dam Carbon Capture Project, Carbon Capture & Storage Initiatives SaskPower 12W — 2025 Victoria Avenue Regina, SK Canada S4P 0S1, Retrieved from http://www.saskpowerccs.com/ccs-projects/boundary-dam-carbon-capture-project/7913%20CSS%20Factsheet-Boundary%20Dam-newtense.pdf.

Moretti, A.L. and Jones, C.S., (2012), *Advanced Emissions Control Technologies for Coal-Fired Power Plants*, BR 1886, Presented at Power-Gen Asia, Bangkok, Thailand, Pages 2 – 11.

Nigerian Electricity Regulatory Commission NERC, (2005), *Electric Power Sector Reform Act of 2005*, Published by The Federal Government Press, Lagos, Nigeria Retrieved from http://www.power.gov.ng/download/Electric%20Power%20Sector%20Reform%20Act%202005.pdf .

Nyakuma, B. B., (2015), *Physicochemical Characterization of Low Rank Nigerian Coals*, arXiv preprint arXiv:1506.02068.

Obaje, N. G. (2009), *Geology and Mineral Resources of Nigeria*, Springer Science & Business Media.

Odesola, I. F., Samuel, E., & Olugasa, T., (2013), Coal Development in Nigeria: Prospects and Challenges, *International Journal of Engineering and Applied Sciences*, Volume 4, No. 1, Pages 64-73.

Ogunsola, O. (2008), Personal Communication with Dr. Olubunmi Ogunsola, TEMEC. July. Data extracted from: http://www.methanetomarkets.org/coalmine/index.htm# profiles on 10th May, 2010.

Ogunsola, O. I., (1990), *History of Energy Sources and Their Utilization in Nigeria, Energy Sources 12*, Mechanical Engineering Department, Covenant University, Ota, Pages 181 – 198.

Parr, S. W., (1922), The Classification of Coal, *Industrial & Engineering Chemistry*, Volume 14, Issue 10, Pages 919-922.

Sourcewatch, (2016), Edwardsport Plant, Retrieved from http://www.sourcewatch.org/index.php/Edwardsport_Plant.

Subbarao, P. M. V., (2010), *Integrated Gasification Combined Cycles*, Lecture Notes, Mechanical Engineering Dept, Indian Institute of Technology Delhi, India.

Sichinga, J. and Buchanan, A., (2005), *Unlocking the Potential Wealth of Coal Introducing Sasol's Unique Coal-To-Liquids Technology*. Sasol Synfuels International (Pty) Ltd., Johannesburg.

Walter, K., 2007, *Fire in the hole,* Science & Technology, Lawrence Livermore National Laboratory, No. 4, Pages 12-18.

Watson, J. and Oldham, G., (1999): *International Perspectives on Clean Coal Technology Transfer to China*, First Report to the Working Group on Trade and Environment, CCICED, Pages 1 – 26.

World Coal Association (WCA), 2016, *Uses of Coal*, Retrieved 15-August-2016 from http://www.worldcoal.org/coal/uses-coal.

World Coal Institute, (2005), *The Coal Resource - A Comprehensive Overview of Coal*, World Coal Institute, Cambridge House, 180 Upper Richmond Road, Putney, London SW15 2SH, UK.Zhu, Q., (2015), *High-Efficiency Power Generation – Review of Alternative Systems*, IEA Clean Coal Centre, ISBN 978-92-9029-569-3.

IN SITU GENERATED DISPERSED SUBMICRON NI-CO-MO-BASED CATALYST FOR THE UPGRADING OF HEAVY CRUDE OIL

***Shuwa, S. M.[1], Al-Hajri, R.S.[2] and Jibril' B.Y.[1]**
[1]Department of Chemical Engineering, Ahmadu Bello University, Zaria, Nigeria
[2]Petroleum and Chemical Engineering Department, Sultan Qaboos University, Muscat, Oman
*: Corresponding author. Tel.: +234 8065400736. E-mail address:smshuwa@yahoo.com smshuwa@abu.edu.ng

ABSTRACT
A batch-reactor study for the upgrading of the heavy oil was conducted using an in-situ prepared, dispersed submicron trimetallic catalyst based on nickel, cobalt and molybdenum in the presence of hydrogen. Response surface methodology was used to design the experiments. The influence of reaction temperature, time and catalyst amount on the upgrading of the heavy oil was investigated. The results showed significant upgrading of the oil in terms of viscosity reduction (95%), API gravity increase (45%), sulfur removal (27wt %) and coke formed (0.05wt%) at temperature; 340^oC, time; 28hours, catalyst amount; 2500ppm. Reaction temperature proved to be the most influential with highest impact of all the reaction parameters investigated. Further characterization of liquid and gaseous products from selected experimental runs showed catalytic hydrocracking playing a significant role in the upgrading process. XRD and SEM-EDS analyses of solid recovered confirmed the in-situ generation of submicron catalyst based on nickel, cobalt and molybdenum.
***Keywords**: trimetallic catalyst, response surface methodology, viscosity reduction, sulfur removal, coke, hydrocracking*

1. INTRODUCTION

Unconventional hydrocarbon resources - heavy oil and bitumen - reserves account for over 70% of the total quantity of petroleum in the world (Herron 2000, Chen, He et al. 2010, Chao, Chen et al. 2012). Depleting reserves of conventional crude oil coupled with growing demands for high quality fuels and petrochemical feedstock led to more research in the area of exploration and exploitation of unconventional resources.

Thus, many enhanced oil recovery (EOR) techniques have been developed and adopted for exploiting heavy crudes (Al-Adasani and Bai , Gogarty 1983, Donaldson, Chilingarian et al. 1985, Green and Willhite 1998, S. Thomas 2001, Shah, Fishwick et al. 2010, Hart, Leeke et al. 2014). Catalysts have been used for decades in refineries to improve and extract the maximum value from each barrel of produced oil. The catalysts facilitate the conversion of some components of the oil to components that result in lower viscosity with high value. Based on this, in-situ catalytic upgrading and recovery of heavy crudes and bitumen has received considerable attention in recent times (Hashemi and Pereira-Almao 2011, Chao, Chen et al. 2012, Hashemi, Nassar et al. 2013, Hashemi, Nassar et al. 2013, Hashemi, Nassar et al. 2014). A series of chemical reactions such as, pyrolysis, hydrocracking, hydrotreating, aquathermolysis etc. is expected to take place within the porous media during the process (Weissman and Kessler 1996, Weissman, Kessler et al. 1996, Cavallaro, Galliano et al. 2005, Galarraga and Pereira-Almao 2010, Zamani, Maini et al. 2010, Shuwa, Al-Hajri et al. 2015). Near-well-bore catalytic upgrading has been demonstrated and shown to decrease sulphur content and increase API gravity (Weissman and Kessler 1996, Weissman, Kessler et al. 1996, Cavallaro, Galliano et al. 2005, Mohammad and Mamora 2008, Gallaraga 2011, Chao, Chen et al. 2012). Moore *et al* and Weissman *et al* were the first to propose the concept of in-situ catalytic upgrading of heavy oil during in-situ combustion(Weissman and Kessler 1996, Weissman, Kessler et al. 1996, Cavallaro, Galliano et al. 2005).

A number of researches have been conducted to investigate the performance of various catalysts in upgrading heavy crude oil and residua (Tian, Mohamed et al. 1998, Fan, Liu et al. 2001, Nares, Schacht-Hernandez et al. 2006, Wen, Zhao et al. 2007, Mohammad and Mamora 2008, Chen, Wang et al. 2009). In our previous study (Shuwa, Al-Hajri et al. 2015), we investigated the effect of dispersed catalysts based on molybdenum in upgrading the same heavy crude oil of Oman deposits. The batch-reactor study of the upgrading processes showed that the catalyst has the potentials to be used for in-situ upgrading and recovery of the heavy oil.

However, the low stability of the water-in-oil emulsion formed which was caused by the presence of the deep eutectic solvent and absence of surfactants, and the formation of solid precipitate of micronic scale are some of the drawbacks observed. Hence, the use of dispersed catalyst from stable water-in-oil emulsion may offer a better approach for upgrading the heavy oil. Very high levels of catalyst dispersion can be achieved by introducing finely divided powders, water-soluble or oil-soluble precursor compounds into the feed (Panariti, Del Bianco et al. 2000, Liu, Gao et al. 2009). In situ upgrading using dispersed catalysts of nanometric or sub-micronic scale is a promising alternatives from both economic and environmental perspectives (Galarraga and Pereira-Almao 2010, Almao 2012, Hashemi, Nassar et al. 2013). Such catalyst is expected to minimize the

formation damage problems caused by pore plugging in the reservoir (Zamani, Maini et al. 2010, Shokrlu and Babadagli 2011, Zamani, Maini et al. 2011, Shuwa, Jibril et al. 2015). Water-in-oil emulsion are particularly attractive reaction media for the preparation of solid catalyst particles of submicron dimension through a complex process (Eriksson, Nylén et al. 2004). They have been applied in producing catalysts based on transition metals for hydrogenation and hydrocracking reactions (Ng and Milad 2000, Thomson 2008, Galarraga and Pereira-Almao 2010). The formation of water-in-oil (w/o) emulsions is driven by strong hydrophilic interactions of the polar head of the surfactant (emulsifier) molecule (López-Quintela 2003, Capek 2004). Based on the foregoing, we found of interest to study the effect of dispersed catalysts in water-in-oil emulsion. Here we present results of the performance of a new trimetallic catalyst based on molybdenum, nickel and cobalt in upgrading heavy crude oil. The catalyst was prepared in-situ.

2. EXPERIMENTAL

2.1 Materials

Heavy crude oil sample from an Omani oilfield used for the upgrading experiments (properties given in Table 1). All chemicals were used without further treatment.

Table 1: Properties of the Heavy crude oil

Property	Value
Density (30^{o}C), g/cm3	0.9660
API gravity, ^{o}	14.31
Viscosity (30^{o}C), cP	3951
Sulfur, wt%	3.67
Asphaltenes, wt%	4.0

2.2 Preparation of catalytic emulsion

Prior to the upgrading experiment, water-in-oil emulsion was formulated by mixing the water phase containing the metal catalyst precursors with the organic phase containing the surfactants (Eriksson, Nylén et al. 2004, Nassar and Husein 2007, Husein, Patruyo et al. 2010). The water phase which contains the metal precursor solutions was prepared in order to get the final loading of the metals to satisfy the atomic ratio: Ni/(Ni + Co + Mo) = 0.3 and Mo/Co = 3 (Gallaraga, Scott et al. 2009). The water-in-oil emulsion was formulated by mixing the water phase containing the metal catalyst precursors with the organic phase containing the surfactants. The two surfactants polyethylene sorbitan monoleate (TWEEN 80^{TM}, HLB = 14) and sorbitan monoleate (SPAN 80, HLB = 4.5) were mixed in combination to give a surfactant with HLB of 8 (Galarraga and Pereira-Almao 2010). The mixing was conducted with ultrasound mixer at 40^{o}C for 30mins at a mixer speed of 4000rpm. Fig.1 shows the schematic representation of the process.

2.3 Upgrading Experiment

Upgrading experiments of the heavy crude oil was carried out using a 300mL capacity batch-type laboratory reactor (4560 series, Parr Instrument Company). The following constant reaction conditions were utilized: 40bar initial hydrogen pressure and 750rpm stirring speed. Detailed experimental method was reported elsewhere (Shuwa et al., 2015)

Response Surface Method (RSM) was used to design the experiments to study the impact of variables; reaction temperature, reaction time and catalysts amounts on viscosity reduction, API increase, sulfur reduction, hydrogen pressure reduction and coke formed from the upgrading experiments. The independent design variables and their levels are presented in Table S1 (supporting Information). Table S2 presents actual and coded levels of variables with corresponding values of all the responses evaluated. At the end of the reaction time, the reactor was cooled to room temperature. Samples of the reactor contents were taken and analyzed for GC, sulfur content, asphaltene content, coke, FTIR, XRD, SEM-EDS, viscosity, density and API gravity. Refer to Table S3 for the results of these measurements.

3. RESULTS AND DISCUSSION

3.1 Preliminary Investigation

Three experimental runs were conducted to investigate the performance of the catalysts in upgrading the heavy crude oil based on conditions as indicated in Table S3.

`

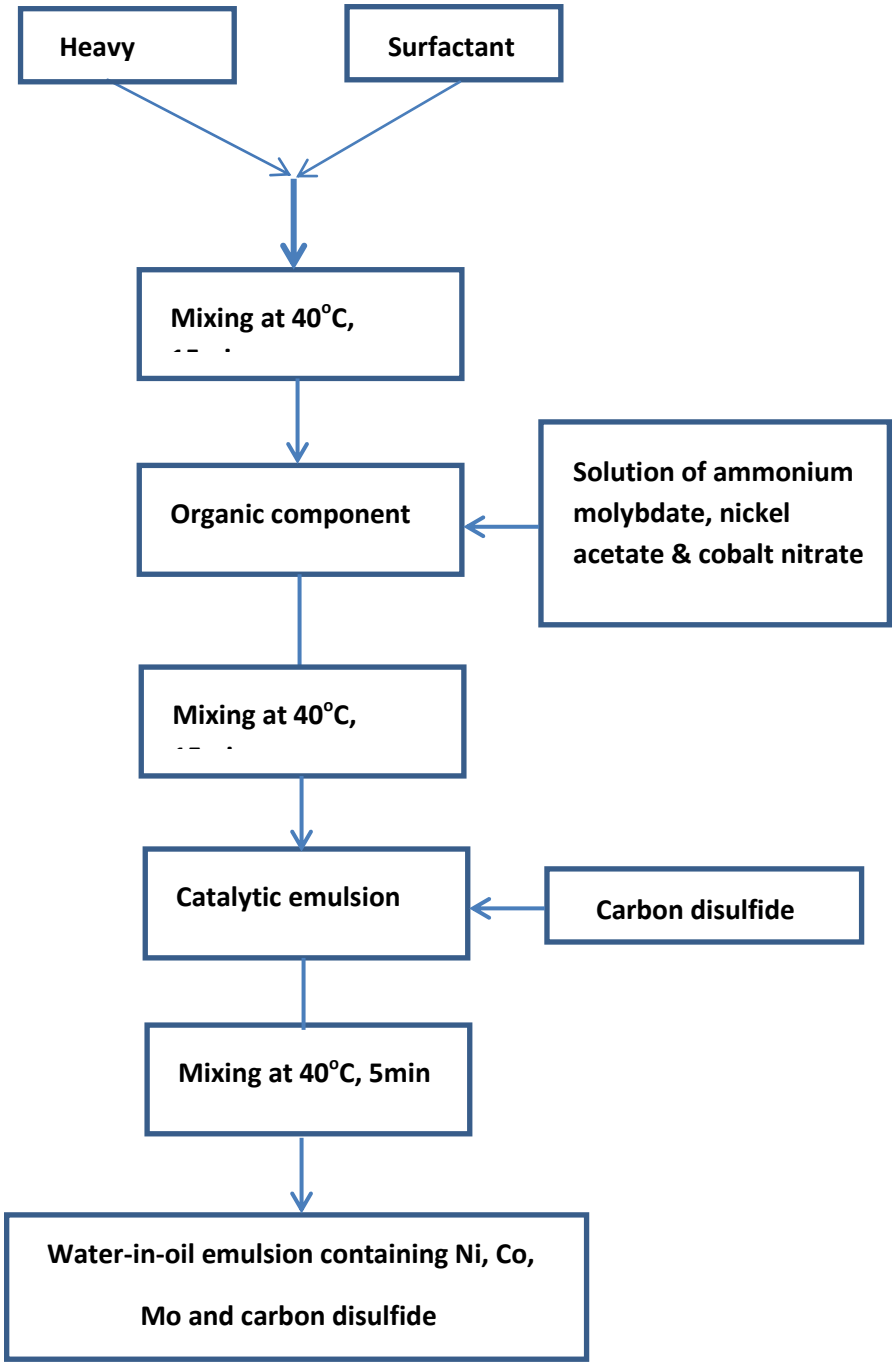

Fig.1: Schematic diagram for the preparation of the water-in-oil catalytic emulsion

The following conditions were kept constant during the runs: temperature of 300°C, initial hydrogen pressure of 40bar, reaction time of 24hours and catalyst amounts of 2000ppm (0.2wt%). About 29% reduction in viscosity was observed when only water was added to the oil after 24hours of reaction at 300^0C as shown in Fig.2 (in P1).

Further reduction to about 48% (as in P2) and 58% (in P3) was recorded when the surfactants and surfactants containing catalysts respectively were added to the oil sample. This shows the catalysts and surfactants are effective in reducing the viscosity of the heavy oil at the given conditions. Similar trend could be observed with API gravity increase for the three runs. catalyst's activity in desulfurizing the heavy crude oil samples. The catalyst proved to adding catalysts and surfactants to the oil (as in P3) led to further sulfur reduction (16% in P3) compared to when there was no catalysts (about 10% for both P1 and P2). This demonstrates its effectiveness in upgrading the oil by reducing viscosity and sulfur and increasing API gravity. Having established that the catalyst is effective in upgrading the

heavy crude oil, the runs were designed and implemented. The study evaluates the solid, liquid and gaseous products of the reaction in order to be able to assess the performance of the catalyst in upgrading the heavy crude oil. To achieve that, some selected runs (conditions given in Table 2) out of the total 17 runs (results given in Table S2 and S3 of supporting material) were selected and reported here to aid the discussion of result.

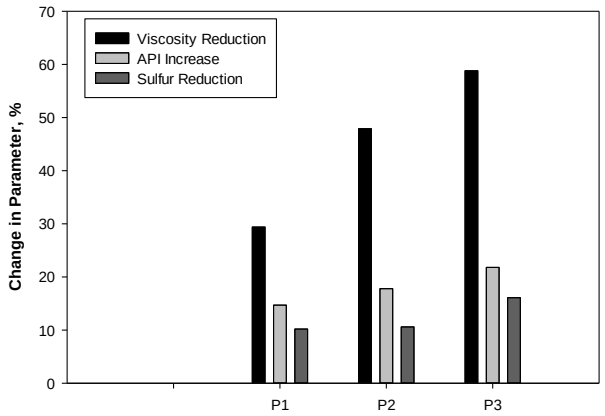

Fig. 2: Results from the preliminary runs; P1 = oil + H_2O, P2 = oil + H_2O + surfactant, P3 = oil + H_2O + surfactant + catalyst

Table 2: Operating conditions of four selected runs

Run number	Reaction temperature, ^oC	Reaction time, hours	Catalyst amounts, ppm
R10	340	28	2500
R11	340	28	500
R12	300	28	1500
R16	260	8	1500

3.2 physical properties of the heavy oil after reaction

Viscosity and API gravity are the two most important physical properties of heavy crudes; hence the heavy crude oil was analyzed to see changes in these properties after reaction. The results are shown in Table 3. Results of oil samples from other runs is shown in Table S3 (supporting material). The change in viscosity and API gravity was calculated according to the following equation:

$$\Delta M = \frac{Mo - M}{Mo} X\ 100\%$$

Where ΔM is the change in property [viscosity (mPas, 30^{o}C)] or API gravity (@ 15 ^{o}C)], Mo is the initial property (viscosity or API gravity), M is the property of the sample after reaction.

Table 3: viscosity and API gravity of reacted oil samples

Oil sample	Viscosity, cP	API gravity, ^{o}	Viscosity reduction, %	API gravity increase, %
Fresh oil	3951	14.31	NA	NA
R10	182	20.61	95.4	43.9
R11	194	20.5	95.1	43.3
R12	1768	17.5	55.3	22
R16	3695	16.1	6.5	12.6

The upgrading reaction achieved a viscosity reduction of over 95% at the maximum reaction temperature of 340^{o}C as shown in Table 3 for oils analyzed from runs R10 and R11. However, despite the difference in amounts of catalyst used between R10 and R11, there was no significant difference in viscosity reduction between the two runs. This shows that temperature plays a significant and influential role in reducing the viscosity of heavy crudes. The temperature effect is even more pronounced at high temperatures than the amounts of catalyst. A substantial reduction in viscosity of about 55% was also recorded at a moderate temperature of 300^{o}C. However, and insignificant reduction in viscosity (6.5%) was observed at 260^{o}C and 1500ppm of catalysts. This could be attributed to low operating conditions evidenced by the low temperature and reaction time. Furthermore, it could be as a result of inability of the catalyst to accelerate the chemical reactions that normally results into transformation of heavier components to lighter ones. The catalyst may not have been activated at that operating conditions since sulfiding of the precursor compounds and hydrocarbon decomposition normally take place at around 300^{o}C (Thomson 2008). Table 3 also evidences that API gravity increases with the operating temperature, an indication of progressive transformation of heavy crude oil to lighter oil. Both viscosity and API gravity showed similar trend. This does not mean that they are directly correlated as oils varying widely in viscosity may have similar API gravity. This is not surprising because different factors are involved in determining the values of viscosity and API gravity (Ancheyta, Rana et al. 2005, Hinkle, Shin et al. 2008).

3.3 Sulfur content of the heavy oil after reaction

The sulfur content and the percent desulfurization of the fresh and reacted heavy oil samples from five selected runs are given in Table 4.. Refer to Table S3 for the results of all runs with experimental error of measurements. The maximum desulfurization (among the four selected runs) of about 24wt% was recorded for sample obtained from run R10. Whereas oil sample recovered from run R11 achieved only 14.5wt% sulfur removal in spite of the fact that both runs were subjected to same operating conditions with an only difference in amounts of catalyst used. This shows that unlike in

viscosity and API gravity, the catalyst amount plays a significant role in reducing the sulfur contents of the reacted oil samples as demonstrated in the difference in desulfurization values between runs R10 and R11. Comparing sulfur contents of oil recovered from runs R12 and R16 shows the significance of reaction temperature and time to the desulfurization process. It could be possible that the 1.7wt% sulfur removal achieved was due to the effect of thermal processes. This can be explained with the fact that the aquathermolysis process (thermal effect in the presence of water) involves breaking of the weak C-S bond which results into sulfur reduction (Fan, Liu et al. 2001, Wen, Zhao et al. 2007, Chen, Wang et al. 2009, Maity, Ancheyta et al. 2010, Chao, Chen et al. 2012). The catalyst's desulfurization performance increases with temperature and time as shown by the reduction in hydrogen partial pressure after reaction (Table 4). Hydrogen is required for reactions to progress and its enhanced consumption indicates catalyst's activity. It is evident in Table 4 and Table S3 that hydrogen pressure reduces with reaction temperature whenever the catalyst was used. In other words hydrogen consumption increases with temperature in the presence of the catalyst. This can be linked to ability of the catalyst to make the hydrocarbons consumed more hydrogen at high temperature due to catalyst's high activity at such temperatures.

Table 4: Chemical Properties of oil samples obtained from selected runs

Run	Sulfur content, wt %	Desulfurization, %	Coke, wt %	Asphaltene content, wt%	Reduction in H_2 pressure, bar
Fresh oil	3.67	NA	NA	4.0	NA
R10	2.86	24.2	0.05	0.9	13
R11	3.14	14.5	0.15	1.6	10
R12	3.14	14.5	0.2	1.1	7
R16	3.60	1.7	0.49	2.9	3

3.4 Coke content of the heavy oil after reaction

The coke contents of the fresh heavy oil and reacted oil samples from the four selected runs are shown in Table 4. In in-situ upgrading processes for recovering heavy crudes, coke formation is not desired because of its capacity to deactivate the catalyst (Dehkissia, Larachi et al. 2004, Ortiz-Moreno, Ramírez et al. 2012) and block pores of reservoir matrix which is responsible for pore plugging that causes damage to the formation. Formation of coke after upgrading reactions also leads to reduction of yield of liquid products commonly desired in hydroprocessing operations (Speigth 1999, Ancheyta, Rana et al. 2005, Eom, Lee et al. 2014).

The highest amounts of coke were recorded for R16 while the least amount of coke formed was observed for run R10. The coke formed by run R16 is even higher than that formed by run P1 (0.42wt%, Table S3) which is a preliminary run (base run) conducted without catalyst at 300^{o}C for 24hours. Also, run R17 (Table S3) which was conducted at the same temperature with R16 but at a longer reaction time (28hours) and higher amounts of catalyst (2500ppm) recorded 0.44wt% coke, which is still lower than that of R16.

All this demonstrate that temperature, reaction time and catalyst amount play a significant role in determining the amounts of coke formed after reaction. It can be interpreted from the results that increasing all the three parameters within the range tested leads to effective reduction of coke after reactions. Similar trend was observed with the reduction in hydrogen pressure. The least the amount of coke formed, the higher the consumption of hydrogen. This clearly reveals that it is the increase in catalyst activity that leads to low amount of coke formed.

Since thermal and catalytic reactions are known to proceed via free radical chain reactions, a higher proportion of free radicals are expected to form, which subsequently lead to formation of higher amount of coke. However, when an effective catalyst coupled with high partial pressure of hydrogen are present, the free radicals will be stabilized and such reactions that lead to formation of coke suppressed. It is expected that catalytic thermal decomposition would result in less amount of coke because catalyst can create new pathways in the reaction schemes (Hashemi, Nassar et al. 2014).

3.5 FTIR and GC analyses of produced oil samples

FTIR spectra of liquid samples recovered from some selected few runs were acquired and presented in Fig.3. The transmission bands at 2925 and 2852cm-1 assigned to C-H stretching vibration (Pecsok, Shields et al. 1976, Chen, Wang et al. 2009, Chen, Yang et al. 2010, Chao, Chen et al. 2012) found in saturated hydrocarbons became much stronger after reactions (in R10, R11,R12 and R16) as demonstrated by the increase in intensity of their respective spectrum. Also, the absorption bands at 1460 and 1376cm^{-1} attributed to C-H bending vibrations (Pecsok, Shields et al. 1976, Chen, Wang et al. 2009) found in alkanes became stronger after reactions as shown in the spectra for all the runs compared to fresh oil sample.

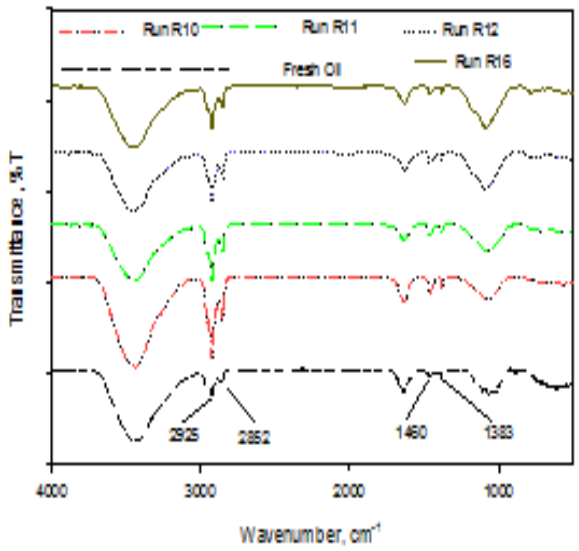

Fig. 3: FTIR Spectra of oil recovered from runs: fresh heavy oil, R10; 340°C, 28h, 2500ppm catalysts R11; 340°C, 28h, 500ppm catalyst, R12; 300°C, 28h, 2500ppm catalyst, R16; 260°C, 28h, 1500ppm

All these point to production of more saturates from the unsaturates presents in the initial fresh raw oil. This may be attributed to the conversion of unsaturated compounds in the other fractions of the oil such as resins and asphaltenes to saturates (Chen, Yang et al. 2010).

This was also confirmed by the reduction in asphaltene content of the oil after upgrading reactions as shown in Table 4. About 76% reduction in asphaltene content was observed for run R10 alone, which was conducted at 340°C, 2500ppm of catalyst for 24hours. Even run R12 which was conducted at a lower temperature compared to R10 achieved 73% reduction in asphaltenes content. However run R11 which was carried out at 40°C higher temperature than R12 but 2000ppm, lower catalyst amounts achieved only 60% reduction in asphaltene content. This shows how catalyst amounts plays a significant role in converting asphaltenes to other fractions of the oil. Just like sulfur and coke contents, asphaltene content has parallel behavior with temperature, catalyst concentration and reaction time.

The GC chromatograms of saturated hydrocarbons from these selected oil samples from the runs showed similar observations when compared with fresh heavy oil sample. There was increase in intensity of peaks of saturated hydrocarbons from the four selected runs when compared with that of fresh heavy oil. See the GC chromatograms of these oil samples as shown in Figs.S4 to S8 in supporting material document.

Table 5 presents the results of gases identified from selected four runs in terms of product distribution. Analysis of the gaseous products revealed the presence of C1-C6 hydrocarbons and substantial amounts of hydrogen sulfide in some of the runs analyzed. The amounts of CH_4 decreases with temperature and increase with amounts of catalysts as s shown in Table 5. Similar trend was observed for the desulfurization behavior of the oils from the selected runs as shown in the H_2S weight (Table 5). This shows that operating at high temperatures for longer reaction time with high amounts of catalysts (within the range tested) gives better upgrading conditions. Since the results of sulfur, coke, asphaltene and hydrogen consumption revealed that the catalyst is only active at high temperatures (300-340°C), it is logical to link the preferential generation of light hydrocarbon liquids to the high activity of the catalyst at such temperatures.

Table 5: Gaseous products distributions from selected runs after upgrading reactions

Identified gases	Weight %			
	Run R10	Run R11	Run R12	Run R16
CH_4	1.7	13.29	8.74	27.74
C_2H_4	7.67	9.63	8.34	13.47
H_2S	11.01	6.20	5.70	ND
C_3H_8	0.21	6.65	6.78	8.45
i-C_4H_8	ND	4.11	2.34	ND
n-C_4H_{10}	0.51	ND	1.21	0.53
i-C_5H_{10}	ND	ND	ND	4.69
n-C_5H_{12}	ND	60.11	ND	ND
n-C_6H_{14}	78.9	ND	66.89	45.13
Total	**100**	**100**	**100**	**100**

The presence of the catalyst at such temperatures enhances the hydrocracking reactions. This is expected in hydrocracking process as it leads to production of liquid distillate fractions at the expense of gaseous and solid products (Dehkissia, Larachi et al. 2004, Speight 2006).

3.6 Characteristics of solids recovered after reactions

XRD and SEM-EDS analyses were performed on recovered solids from some of the runs. The solids, a non-soluble filter cake from the filtration process, consist of the catalytic particles generated in situ and were characterized.

3.6.1 X-Ray diffraction

The XRD diffractograms of solids recovered from runs R10 and R12 are presented in Figs 4 and 5 respectively. The XRD patterns of the solids recovered from run R10, which was carried out at 240°C, 28hours with 2500ppm of catalyst indicated the presence of highly crystalline materials as demonstrated by the resolution and intensity of the peaks recorded. The peak at $2\Theta = 26.6$ is attributed to the presence of β-$NiMoO_4$ (Jeon, Na et al. 2011). This diffraction peak was found out in both samples (R10 &R12) an indication of low sulfidation state of the catalyst precursor compounds. This diffraction peak is more pronounced in solid from run R12 than R10, which can be attributed to the poor sulfidation behavior in R12 compared to R10 at low temperature. In addition to that ,the sulfidation state of

such compounds are found to be low and very sensitive to water (Fixari, Peureux et al. 1994). In spite of the presence of this peak, a diffraction pattern similar to that of molybdenite (MoS_2), an active form of molybdenum hydrocracking catalyst was observed. The diffraction peaks at 2Θ = 14, 33, 34 and 44 were observed in the XRD patterns of the solids from the two runs (R10 and R12) and are due to the presence of the active form of the catalyst (Fixari, Peureux et al. 1994, McFariane, Hawkins et al. 1998, Panariti, Del Bianco et al. 2000, Gallaraga 2011).

The XRD pattern of solids from run R10 showed a crystallize as sulfides with a pyrrhotite-like structure. These are characteristics of sulfides derived from other metals (Ni, Co ,Fe etc.) and generally form a three-dimensional pyrrhotite-like crystalline structure (Panariti, Del Bianco et al. 2000). This shows the formation of the sulfides of Ni and Co which were used as promoters in this work.

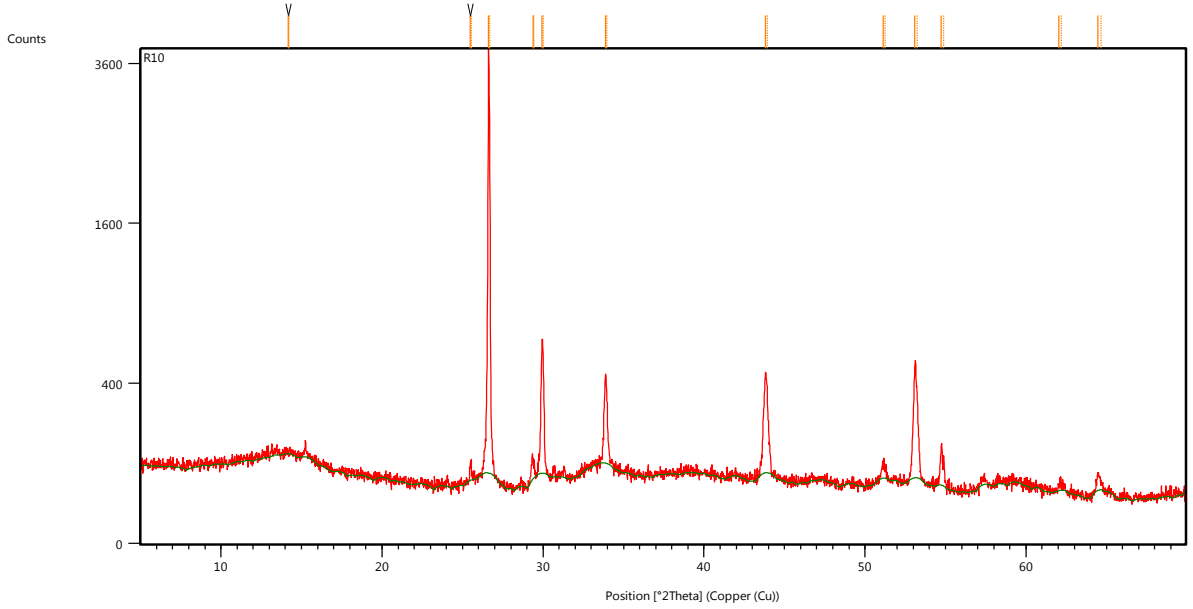

Fig.4: X-ray Diffractogram of solid recovered from run R10 at 340°C, 28h, 2500ppm catalyst

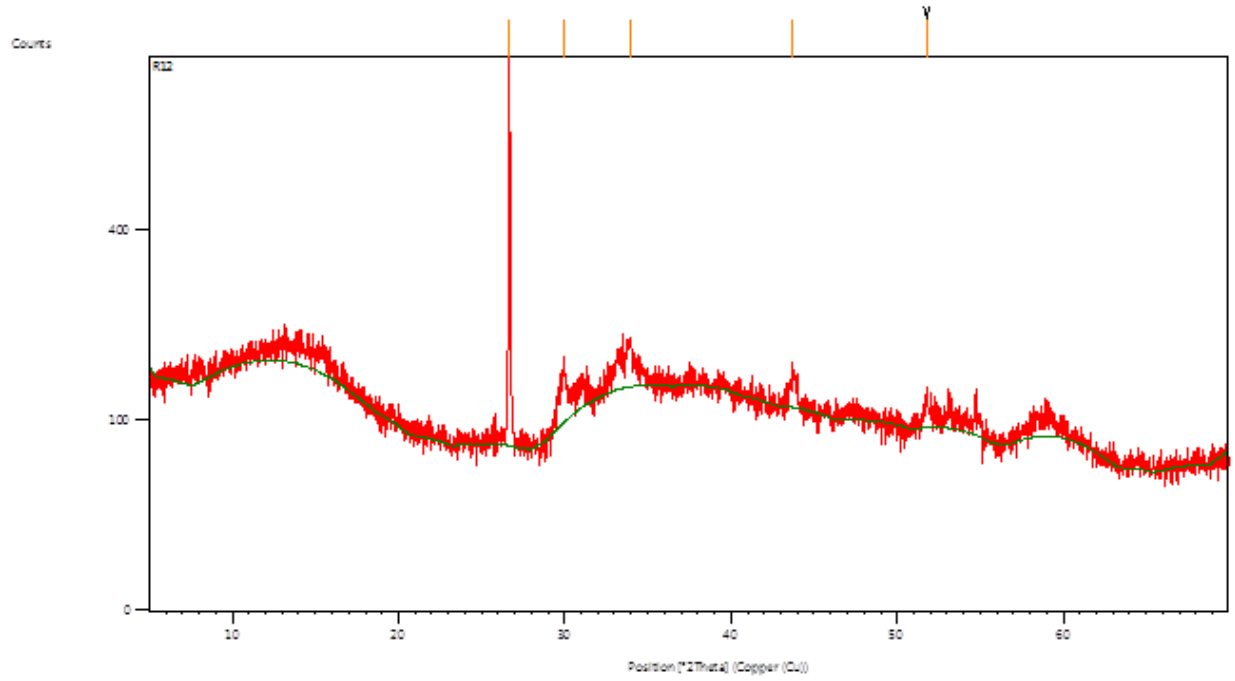

Fig.5: X-ray Diffractogram of solid recovered from run R12 at 300°C, 28h, 2500ppm catalyst

3.6.2 SEM-EDS analysis

Figs.6 and 7 show the SEM microphotographs of the solid recovered from runs R10 and R12 respectively. Two types of morphologies could be observed from the SEM images as shown in the figures; the needle-like type with the small particle size (approximately 240nm on the average as shown in Fig.6) and the near round particle with a both small and a bit larger particle size (1.43-2.6µm shown in Fig.6 and 7). EDS analysis of this near-round particles revealed they composed principally of the catalytic metals used. The main structure of similar molybdenum and nickel catalyst aggregates and agglomerates are reported to have similar morphologies (Thomson 2008, Hashemi, Nassar et al. 2014). In contrast to the sizes of the catalytic particles obtained in R10, an approximate particle size of 400nm was found for run R12 as shown in Fig.7. The difference between this run and run R10 is the reaction temperature; R10 was carried out at 340^{o}C whereas R12 was conducted at 300^{o}C. This shows that the higher the temperature the larger the size of the catalyst particles. Similar observation of increase in particle size with decomposition temperature was made by Wang (Wang 2004).

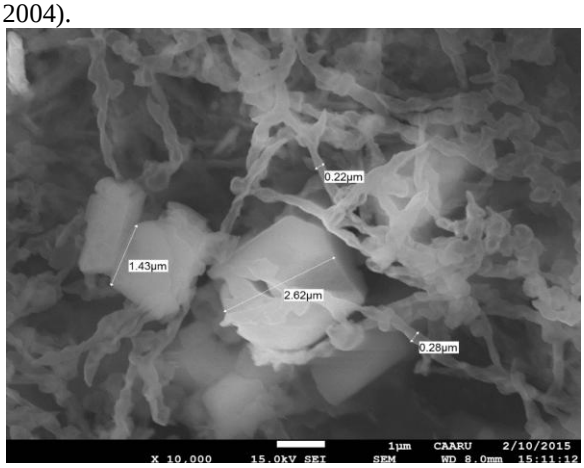

Fig.6: SEM image of filtered solid recovered from run R10 obtained at 340^{o}C, 2500ppm of catalyst for 28h

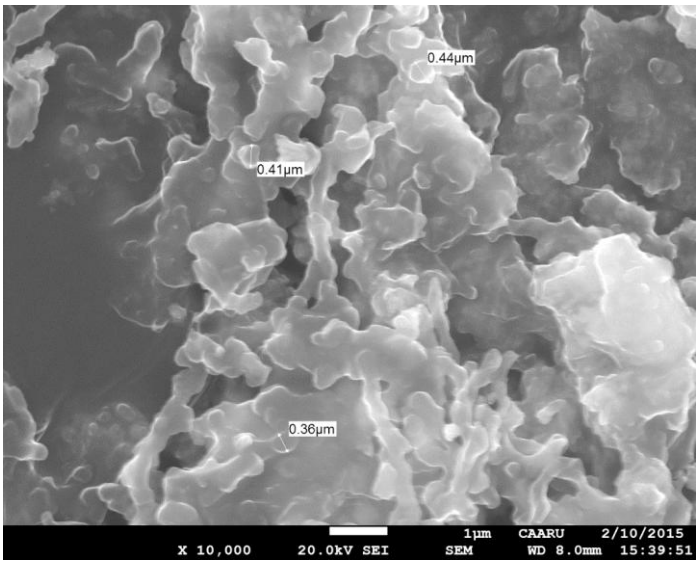

Fig.7: SEM image of filtered solid recovered from run R12 obtained at 300^{o}C, 2500ppm, 28h

Figs.8 and 9 show the EDS spectra and the quantification results of the elemental analysis of the two runs (R10 and R12). The results of the EDS analysis were presented on right hand side of the figures while SEM images of the zones used for the EDS were presented on the left hand side. The EDS analysis in Fig.8 was for spectrum 2 and spectrum 15 was chosen in Fig.9 as shown in SEM images in the figures.

The samples in the selected spectra 2 and 15 are composed mainly of O, Mo, S, Ni, Co and N as shown in the EDS elemental result. This is expected as the oil originally composed of heteroatoms in form O, N and S while Mo, Ni and Co from the catalyst particles used. Considering the three metals used for the formulation of the catalysts, Ni, Co and Mo, their amounts in the selected spectrum 2 were 11, 4.5 and 28.1%wt respectively. The equivalent amounts in atomic percent as shown in Table 6 is 5.3, 2.2 and 8.3% for Ni, Co and Mo respectively.

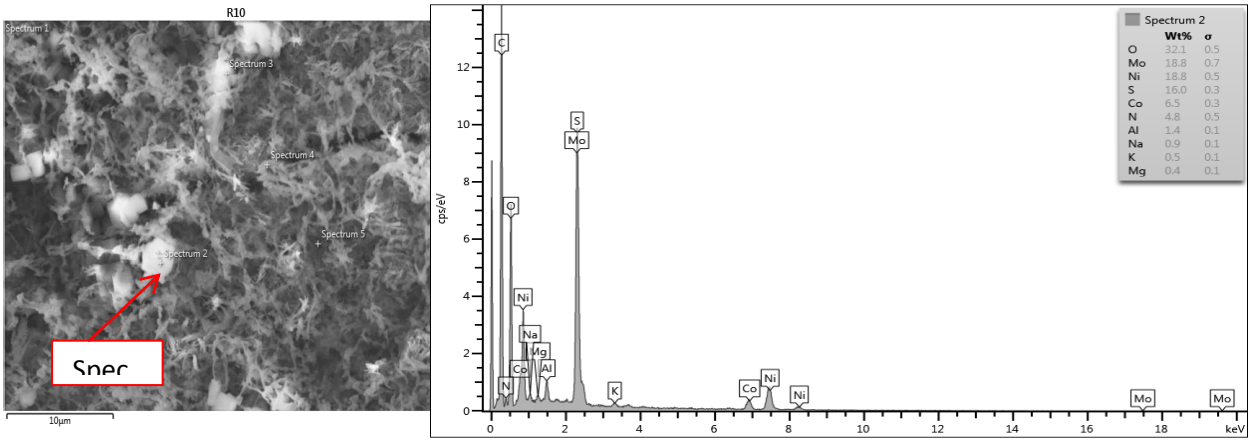

Fig.8: SEM image, EDS spectra and elemental result of solid recovered from run R10

This is close to the quantities introduced in to the reaction media. The ratio of Ni to the total metals [Ni/(Ni+Co+Mo)] or Ni/Me introduced to the reaction media through the catalytic emulsion was 0.3 and a value of 0.33 was found from the elemental analysis of the recovered solid

The ratio Mo/Co was 3 as introduced into the reaction media and a ratio of 3.77 was found from the elemental analysis. Contrary to that, there is a deviation in quantities of the metals introduced with the EDS elemental quantification results for solids recovered from R12 as shown in Table 6. This could be attributed to inhomogeneous distribution of the catalyst particles in the solids after the reaction

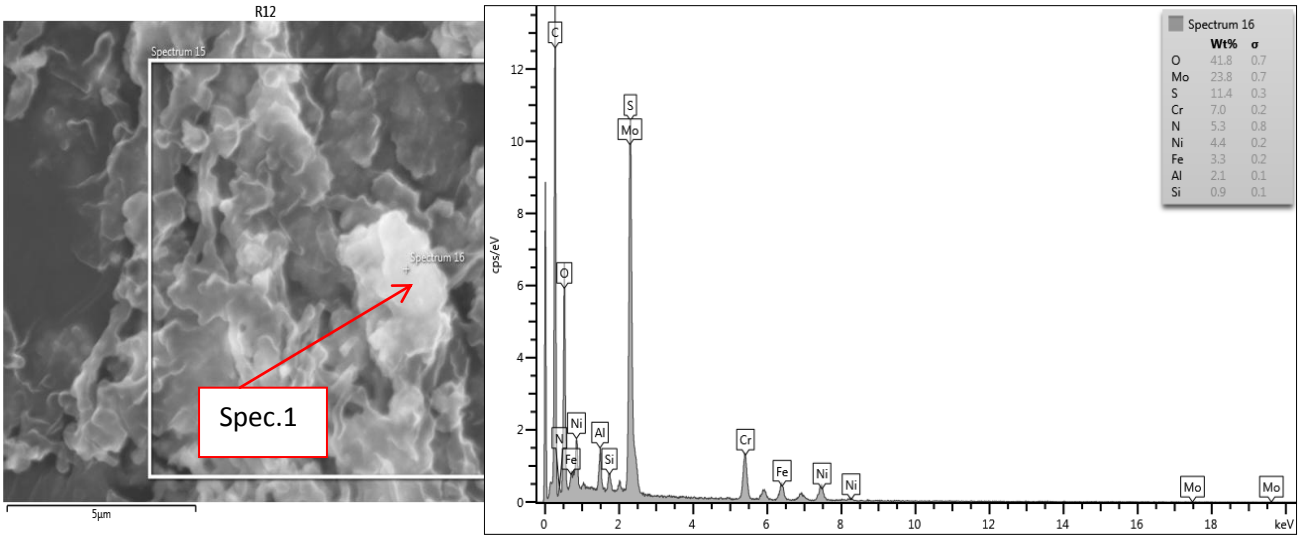

Fig.9: SEM image, EDS spectra and elemental result of solid recovered from run R12

Table 6: Chemical composition results of selected spots of solids recovered from runs R10 and R12

Element	Spectrum 2, R10		Spectrum 15, R12	
	Weight %	Atomic %	Weight %	Atomic %
Mo	28.1	8.3	32.3	9.3
Ni	11.0	5.3	5.6	2.7
Co	4.5	2.2	3.8	2.1
O	32.1	56.9	31.1	53.9
S	16.0	14.2	15.0	13.0
N	4.8	9.7	7.6	15.1
Al	1.4	1.5	1.7	1.8
Na	0.9	1.1	1.0	1.2
K	0.5	0.4	1.8(Fe)	0.9
Mg	0.4	0.4	ND	_
Ni/Me		0.33		0.19
Mo/Co		3.77		4.42

4. CONCLUSION

Preliminary evaluation showed the catalyst to be very effective in upgrading the heavy crude oil. Results showed that the catalyst can be used in upgrading the heavy crude oil as significant improvement in qualities of the oil after reaction was achieved. After analyzing the results from the heavy crude oil upgrading reactions in the presence of the catalyst at varying operating conditions, the following specific conclusions can be drawn:

1. While the presence of the catalyst appeared to have improved on API gravity and viscosity of the heavy oil after reaction based on preliminary investigation conducted; however, there was no significant change in these properties when the catalyst amount was varied from 500 to 2500ppm.
2. Varying the catalyst concentration from 500 to 2500ppm showed to have significant impact on the sulfur, asphaltenes and coke contents of the heavy oil after reaction. This indicates that the catalyst

have impacted more on the chemical properties of the heavy oil than on physical properties.

3. Sulfur, asphaltene and coke contents of the heavy oil after reaction have parallel behavior with temperature. In other words, raising temperature led to a significant reduction in the quantities.
4. XRD and SEM-EDS analyses of the recovered solids from some of the runs after reaction confirmed the in-situ formation of the dispersed submicron catalytic particles based on Nickel, cobalt and molybdenum.

ACKNOWLEDGEMENTS

The authors would like to thank The Research Council of Oman for providing financial support to this work through the research grant; RC/ENG/PCED/11/01. The authors are also grateful to Sultan Qaboos University Oman and Ahmadu Bello University Zaria, Nigeria for allowing the use of their facilities and other supports offered.

REFERENCES

Al-Adasani, A. and B. Bai *Recent Developments and Updated Screening Criteria of Enhanced Oil Recovery Techniques, Society of Petroleum Engineers.*

Almao, P. P. (2012). "In situ upgrading of bitumen and heavy oils via nanocatalysis." *The Canadian Journal of Chemical Engineering* **90**(2): 320-329.

Ancheyta, J., M. S. Rana and E. Furimsky (2005). "Hydroprocessing of heavy petroleum feeds: Tutorial." *Catalysis Today* **109**(1–4): 3-15.

Capek, I. (2004). "Preparation of metal nanoparticles in water-in-oil (w/o) microemulsions." *Advances in Colloid and Interface Science* **110**(1–2): 49-74.

Cavallaro, A. N., G. R. Galliano, R. G. Moore, S. A. Mehta, M. G. Ursenbach, E. Zalewski and P. Pereira (2005). In Situ Upgrading of Llancanelo Heavy Oil Using In Situ Combustion and a Downhole Catalyst Bed. *Canadian International Petroleum Conference, Calgary, Petroleum Society; Canadian Institute of Mining, Mettalurgy & Petroleum.*

Chao, K., Y. Chen, J. Li, X. Zhang and B. Dong (2012). "Upgrading and visbreaking of super-heavy oil by catalytic aquathermolysis with aromatic sulfonic copper." *Fuel Processing Technology* **104**(0): 174-180.

Chao, K., Y. Chen, H. Liu and J. L. X Zhang (2012). "Laboratory Experiments and Field Test of a Difunctional Catalyst for Catalytic Aquathermolysis of Heavy Oil." *Energy & Fuels* **26**: 1152-1159.

Chen, Y., J. He, Y. Wang and P. Li (2010). "GC-MS used in study on the mechanism of the viscosity reduction of heavy oil through aquathermolysis catalyzed by aromatic sulfonic H3PMo12O40." *Energy* **35**(8): 3454-3460.

Chen, Y., Y. Wang, J. Lu and C. Wu (2009). "The Viscosity Reduction of Nano-Keggin-K3PMoO40 in Catalytic Aquathermolysis of Heavy Oil." *Fuel* **88**: 1426-1434.

Chen, Y., Y. Wang, J. Lu and C. Wu (2009). "The Viscosity Reduction of Nano-Keggin-K3PMoO40 in Catalytic Aquathermolysis of Heavy Oil." *Fuel* 88: 1426-1434.

Chen, Y., Y. Wang and J. Lu, Wu, Chuan (2009). "The Viscosity Reduction of Nano-Keggin-K3PMoO40 in Catalytic Aquathermolysis of Heavy Oil." *Fuel* 88: 1426-1434.

Chen, Y., C. Yang and Y. Wang (2010). "Gemini Catalyst for Catalytic Aquathermolysis of Heavy Oil." *Journal of Analytical and Applied Pyrolysis* **89**: 159-165.

Dehkissia, S. n., F. ç. Larachi and E. Chornet (2004). "Catalytic (Mo) upgrading of Athabasca bitumen vacuum bottoms via two-step hydrocracking and enhancement of Mo–heavy oil interaction." *Fuel* **83**(10): 1323-1331.

Donaldson, E. C., G. V. Chilingarian and T. F. Yen (1985). *enhanced oil recovery, I fundamentals and analyses. Amsterdam, Elsevier*.

Eom, H.-J., D.-W. Lee, S. Kim, S.-H. Chung, Y. G. Hur and K.-Y. Lee (2014). "Hydrocracking of extra-heavy oil using Cs-exchanged phosphotungstic acid (CsxH3−xPW12O40, x = 1–3) catalysts." *Fuel* **126**(0): 263-270.

Eriksson, S., U. Nylén, S. Rojas and M. Boutonnet (2004). "Preparation of catalysts from microemulsions and their applications in heterogeneous catalysis." *Applied Catalysis A: Genera*l **265**(2): 207-219.

Fan, H., Y.-J. Liu and L.-G. Zhong (2001). "Studies on the Synergetic Effects of Minerals and Steam on the Composition Changes of Heavy Oils." *Energy & Fuels* 15: 1475-1479.

Fan, H., Y. Liu and L. Zhong (2001). "Studies on the Synergetic Effects of Minerals and Steam on the Composition Changes of Heavy Oils." *Energy & Fuels* **15**: 1475-1479.

Fixari, B., S. Peureux, J. Elmouchnino, P. Le Perchec, M. Vrinat and F. Morel (1994). "New Developments in Deep Hydroconversion of Heavy Oil Residues with Dispersed Catalysts. 1. Effect of Metals and Experimental Conditions." *Energy & Fuels* **8**(3): 588-592.

Galarraga, C. E. and P. Pereira-Almao (2010). "Hydrocracking of Athabasca Bitumen Using Submicronic Multimetallic Catalysts at Near In-Reservoir Conditions." *Energy & Fuels* **24**(4): 2383-2389.

Gallaraga, C., E., C. E. Scott and P. Pereira-Almao (2009). Hydrocracking of Athabasca bitumen using ultradispersed Ni-W-Mo catalysts. *World Congress on Chemical Engineering, Montreal.*

Gallaraga, C. E. (2011). Upgrading Athabasca Bitumen using Submicronic NiWMo Catalysts at Conditions near to In-reservoir Operation. *PhD PhD Dissertation, University of Calgary.*

Gogarty, W. B. (1983). "Enhanced Oil Recovery Through the Use of Chemicals." *Journal of Petroleum Technology* ***Distinguished Author Series****:* 1581-1590.

Green, D. W. and G. P. Willhite (1998). E*nhanced Oil Recovery*. Texas, SPE International.

Hart, A., G. Leeke, M. Greaves and J. Wood (2014). "Down-hole heavy crude oil upgrading by CAPRI: Effect of hydrogen and methane gases upon upgrading and coke formation." *Fuel* **119**(0): 226-235.

Hashemi, R., N. N. Nassar and P. Pereira Almao (2013). "Enhanced Heavy Oil Recovery by in Situ Prepared Ultradispersed Multimetallic Nanoparticles: A Study of Hot Fluid Flooding for Athabasca Bitumen Recovery." *Energy & Fuels* **27**(4): 2194-2201.

Hashemi, R., N. N. Nassar and P. Pereira Almao (2013). "In Situ Upgrading of Athabasca Bitumen Using Multimetallic Ultradispersed Nanocatalysts in an Oil Sands Packed-Bed Column: Part 1. Produced Liquid Quality Enhancement." *Energy & Fuels* **28**(2): 1338-1350.

Hashemi, R., N. N. Nassar and P. Pereira Almao (2014). "In Situ Upgrading of Athabasca Bitumen Using Multimetallic Ultradispersed Nanocatalysts in an Oil Sands Packed-Bed Column: Part 2. Solid Analysis and Gaseous Product Distribution." *Energy & Fuels* **28**(2): 1351-1361.

Hashemi, R. and P. Pereira-Almao (2011). Experimental Study of Simultaneous Athabasca Bitumen Recovery and Upgrading Using Ultradispersed Catalysts Injection. *Canadian Unconventional Resources Conference. Calgary, Alberta, Canada. 15-17 November, Society of Petroleum Engineers.*

Herron, H. E. (2000). "Heavy Oil: A Solution to Dwindling Domestic Oil Supplies." Retrieved 21st December, 2014, from http://www.petroleumequities.com/HeavyOilReport.htm .

Hinkle, A., E.-J. Shin, M. W. Liberatore, A. M. Herring and M. Batzle (2008). "Correlating the chemical and physical properties of a set of heavy oils from around the world." *Fuel* **87**(13–14): 3065-3070.

Husein, M. M., L. Patruyo, P. Pereira-Almao and N. N. Nassar (2010). "Scavenging H2S(g) from oil phases by means of ultradispersed sorbents." *Journal of Colloid and Interface Science* **342**(2): 253-260.

Jeon, S. G., J.-G. Na, C. H. Ko, K. B. Lee, N. S. Rho and S. B. Park (2011). "A new approach for preparation of oil-soluble bimetallic dispersed catalyst from layered ammonium nickel molybdate." *Materials Science and Engineering:* B **176**(7): 606-610.

Liu, Y., L. Gao, L. Wen and B. Zong (2009). "Recent Advances in Heavy Oil Hydroprocessing Technologies." *Recent Patents on Chemical Engineering* 2: 22-36.

López-Quintela, M. A. (2003). "Synthesis of nanomaterials in microemulsions: formation mechanisms and growth control." *Current Opinion in Colloid & Interface Science* **8**(2): 137-144.

Maity, S. K., J. Ancheyta and G. Marroquin (2010). "Catalytic Aquathermolysis Used for Viscosity Reduction of Heavy Crude Oils: A Review." *Energy & Fuels* 24: 2809-2816.

McFariane, R. R., R. W. T. Hawkins and T. Cyr (1998) "*DISPERSION AND ACTIVITY OF INORGANIC CATALYST PRECURSOR IN HEAVY OIL* ", 496-500.

Mohammad, A. A. and D. D. Mamora (2008). In Situ Upgrading of Heavy Oil Under Steam Injection with Tetralin and Catalyst. *SPE International Thermal Operations and Heavy Oil Symposium, Calgary, SPE International.*

Nares, H. R., P. Schacht-Hernandez, M. C. Cabrera-Reyes, M. Ramirez-Garnica and O. Cazarez-Candia (2006). Upgrading of Heavy Crude Oil with Supported and Unsupported Transition Metals. *Canadian International Petroleum Conference (57th Annual Technical Meeting), Calgary, Petroleum Society.*

Nassar, N. N. and M. M. Husein (2007). "Effect of microemulsion variables on copper oxide nanoparticle uptake by AOT microemulsions." *Journal of Colloid and Interface Science* **316**(2): 442-450.

Ng, F. T. T. and I. K. Milad (2000). "Catalytic desulphurization of benzothiophene in an emulsion via in situ generated H2." *Applied Catalysis A: General* **200**(1–2): 243-254.

Ortiz-Moreno, H., J. Ramírez, R. Cuevas, G. Marroquín and J. Ancheyta (2012). "Heavy oil upgrading at moderate pressure using dispersed catalysts: Effects of temperature, pressure and catalytic precursor." *Fuel* **100**(0): 186-192.

Panariti, N., A. Del Bianco, G. Del Piero and M. Marchionna (2000). "Petroleum Residue Upgrading with Dispersed Catalysts Part 1. Catalysts Activity and Selectivity." *Applied Catalysis A: General* 204: 203-213.

Panariti, N., A. Del Bianco, G. Del Piero and M. Marchionna (2000). "Petroleum residue upgrading with dispersed catalysts: Part 1. Catalysts activity and selectivity." *Applied Catalysis A: General* **204**(2): 203-213.

Pecsok, R. L., D. L. Shields, T. Cains and I. G. McWilliam (1976). *Modern Method of Chemical Analysis*. New York, United States of America, John Wiley & Sons.

S. Thomas, S. M. F. A. (2001). "Micellar Flooding and ASP—Chemical Methods for Enhanced Oil Recovery." *Journal of Canadian Petroleum Technology*, Volume 40, No. 2: 46-47.

Shah, A., R. Fishwick, J. Wood, G. Leeke, S. Rigby and M. Greaves (2010). "A review of novel techniques for heavy oil and bitumen extraction and upgrading." *Energy & Environmental Science* **3**(6): 700-714.

Shokrlu, Y. H. and T. Babadagli (2011). Transportation and Interaction of Nano and Micro Size Metal Particles Injected to Improve Thermal Recovery of Heavy-Oil. *SPE Annual Technical Conference and Exhibition. Denver, Colarado, USA*, 30 October- 2 November 2011, Society of Petroleum Engineers.

Shuwa, S., B. Jibril, Y. Al-Wahaibi and R. Al-Hajri (2015). "Heavy-Oil-Recovery Enhancement With Choline Chloride/Ethylene Glycol-Based Deep Eutectic Solvent." *SPE Journal* **20**(01).

Shuwa, S. M., R. S. Al-Hajri, B. Y. Jibril and Y. M. Al-Waheibi (2015). "Novel Deep Eutectic Solvent-Dissolved Molybdenum Oxide Catalyst for the Upgrading of Heavy Crude Oil." *Industrial & Engineering Chemistry Research* **54**(14): 3589-3601.

Speight, J. G. (2006). *The Chemistry and Technology of Petroleum*, Fourth Edition. New York, CRC Press.

Speigth, J. G. (1999). *Refining Heavy Feedstocks The Chemistry and Technology of Petroleum*
New York, CRC Press.

Thomson, J. (2008). The synthesis and evaluation of molybdenum-based ultra-dispersed hydroprocessing catalysts. *MSc MSc Thesis, University of Calgary*.

Tian, K. P., A. R. Mohamed and S. Bhatia (1998). "Catalytic Upgrading of Petroleum Residua Oil by Hydrotreating Catalysts: A Comparison Between Dispersed and Supported Catalystsl." *Fuel* 77: 1221-1227.

Wang, J. (2004). Synthesis and Characterization of Submicron Molybdenum Catalyst Particles Obtained from Water/Oil Emulsions for Heavy Oil Upgrading. *MSc, University of Calgary.*

Weissman, J. G. and R. V. Kessler (1996). "DownHole Heavy Crude Oil Hydroprocessing." *Applied Catalysis A: General* 140: 1-16.

Weissman, J. G. and R. V. Kessler (1996). "DownHole Heavy Crude Oil Hydroprocessing." A*pplied Catalysis A: General* **140**: 1-16.

Weissman, J. G., R. V. Kessler and R. A. Sawicki (1996). "Down-Hole Catalytic Upgrading of Heavy Crude Oil." *Energy & Fuels* 10: 883-889.

Weissman, J. G., R. V. Kessler, R. A. Sawicki, J. D. M. Belgrave, C. J. Laureshen, S. A. Mehta, R. G. More and M. G. Ursenbach (1996). "Down-Hole Catalytic Upgrading of Heavy Crude Oil." *Energy & Fuels* **10**: 883-889.

Wen, S., Y. Zhao, Y. Liu and S. Hu (2007). A Study on Catalytic Aquathermolysis of Heavy Crude Oil During Steam Stimulation. *SPE International Symposium on Oilfield Chemistry, Houston-Texas*, SPE International.

Zamani, A., B. Maini and P. Pereira-Almao (2010). "Experimental Study on Transport of Ultra-Dispersed Catalyst Particles in Porous Media." *Energy & Fuels* **24**(9): 4980-4988.

Zamani, A., B. B. Maini and P. Pereira-Almao (2011). Propagation of Nanocatalyst Particles Through Athabasca Sands. *Canadian Unconventional Resources Conference. Calgary, Alberta, Canada*, 15-17 November 2011, Society of Petroleum Engineers.

SUPLEMENTARY DATA

Table S1: Amounts and levels of the experimental independent design variables

Variable	Unit	lower level (-1)	center point (0)	higher level (+1)
Reaction temperature(X1)	^{0}C	260	300	340
Catalyst amounts (X2)	ppm	500	1500	2500
Reaction time (X3)	hour	8	28	48

Table S2: Coded and actual levels of variables and corresponding responses

Run	Coded levels of variables			Actual levels of variables			Responses				
	X1	X2	X3	X1	X2	X3	Viscosity, cP	Sulfur, wt%	API incr.	H_2 P,bar	coke, %wt
1	0	0	0	300	1500	28	1798	14.1	19.2	7	0.22
2	1	0	1	340	1500	48	272	27	38.6	12	0.12
3	0	-1	-1	300	500	8	3212	8.5	17	3	0.33
4	0	1	-1	300	2500	8	2510	11.2	19.4	4	0.39
5	-1	0	1	260	1500	48	4545	6.2	6.2	5	0.41
6	0	0	0	300	1500	28	1765	13.7	22	6	0.21
7	-1	1	0	260	2500	28	4285	6.9	14.2	5	0.49
8	0	0	0	300	1500	28	1828	14	18.9	6	0.21
9	0	1	1	300	2500	48	2208	10.3	17.8	8	0.18
10	1	1	0	340	2500	28	182	24.2	43.9	13	0.05
11	1	-1	0	340	500	28	194	14.5	43.3	10	0.15
12	0	0	0	300	1500	28	1768	14.5	22	7	0.20
13	1	0	-1	340	1500	8	852	13.1	26.2	5	0.11
14	0	0	0	300	1500	28	1768	13.7	22	6	0.24
15	0	-1	1	300	500	48	1424	10.5	23.1	7	0.28
16	-1	0	-1	260	1500	8	3695	1.7	12.6	3	0.49
17	-1	-1	0	260	500	28	3992	1.9	4.8	3	0.44

Table S3: Results with experimental errors for all the 20runs conducted

Run No.	Density, g/cm3	Viscosity, cP	API Gravity, $^\circ$	Sulfur, wt%	Coke, wt%	H_2 P red., bar
Fresh Oil	0.9591 ± 0.003	3951 ± 3	14.32 ± 0.01	3.67 ± 0.124	-	-
P1	0.9459 ± 0.00005	2790 ± 10	16.42 ± 0.02	3.30 ± 0.005	0.42	2
P2	0.9432 ± 0.00006	2060 ± 0	16.87 ± 0.003	3.28 ± 0.002	0.41	2
P3	0.9394 ± 0.0004	1628 ± 5	17.44 ± 6x10^{-4}	3.08 ± 0.006	0.19	7
R1	0.9419 ± 0	1798 ± 5	17.07 ± 0	3.16 ± 0.02	0.22	7
R2	0.9240 ± 0.0005	272 ± 3	19.85 ± 0.07	2.67 ± 0.009	0.12	12
R3	0.9438 ± 0.0002	3212 ± 3	16.76 ± 0.02	3.36 ± 0.02	0.33	3
R4	0.9418± 0.00008	2510 ± 5	17.1 ± 0.06	3.26 ± 0.03	0.39	4
R5	0.9540 ± 0.0002	4545 ± 6	16.49 ± 0.003	3.45 ± 0.02	0.41	5
R6	0.9391 ± 0.0008	1765 ± 5	17.47 ± 0.09	3.17 ± 0.04	0.21	6
R7	0.9462 ± 0.001	4285 ± 5	16.36 ± 0.1	3.42 ± 0.03	0.49	5
R8	0.9420 ± 0.0009	1828 ± 8	17.02 ± 0.09	3.13 ± 0.008	0.21	6
R9	0.9437 ± 0.0004	2208 ± 3	16.87 ± 0.2	3.29 ± 0.009	0.18	8
R10	0.9189 ± 0.0003	182 ± 3	20.61 ± 0.007	2.86 ± 0.02	0.05	13
R11	0.9196 ± 0.001	194 ± 2	20.52 ± 0.1	3.14 ± 0.02	0.15	10
R12	0.9391 ± 0.0004	1768 ± 3	17.47 ± 0.09	3.14 ± 0.04	0.20	7
R13	0.9353 ± 0.003	852 ± 3	18.07 ± 0.5	3.19 ± 0.02	0.11	5
R14	0.9391 ± 0.0008	1768 ± 3	17.47 ± 0.09	3.17 ± 0.04	0.24	6
R15	0.9378 ± 0.0002	1424 ± 7	17.63 ± 0.05	3.29 ± 0.03	0.28	7
R16	0.9481 ± 0	3695 ± 4	16.13 ± 0.06	3.60 ± 0.1	0.49	3
R17	0.9515 ± 0	3992 ± 8	15.01 ± 0.2	3.61 ± 0.1	0.44	3

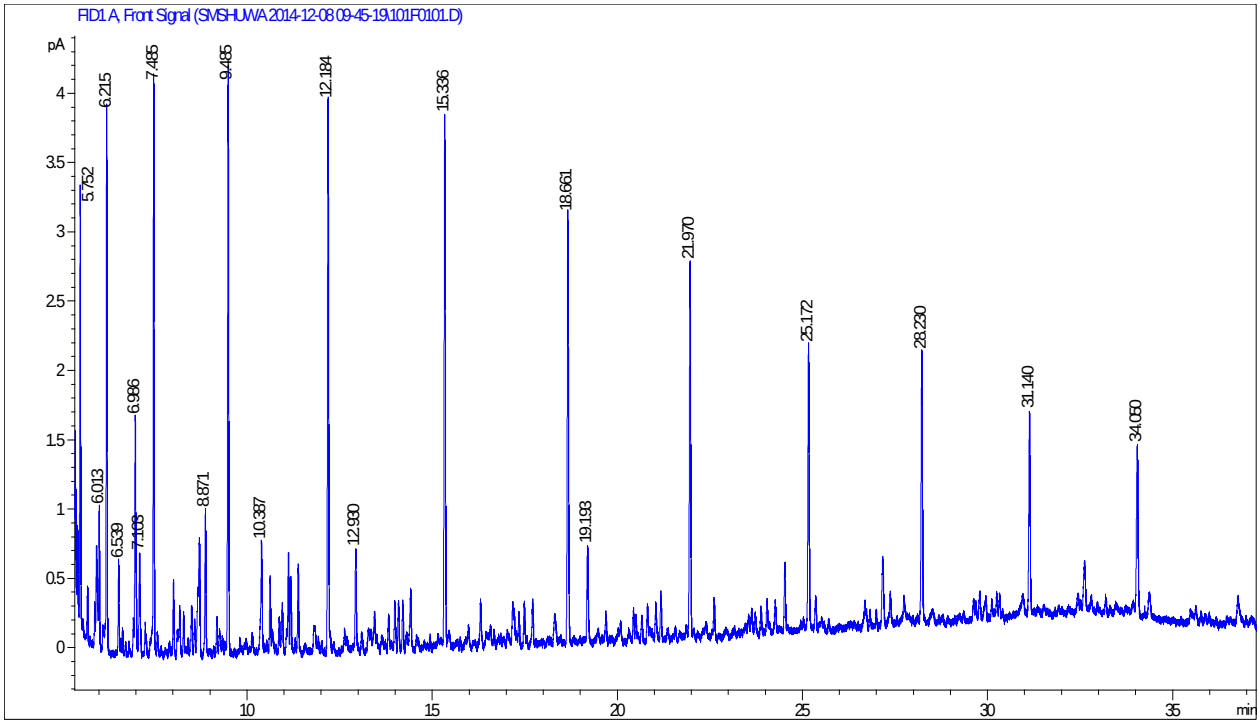

Figure S4: GC chromatogram of oil fresh Amal West heavy crude oil sample

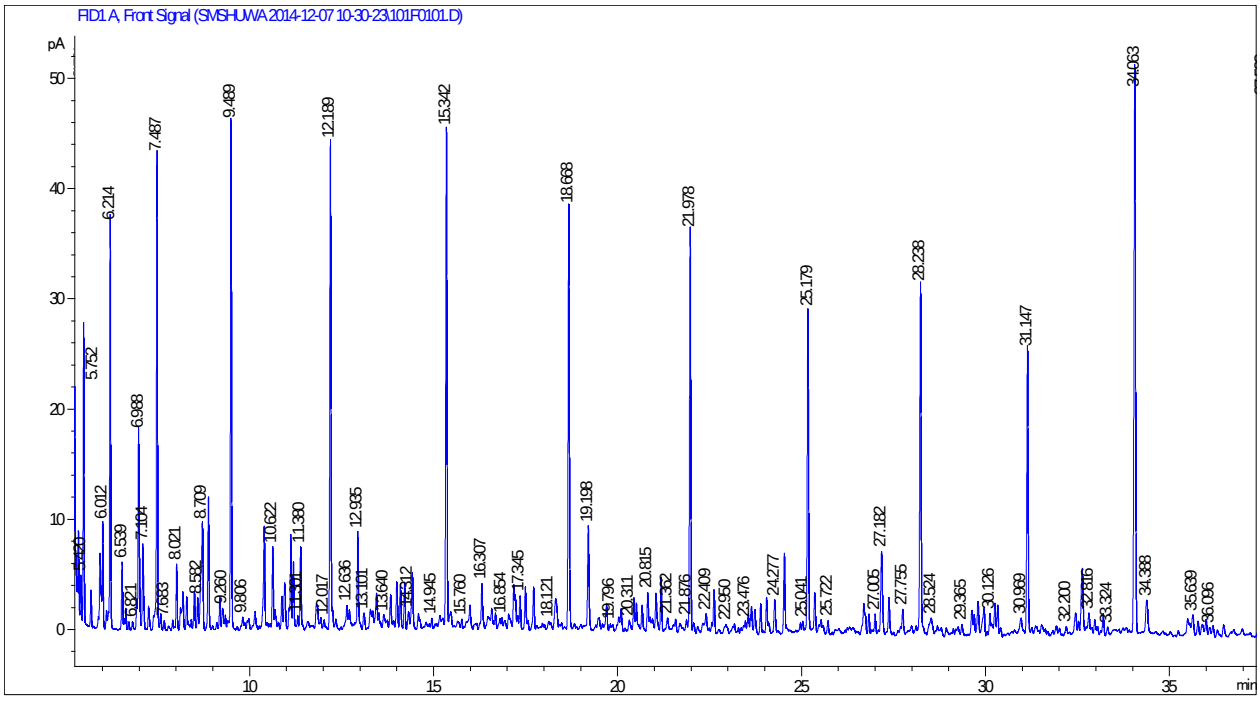

Figure S5: GC chromatogram of oil recovered from run R10 conducted at 340°C, 28h and 2500ppm catalyst amounts

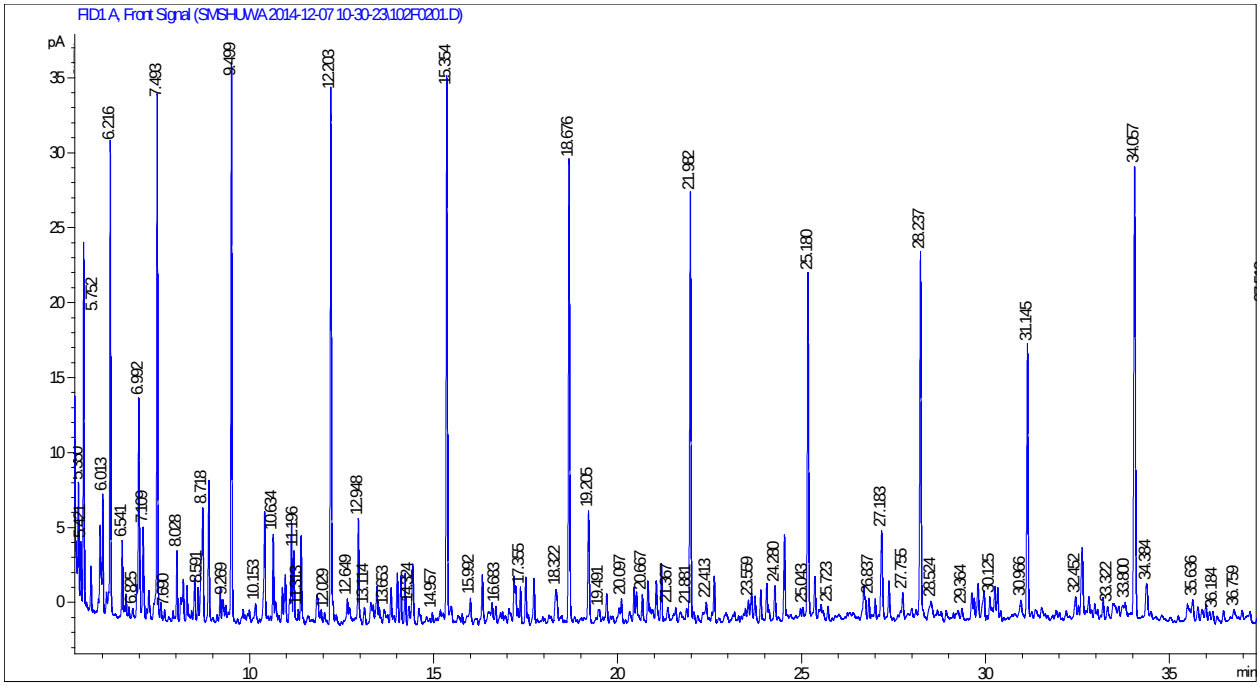

Figure S6: GC chromatogram of oil recovered from run R11 conducted at 340oC, 28h and 500ppm catalyst amounts

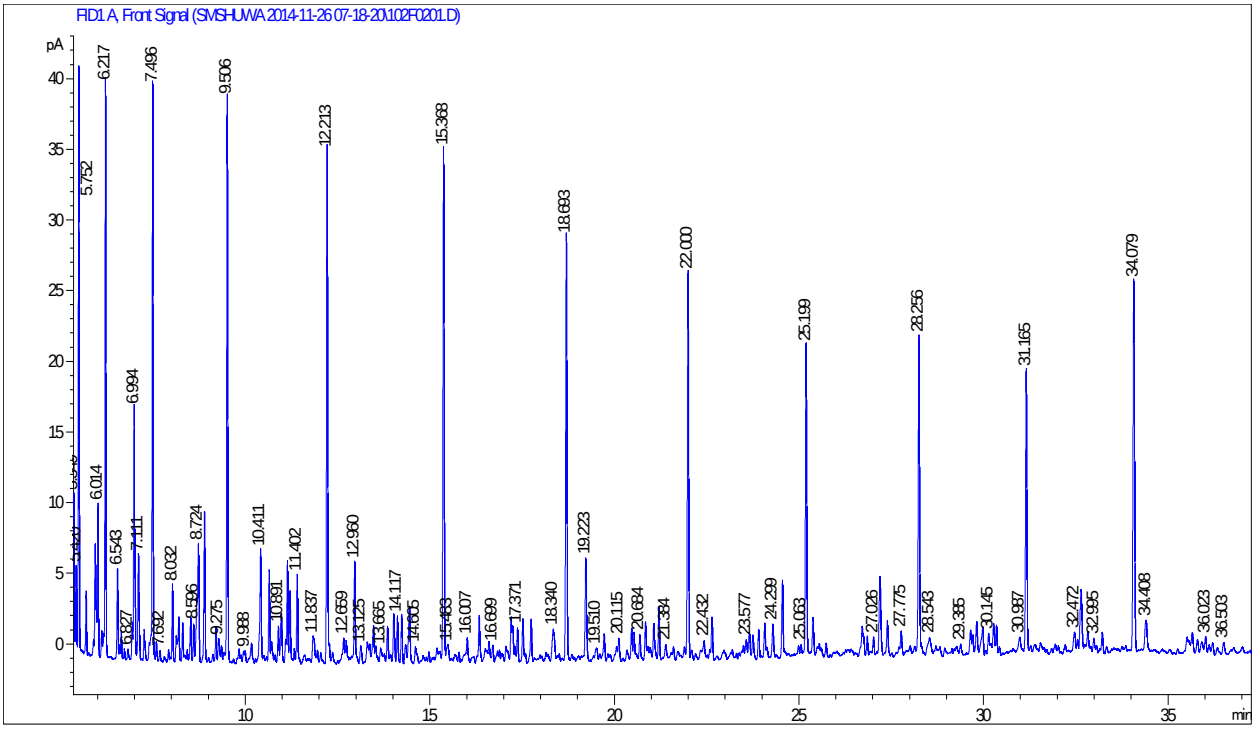

Figure S7: GC chromatogram of oil recovered from run R12 conducted at 300oC, 28h and 2500ppm catalyst amounts

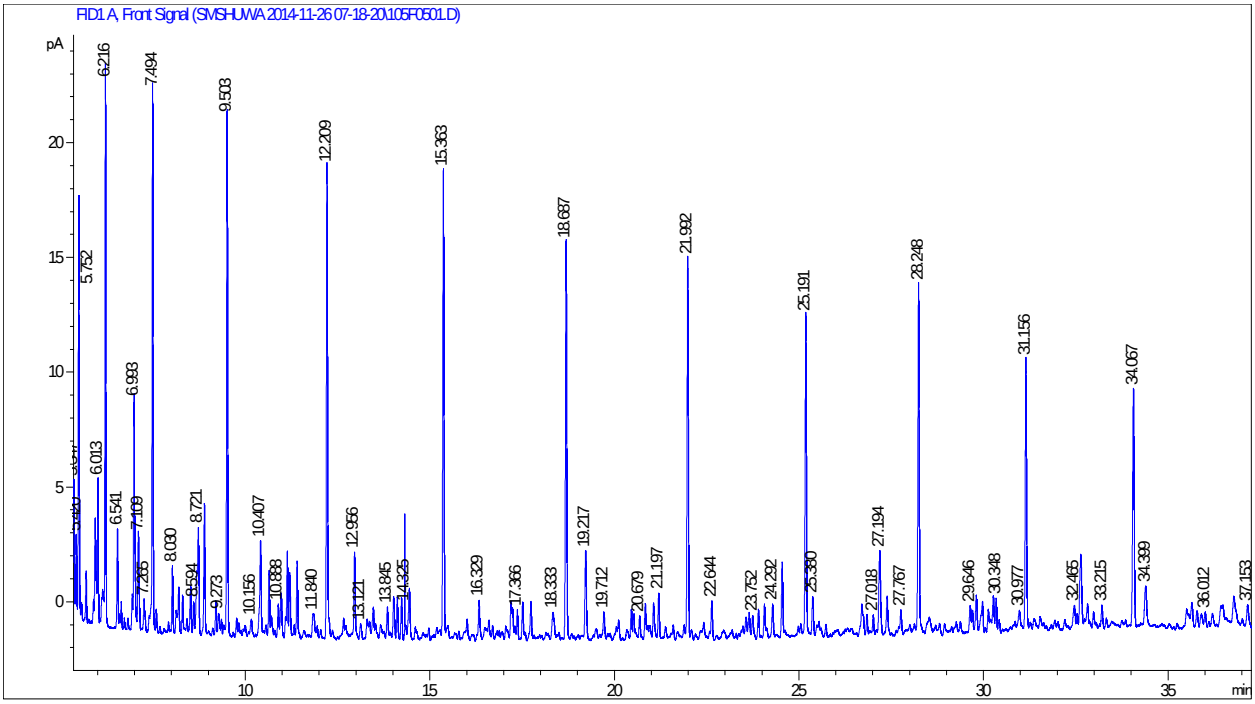

Figure S8: GC chromatogram of oil recovered from run R16 conducted at 260oC, 8h and 1500ppm catalyst amounts

SIMULTANEOUS ADSORPTION OF LEAD (II), CADMIUM (II) AND MANGANESE (II) IONS FROM INDUSTRIAL WASTEWATER ONTO DIJAH-MONKIN NATURAL BENTONITE CLAY

***Abdulsalam, S.[1], El-Nafaty, U. A.[1], Jock, A. A.[2] and Zaini, M. A. A.[3]**

[1]Department of Chemical Engineering, Abubakar Tafawa Balewa University, Bauchi, Nigeria

[2]Chemical & Petroleum Option, Department of Science Laboratory Technology, University of Jos, Nigeria

[3]Centre of Lipids Engineering & Applied Research (CLEAR), Ibnu Sina Institute for Scientific & Industrial Research (ISI-SIR), Univertiti Teknologi Malaysia, Johor Bahru, Malaysia.

*Corresponding author: S. Abdulsalam, Ph.D., e-mail: surajudeen_abdulsalam@yahoo.com

ABSTRACT

Pollution posed by toxic heavy metals contamination as a result of industrial activities is at the increase and it has devastating effects on human and the environment at large. Activated carbon used as adsorbent has been successful in the treatments of toxic heavy metal ions from aqueous solutions although expensive. Therefore, the need for a safe, effective and low cost technology. As a result of the aforementioned, the potential of the Dijah-Monkin bentonite as adsorbent for the removals of Pb (II), Cd (II) and Mn (II) were investigated in a multi-component aqueous solution in batch mode. Characterization of the bentonite showed that the major components in the clay were silica (62.30 wt%) and alumina (21.00 wt.%). In addition, the specific surface area and cation exchange capacity were 23.50 m^2/g and 47.70 mEq/100g respectively. The surface morphology and the micro structure of clay showed the presence of pores that can allow favourable sorption to take place. The percentage removal of the metal ions were 58%, 27% and 15% for Pb (II), Cd (II) and Mn (II) respectively in the order: Pb (II) > Cd (II) > Mn (II). The equilibrium isotherm and kinetics studies of the data obtained revealed that the Langmuir model and the pseudo second order kinetics better described the adsorption process.

Keywords: Multicomponent; batch adsorption; heavy metals; wastewater; Dijah-Monkin bentonite; low cost.

1.0 INTRODUCTION

Environmental pollution has become a global concern and attracts much attention. Water bodies and soil are the most common natural resources that have been contaminated as a result of different human activities. One of the most important environmental problems related to water pollution throughout the world is the contamination of water bodies by heavy metal ions because of their toxic effects on the environment and human health (Saad *et al.,* 2015). Heavy metals in wastewater can have detrimental effects on all forms of life even at low concentrations when discharged directly into the environment (Mahdavi *et al.,* 2013). They are usually stable and non-biodegrable within the ecosystem. As a result, they tend to bioaccumulate in living tissues thereby causing health concerns (Lukman *et al.,* 2013). Every year at least five million people die from water-related diseases worldwide ***(***Ghasemi *et al.*, 2015***)***. Thus, it is very important to determine effective methods for remediating toxic heavy metal contamination.

Among heavy metals, lead, cadmium and manganese are the most widely used in western society for the manufacture of metal alloys and plating, batteries, fertilizer, oil, paint, electronic, glass, ceramics, etc. (Vieira *et al.,* 2010; Pawar *et al.,* 2016; Akpomie *et al.*, 2016). Lead is highly toxic to organisms, including humans, even at extremely low concentrations. Lead poisoning in humans causes severe damage to the kidneys, nervous system, reproductive system, liver, and brain. Severe exposure to lead (II) is associated with various neurodevelopmental effects, cardiovascular diseases, mental retardation, sterility, abortion, stillbirth, and neonatal deaths (Pawar *et al.,* 2016). Cadmium is widely used and highly toxic in relatively low dosages, with cumulative effects causing kidney damage, renal disorder, high blood pressure, bone fracture and destruction of red blood Cells (Kumar *et al.,* 2010). Manganese is usually present in groundwater as a divalent ion and is considered a pollutant mainly because of its organoleptic properties (Akpomie *et al.*, 2016).

Several techniques have been developed for heavy metal removal from aqueous solution such as chemical precipitation, electrochemical treatment, evaporation, ion-exchange, filtration, oxidation/reduction, solvent extraction, membrane technologies and adsorption (Akpomie *et al.,* 2015). Among the various removal technologies available for the treatment of heavy metals-containing wastewater, adsorption has been proven to be an effective and affordable method, due to the low initial cost, flexibility and simplicity of design as well as ease of operation (Gao *et al.,* 2016).

Owing to the low cost of natural clay minerals, their abundance in most continents of the world, and high sorption properties, they have been used for sorption or elimination of heavy metals present in effluents (Gao *et al.,* 2016). The cost of clays is relatively low as compared to other alternative adsorbents, including

activated carbon, natural and synthetic zeolites, ion-exchange resins, and other adsorbent materials (Zhu *et al.,* 2016). Clay minerals such as montmorillonite, vermiculite, illite, kaolinite and bentonite are among the natural materials that have been investigated as heavy metal adsorbents (Vieira *et al.,* 2010). Other advantages in using clays as adsorbents are their intrinsic properties, such as large specific surface area, excellent physical and chemical stabilities, and a number of other structural and surface properties (Zhu *et al.,* 2016).

In this study, bentonite clay from Dijah-Monkin occurrence in Taraba State, Nigeria was investigated for simultaneous adsorption of lead (II), cadmium (II) and manganese (II) in a mixed aqueous solution. The adsorption data were interpreted using the isotherm and kinetic models. The choice of this clay material was based on its low cost and availability in Nigeria while heavy metals chosen were due to their health risk and wide areas of application.

2.0 MATERIALS AND METHODS

2.1 Sample collection and preparation

The raw bentonite clay sample was collected from a typical site at Dijah-Monkin town in Zing L.G.A, Taraba state of Nigeria. Ten kilograms (10 kg) of the clay was crushed to fine powder and soaked in water for 24 h. The clay-water mixture was blunged (stirred) for 3 h at 25^{o}C and was allowed to age for four days for the quartz impurities to settle to the bottom leaving colloidal solution of clay and suspended particles at the top. At each day of sedimentation, decantation of the overflow was done and replaced with fresh tap water to the fourth day when the overflow has become less milky and free from suspended particles. The colloid clay sample was then collected and separated from the quartz sediments and sieved through a 230 mesh Tyler sieve (63 µm sieve opening) to further remove coarse impurities and organic particles present in the clay. The thick slurry clay was put in a filter cloth and pressed under heavy mass of 10 kg to squeeze out the water. The resulting cake was sun dried and also oven dried at 110^{o}C to a constant weight. The dried clay was milled and sieved with a 125 µm mesh. The sieved clay was then stored in large polyethylene bag for analysis and subsequent experiments were carried out according to procedure described by Nwafulugo *et al.* (2014).

2.2 Characteristic of the Bentonite Clay

The bentonite clay was characterized for chemical composition using analysis X- ray fluorescence (model Mini PAC4 EDXRF, Rigaku, Japan). The morphological structure of the bentonite clay was determined by a field emission scanning electron microscope (model SU8020, Hitachi, Japan) coupled with energy dispersive spectrophotometer (EDS) of Oxford Instrument while the specific surface area was determined using the adsorption and desorption nitrogen isotherms, at liquid nitrogen temperature of -196^{o}C on Surfer Thermo Scientific (Thermo Scientific, USA). The FTIR spectra were recorded with a FTIR spectrophotometer (model Spectrum One, PerkinElmer, USA) using KBr pressed disk technique and the cationic exchange capacity of the clay was estimated using the ammonium acetate NH_4OAc method (Burt, 2004). The thermogravimetric (TGA) curves were obtained using a Q500 equipment (TA Instruments, USA). All the analyses were carried out at the Central laboratory, Universiti Teknologi Malaysia.

2.3 Batch Adsorption

2.3.1 Preparation of stock solution

Heavy metals solutions were prepared using $Pb(NO_3)_2.4H_2O$, $Cd(NO_3)_2.4H_2O$ and MnO_2 for lead (II), cadmium (II) and manganese (II), respectively. Distilled water was used for solution preparation and dilution to desired concentrations of 10, 20, 30, 40 and 50 mg/L for each metal ion. All the reagents used in this study were of high grade quality.

2.3.2 Equilibrium experiments

Fifty milligrams (50 mg) of the oven dried powdered clay (bentonite) was mixed with 50 mL of metal solution prepared at different concentrations. Batch adsorption was carried out on heavy metal ions (lead (II), cadmium (II) and manganese (II)) in aqueous solution (the three metal ions present simultaneously). The mixtures were shaken on orbital shaker (SASTEC^{TM}) at 25^{o}C and speed of 110 rpm for 72 h (Plate I). The contact period is presumably sufficient for the adsorption of heavy metals to attain the equilibrium (Hajahmadi *et al.*, 2015). Then, the suspension was filtered using a 0.45 µm syringe filter. The residual metal ions concentration was measured using ICP-OES. The removal of Pb (II), Mn (II) and Cd (II) ions from aqueous solution was calculated using mass balance equation,

$$q_e = \frac{C_o - C_e}{m} V \qquad (1)$$

where, q_e (mmol/g) is the adsorption capacity, C_o and C_e (mM) are the initial and equilibrium concentrations, respectively, V (L) is the solution volume and m (g) is the mass of adsorbent.

Plate I: Experimental setup for batch adsorption process

2.3.3 Kinetic experiments

Batch adsorption kinetic experiments were conducted on the mixed metals solution (10, 30 and 50 mg/L) by varying agitation (contact) time. Zero point five grams (0.05 g) of clay was brought into contact with a series of 50 mL multicomponent heavy metals solution of known concentration in 250 mL Erlenmeyer flasks. The mixtures were shaken on orbital shaker (SASTEC^{TM}) at a speed of 110 rpm, and 25^{o}C. The contact time was varied from 0 to 720 min. At predetermined time intervals (0-720 min), the suspension was withdrawn and filtered using a 0.45 µm syringe for concentration measurement using ICP-OES.

3. 0 RESULTS AND DISCUSSION

3.1 Characterization of bentonite clay

The result of chemical analysis (wt%) in Table 1 shows that the clay consists mainly of silica and alumina, with metallic oxides such Fe_2O_3, K_2O, CaO and TiO_2 present in minute quantities. The brownish colour observed in the clay may be due to the relatively high concentration of Fe_2O_3 (8.20 wt.%). The presence of CaO in the clay and the absent of Na_2O (Table 1), suggests that the predominant clay mineral is the Ca-rich type (Nweke *et al.,* 2015). In Table 1, the chemical composition was obtained from XRF while the ICPOES was used to measure the concentration of the cations for CEC determination and the specific area was obtained using BET method.

Table 1 Characteristics of bentonite samples

Sample	Chemical composition (wt.%)						Specific area, S_{BET} (m^2/g)	CEC (meq/100 g)
	SiO_2	Al_2O_3	Fe_2O_3	CaO	K_2O	TiO_2		
NB	62.3	21.0	8.20	1.17	4.59	1.22	23.5	47.70

Figure 1 shows the EDX spectra of bentonite samples consisting mainly of silicon (Si) and aluminium (Al). Other elements present include calcium (Ca), magnesium (Mg), potassium (K), iron (Fe) and titanium (Ti). The result of the EDX is in agreement with the chemical analysis obtained from XRF (Table 1) and the major components in the clay sample were Si and Al, which are the basic elements for smectite clay group (Araujo *et al.*, 2013).

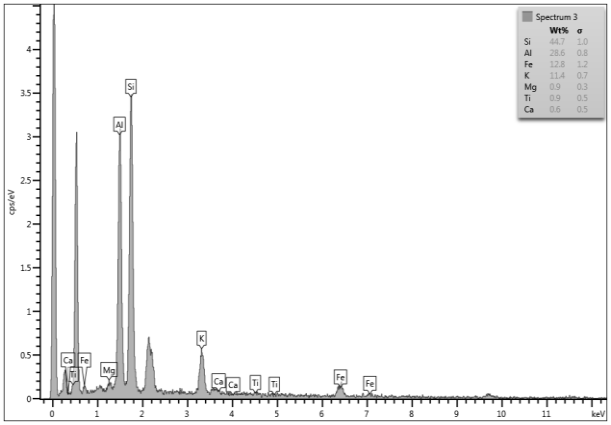

Figure 1: EDX spectra of natural bentonite

Similarly, the clay sample can be designated as polycationic bentonite due to the presence of Ca^{2+} and Mg^{2+} cations, which are suitable for adsorption process (Bertagnolli *et al.,* 2011).

The specific area of the bentonite clay in Table 1, is adequate for adsorption to occur and according to IUPAC definition, the clay is predominantly mesoporous materials with average pore diameter in a range of 2-50 nm (Budsaereechai *et al.,* 2012).

The cation exchange capacity described the ability of a clay to exchange cations in aqueous solution. From Table 1 and Figure 1, the major cations in bentonite sample were Ca^{2+} and Mg^{2+}. The clay exchange sites contain mostly calcium, and a higher CEC value allows a higher capacity to trap trace elements, which is also beneficial in the adsorption of positively-charged pollutants (Zhansheng *et al*., 2006). The cation exchange capacity of calcium montmorillonite ranges from 40 to 70 mEq/100 g, while that of sodium montmorillonite is between 80 and 150 mEq/100 g (Murray, 2007). Therefore, the bentonite sample with a cation exchange capacity of 47. 7 mEq/100 g (Table 1) has the tendency of exchanging its cation with heavy metals in solution.

The surface morphology and the micro structure of adsorbent materials play a vital role in knowing the surface heterogeneity and presence of pores that can allow sorption to take place. The SEM image and morphology of bentonite clay is shown in Plate II.

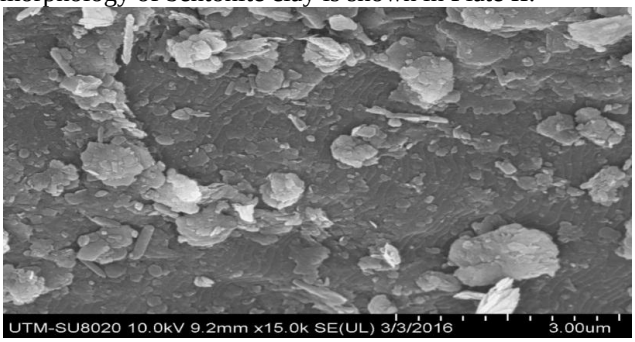

Plate II: SEM images of natural bentonite (magnification: x 15, 000)

Bentonite clay (montmorillonite) generally exhibits ultrafine, thin, leaf-like crystals forming a dense aggregates, or open honeycomb texture (Zuzana *et al.*, 2012). The micrograph of the clay in Plate II shows that the bentonite grains are aggregated mass of irregularly shape particles that appeared to have been formed by several flaky particles stacked together in the form of agglomerates.

Figure 2 shows the nitrogen adsorption-desorption isotherms of bentonite clay sample. It can be seen that it shows type IV isotherm according to IUPAC classification (Budsaereechai *et al.*, 2012). The volume of adsorbed gas decreases in relation with the relative pressure.

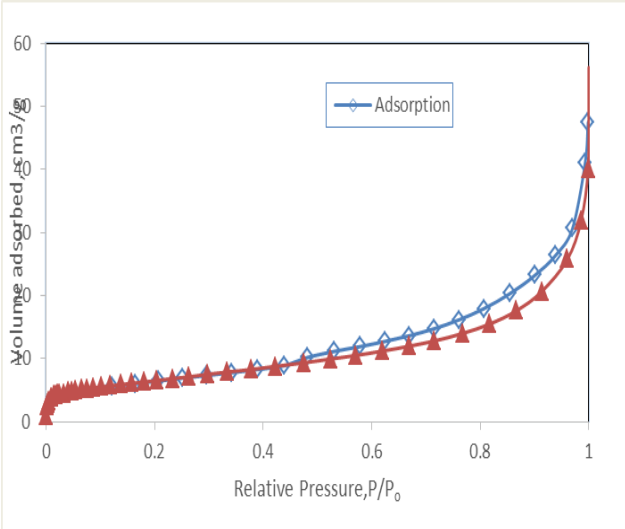

Figure 2: Adsorption and desorption isotherms of bentonite clay sample

The FTIR spectrum serves not only as a fingerprint for mineral identification, but also gives unique information about the mineral structure, including the family of minerals to which the specimen belongs, the degree of regularity within the structure, nature of isomorphic substituents, the distinction of molecular water from constitutional hydroxyl, and the presence of both crystalline and non-crystalline impurities (Djomgoue and Njopwouo, 2013).

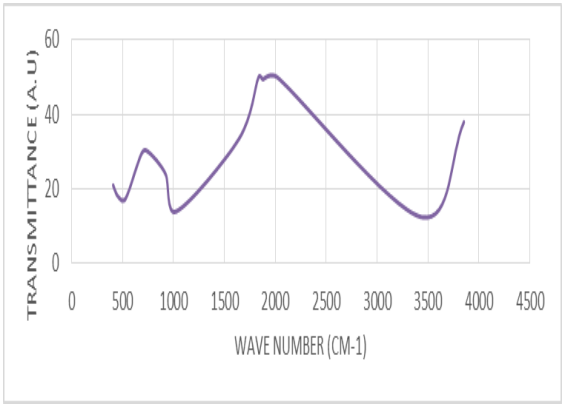

Figure 3: FTIR spectra of bentonite clay material

Figure 3 shows the spectra of bentonite clay sample in the wave number range of 4000-400 cm^{-1}. The bands corresponding to the water molecules in the interlayers, and the structural hydroxyl groups in the clay layers are in the region between 3750 and 3500 cm^{-1}, and the characteristic silicate bands are found between 1200 and 700 cm^{-1}. The bands at 600-400 cm^{-1} could be originated from Si-O bending and Al-O stretching vibration (Tomul and Balci, 2007). Water molecules basically exhibit three types of vibration: symmetric and asymmetric stretching and angular deformation of H-O-H group.

In addition, the 1600 to 1700 cm^{-1} range corresponds to angular deformation of H-O-H, while the 3100 to 3700 cm^{-1} range corresponds to the O-H stretching (Bertagnolli *et al.*, 2011). The peaks at 3433 and 3439 cm^{-1} are assigned to OH stretching, and are within the range of 3420-3450 cm^{-1} for water in montmorillonite that gives a broad band (Zuzana *et al.*, 2012). The peaks at 1030, 1045 and 1049 cm^{-1} are assigned to stretching vibration of Si-O, and the band observed at 922 cm^{-1} corresponds to Al-Al-OH (Er-ramly and Ider, 2014). Various bands at 733, 750 and 752 cm^{-1} are assigned to Al-O-Si, while peak at 685 cm^{-1} indicates OH deformation (Davarcioglu and Ciftci, 2010). The functional groups in bentonite clay include Al-OH, Al-O, Si-O, Si-OH, Al-Al-OH, Al-Mg-OH (Araujo *et al.*, 2013; Yu *et al.*, 2016). The main surface functional groups in clay that generate loads for possible adsorption are the pH dependent Si-OH and Al-OH groups (Araujo *et al.*, 2013).

3.2 Equilibrium studies of heavy metals adsorption

Adsorption at equilibrium indicates the uptake capacity of adsorbent at which the rate of adsorption is equal to the rate of desorption. The metal uptake for all the three metals increased from low concentrations to a saturation points, where their uptakes remain almost constant even when their concentrations were increased as shown in Figure 3.

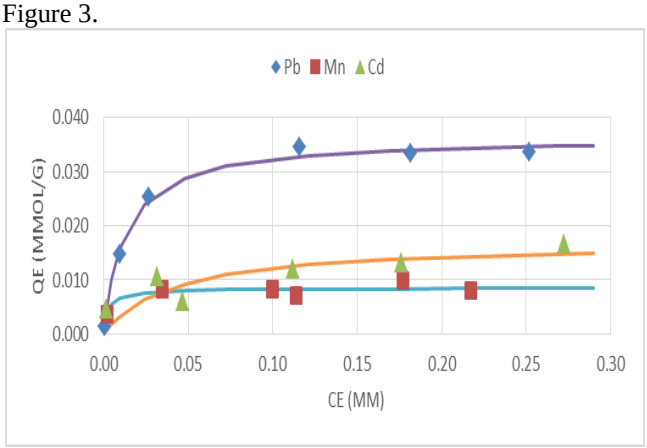

Figure 4: Equilibrium adsorption of lead (II), cadmium (II) and manganese (II) ions onto natural bentonite

Figure 4 shows the equilibrium adsorption of heavy metals in multicomponent system. The adsorption of Pb (II), Mn (II) and Cd (II) onto the bentonite sample could be prompted by the surface area in addition to the surface functional groups via ion-exchange mechanism between the metal ions and the surface active sites of bentonite (Vhanangwele and Mugera, 2015).

The difference in adsorption capacities between metals are commonly explained using hydration energy, hydrolysis constant, electro-negativity, and hydroxide solubility product of the metals (Nguyen *et al.*, 2015). From Figure 5, Pb (II) ions were favourably adsorbed over Mn (II) and Cd (II) ions.

The Langmuir and Freundlich models both incorporated three parameters into an empirical isotherm were employed to test for the fitness of the experimental data. The models were solved through non-linear regression using *Solver* for the least sum of squared error and optimum correlation of determination (R^2). The respective constants are summarized in Tables 2. The data for the adsorption of all the metals from the mixed metals solution satisfactorily fitted to the Langmuir model. This suggests that the adsorption sites were homogeneous with monolayer adsorption (Nguyen *et. al.* 2015). The values of maximum uptake (Q_m) predicted by the Langmuir model were in accordance with the experimental data (Figure 4).

Table 2: Isotherm constants for multicomponent adsorption of Pb (II), Cd (II) and Mn (II) onto bentonite clay

	Langmuir				Freundlich			
Heavy Metal	Q_m (mmol/g)	K_L (L/mmol)	SSE	R^2	K_F (mmol/g) (L/mmol)$^{1/n}$	$1/n$	SSE	R^2
Pb (II)	0.0363	79.6	5.9×10^{-6}	0.993	0.0534	0.261	8.6×10^{-5}	0.910
Mn (II)	0.0085	391.0	4.3×10^{-6}	0.802	0.0113	0.152	6.2×10^{-6}	0.714
Cd (II)	0.0170	25.0	3.9×10^{-5}	0.743	0.0233	0.283	1.8×10^{-5}	0.819

The maximum uptakes (% removal) for the metal ions were 0.036 mmol/g (58.1%) for Pb (II), 0.017 mmol/g (27.4%) Cd (II) and 0.009 mmol/g (14.5%) Mn (II). It indicates that lead (II) uptake was predominant as compared to those for cadmium (II) and manganese (II). The sorption capacities of metal ions was in the following order: Pb (II) > Cd (II) > Mn (II). This trend is in agreement with the increasing order of hydrated ionic radii of metal ions of 0.401, 0.426 and 0.438 nm for Pb (II), Cd (II) and Mn (II) ions respectively (Wang *et al.*, 2011). The smallest cations should ideally be adsorbed faster and in larger quantities compared to the larger cations, since the smaller cations can pass through the micropores and channels of the bentonite structure with ease (Afordita and Mirjana, 2014).

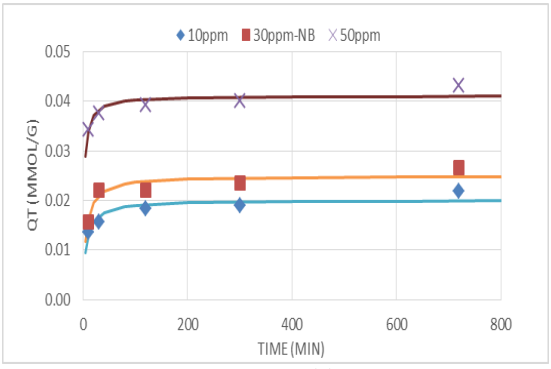

(a)

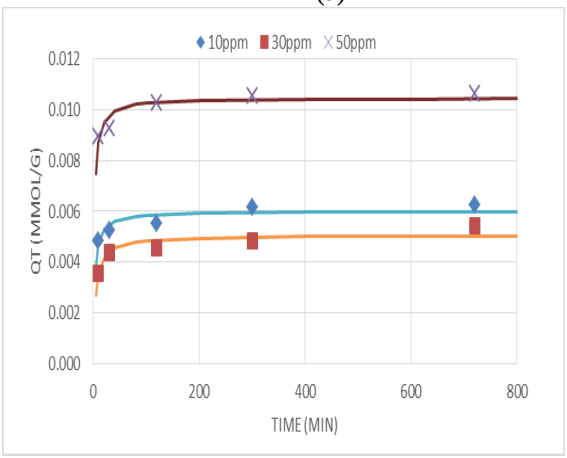

(b)

3.3 Kinetics of Multicomponent Adsorption

Simultaneous adsorption of lead (II), cadmium (II) and manganese (II) was measured at different time intervals and concentrations. The results shown in Figures 5a, b and c are the effects of contact time on the adsorption of lead (II), cadmium (II) and manganese (II), respectively. The uptakes at equilibrium remained constant even with increasing initial concentrations. Lead (II) ions were favourably adsorbed at all concentrations used over Mn (II) and Cd (II) ions. This was also similar with the decreased order of hydrated ionic radii of metal ions earlier discussed.

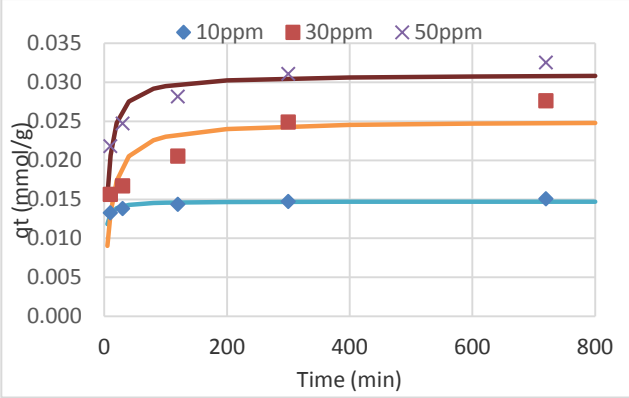

(c)

Figure 5: Effect of contact time on (a) lead (II), (b) cadmium (II) and (c) manganese (II) adsorption

The kinetics data were evaluated using the pseudo first and pseudo second order kinetics. These models revealed the nature and mechanism of adsorption process. The constants were also determined using *Solver* and the values sumarized in Tables 3. Comparing the regression coefficient (R^2) values, the pseudo second order model fitted better the adsorption kinetics than the pseudo first order model. The better fit of the pseudo second order model suggests that chemical process may be the rate-limiting step in the adsorption (Nguyen *et al.*, 2015).

Table 3 Rate constants of pseudo-kinetics models for multicomponent heavy metals adsorption

Heavy metal	Initial conc. (mg/L)	$q_{e,exp}$ (mmol/g)	Pseudo-first order kinetic				Pseudo-second-order kinetic			
			$q_{e,cal}$ (mmol/g)	K_1 (min^{-1})	SSE	R^2	$q_{e,cal}$ (mmol/g)	K_2 (mmol/g.min)	SSE	R^2
Pb(II)	10	0.022	0.019	0.110	1.6×10^{-5}	0.604	0.020	8.77	7.1×10^{-6}	0.825
	30	0.027	0.024	0.103	1.1×10^{-5}	0.823	0.025	7.14	8.6×10^{-6}	0.865
	50	0.043	0.040	0.192	1.7×10^{-5}	0.614	0.041	11.4	7.9×10^{-6}	0.815
Cd(II)	10	0.006	0.006	1.00	1.4×10^{-6}	0.533	0.006	58.7	2.9×10^{-7}	0.802
	30	0.005	0.005	1.00	1.9×10^{-6}	0.652	0.005	45.1	3.0×10^{-7}	0.840
	50	0.011	0.010	1.00	2.4×10^{-6}	0.525	0.010	47.7	3.8×10^{-7}	0.843
Mn(II)	10	0.015	0.014	1.00	2.1×10^{-6}	0.581	0.015	55.4	3.2×10^{-7}	0.845
	30	0.028	0.024	0.079	5.7×10^{-5}	0.506	0.025	4.48	2.9×10^{-5}	0.736
	50	0.033	0.030	0.121	3.1×10^{-5}	0.617	0.031	6.40	1.1×10^{-5}	0.866

4. CONCLUSIONS

The potentials of Dijah-Monkin bentonite for simultaneous adsorption of lead (II), cadmium (II) and manganese (II) ions in aqueous solution in a batch were investigated and from the results obtained, the following conclusions were drawn:

(i) Adsorption of each metal ion increases with increased in initial concentration until equilibrium was attained and the order of selectivity of metal ions was Pb (II) > Cd (II) > Mn (II).

(ii) The adsorption efficiencies were 58, 27 and 15% for Pb (II), Cd (II), Mn (II) respectively.

(iii) The Langmuir isotherm model yields a better fit to the experimental data.

(iv) The pseudo second order model appeared to fit the data satisfactorily.

The overall result of the study shows that Dijah-Monkin bentonite clay is a promising low-cost adsorbent for effective removal of mixed heavy metals ions from aqueous solution.

REFERENCES

Afordita Z, Mirjana G (2014) Effect of competing cations (Cu, Zn, Mn, Pb) adsorbed by natural zeolite. *International Journal of Science, Engineering and Technology* 2(5): 483-492.

Akpomie K.G, Dawodu F.A. and Adebowale K.O. (2015) Mechanism on the sorption of heavy metals from binary-solution by a low cost montmorillonite and its desorption potential. *Alexandria Engineering Journal* 54: 757–767

Araujo ALP, Bertagnolli C, Silver MGC, Gimenes ML, Barros MAS (2013) Zinc adsorption in bentonite clay: Influence of pH and initial concentration. *Acta Scientiarum Technology* 35(2): 325-332.

Bertagnolli C, Kleinubing SJ, Silver MGC (2011) Preparation and characterization of a Brazilian bentonite clay for removal of copper in porous beds. *Applied Clay Science* 53: 73-79.

Budsaereechai S, Kamwialisak K, Ngernyen Y (2012) Adsorption of lead, cadmium and copper on natural and acid activated bentonite clay. *KKU Res. J.* 17(5): 800-810.

Davarcioglu, B. and Ciftci, E. 2010. Spectral characterization of Kolsuz-Ulukisla-Nigde clays, central Anatolian region-Turkey and petroleum exploration. *Journal of petroleum and Gas Engineering* 1(3): 41-53.

Djomgoue, P. and Njopwouo, D. 2013. FT-IR spectroscopy applied for surface clays characterization. *Journal of Surface Engineered Materials and Advanced Technology* 3(4): 275-282.

Er-ramly, A. and Ider, A. 2014. Physicochemical and mineralogical characterization of Moroccan bentonite of Trebia and its use in ceramic technology. *American Journal of Physical Chemistry* 3(6): 96-101.

Gao Y., Guo Y. and Zhang H. (2016) Iron modified bentonite: Enhanced adsorption performance fororganic pollutant and its regeneration by heterogeneous visible lightphoto-Fenton process at circumneutral pH. *Journal of Hazardous Materials* 302 (2016) 105–113

Ghasemi M., Ghoreyshi A.A., Younesi H. and Khoshhal S. (2015) Synthesis of a high characteristics activated carbon from walnut shell for the removal of Cr (VI) and Fe (II) from aqueous solution: single and binary solutes adsorption *Iranian Journal of Chemical Engineering 12(4): 1-24*

Hajahmadi Z, Younesi H, Bahramifar N, Khakpour H, Pirzadeh K (2015) Multicomponent isotherm for biosorption of Zn(II), CO(II) and Cd(II) from ternary mixture onto pre-treated dried Aspergillus niger biomass, *Water Resources and Industry* 11: 71-80.

Kumar P.S., Ramakrishnan K., Kirupha S.D. and Sivanesan S. (2010) Thermodynamic and kinetic studies of cadmium adsorption from aqueous solution onto rice husk. *Brazilian Journal of Chemical Engineering* 27(2): 347 – 355.

Lukman S., Essa M. H., Muazu D. M., Bukhari A. and Basheer C., (2013), "Adsorption and desorption of Heavy Metals onto Natural Clay Materials: Influence of Initial pH", *Journal of Environmental Science and Technology*, 6: 1-15.

Mahdavi S., Jalali M. and Afkhami A. (2013) Heavy Metals Removal from Aqueous Solutions Using TiO2, MgO, and Al2O3 Nanoparticles. *Chemical Engineering Communications*: 1-24

Murray H.H (2007) *Applied clay mineralogy*, Elsevier: 111-130.

Nguyen, T.C., Loganathan P., Nguyen T.V., Vigneswaran S., Kandasamy J. and Naidu R. 2015. Simultaneous adsorption of Cd, Cr, Cu, Pb, and Zn by an iron-coated Australian zeolite in batch and fixed-bed column studies. *Chemical Engineering Journal* 270: 393–404

Nweke MO, Igwe EO, Nnabo PN (2015) Comparative Evaluation of Clays from Abakaliki Formation with Commercial Bentonite Clays for Uses as Drilling Mud. *African Journal of Environmental Science and Technology* 9(6): 508-518.

Pawar R.R., Lalhmunsiama , Bajaj H.C. and Lee S.M. (2016) Activated bentonite as a low-cost adsorbent for the removal of Cu(II) and Pb(II) from aqueous solutions: Batch and column studies.

Saad D.M., Cukrowska E. and Tutu H. (2015) Column adsorption studies for the removal of U by phosphonated cross-linked polyethylenimine: modelling and optimization *Appl Water Sci.* 5:57–63

Tomul, F. and Balci, S. 2007. Synthesis and characterization of Al-pillard interlayered bentonite. *G.U. Journal of Science* 21(1): 21-31.

USDA, 2014. Soil survey laboratory methods manual - Soil Survey Investigations Report No. 42, Version 5, Nebraska: United States Department of Agriculture.

Vhahangwele M. and Mugara G.W. (2015) The potential of ball-milled South African bentonite clay for attenuation of heavy metals from acidic wastewater: Simultaneous sorption of Co^{2+}, Cu^{2+}, Ni^{2+}, Pb^{2+} and Zn^{2+} ions. *Journal of Environmental Chemical Engineering* 3: 2416-2425.

Vieira M.G.A., Neto A.F.A., Gimenes M.L. and Silva M.G.C (2010) Sorption kinetics and equilibrium for the removal of nickel ions from aqueous phase on calcined Bofe bentonite clay. *Journal of Hazardous Materials 177: 362–371*

Wang X.S., Miao H.H., He W. and Shen H.L. (2011) Competitive adsorption of Pb(II), Cu(II), and Cd(II) ions on wheat residue derived black carbon. *J. Chem. Eng. Data* 56: 444-449.

Yu Y, Li X, Cheng J (2016) A Comparison Study of Mechanism: Cu^{2+} Adsorption on Different Adsorbents and Their Surface-Modified Adsorbents. *Journal of Chemistry:* 1-8.

Zhansheng W, Xifang CLS, Xiaolin X, Bin D, Jin'e L, Hongsheng Z (2006) Characterization, Acid Activation and Bleaching Performance of Bentonite from Xinjiang. *Chinese J. Chem. Eng*. 14(2):253-258.

Zhu, R., Chen, Q., Zhou, Q., Xi. Y., Zhu, J. and He, H. 2016. Adsorbents based on montmorillonite for contaminant removal from water: A review. *Applied Clay Science* 123: 239-258.

Zuzana, O., Annamaria, M., Silva, D. and Jaroslav, B. 2012. Effect of thermal treatment on bentonite properties. *Arhiv Za Tehnicke Nauke* 7(1): 49-56.

MODEL DEVELOPMENT FOR ASSESSING BULK CHLORINE DECAY RATE IN WATER FROM TREATED WATER SUPPLY IN KADUNA – NIGERIA

[*]Abdullahi, M. E.[1], Ibrahim, Y.[2] and Baba, M. B.[3]
[1]Department of Chemical Engineering, University of Abuja-Nigeria, [2]Kaduna Refinery and Petrochemical Company, Kaduna-Nigeria, [3]Department of Chemical Engineering, Kaduna Polytechnic, Kaduna-Nigeria
Corresponding author: evutimohd@yahoo.com

ABSTRACT

Residual chlorine in water distribution systems is an important parameter needed for ensuring the standard of potable water supplies. This research investigates the bulk chlorine decay rate in water from public treated water supply from Kaduna North water treatment plant, Malali-Kaduna, Nigeria. The data generated from the study was used to validate a mathematical model of residual chlorine versus time developed using POLYMATH 6.10 professional software. The initial average residual chlorine value of 0.323 mg/l of the treated water obtained is lower than the recommended World Health Organization (WHO) value of 0.5 mg/l. The resultant model was found to be: $R_{ch} = 0.2808687 - 0.0030073t$. *Comparison of the results of the simulation of this model and the experimental data shows a good correlation with values of* R^2 *(a measure of the closeness of the data to the fitted regression line) and* R^2 *adj as 0.961 and 0.956 respectively. The model can therefore be used as an alternative to the manual method of determining the variation of residual chlorine along the treated water distribution network. The research revealed the need for booster chlorination after one hour along the distribution line or application of higher mass rate of chlorine at the source to maintain the minimum residual chlorine up to the farthest end.*

Key words*: Chlorine, Decay Rate, Water Distribution System, Modeling, Simulation*

1. INTRODUCTION

According to American Water Works Association (AWWA), 2004, the earliest recorded use of chlorine directly for water disinfection was on an experimental basis in connection with filtration at Louisville, KY in 1896. The advantages of chlorine disinfection include simplicity, low cost and a broad range of effectiveness such as controlling aesthetic quality, removing iron, manganese, and hydrogen sulphide; sterilizing mains and storage tanks; restoring and preserving pipeline capacity and maintaining distribution system bacterial quality by reducing the growth of microorganism and slimes (Abdullahi and Abdulkarim, 2010; Hua *et al*., 1999; Vasconcelos *et al*., 1997).

When chlorine is dissolved in water, it hydrolyzes to form hypochlorous and hydrochloric acid as follows;

$Cl_2 + H_2O \rightarrow HOCl + HCl$ (1)

The hypochlorous acid further ionizes or dissociates into hydrogen and hypochlorite ions as follows;

$HOCl \leftrightarrow H^+ + OCl^-$ (2)

The oxidizing effect on micro-organisms is produced by both hypochloric acid and hypochlorite ions (Eryilmaz and Palabiyik, 2013). When Chlorine is used for disinfection, it reacts readily with oxidizable substances such as Fe^{2+} and Mn^{2+} and other organic matters. Thereafter, chlorine reacts with ammonia to form chloramines (monochloramine, NH_2Cl and dichloramine, $NHCl_2$) which further oxidize with more chlorine to trichloramine NCl_3 (Nitrogen trichloride). Research results have also revealed that chlorine decay occurs due to reactions with materials associated with the pipe wall resulting in corrosion and biomass growth on the inner pipe walls (Kowalska *et al*., 2006). The break point is reached when these reactions are completed so that continued addition of chlorine produces free residual chlorine (White, 1986). Therefore, residual chlorine can be defined as the concentration of all oxidizing agents produced by chlorination of natural water that remains after a certain period of time. Its measurement is done to determine the efficiency of disinfection.

Chlorine dosages in distribution systems are determined primarily by the need to ensure minimum chlorine residual in the distribution system water so as to eliminate disease causing microorganisms or substances that adversely affect the taste and quality of the distributed water as well as the condition of the distribution system. On the other hand, control of excess chlorine doses is required to reduce the extent of

formation of disinfection byproducts (DBPs) that are known for causing health related risks in humans (Tiruneh *et al*., 2016). Rossman *et al*. (2001) define the bulk chlorine decay as chlorine reaction with dissolved and suspended matter, mostly natural organic matter (NOM) in the water, thus the chlorine reactions with compounds attached to or derived from pipe materials can be ignored. In most waters, the reactions of chlorine with NOM make up the majority of the chlorine demand. Bulk decay may be isolated from wall decay by carrying out chlorine decay experiments on the source water under controlled conditions in laboratory (Hua *et al*., 1999)

A water distribution system (WDS) is a hydraulic conveyance system laid on road shoulders where topology and topography are known and that transmit water from the source to the consumers. It consists of elements such as pipes, valves, pumps, tanks and reservoirs, flow regulating and control devices (Bello *et al*., 2015). According to Vasconcelos *et al*. (1997), proper understanding, characterization, and prediction of water quality behavior in the water distribution systems are critical to meeting regulatory requirement and consumer-oriented expectations. This can be achieved through computer-based modeling and simulation of the water quality variables along the distribution systems with time.

A model is a simplified representation of a system intended to enhance our ability to understand, explain change, preserve, predict and possibly control the behaviour of a system. Modeling is thus the process of establishing inter-relationship between important entities of a system (Abdulkareem, 2000); while simulation is a means of gaining relevant information on the characteristics of full size prototypes without incurring the expenses of building a full size prototype to test (Morley, 1979). According to Kowalska *et al*. (2006), it is difficult to predict chlorine decay in large distribution systems, especially if they work under poor hydraulic conditions (aged pipes, small velocities, etc.). Therefore, when testing chlorine decay, it seems easier to separate the reactions associated with the bulk liquid from those associated with the pipe wall. Mathematical modeling of chlorine decay in distribution systems is essential in order to be able to predict chlorine residuals with reasonable accuracy and reduce the cost and time associated with monitoring. In large distribution systems, monitoring of chlorine residuals may be prohibitively expensive (Tiruneh *et al*., 2016). Therefore, computer based model will be a promising cost effective alternative (Vasconcelos *et al*., 1997).

In recognition of the importance of residual chlorine as an essential final check to the quality of water supply to the consumer, a number of researches have been conducted on chlorine decay kinetics and development of model to predict chlorine decay in drinking water in recent time (Castro and Neves, 2003; Georgescu and Georgescu, 2012; Goyal and Patel, 2014; Hua *et al*., 1999; Kowalska *et al*., 2006; Tiruneh *et al*., 2016; Vasconcelos *et al*., 1997). However, there is still need for further research in this area particularly in developing countries like Nigeria, where water distribution system is characterized with over dependence due to excessive growth in population and intermittent supply of water. To cope with high demand, the service areas are usually divided into few zones and each zone receives supply for limited hours which leads to the stagnation of water in pipes during non-supply hours and decay of chlorine for rest of the hours. The intermittent supply scenario exposes consumers to health risks due to the higher likelihood of contamination of water pipelines through joints and damaged segments during periods when the system is not pressurized. Also, there is a problem related to maintenance of pressure at the farthest node in intermittent water supply.

According to Kowalska *et al.* (2006), the residence time of water in any distribution system changes the quality of the water, because the values of many parameters decrease or increase as a result of chemical and biological reactions which depend on the environment in the distribution system. This research investigates the variation of residual chlorine with time in water from public treated water supply from Kaduna North water treatment plant, Malali-Kaduna, Nigeria and to use the data generated to develop a mathematical model relating residual chlorine with time using polymath software. This study is significant because the effect of residence time on concentration of residual chlorine is a necessary check for both the chlorine application strategy which guides the selection of supply hours of water to achieve the effectiveness of booster chlorination strategy for the intermittent water supply.

2. MATERIALS AND METHODS

Study Site and Sample Collection

The study area is the Kaduna North water treatment plant, Malali-Kaduna, Nigeria. The treated water samples were collected using sample bottles sterilized

with sulphuric acid and washed thoroughly with distilled water. The samples were taken at the point of discharge to consumers at the water treatment plant once weekly for a period of three weeks.

Determination of Residual Chlorine

The residual chlorine was determined using a NN Diethyl-Pthenogene Diamine reagent (DPD test). The test was carried out in a British Drig House (BDH) comparator which comprises of two 10 ml cuvettes, two standard discs, 3/40/A and 3/40/B disc with range of residual chlorine measurements of 0.1 – 1.00 and 0.2 – 0.4 mg/l respectively. The first tests were carried out at the point of collection to avoid any time lapse, while the subsequent tests where carried in the laboratory.

For each batch of test, a cuvette was filled with 10ml of the sample and inserted into the left compartment of the BDH comparator. The second cuvette was then filled to about 2cm of its depth with the same sample and a DPT tablet was then dropped into it and allowed to dissolve completely. The mixture was then inserted into the right compartment of the comparator and then observed. A pink colour development indicates the presence of residual chlorine. The value of the residual chlorine was determined by rotating one of the discs until a colour march is attained in the viewing window and the residual chlorine was directly read through the window in the lower right hand corner of the comparator. This was repeated for all the samples at intervals until no residual chlorine was observed.

Modeling Procedure and Statistical Analysis

A simple linear regression model for an outcome y as a function of a predictor x takes the form:

$$y_i = \beta_0 + \beta_1 x_i + c_i \quad (3)$$

for $i = 1, \ldots\ldots, n$

Where n represents the number of observations (rows) in the data set (Model Data Science with R, 2017).

Kowalska *et al.* (2006) states that the water quality parameter changes with the residence time of water in any distribution system. A study by Franson (1994) shows that chlorine demand for water disinfection is dependent on the time of contact. The relationship between the residual chlorine and time can be expressed mathematically as (Abdullahi and Abdulkarim, 2010):

$$R_{cl} = f(t) \quad (4)$$

Introducing a constant, Equation (4) becomes:

$$R_{cl} = a_1 t \quad (5)$$

To correct variations from other factors such as temperature, pH etc. (Zheng, 2013) not accounted for, a constant a_0 is introduced, thus Equation (5) becomes:

$$R_{cl} = a_0 + a_1 t \quad (6)$$

Where: R_{cl} = Residual Chlorine

a_0 and a_1 are constants

t = time

Using POLYMATH 6.10 professional software, the values of these constants can be evaluated and substituted into Equation (6) to obtain the model equation.

The statistical analysis and the linear fit of plot of predicted versus actual experimental residual chlorine values was obtained using OriginPro 8.0 software.

3. RESULTS AND DISCUSSION

Effect of residence time on Chlorine concentration in treated water samples

The values of residual chlorine determined from the treated water samples with respect to time once per week for a period of three weeks and the average values are presented in Table 1. An initial average observed value of 0.323 mg/l can be considered inadequate because according to WHO (1993), a residual concentration of free chlorine of greater than or equal to 0.5 mg/L (0.5 ppm or parts per million) after at least 30 minutes contact time at pH less than 8.0 is recommended for treated water (CDC, 2014). However, this will only be appropriate when users drink water directly from the flowing tap. It has been found that while a residual chlorine level of 0.5 mg/L at the treatment plant may be enough to maintain the quality of water throughout the distribution network; however, it is most likely not to be adequate to maintain the quality of the water at this residual chlorine level when the water is stored at home in a bucket or jerry can for over 24 hours. The United States Centre for Disease Control and Prevention therefore recommends initial residual chlorine of 2.0 mg/L at the point of dosage.

Table 1: Experimental values of Residual Chlorine

S/No.	Time (Min)	Residual Chlorine (mg/l)			
		Week 1	Week 2	Week 3	Average
1	0	0.3	0.32	0.35	0.323
2	5	0.25	0.28	0.27	0.267
3	23	0.2	0.21	0.22	0.21
4	30	0.15	0.16	0.15	0.153
5	45	0.125	0.13	0.125	0.127

S/No.	Time (Min)	Residual Chlorine (mg/l)			
		Week 1	Week 2	Week 3	Average
6	55	0.1	0.1	0.1	0.1
7	70	0.07	0.08	0.07	0.073
8	80	0.03	0.03	0.04	0.043
9	95	0	0	0	0
10	100	0	0	0	0

Figure 1 shows a gradual decrease in average residual chlorine values from 0.323 mg/l at 0 minute to 0 mg/l after a residence time of 95 minutes. This is as a result of further reactions of chlorine with dissolved and suspended matter which are usually natural organic matter (NOM) in the water along the distribution line. This is in accordance with the findings of Kowalska *et al*. (2006) which states that the water quality parameter changes with the residence time of water in any distribution system. This decrease in chlorine concentration with time is referred to as chlorine decay (Goyal and Patel, 2014). The result also shows the need for booster chlorination along the distribution network after every 60 minutes residence time of treated water in the supply pipeline. The booster chlorination helps in maintaining proper balance between the minimum and maximum residual chlorine concentrations. Alternatively, to cope up with the decay in chlorine, higher mass rate of chlorine is applied at the source to maintain the minimum residual chlorine up to the farthest end, however, studies have also shown that this may result in harmful disinfection by-products (DBP) formation at the nearest locations to the source and less concentration of residual chlorine at farthest location (Goyal and Patel, 2014).

Modeling and Statistical Analysis

The model of the relationship between the average chlorine value and time was determined by substituting the experimental average residual chlorine values into the POLYMATH 6.10 professional software. The resultant model was found to be:

$$R_{ch} = 0.2808687 - 0.0030073t \quad (7)$$

The result of the simulation of the model (Equation 7) is shown in Table 2.

Table 2: Simulated Values of Residual Chlorine

S/No.	Time (Min)	Residual Chlorine (mg/l)
1	0	0.2809
2	5	0.2658
3	23	0.2117
4	30	0.1906
5	45	0.1455
6	55	0.1155
7	70	0.0704
8	80	0.0403
9	95	-0.0048
10	100	-0.0199

A plot of simulated residual chlorine values against time (Figure 2) gave a straight line which shows a regular decrease in the simulated residual chlorine values (ideal situation) with negative residual chlorine values of -0.0048 and -0.0199 at 95 and 100 minutes respectively which are not obtainable in real situations. This may be attributed to the effect of other factors such as pH and temperature not taking into consideration during the development of the model (Zheng, 2013).

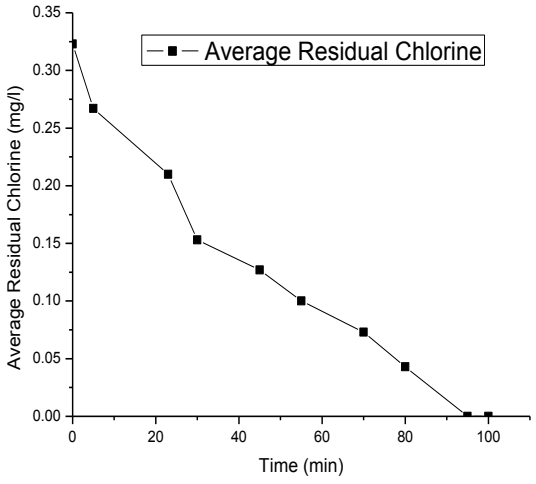

Figure 1: A plot of Average Residual Chlorine (mg/l) against time (min)

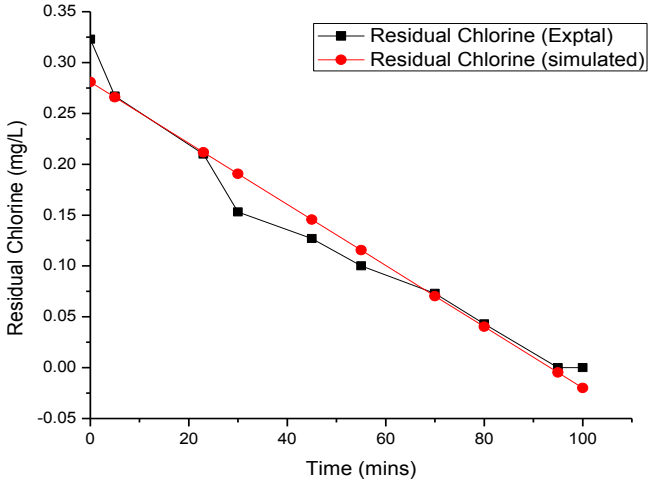

Figure 2: A plot of experimental and simulated residual chlorine values against time

Statistical analysis of the result using OriginPro 8.0 software gave the values of the correlation coefficient (R^2) and adjusted R^2 as 0.961 and 0.956 respectively. *R-squared* is a statistical measure of how close the data are to the fitted regression line. It is also known as the coefficient of determination, or the coefficient of multiple determinations for multiple regressions. The R^2 coefficient gives the proportion of the total variation in the response predicted by the model, indicating ratio of sum of squares due to regression (SSR) to total sum of squares (TSS). The R^2 value was found to be closed to adjusted R^2 value of 0.961 showing a good relationship between simulated and experimental values. A high R^2 value, close to 1, is desirable and a reasonable agreement with adjusted R^2 is necessary (Ghafari *et al*., 2009). A high R^2 coefficient ensures a satisfactory adjustment of the model to the experimental data.

The linear fit of plot of predicted versus actual experimental residual chlorine values (Figure 3) shows a straight line with an error of 0.0408. This indicates good prediction of experimental data using the model. Actual values are the measured values for a particular experiment, whereas predicted values are generated by using the approximating functions.

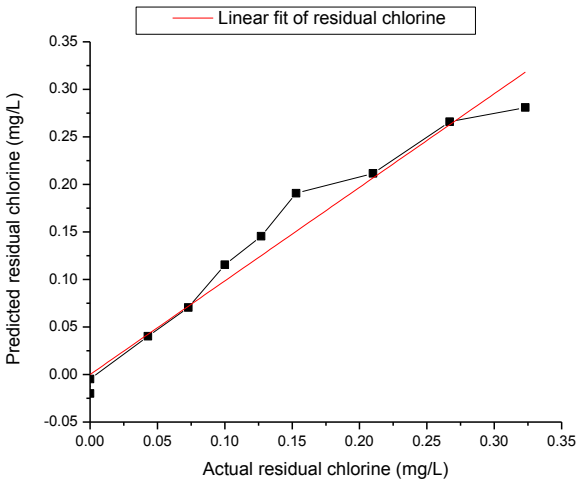

Figure 3: A plot of predicted versus actual experimental residual chlorine values

4. CONCLUSION

The objective of this research was to assess the bulk chlorine decay of treated water samples from Kaduna North water treatment plant, Malali-Kaduna, Nigeria under controlled conditions in laboratory and to use the results obtained to validate a model of the change in residual chlorine versus time developed using POLYMATH 6.10 professional software. The major conclusions drawn from the results are:

1. The initial average residual chlorine value of 0.323 mg/l of the treated water is lower than the recommended WHO value of 0.5 mg/l.
2. The result revealed the sensitivity of residence time to residual chlorine hence the need for booster chlorination after one hour (1 hr) along the distribution line or application of higher mass rate of chlorine (0.5 mg/l) at the source to maintain the minimum residual chlorine up to the farthest end.
3. The resultant model gave a good prediction with values of R^2 and R^2 adj as 0.961 and 0.956 respectively. The model can therefore be used as an alternative to the manual method of determining the variation of residual chlorine along the treated water distribution network.

5. RECOMENDATION

Further researches should focus on the effect of reactions with materials associated with the pipe wall resulting in corrosion and biomass growth on the inner pipe walls on residual chlorine.

REFERENCE

Abdullahi M. E. and Abdulkarim, B. I. (2010). Development of mathematical model for determining the quantity of chlorine required for water treatment, *Journal of Applied Sciences Research*, 6(8), 1002-1007.

American water works Association, 2004. *Water treatment plant design*; 4th Edition Mc. Graw Hill, international, U.S.A.

Bello, A. D., Alayande, W. A., Johnson A. Otun, J. A., Ismail, A. and Lawan, U. F. (2015). Optimization of the Designed Water Distribution System Using MATLAB. *International Journal of Hydraulic Engineering*, 4(2), 37-44.

Castro, P. and Neves, M. (2003). Chlorine Decay in water distribution systems Case Study-Lousada Network. *Environmental 2010: Situation and Perspectives for the European Union, 6-10 May 2003. Porto, Portugal paper G11,* 1-6.

Centre for Disease Control and Prevention (CDC), (2014). The safe water system. http://www.cdc.gov/safewater/chlorine-residual-testing.html

Eryilmaz, M. and palabiyik, I. M. (2013). Hypochlorous Acid-Analytical Methods and Antimicrobial Activity. *Tropical Journal of Pharmaceutical Research*, 12(1), 123-126.

Franson, M. A. H. (1994). *Standard Methods for the Examination of Water and Waste Water*, 18th edition, American Public Health Association Washington DC.

Ghafari, S., Abdul Aziz, H., Isa, M. H. and Zinatizadeh, A. (2009). Application of response surface methodology (RSM) to optimize coagulation–flocculation treatment of leachate using poly-aluminum chloride (PAC) and alum. *Journal of Hazardous Materials*. 163, 650-656.

Georgescu, A. M. and Georgescu, S. C. (2012). Chlorine Concentration Decay in the Water Distribution System of a Town With 50000 Inhabitants. *University POLITEHNICA of Bucharest Science Bulletin, Series D*, 74(1), 103-114.

Goyal, R. V. and Patel, H. M. (2015). Analysis of Residual Chlorine in Simple Drinking Water Distribution System with Intermittent Water Supply, *Applied Water Science* 5, 311-319.

Hua, F., West, J.R., Barker, R.A., Forster, C.F. (1999). Modelling of Chlorine Decay in Municipal Water System, *Water Research*, 33(12), 2735–2746.

Kowalska, B., Kowalski, D. and Musz, A. (2012). Chlorine Decay in water distribution systems. *Environmental Protection Engineering*, 32(2), 2006.

Model Data Science with R, (2017). CRC Press, *https://mdsr-book.github.io/excerpts/mdsr-regression.pdf*

Morley, D. A. (1979). *Mathematical Modeling in Water and Waste Water Treatment*, Applied Science Publishers Ltd, London.

Rossman, L. S., Brown R. A., Singer, P. C., Nuckols, J. R. (2001). DBP formation kinetics in a simulated distribution system, *Water Research*, 14, 3483–3489.

Tiruneh, A, T., Fadiran, A. O., Nkambule, S. J. and Zwane, L. M. (2016). Modeling of Chlorine Decay Rates in Distribution Systems Based on Initial Chlorine, Reactant Concentrations and Their Distributions. *American Journal of Science and Technology*. 3(3), 53-62.

Vasconcelos, J. J., Rossman, L. A., Grayman, W. M., Boulos, P. F. and Clark, R. M. (1997). Kinetics of Chlorine Decay, *Journal of American Water Works Association*, 86(7), 54-65.

White, G.C. (1986). *Handbook of Chlorination*. Van Nostrand Rain Bold, New York. 150-256.

Zheng, M. (2013). Factors Contributing to Chlorine Decay and Microbial Presence in Drinking Water Following Stagnation in Premise Plumbing. *An Unpublished Master's Thesis submitted to the University of Tennessee*. http://trace.tennessee.edu/utk_gradthes/2485

NUMERICAL SIMULATION OF TRANSIENT TURBULENT COMPRESSIBLE FLOW IN A NATURAL GAS PIPELINE

Effiong, E. E.[1], Orga, A. C.[1], Ibe, E. C.[1], *Ekeke, I. C.[1] and Nzebuka, C. G.[2]

[1] Chemical Engineering Department, [2] Materials and Metallurgical Engineering Department
Federal University of Technology, Owerri, Imo State, Nigeria
Author for correspondence; e-mail: ifyekeke@yahoo.com

ABSTRACT

Transient compressible natural gas flow through a pipeline was studied by the use of a finite volume method in 2D axisymmetric cylindrical coordinates. To account for turbulence within the pipeline system, the standard $k-\varepsilon$ turbulence equations were modeled together with the Navier Stokes equations via the Reynolds-Averaged method. The equation of state employed was the Soave-Redlich-Kwong equation. The Pressure Implicit with Splitting of Operators (PISO) algorithm was then used for calculating the pressure and velocities on a staggered grid. Computer simulation was carried out to determine pressure variation, density variation, velocity variation and temperature variation within the pipeline system. The shapes of the profiles obtained from the results were in agreement with those obtained in validated literature results.

Keywords: *Transient, compressible, cylindrical, axisymmetric, pipeline and turbulence.*

1. INTRODUCTION

Unsteady flow of natural gas in pipelines involves change of certain flow variables such as pressure, velocity, density, temperature with respect to time or distance as a result of disturbances in the system. The accurate prediction of these variables is therefore very important since this information gives the pipeline operator an insight into the behaviour of the system at any given point in time.

Many researchers in the past have modelled compressible flow in pipelines using various numerical methods. Siögreen (1995) employed the use of centered finite difference methods of general order of accuracy 2p to solve the compressible Navier-Stokes equations. Kessal et al (2014) analytically and numerically analysed a set of equations governing an isothermal compressible fluid flow in short pipeline. The equations were written in characteristics form and solved by a predictor-corrector lambda scheme for the interior mesh points. The method of characteristics was used for the boundaries. Accurate grid-converged results were obtained.

Behbahani-Nejad, et al (2008) presented an effective transient flow simulation based on the transfer function models and Matlab Simulink for gas pipelines and networks. In the paper by Nouri-Borujerdi (2011), simulation of transient 1D compressible adiabatic gas flows in a long pipeline following a catastrophic failure using a finite difference scheme was carried out. The advantages of this scheme are reduction of grid points, less computational effort and time with high accuracy. Noorbehesht (2012) modelled compressible natural gas flow in a transmission line at steady state in 2D cylindrical coordinates. The Navier Stokes equation, the ideal gas equation of state and the k-ε turbulence models were applied. A finite volume method, involving the SIMPLER algorithm (Patankar and Spalding, 1972; Patankar, 1980) was then used for the solution of the equations. Results obtained by this method agreed very well with experimental data obtained from the National Iranian Gas Company. An approximate 4% error proved the accuracy of this method. Finally, effect of variation in temperature of inlet gas, gas' flow rate, and ambient temperature on pressure drop and system's parameters were studied. In another paper, Noorbehesht, et al, (2013) investigated the dynamic behavior of natural gas in transmission line by same finite volume method applied earlier. The accuracy of this method was verified by comparing the experimental field data with this approach, showing errors of approximately 4 to 4.5%, which shows the precision of this approach. Finally, a case study was used as an application for the model and the best possible operating solution was proposed for a compressor station failure during winter. Nouri-Borujerdi et al (2007) investigated the numerical modeling of the dynamic behavior of compressible gas flow in pipelines by a finite-volume based finite-element method. The numerical simulation was performed by solving the coupled conservation form of the governing equations for 2D laminar, viscous, supersonic flows in

the developing region under different thermal boundary conditions. The results indicated that heating the gas flow leads to an increase in pressure loss. Nouri-Borujerdi et al (2010) again presented a study on 2D unsteady turbulent compressible high pressure gas flow with a rupture at its center numerically. A computer code based on a mixed finite element-finite volume formulation for an unstructured grid was used to solve the problem. The turbulence modeling is based on the $k-\boldsymbol{\varepsilon}$ model, followed by a two layer technique near the wall. His results show that the numerical scheme employed is stable and accurate.

So many other works have been carried out by researchers which cannot be listed here. Most of these works have been done in Cartesian coordinates. Few have been carried out in cylindrical coordinates. This work therefore presents a finite volume method for solving 2D transient gas flow in cylindrical coordinates using the real gas Soave-Redlich Kwong equation of state. The finite volume method involves the use of the Pressure Implicit Scheme with Splitting of Operators to solve the Reynolds-Averaged Navier Stokes equation in 2D axisymmetric cylindrical coordinates. The $k-\boldsymbol{\varepsilon}$ turbulence model is incorporated to enable the prediction of turbulent eddy viscosity. To the authors' knowledge, no work has been published which employs this same method of simulation. To validate the model, pressure data published by Noorbehesht (2012) which he obtained from the National Iranian Gas Company for the validation of the model he proposed were used. The geometry of the pipeline he considered for simulation was scaled down for the purpose of this simulation and a scale factor obtained. This scale factor was then used to calculate the inlet and outlet pressures employed in the present work to obtain an accurate result for the pressure profile. The profile is similar to that obtained by Noorbehesht (2012). This proves the accuracy of the solution used for the model. Profiles for temperature, density, velocity along the pipeline were also obtained.

2. THE MATHEMATICAL MODEL

The basic equations used to model flow in pipelines and employed in this work are the compressible Navier-Stokes equations. In carrying out this work, it was assumed that the cross-sectional area of the pipe is constant. Another assumption made is that the gas flow is highly turbulent.

2.1 Conservation of mass or continuity equation: In its general form, the continuity equation is expressed as *(*Bird et al, 2002);

$$\frac{\partial \rho}{\partial t}+\frac{1}{r}\frac{\partial}{\partial r}(\rho r V_r)+\frac{\partial}{\partial z}(\rho V_z) = 0 \quad (1)$$

2.2 Conservation of Momentum equation in terms of $\boldsymbol{\tau}$ in the r and z-directions: For gas flows in a pipe, the compressible Navier-Stokes equations can be written for the axial and radial directions, respectively (Bird *et al*., 2002) as;

$$\frac{\partial(\rho V_r)}{\partial t}+\frac{1}{r}\frac{\partial(r\rho V_r V_r)}{\partial r}+\frac{\partial(\rho V_r V_z)}{\partial z} = -\frac{\partial P}{\partial r}-\frac{1}{r}\frac{\partial}{\partial r}(r\tau_{rr})-\frac{\partial}{\partial z}\tau_{zr}+\frac{\tau_{\theta\theta}}{r} \quad (2)$$

$$\frac{\partial(\rho V_z)}{\partial t}+\frac{1}{r}\frac{\partial(r\rho V_r V_x)}{\partial r}+\frac{\partial(\rho V_z V_z)}{\partial z} = -\frac{\partial P}{\partial r}-\frac{1}{r}\frac{\partial}{\partial r}(r\tau_{zr})-\frac{\partial}{\partial z}\tau_{zz} \quad (3)$$

where

$$\tau_{rr} = -\mu_{eff}\left(2\frac{\partial V_r}{\partial r}-\frac{2}{3}(\nabla . v)\right) \quad (4)$$

$$\tau_{xz} = -\mu_{eff}\left(2\frac{\partial V_z}{\partial z}-\frac{2}{3}(\nabla . v)\right) \quad (5)$$

$$\tau_{xr} = -\mu_{eff}\left(\frac{\partial V_r}{\partial z}+\frac{\partial V_z}{\partial r}\right) \quad (6)$$

$$\tau_{\theta\theta} = -\mu_{eff}\left(2\frac{V_r}{r}-\frac{2}{3}(\nabla . v)\right) \quad (7)$$

$$\nabla . v = \frac{1}{r}\left(\frac{\partial}{\partial r}\right)(rV_r)+\frac{\partial V_z}{\partial z} \quad (8)$$

$\mu_{eff} = \mu + \mu_t = effective\ viscosity$ (Blazek, 2001)

2.3 Conservation of Energy Equation; The energy equation in its basic form in terms of temperature is;

$$\frac{\partial}{\partial t}(\rho c_p T)+\frac{\partial}{\partial z}(\rho c_p V_z T)+\frac{1}{r}\frac{\partial}{\partial r}(r\rho c_p V_r T) = \frac{\partial}{\partial z}\left(\left(\lambda+\frac{c_p\mu_t}{G_T}\right)\frac{\partial T}{\partial z}\right)+\frac{1}{r}\frac{\partial}{\partial r}\left(r\left(\lambda+\frac{c_p\mu_t}{G_T}\right)\frac{\partial T}{\partial r}\right)+S_T \quad (9)$$

2.4 Equation of State

The equation of state adopted in this work is the Soave-Redlich-Kwong equation stated as follows (Perry et al, 1997, Soave (1972)):

$$P = \frac{RT}{V-b}-\frac{a(T)}{V(V+b)} \quad (10)$$

$$where \quad a(T) = 0.4274\left(\frac{R^2T_c^2}{P_c}\right)\left\{1 + m\left[1-\left(\frac{T}{T_c}\right)^{0.5}\right]\right\}^2 \quad (11)$$

$$m = 0.480 + 1.57\omega - 0.176\omega^2 \quad (12)$$

$$b = 0.08664\frac{RT_c}{P_c} \quad (13)$$

The kinetic energy of turbulence, k and the turbulence dissipation term, ε are computed by solving the following two transport equations;

$$\frac{\partial}{\partial t}(\rho k) + \frac{\partial}{\partial x}(\rho V_x k) + \frac{1}{r}\frac{\partial}{\partial r}(r\rho V_r k) = \frac{\partial}{\partial x}\left(\left(\mu + \frac{\mu_t}{G_k}\right)\frac{\partial k}{\partial x}\right) + \frac{1}{r}\frac{\partial}{\partial r}\left(r\left(\mu + \frac{\mu_t}{G_k}\right)\frac{\partial k}{\partial r}\right) + S_k \quad (14)$$

$$\frac{\partial}{\partial t}(\rho \varepsilon) + \frac{\partial}{\partial x}(\rho V_x \varepsilon) + \frac{1}{r}\frac{\partial}{\partial r}(r\rho V_r \varepsilon) = \frac{\partial}{\partial x}\left(\left(\mu + \frac{\mu_t}{G_\varepsilon}\right)\frac{\partial \varepsilon}{\partial x}\right) + \frac{1}{r}\frac{\partial}{\partial r}\left(r\left(\mu + \frac{\mu_t}{G_\varepsilon}\right)\frac{\partial \varepsilon}{\partial r}\right) + S_\varepsilon \quad (15)$$

In the above equations, $S_k = \mu_t g - \rho\varepsilon$, $S_\varepsilon = C_1 g \mu_t \varepsilon k - C_2 \rho \frac{\varepsilon^2}{k}$ and $\mu_t = C_\mu \rho \frac{k^2}{\varepsilon}$, $C_\mu = 0.09, C_1 = 1.4, C_2 = 1.92, G_k = 1.00, G_\varepsilon = 1.3, G_T = 0.85$, V_r and V_z are the radial and axial velocity components (m/s), k is the thermal conductivity (W/mK), ρ is density (kg/m^3), μ is dynamic viscosity (Ns/m^2), τ is shear stress (N/m^2); r, z and θ are the radial, axial and azimuthal directions respectively; T, P, t, C_p and q are temperature (K), pressure (N/m^2), time (s), constant pressure specific heat capacity $(J/kgK)$and heat flux (W/m^2)respectively.

3. NUMERICAL TECHNIQUE

The finite volume method is the numerical solution method adopted in this work. It is one of many methods that come under a general name - Computational Fluid Dynamics. In using the finite volume method, the general form of the conservation equations of fluid for the geometry considered in this work, for any scalar variable ϕ can be represented as follows;

$$\frac{\partial}{\partial t}(\rho\phi) + \frac{\partial}{\partial x}(\rho V_x \phi) + \frac{1}{r}\frac{\partial}{\partial r}(r\rho V_r \phi) = \frac{\partial}{\partial x}\left(\Gamma\frac{\partial \phi}{\partial x}\right) + \frac{1}{r}\frac{\partial}{\partial r}\left(r\Gamma\frac{\partial \phi}{\partial r}\right) + S_\phi \quad (16)$$

ϕ represents any of the variables, $V_r, V_x, T, k \; and \; \varepsilon$ while $\boldsymbol{\Gamma}$ represents μ and k. In employing the method, bracketed smaller contributions to the viscous stress terms in the transport equation are hidden (Versteeg and Malalasekera, 2007). Equations 1, 2, 3, 10, 15 and 16 are then integrated over a control volume after which Gauss' divergence theorem is applied to give the following;

$$\int_{CV}\frac{\partial}{\partial t}(\rho\phi)dV + \int_A n.(\rho V_x \phi)dA + \int_A n.(r\rho V_r \phi)dA = \int_A n.\left(\Gamma\frac{\partial \phi}{\partial x}\right)dA + \int_A n.\left(r\Gamma\frac{\partial \phi}{\partial r}\right)dA + \int_{CV} S_\phi dV \quad (17)$$

The solution region comprising of a grid is then divided into discrete control volumes (CV). The CV surface consists of four (in 2D) plane faces, denoted by lower-case letters corresponding to their direction (e, w, n, s) with respect to the central node (P) (Ferziger and Peric, 2012)

The governing equations are then integrated over the CV to obtain a discrete equation on node P. The equation is as follows;

$$\frac{\rho_p(\phi_p - \phi_p^0)\Delta V}{\Delta t} + (\rho V_x A\phi)_e - (\rho V_x A\phi)_w + (\rho V_r A\phi)_n - (\rho V_r A\phi)_s = \left(\Gamma A\frac{\partial \phi}{\partial x}\right)_e - \left(\Gamma A\frac{\partial \phi}{\partial x}\right)_w + \left(\Gamma A\frac{\partial \phi}{\partial r}\right)_n - \left(\Gamma A\frac{\partial \phi}{\partial r}\right)_s + (S_p\phi_p + S_u)\Delta V_p \quad (18)$$

The integration of the continuity equation also gives;

$$\frac{(\rho_p - \rho_p^0)r\Delta x\Delta r}{\Delta t} + (\rho UA)_e - (\rho UA)_w + (\rho VA)_n r - (\rho VA)_s r = 0 \quad (19)$$

In the discretization of the governing equations, implicit discretization was employed in the temporal terms. A time step of 2.85596×10^{-6} seconds was used. Implicit discretization for unsteady flows has the advantage of producing unconditionally stable results. Central differencing scheme was used in the spatial diffusion terms while second order upwind differencing scheme was employed in the spatial convection terms.

The general discrete equation is then;

$$a_P\phi_P = a_W\phi_W + a_E\phi_E + a_S\phi_S + a_N\phi_N + a_P^0\phi_P^0 + S_U \quad (20)$$

where $a_P = a_W + a_E + a_S + a_N + a_P^0 + \Delta Fr - S_P$, $\Delta Fr = (F_e r - F_w r) + (F_n r - F_s r)$, $F_e = (\rho U)_e A_e$, $F_w = (\rho U)_w A_w$, $F_n = (\rho U)_n A_n$, $F_s = (\rho U)_s A_s$

In solving the above equation, the staggered grid arrangement was used. The reason for using staggered grid in solving pressure-velocity coupling equation is as a result of a uniform pressure field that would be obtained if velocity and pressure were stored at the same nodal points.

Next, a pressure-velocity calculation procedure, known as, Pressure-Implicit with Splitting of Operators (PISO) originally developed by Issa (1986) for the non-iterative computation of unsteady compressible flows was employed in the computation. It is a guess-and-correct procedure and has been adapted by Versteege and Malalasekera (2007) for steady flows. It involves one predictor step and two corrector steps. The method is an improvement to Semi-Implicit-Pressure Link Equation (SIMPLE) algorithm originally invented by Patankar and Spalding (1972) in the sense that it has an additional corrector step to enhance it. Furthermore, it is efficient and fast (Versteege and Malalasekera, 1995).

Boundary conditions

The boundary conditions for gas flow in pipeline in a 2D geometry are as shown in Figure 1.

Steady state condition

- *Fluid boundaries:*
  a. Inlet: $P, u \text{ and } T$ are defined and ρ is defined by state equation.
  b. Outlet: general condition of fluid which is almost commonly applied in finite volume method is as follows (Versteeg and Malalasekera, 1995, Noorbehesht,2012):

$$\frac{\partial T}{\partial n} = 0 \text{ and } \frac{\partial u_n}{\partial n} = 0$$

And a defined P_{out} aiming considered mass flow rate, and n is the normal outward vector of outlet surface.

- *Solid boundary:*

No slip condition; $u = u_w = 0$

Constant temperature on the wall; $T = T_w$

Symmetric boundary condition; $\frac{\partial \phi}{\partial n} = 0$

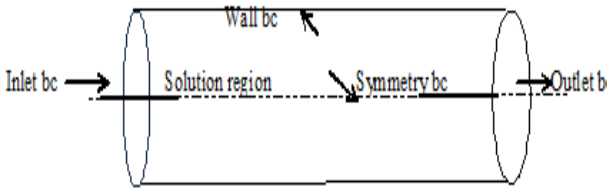

Figure 1: Flow domain and boundary conditions (Noorbehesht, 2012)

Initial Conditions for Unsteady State

The parameters $P, u, T \text{ and } \rho$ must be specified according to their initial values at $t = 0$ Therefore, the steady state condition data are also the initial conditions of the unsteady state.

Operating *Conditions*;

Pipe diameter D = 0.35m, pipeline length L = 500m; inlet pressure $P_{in} = 26337.01Pa$; outlet pressure $P_{out} = 20574.05Pa$; inlet temperature $T_{in} = 46.86$ ℃ ; outlet temperature $T_{out} = 34^oC$; *Physical properties of gas*; the current properties of the gas are assumed constant. Molecular weight $M_w = 19$; thermal conductivity k = 0.0332 W/mK ; specific heat at constant pressure $C_p = 2530\ J/kgK$;; viscosity, μ = $1.56 \times 10^{-5}\ kg/ms$.

4 RESULTS

Model Validation and Simulation

To validate the model, pressure data published by Noorbehesht (2012) which he obtained from the National Iranian Gas Company for the validation of a model he proposed were used. The pipeline he considered for simulation was 135km in length. Inlet and outlet pressures were 71.11bar and 55.55bar respectively while inlet and outlet temperatures were 46.86°C and 34°C respectively. For the purpose of validation of the model considered in this work, this pipeline length was scaled down to 500m. The scale factor was calculated by the method of geometric similarity presented by Rajput (1998). It was then used to obtain the inlet and outlet pressure values stated above (i.e. $26337.01Pa$ and $20574.05Pa$). The temperatures employed in the present simulation remained 46.86°C at the inlet and 34°C at the outlet. Steady state results were first obtained and then used as initial conditions for the unsteady state simulation. ANSYS FLUENT, a finite volume simulation software was used for simulation. The profile for pressure is similar to that obtained by Noorbehesht (2012). This proves the accuracy of the solution used for the model. Profiles for temperature, density, velocity, along the pipeline were also obtained. They are presented below.

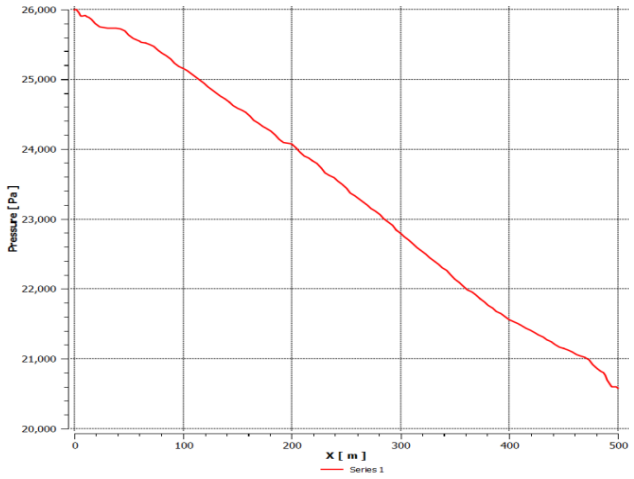

Figure 2: Graph of pressure distribution along the length of the pipeline

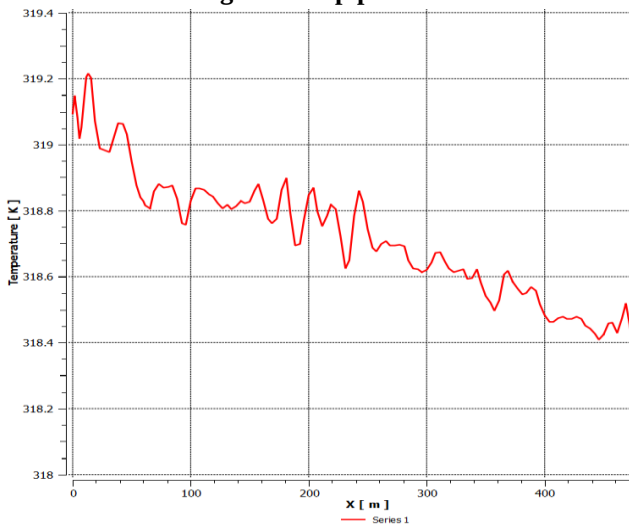

Figure 3: Graph of temperature distribution along the length of the pipeline

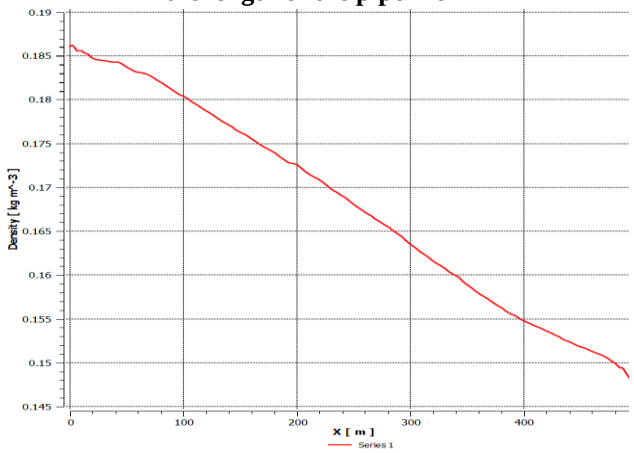

Figure 4: Density distribution along the pipeline length

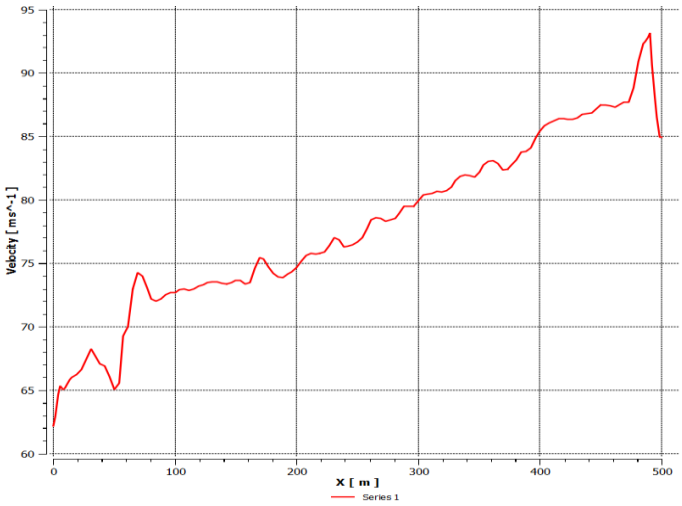

Figure 5: Velocity distribution along the length of the pipeline

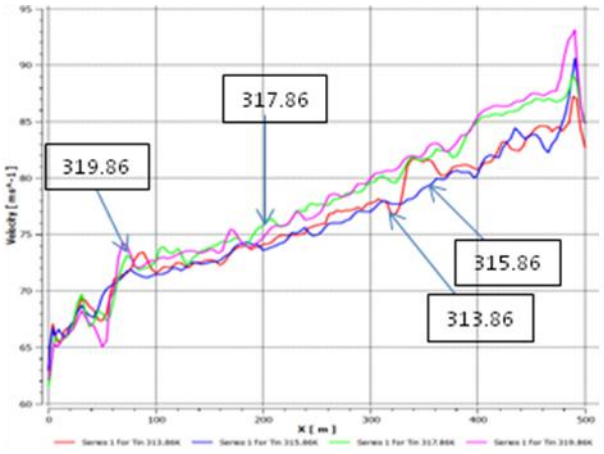

Figure 6: Variation of velocity along the pipeline length at different inlet temperatures

5. DISCUSSIONS

Figure 2 above shows a plot of the distribution of pressure along the pipe at transient condition. A drop in pressure from 26,000Pa at the pipe entrance to 20,600Pa 500m downstream of the pipe can be seen. This is to be expected since for a fluid flowing down a conduit, there's usually a pressure drop due to frictional resistance. The plot shows same trend as that obtained by Noorbehesht (2012), Noorbehesht and Ghaseminejad (2013), Nouri-Borujerdi (2011). The Figure 3 above shows a plot of the temperature distribution in the pipe at transient condition. There is also a decrease in temperature. This trend is the same as that of the pressure as can be seen since from the equation of state, pressure is directly proportional to temperature (Perry et al, 1997; Bansal, 2008).

Figure 4 and Figure 5 show plots of density and velocity respectively. It can be seen that density decreases along the length of the pipeline while the velocity plot shows a

reverse trend. This is in consonance with the mass flow rate equation shown below (which shows that velocity increases with density decrease);

$$m = \rho u A \quad (21)$$

Where $m = mass\ flow\ rate., kg/s, \rho = density\ of\ gas, kg/m^3, u = axial\ velocity, m/s$ $and\ A = cross-sectional\ area\ of\ pipeline, m^2$.

Figure 6 shows variation of velocity of gas with inlet temperature along the pipeline. Inlet velocity increases due to inlet temperature increase. The inlet temperatures include 313.86K, 315.86K, 317.86K and 319.86K. The increase of course stems from the fact that motion of gas molecules (hence their velocity) increases as temperature increases in a given system (Noorbehesht, 2012). This same trend is seen towards the end of the pipeline though the velocity values for the 315.86K and 317.86K inlet temperatures tend to be the same.

6. CONCLUSIONS

A method for predicting flow properties in a natural gas pipeline has been presented in this work. First, transient compressible natural gas flow was modeled via the continuity, momentum and energy equations together with the $k-\boldsymbol{\varepsilon}$ turbulence equations. The real gas Soave-Redlich-Kwong equation was included as an auxiliary equation. The method of simulation involved the use of the PISO algorithm on a staggered grid. ANSYS FLUENT was then used to carry out the simulation. The results of the simulation show that the method employed is adequate for predicting flow properties in a pipeline system. The method can be employed by the Oil and Gas industries for the knowledge/control of natural gas pipeline system behaviour.

REFERENCES

Bansal, R. K., (2008). A Textbook of Fluid Mechanics, (p. 19). Laxmi Publications (P) Limited, New Delhi.

Blazek, J., (2001). *Computational Fluid Dynamics: Principles and Applications*. Elsevier.

Behbahani-Nejad, M and Bagheri, A., (2008). A MATLAB Simulink Library for Transient Flow Simulation of Gas Networks. *World Academy of Science, Engineering and Technology*, 19.

Bird, R. B., Stewart, W. E. and Lightfoot, E, N., (2002). *Transport Phenomena* (p. 337). John Wiley and Sons, Inc.

Ferziger, J. H. and Peric, M., (2002), Computational Methods for Fluid Dynamics. Springer. 3rd edition.

Issa, R. I., (1986). Solution of Implicitly Discretised Fluid Flow Equations by Operator-Splitting. *J. Comput. Phys*., 62, 40–65.

Kessal, M., Boucetta, R., Zamoum, M. and Tikobaini, M., (2014). Numerical Modelling of transients in gas pipeline. *International Journal of Physical Sciences*, 9(5), 82-90.

Noorbehesht, N., (2012). Numerical Simulation of Natural Gas Flow in Transmission Lines through CFD Method Considering Effective Parameters. *J. Basic. Appl. Sci. Res*., 2(8), 7473-7487.

Noorbehesht, N. and Ghaseminejad, P., (2013). Numerical Simulation of the Transient Flow in Natural Gas Transmission Lines Using a Computational Fluid Dynamic Method. *American Journal of Applied Sciences*, 10 (1): 24-34.

Nouri-Borujerdi, A. and Ziaei-Rad, M., (2007). Numerical Prediction of Developing Flow in Gas Pipelines. *5th International Conference on Heat Transfer, Fluid Mechanics and Thermodynamics.*

Nouri-Borujerdi, A. and Ziaei-Rad, M., (2010). Numerical Modeling of Transient Turbulent Gas Flow in a Pipe Following a Rupture. *Transaction B: Mechanical Engineering*, 17(2), 108-120. © Sharif University of Technology, Tehran, Iran.

Nouri-Borujerdi, A., (2011). Transient modeling of Gas Flow in Pipelines following catastrophic failure. *Mathematical and Computer Modeling*, 54, 3037–3045.

Perry, R. H., Green, D. W. and Maloney, J. O., (1997). Perry's Chemical Engineers' Handbook, Seventh Edition (p. 4-21). McGraw-Hill.

Rajput, R.K., (1998). Fluid mechanics and Hydraulic Machines, S Chand and Company Limited.

Soave, G. (1972). Equilibrium constants from a modified Redlich-Kwong equation of state. Chemical Engineering Science. 27(6), 1197-1203.

Siögreen B., (1995). High Order Centered Difference Methods for the Compressible Navier-Stokes Equations. *Journal of Computational Physics*, 117, 67-78.

Versteeg, H K and W Malalasekera, W., (1995). *An introduction to computational fluid dynamics the finite volume method, First edition*. Longman Scientific and Technical.

Versteeg, H K and W Malalasekera, W., (2007). *An introduction to computational fluid dynamics the finite volume method, second edition*. Longman Scientific and Technical.

NOMENCLATURE

V_r	Velocity in the radial (r) direction, m/s
V_z, U, u	Velocity in the axial (z) direction, m/s
r	Radial direction
x, z	Axial direction, m
T	Temperature, K
t	Time, s
E	Total internal energy, J
k	Thermal conductivity, W/mK
$k,$	Kinetic energy of turbulence, J/kg
m	Mass flow rate, kg/s
A	Cross-sectional area, m^2
P	Pressure, N/m^2
L	Pipeline length, m
V	Volume, m^3
D	Pipeline diameter, m
C_p	Constant pressure specific heat capacity, J/kgK
q	Heat flux, W/m^2
g	Acceleration due to gravity, m^2/s
$\bar{Z}$	Average value for compressibility factor
R	Gas constant
Greek Characters	
μ	Dynamic viscosity, Ns/m^2
ρ	Density, kg/m^3
τ	Shear stress tensor, N/m^2
θ	Azimuthal direction
ε	Turbulence dissipation rate, m^2/s^3

DEVELOPMENT OF SOLID MINERALS IN AN ENVIRONMENTALLY AND SOCIALLY SUSTAINABLE MANNER

***Tsado, D. G.[1,2] and Ugwu, O. G.[2]**

[1]Department of Chemical & Process Engineering, Faculty of Engineering & Physical Sciences, University of Surrey, GU2 7XH, Guildford UK

[2]Department of Chemical Engineering, The Federal Polytechnic, P.M.B 55, Bida. Niger State. Nigeria

Correspondence e-mail: *davidadule@yahoo.co.uk*

ABSTRACT

In the development of solid mineral in any nation, the most important issue of noteworthy is that whereas mineral industries appreciate that they mine and process mineral to maintain and advance standard of living of humanity, they must do so in a manner that protects the earth and its environs so that the generations unborn are not adversely impacted and can enjoy its bounties. However, this paper explores solid mineral mining in the perspective of sustainable development or sustainability, and provides some guiding principle for mining industries wanting to operate more sustainably. Social and environmental issues are highlighted. Some sustainable practices for solid mineral development were brought to light which includes sustainable mining practices (safety, economy, resource efficiency, environment, community). Others sustainable practices discussed comprise environmentally sustainable mining, which recommended reduction in both the input (water, energy, land disruption) and output (waste, acid rock drainage) flow into mining system; and framework for responsible/ sustainable solid mineral development. Now that Nigerian government has recently revisited solid mineral roadmap with the view of license issuance to prospective miners, it will become increasingly important that mines should start pursuing socioeconomic and environmental issues with improved strategy that involves sustainable development into mode of operations in the companies.

Key Words: *environment, social, sustainable development, mining*

1.0 INTRODUCTION

Minerals are considered to be the key to development and the foundation upon which our modern society is built. Goods made from mineral raw materials are the basis of all advanced societies. Adequate supplies of mineral materials and wise usage of mineral resources have always been the most important determinants of a nation's survival (Adekeye, 1999). Minerals and metals have brought huge benefits to society – they are vital commodities that serve as a foundation to society's material quality of life. In today's world, population growth, urbanization, social and economic development and even demands for a green (or low carbon) economy are all contributing to an increase in the demand for minerals. However meeting that demand and achieving the benefits comes at a cost (ICMM, 2012; Adekeye, 1999).

There have been disputes over land use, property rights and environmental damage, concerns about revenue transparency and corruption and a growing debate about the distribution of the benefits of mineral wealth. Tensions within communities and regions have often been the result. In the extreme, there has been conflict. However, mining is a key contributor to economic growth and improved material quality of life. Mining's long time horizon, its need for both skilled and unskilled labour, its links to regional infrastructure and service development as well as the importance of the products that it produces, means that its activities should be conducted in a manner which is environmentally and socially acceptable to be able to contribute sustainable development. With responsible public and private management, the mining and metals industry can contribute to poverty alleviation across the world while maintaining ecosystem integrity (ICMM, 2012).

To date, it appears that the main constraints to sustainability in the mining sector derive from the ever-increasing demand for mined resources; the consumption of resources (mostly energy and water) needed to extract and process metals; and the increasing pollution generated by the extraction process. This holds true for both large-scale, often multinational corporate, operations as well as for small-scale or artisanal ventures (SDKP, 2016). Unless the environmental and social issues that are associated with solid mineral development are managed, the considerable disruption to livelihoods and to the social fabric of communities in the mines can negate any positive and long- term benefits that solid mineral mining brings (Rajaram *et al.*, 2005).

From the perspective of mining companies, reducing impacts and risks eventually translate into lower costs of doing business—and provide opportunities for building relationships with local communities. Better community relations reduce the chances of conflict between the mining industry and those who work in or live nearby mining operations. Poor community relations can even

lead to the militarization of the mining site and draw the company into wider conflict (Rajaram *et al.,* 2005).

Transparency, effective regulation and good corporate governance can unlock the potential for extractive industries to operate as a force for social progress. In this work, solid mineral mining operations are thoroughly explored in light of sustainable development for responsive social and environmental practices.

2.0 SUSTAINABILITY IN RELATION TO SOLID MINERAL INDUSTRIES

The concept of sustainability has been defined as "meeting the needs of the present without compromising the ability of the future generations to meet their needs" (WCED, 1987). To the perspective of solid mineral development, sustainability should mean to meet the people's need at a safe, low cost, and low environmental harms pending the availability of an appropriate alternative energy resource is put in place; and not to mean production sustenance of the energy source for indefinite time (Lyn, 2003). In a nut shell, the various competitive needs of human needs have to be balanced economically, socially and environmentally in the domain of sustainable development (Sustainable Development Commission, 2011; WCED, 1987).

Furthermore, sustainable development can be seen by solid mineral industries, firstly, in terms of concern on environment that results from the way and manner they operate. Their manner of industrial operations can lead to damages on the environment, for example, air, soil and water pollution, disruption of vegetation and wildlife, waste, and greenhouse harms. Secondly, in terms of development which explains the big role private sector can play in poverty reduction and educational improvement through practices of social responsibility. Development is still an aspect of social problems which also includes health, human rights, safety, and issues relating to the harmful impacts of industrial activities on indigenous communities in developing countries (Jenkins, 2005).

3.0 SOCIAL ISSUES IN MINING SOLID MINERALS

In most of resource-rich countries, especially the developing countries, extractive industries employ relatively few people. But their operations have wider effects on local communities, which often feel excluded from the benefits and the wealth that extractive industries generate, and harmed by the disruption or ecological impacts of extraction (Africa Progress Report, 2013). In respect of this, there is need for effective social responsibility, which is the responsibility of an organisation for the impacts of its decisions and activities on society and the environment, through transparent and ethical behaviour that:

- contributes to sustainable development, including health and the welfare of society;
- takes into account the expectations of stakeholders;
- is in compliance with applicable law and consistent with international norms of behaviour; and
- is integrated throughout the organisation and practised in its relationships (ISO, 2010).

The following are "Big Five –Tough" Social Issues as it relates to solid mineral development (SRK Consulting, 2015).

i. Involuntary resettlement. Economic and physical displacement of communities often accompanies mining projects. Resettlement is an emotional issue, with human rights a prominent concern. When resettlement processes are badly managed, reputations can be severely damaged, and the process is difficult to reverse. There is need to develop best-practice Resettlement Frameworks and Action Plans, incorporating provisions to restore livelihoods and to improve quality of life.

ii. Indigenous peoples. Indigenous peoples have strong links with the natural environment, and especially with land. Miners seeking to work in areas where land and other traditional rights are in play face complex issues, and sometimes get limited help from governments reluctant to deal with traditional rights. So it is required to plan and undertake appropriate consultation with local indigenous communities.

iii. Artisanal mining. Artisanal mining provides a living for many poor people in resource-rich developing countries. The sector is often unregulated, with formal miners having to compete with artisanal diggers for their own resources. Governments often deal erratically with artisanal miners, and some companies that have taken strong action have been accused of rights abuses. There is need to develop Strategies and Action Plans to address volatile artisanal mining situations.

iv. Corporate governance and standards. Many developing countries have weak legislation on the management of mining impacts, and the use of tax and royalty revenues. This may allow some officials to adopt corrupt practices, and some miners to dodge responsibilities. Therefore it is advisable that the mining industries to make use of international instruments that promote financial transparency (for example, the Extractive Industries Transparency Initiative), and on internal arrangements to promote and entrench best-practice governance.

v. Corporate social investment (CSI). Mining contributes to the economies of many developing countries; however, the wealth may not reach local communities. Responsible miners often seek to contribute to local development, but they face a number of challenges, including unrealistic expectations and a plethora of deserving projects. The mining industries should pursue CSI strategies that are defensible and sustainable. They should also establish Development Foundations, based on a partnership between mines and communities.

4.0 ENVIRONMENTAL ISSUES IN MINING SOLID MINERALS

Mining activities are carried out in various stages, each of which raises specific environmental concerns. Broadly speaking, these stages are: deposit prospecting and exploration, mine development and preparation, mine exploitation, and treatment of the minerals obtained at the respective installations with the aim of obtaining marketable products. The most important environmental impact as a result of solid mineral development includes: impacts on water resources (acid mine drainage and contaminant leaching; erosion of soils and mine wastes into surface waters; impacts of tailing impoundments, waste rock, heap leach, and dump leach facilities; and impacts of mine dewatering). Others are impacts of mining projects on air quality as a result of emissions; impacts of mining projects on wildlife (habitat loss; and habitat fragmentation); impacts of mining projects on soil quality; leakages of chemicals; and lastly, climate change considerations (EIAs, 2015).

Environmental impacts thus become economic and social issues as livelihoods are disrupted. Environmental impacts continue well after the mine has been exhausted, so it is local communities that bear the long-term burden of mining. The environmental legacy of mining in Africa is generally that of large unfilled holes and abandoned artisanal mining sites (*Kaushik and Kaushik, 2010).*

5.0 SUSTAINABLE MINING PRACTICES IN SOLID MINERAL INDUSTRIES

A body of literature exists suggesting that mining can contribute to sustainable development by focusing on successful economic, environmental and community outcomes. However, in a mining context, these pillars (the triple bottom-line) fail to adequately account for two important areas, essential for a sustainable mining operation, as illustrated by the Broken Hill example. One "missing" dimension is safety, which receives more attention in the mining sector than arguably any other industry. The media coverage and political focus applied to any mine "accident" exceeds virtually all other industries. It is not unusual for regulators to force a mine to close on the basis of a poor mine safety record (DRET, 2011).

The second missing dimension is a focus on extraction practices of the mineral resource itself. In the literature, researchers have tended to concentrate on the exhaustibility of the resource as a depleting asset (Auty and Mikesell, 1998). However, the researchers approach the subject from a macro level and usually from an economic perspective. It is suggested that there is a need to focus on the micro level, at the individual mine site, where the resource is managed sustainably or unsustainably. This element or dimension can be termed 'resource efficiency' or simply 'efficiency'. It differentiates mining from other industries and is the basis or platform for any sustainable benefit to flow to the community (DRET, 2011). Mine managers will be on track in establishing a sustainable mining operation if they then focus on the following five areas: safety, environment, economy, efficiency and the community (Laurence, 2011).

Safety

For both ethical and business reasons, a mining operation should aim to prioritise safety. Characteristics of safe mines include a commitment to risk management; appropriate attitudes and behaviours; reporting systems need to be in place; a focus on education and training; and a focus on processes and equipment (Laurence, 2005).

Economy

Unless a mine is profitable, it cannot be sustainable. The aim for mine managers is to generate profit responsibly for as long as possible by keeping costs to a minimum while maximizing revenue. This will also maximize the equitable benefits to all stakeholders, including shareholders, employees, local communities and businesses, which depend on the mine, as well as the governments that benefit by means of taxes and royalties.

Resource Efficiency

A mine also has to be efficient in the way the resource is managed and extracted. Mining engineers, geologists and metallurgists collaborate to optimize resource extraction. Examples of non-sustainable mining practices abound and include "high grading" the ore body, which entails mining only the highest grade material for short term gain. This is a practice used by companies and individuals within those companies with a short time frame. Efficiency also encompasses the management dimension at a mine site, as poor management decisions can often lead to production difficulties or equipment breakdown or industrial relations or other factors that impact on optimum resource extraction (Mitchell et al., 1995).

Environment

Adopting leading environmental management practices on mine sites makes excellent business sense. Unless steps are taken in the planning and operational stages to protect environmental values, long-term liabilities such as acid mine drainage, may result. Thanks in part to the increasing awareness of environmental issues, there is considerable literature relating to the environment and sustainable development.

Community

Finally, a mine needs a 'social licence to operate' Unless the community is engaged and supportive of a mining operation, opposition and confrontation may ensue. Mining operations run by corporations have been disrupted on many occasions in the recent past particularly from local artisanal and small-scale miners, who were mining in many cases before the commencement of the larger-scale operations.

Dysfunctional community interaction will ultimately distract management from its main focus of efficiently running the mine. Enlightened mining companies, particularly those operating in the developing world, maintain their social license to operate by undertaking various initiatives, including preferentially employing

local people; training and providing skills in businesses or enterprises that will endure after the mine closes and so on.

6.0 ENVIRONMENTALLY SUSTAINABLE MINING

Developing and integrating practices that reduce the environmental impact of mining operations can make mining become more environmentally sustainable. These practices include measures such as reducing water and energy consumption, minimizing land disturbance and waste production, preventing soil, water, and air pollution at mine sites, and conducting successful mine closure and reclamation activities.

However, although mining process itself may not consume vast portion of land but the infrastructure and pollution linked to mining activities have a serious potential to affect the health of ecosystems and reduce their ability to provide the goods and services necessary for human and environmental well-being (Rajaram *et al.,* 2005). When the environment is healthy to future generations yet unborn is recognized as satisfying the concept of sustainable development.

In order to be more environmentally sustainable, mining operations are increasingly conducted in a manner that minimizes their impact on the surrounding environment, and leaves mine sites in an acceptable state for re-use by people or ecosystems. A number of management strategies and technologies that should be developed and used by the mining industry to reduce the environmental impacts of mining, and are discussed below:

a. Reducing Inputs

i. Water

In mining, water is used within a broad range of activities including mineral processing, dust suppression, slurry transport, and employee requirements. Water is used in a number of applications at mine sites. By diverting surface water and pumping groundwater, mining operations can reduce both the quantity and quality of water available downstream for aquatic ecosystems and other industrial and municipal water users, especially in areas with arid climates.

In response to water scarcity in many mining regions, a number of innovative water conservation practices are being developed and implemented to reduce water use.

Various control techniques can be used to reduce the potential for water contamination and minimize the volume of water requiring treatment. These techniques include (Lottermoser, 2012):

1. **Intercepting and diverting surface water** (rain and snowmelt runoff, streams, and creeks) from entering the mine site by building upstream dams to reduce the potential for water contamination from exposed ore and waste rock
2. **Recycling water used for processing ore** in order to reduce the volume of water requiring treatment
3. **Capturing drainage water** from precipitation at the mine site through the use of liners and pipes and directing the water to tailings dams in order to prevent potentially contaminated water from entering groundwater or flowing off site
4. **Allowing the water to evaporate in ponds** to reduce the volume of contaminated water; in dry regions, enough water may be evaporated that no water needs to be discharged, resulting in the containment of contaminates at the mine site
5. **Installing liners and covers on waste rock and ore piles** to reduce the potential for contact with precipitation and contamination of groundwater

Different combinations of strategies can be applied, and the selection of strategies is site-specific. (Lottermoser, 2012).

ii. Energy

Mining and metal processing can be very energy-intensive processes. For instance, diesel fuel is used by trucks and excavators during mining, electricity is used to grind ore and refine copper and aluminum, and coal is required in order to smelt iron ore and make steel (Rankin, 2011). The extraction of fossil fuels (coal, oil, and gas), and the construction of infrastructure required for energy generation have their own environmental impacts, including the production of greenhouse gases and increased risk of environmental contamination along the energy supply route. Reducing energy consumption at mines can reduce greenhouse gas emissions and extend the life of fossil fuel reserves in addition to reducing operating costs and therefore the cost of the commodity being mined (Rankin, 2011). Mining companies are also investigating renewable energy sources to reduce costs and reliance on external energy sources including solar power in Chile and wind turbines.

iii. Land disruption

Mine sites currently disturb a small fraction of the Earth's total land surface. However, mining activities use land at every stage of the mine cycle, including exploration, construction, operation, closure, and post-closure (ICMM, 2011). Vegetation is cleared for the construction of buildings, roads, and powerlines, open pits or tunnels are dug to gain access to the ore, and waste storage facilities such as tailings ponds are expanded over the life of the mine, potentially leading to habitat loss and deforestation (ICMM, 2011).

There are a number of ways to reduce the land-use impacts of mining. These include reducing the overall footprint of the mining area, minimizing the amount of waste produced and stored, maintaining biodiversity by transplanting or culturing any endangered plants found on site, and planning mines around existing infrastructure where possible (ICMM, 2011).

b. Reducing Outputs

i. Waste

Mine waste includes solid waste, mine water, and air particles, which can vary significantly in their composition and potential for environmental contamination. In addition to preventing soil, water, and

air pollution, waste management plans are required in order to select and design appropriate storage facilities for the large volumes of waste produced at most mine sites (Rajaram *et al.,* 2005). Methods for minimizing and eliminating wastes in the production of minerals and metal commodities include (Rankin, 2011): using cleaner production techniques; environmental control technologies; using waste as raw material, and reducing the amount of waste produced through process re-engineering.

Water management strategies are used to reduce the volume of waste water produced, and if necessary, to treat it to an acceptable quality before it is released (Rajaram *et al.,* 2005).

ii. Acid Rock Drainage

Acid rock drainage (ARD) or acid mine drainage refers to the acidic water that is created when sulphide minerals are exposed to air and water and, through a natural chemical reaction, produce sulphuric acid (NAP, 2012). ARD has the potential to introduce acidity and dissolved metals into water, which can be harmful to fish and aquatic life. Preventing and controlling ARD is a concern at operating mine sites and after mine closure. ARD can pollute surface and groundwater with acidity and dissolved metals, which can adversely affect aquatic organisms and water users downstream. A number of strategies are used to predict, prevent, and mitigate ARD at mine sites.

iii. Restoring Environmental Function at Mine Sites

Mining is a relatively temporary activity, and mine sites have finite operating lives which are determined by the size and quality of the ore deposit being mined. Mine site reclamation and closure activities aim to restore land disturbed by mining activities to an acceptable state for re-use by people or ecosystems.

7.0 FRAMEWORK FOR RESPONSIBLE/ SUSTAINABLE SOLID MINERAL DEVELOPMENT

To achieve a responsible solid mineral development, the following framework has been highlighted (Doreen, 2016).

i. Builds on MMSD (Mining, Minerals and Sustainable Development) and, ICMM (International Council on Mining & Metals)
ii. Deciding whether a mine is an appropriate use of land. The need to preserve ecologically and culturally significant areas and to weigh land and resource use options is very paramount to sustainable mining development. For instance, Mining should not occur in any marine protected areas or in any site that is categorized as protected or restricted areas, and companies should ensure that their projects provide net conservation benefits that are consistent with maintaining the biological resources and ecosystem services on which local communities depend.
iii. Ensuring environmentally responsible mine development. Once a decision to mine has been made, certain environmental provisions should be in place to avoid negative outcomes and capitalise on benefits. This point details the environmental issues that need to be addressed at each stage of mine development. This includes: exploration management, environmental impact analysis, water contamination and use, air, energy consumption, noise, waste management, cyanide, reclamation and rehabilitation, financial guarantees, and post-closure.
iv. Ensuring that mine development results in benefits to workers and affected communities. This includes issues related to free, prior, and informed consent of communities for mining, health and safety provisions, capturing benefits more broadly, and developing consent agreements with communities. Others include participation of workers and the host communities in decision making/consultation, access to information/disclosure, consent-benefit and compensation agreements, recognizing women's rights and addressing gender-related risks, recognizing labour rights and addressing worker-related risks, resettlement/relocation and compensation, and security issues and human rights.
v. Ensuring that appropriate corporate governance structures are in place. Include broader corporate or national governance provisions to ensure transparency in revenue payments between governments and companies, and reporting company progress made toward implementing responsible practices.

8.0 CONCLUSION

This article presented sustainability as an increasingly prominent discourse, particularly among solid mineral mining companies, clarifying exactly how solid minerals can be developed and operated in an environmentally acceptable and socially responsible manner to be able to gain and sustain the full economic benefit derivable from this natural resource. Since solid mineral development has potentials to impact a wide range of environmental and social units in the mode of operations, there is need for commitment to improve environmental performance, and also collaborate with the stakeholders and community groups from the onset. To make this happen, the concept of sustainability needs to be employed. This paper has also presented some guidance for prospective mining industries that have interest to improve on their sustainable way of operation. Some sustainable practices for solid mineral development were brought to light which includes sustainable mining practices; environmentally sustainable mining which recommended reduction in both the input and output flow into mining system; and framework for responsible/ sustainable solid mineral development. Now that Nigerian government has recently revisited solid mineral roadmap with the view of license issuance to prospective miners (Kayode, 2015; Kayode, 2016), it will become increasingly

important that mines should start pursuing socioeconomic and environmental issues with improved strategy that involves sustainable development into mode of operations in the companies.

REFERENCES

Adekeye ,J. l. D. (1999). Solid Minerals Development: Nigeria's Economic Mirage. *Journal of Earth Sciences Research Communications* 1(1); 10 – 24.

Africa Progress Report, (2013). *Stewarding Africa's Natural Resources for all.* Retreieved from: http://appcdn.acwuploaded.co.uk/wpcontent/uploads/2013/08/2013_APR_Equity_in_Extractives_25062013_ENG_HR.pdf [Accessed 12/8/2016]

Auty, R.M. and Mikesell, R.F., (1998). *Sustainable Development in Mineral Economies*. Clarendon Press, Oxford.

Department of Resources, Energy and Tourism (DRET). (2011). *A guide to leading Practice sustainable Development in mining.* Retrieved from: http://www.industry.gov.au/resource/Documents/LPSDP/guideLPSD.pdf [Accessed 24/7/2016]

Doreen Fedrigo (2016). *Towards a responsible mining industry - The environmental dimension.* Retrieved from: http://www.eesc.europa.eu/resources/docs/fedrigo.pdf [Accessed 29/7/2016]

EIAs, (2015). *Guidebook for Evaluating Mining Project*. Retrieved from: https://www.elaw.org/files/mining-eia-guidebook/Chapter1.pdf [Accessed 24/7/2016]

International Council of Mining and Metals (ICMM) (2012). *Mining's contribution to sustainable development.* Retrieved from: http://hub.icmm.com/document/3716 [Accessed 24/7/2016]

International Council on Mining & Metals (ICMM), (2011) *The Role of Mining and Metals in Land Use and Adaptation*. Retrieved from: http://www.icmm.com/library/inbrief-the-role-of-mining-and-metals-in-land-use-and-adaptation. [Accessed 29/7/2016]

International Standards Organization, (ISO) (2010) ISO 26000 Project Overview. Retrieved from: http://www.iso.org/iso/iso_catalogue/management_and_leadership_standards/social_responsibility/sr_iso26000_overview.htm [Accessed 24/7/2016]

Jenkins, R. (2005). Globalization, corporate social responsibility and poverty. *International Affairs*. volume *81*, issue 3, pp.525-40. Retrieved from: DOI: 10.1111/j.1468-2346.2005.00467.x [Accessed 12/8/2016]

Kayode F. (2015). *State of the Solid Minerals Sector and Way Forward*. Retrieved from:www.ekekeee.com [Accessed 22/8/2016]

Kayode F. (2016). *A Road Map for the Solid Minerals Sector.* Retrieved from:www.thisdaylive.com [Accessed 22/8/2016]

Kaushik Anubha and Kaushik, C.P. (2010). Basics of Environment and Ecology. New Delhi: New Age International (p) Limited, Publishers.

Laurence, D.C. (2011). Establishing a Sustainable Mining Operation—An Overview *Journal of Cleaner Production* Vol. 19, Issue 2-3, Elsevier Science Ltd

Laurence, D.C. (2005). Safety Rules and Regulations on Mine Sites—The Problem and a Solution. *Journal of Safety Research*. Vol. 36, Issue 1, p. 39-50

Lottermoser, B. (2012). *Mine Wastes: Characterization, Treatment and Environmental Impacts*. Springer: New York. p.400

Lyn, A. (2003). HSE Horizons: Sustainable Development in Oil and Gas Industry. *Exploration and Production Environmental Conference.SPE/EPA/DOE*. San Antonio, Texas, 10-12 March 2003. Retrieved from: www.spe.org/jpt/print/archives/2003/.../JPT2003_08_hse_horizons.p... [Accessed 24/7/2016]

Mills, C. (2011). *An Introduction to Acid Rock Drainage*. InfoMine. Retrieved from: http://technology.infomine.com/enviromine/ard/Introduction/ARD.HTM. [Accessed 20/8/2016]

Mitchell M. et al., (1995). *A Methodological Framework for Development of Indicators of Sustainable Development, International Journal of Sustainable Development and World Ecology*, vol. 2, no. 2, p.26-33

NAP: The International Network for Acid Prevention (2012). *Global Acid Rock Drainage Guide Summary*. Retrieved from: http://www.gardguide.com/index.php/Summary. [Accessed 24/7/16]

Rajaram, V., Dutta, S. and Parameswaran, K., (2005). *Sustainable Mining Practices: A Global Perspective.* Taylor and Francis Group, Leiden, The Netherlands. pp. 1-11, 45-89, 193-230.

Rankin, W.J., (2011). *Minerals, metals and sustainability: meeting future material needs*, Collingwood, Vic.: CSIRO Pub.

Mills, C. *An Introduction to Acid Rock Drainage*, 2012 [cited 2012 June 26]; InfoMine. Retrieved from: http://technology.infomine.com/enviromine/ard/Introduction/ARD.HTM.

SRK Consulting, (2016). *Big five - Tough Social Issues in Mining*. Retrieved from: http://www.srk.com/files/File/newsletters/SRKnews41-social-assessment-A4.pdf [Accessed 24/7/2016]

Sustainable Development Knowledge Plateform (SDKP). (2016) *Mining*. Retrieved from: https://sustainabledevelopment.un.org/topics/mining [Accessed 20/8/2016]

World Commission on Environment and Development, WCED. (1987). *Our Common Future*, Oxford University Press, Oxford. Pp 8-46

DEVELOPMENT OF MODEL FOR METHANE FLOW IN COAL AS POROUS MEDIA

***Dagde, K. K., and Ehirim, E. O.**
Department of chemical/petrochemical engineering
Rivers state university of science and technology,
Port Harcourt, Rivers State, Nigeria.
dagde.kenneth@ust.edu.ng

ABSTRACT

The primary objective of this work is to develop a model capable of predicting the single-phase flow of methane through coal as a porous media. The model was developed by applying the principle of conservation of mass on a controlled volume of coal seam and incorporating the Darcy's law for laminar flow of methane. The model was solved numerically using implicit formulation of Finite Difference method. The result was validated with literature data. Predictions were made on the sensitivity of the model by varying parameters such as permeability, cleat distance, temperature, permeability, porosity, viscosity and the partial pressure. The result obtained showed that an increase in permeability led to an increase in effective stress and decrease in flow rate. Permeability and porosity are flow characteristics that influence fluid flow through its pores. The result also indicated that permeability is highly dependent on the applied gas pressure and the rock stress. The model will aid the extraction of methane for economical recovery and use, as well as underground mine degassing for safety reasons and also can be integrated into existing reservoir simulator to predict the variability of reservoir properties and how operating parameters affect performance under real conditions.

Keywords: *Modeling, Coal seam, Porous Media, Darcy's Law, Permeability, Partial Pressure.*

1.0 INTRODUCTION

Substantial amount of methane rich gas are generated and stored in coal formation. The coalification process whereby plant material is progressively converted to coal generates large quantity of methane rich gas, which is stored within the coal structure. In the process of coalification, coals increase in rank from lignite to sub-bituminous, bituminous and anthracite. Coal rank directly influences the gas (methane) storage capacity of coal. The type of organic material, depositional setting, pH, temperature, reducing potential depth of burial and time of burial influence the rank and type of coal formed(Saulsberry *et al.*, 1996). Most commercial coal bed methane is domicile in coals within the rank range of sub-bituminous to low volatile bituminous coal. Coal of this rank usually provides optimum gas (methane) content and natural permeability. The lignite, anthracite and graphite rank are usually low in methane gas because of its extremely low permeability, the lignite has high porosity while the anthracite and graphite are of low porosity and high volatile components drive off (Alpern and Lemos de Sousa, 2002). The presence of this gas has been recognized due to explosion and outburst associated with underground mining [Harpalani and Schraufnagel, 1990]. The recovery process of methane in coal begins with a production well that is often stimulated by fracturing to connect the well bore to the coal natural fracture system through an induced fracture [Mazumder *et al.*,. 2001]. There are two types of fractures that occur in coal, these are termed butt cleat and face cleats. Face cleats develop first and tend to be more continous than butt cleats. Butt cleats usually form at right angle to face cleats and are discontinuous, resulting in lower permeability (Harpalani and Schraufnagel, 1990). When the pressure in the well is reduced by pumping water from the well using artificial lift mechanism, the pressure in the induced fracture is reduced which in turn reduces the pressure in the natural coal fracture system. Initially, when the natural coal fracture system pressure drops the critical desorption pressure, methane starts to desorp from the primary-secondary porosity interface and is released into the secondary porosity system [Andersen, 2003]. As a result, the absorbed gas concentration is the primary porosity system near the natural fractures is reduced. This reduction creates a concentration gradient that result in mass transfer by diffusion through the micro and meso porosity [Mazumder *et al.*, 2001]. Adsorbed methane continues to be released as the pressure is reduced. Methane is extracted from coal mines to majorly reduce its emissions which causes mine explosion and for use as a clean source of fuel [Hargraves, 1984].

The need for reservoir models that can predict and evaluate production capability of coal gas is apparent.

There are many models of reservoir available.of which Karacan *et al.,* (2011; 2007) presented the Finite Element Method Laboratory (FEMLAB) technique for improving gas management in coal mines. Wang (2003) also used the Computational Fluid Dynamic (CFD) modeling technique in investigating the significance of ventilation and gas management during coal mining. Curl (1978) and Hargraves,(1984) have given detailed reviews on the nature and characteristics of methane content in coal seams. Lama and Nguyen (1987) conducted diffusion test, permeability test, desorption test on a cylindrical specimen to determine flow of methane. Wide spread utilization of coal bed methane model has established the tools for analyzing and estimating production from coal bed methane mines. It is the aim of this study to predict the single-phase flow of methane through coal as a porous media [Harpalani & Schraufnagel, 1990]. In this study, a model is developed for the extraction of methane for economical recovery and use, as well as underground mine degassing for safety reasons and also can be integrated into existing reservoir simulator to predict the variability of reservoir properties and how operating parameters affect performance under real conditions. Numerical MATLAB technique was adopted for simulation.

2.0 MODEL DEVELOPMENT

Figure 1 depicts a hypothetical representation of coal cleat with continuous methane flow across its boundary. Methane molecules absorbed from the sites, *diffuse through the coal matrix till they find a cleat [Harpalani & Zhao, 1991]. After entering the cleat system, this flow follows the Darcy's law and come out. The coal bed is made up of small cubic blocks separated by fractures. The spacing of the fractures determines how far the methane has to diffuse before reaching the fracture and the dimension of the fracture decides the quantity of methane that can flow through [Harpalani *et al.*, 1990]. The one dimensional, coal matrix is considered as a prism. This methane diffuse through micro pores and meets the cleats [Gamson et al., 1992]. These cleats allow it to flow to the bore well.

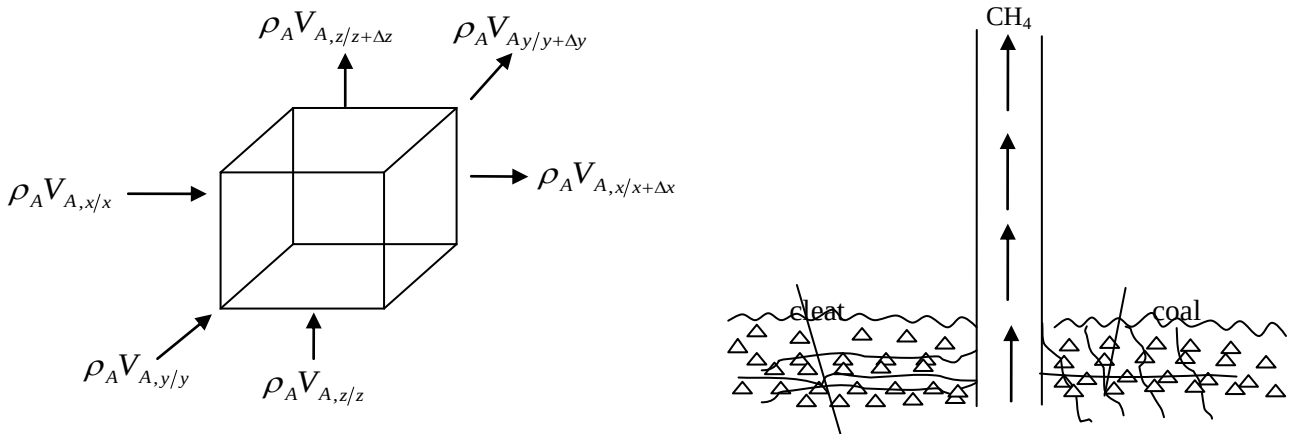

Figure 1A & B: Hypothetical representation of coal body with flow of methane gas

where ρ_A is the density of methane, $V_{A,x,y,z}$ is the velocity of methane in the x, y, z direction respectively, the methane enters at point x, y or z and exists at $x+\Delta x$, $y+\Delta y$ and $z+\Delta z$ respectively.

2.1 Model Assumptions

In the derivation of the model, the following assumptions are made:

1) The flow of methane inside the cleats is considered as laminar and hence Darcy's law is applicable (Lama and Nguyen, 1987; Wang, 2013).
2) The coal body is a rectangular prism.
3) Gravitational effects are negligible
4) The effect of diffusion is neglected in the cleats.
5) Isothermal condition is assumed during degasification process
6) The width and cleat spacing remains constant during the gas flow period
7) No accumulation of methane at the fracture surface.

8) During desorption of methane there exists no matrix shrinkage.
9) Permeability is assumed to be constant while it varies as per the Klinkenberg Law (Lama and Nguyen, 1987). .

Under these conditions, the general relation for mass balance of methane flow in and out of the control volume for a rectangular prism without chemical reaction may be stated as:
[net rate of mass efflux of methane for control volume] + [net rate of accumulation of methane within the control volume] = 0 (1)
Defining each term and substituting appropriate variables into equation (1) yields:

$$\frac{\partial \rho_A V_{A,x}}{\partial x}+\frac{\partial \rho_A V_{A,y}}{\partial y}+\frac{\partial \rho_A V_{A,z}}{\partial z}+\frac{\partial \rho_A \phi}{\partial t}=0 \qquad (2)$$

Assuming that methane is flowing in z-direction only; we have

$$\frac{\partial \rho_A V_{A,x}}{\partial z}+\frac{\partial \rho_A \phi}{\partial t}=0 \qquad (3)$$

The flow of methane in coal as porous media follows the Dancy's law which states that the flow rates of a fluid through a porous media is proportional to the partial pressure gradient; thus:

$$V_{A,Z}=-\frac{kA}{\mu}\frac{\partial P_A}{\partial z} \qquad (4)$$

Recall that one mole of methane contains a mass equivalent to its molecular weight; thus

$$\rho_A = C_A\ M_A \qquad (5)$$

$$C_A=\frac{P_A}{RT} \qquad (6)$$

therefore,

$$\rho_A=\frac{P_A M_A}{RT} \qquad (7)$$

Substituting equation (3) and (6) into equation (2) gives

$$\frac{\partial}{\partial Z}\cdot\left[-\frac{\rho_A KA\,\partial P_A}{\mu.\partial Z}\right]+\frac{\partial}{\partial t}\left[\frac{M_A P_A}{RT}\right]\phi=0 \qquad (8)$$

$$-\rho_A\frac{KA}{\mu}\cdot\frac{\partial^2 P_A}{\partial Z^2}+\frac{\phi M_A}{RT}\frac{\partial P_A}{\partial t}=0$$

let $\rho_A\ \frac{KA}{\mu}=\alpha$ and $\frac{\phi M_A}{RT}=\beta$

$$-\alpha\frac{\partial^2 P_A}{\partial Z^2}+\beta\frac{\partial P_A}{\partial t}=0$$

$$\frac{\partial^2 P_A}{\partial Z^2}=\frac{\beta}{\alpha}+\frac{\partial P_A}{\partial t} \qquad (9)$$

Hence, $$\frac{\partial^2 P_A}{\partial Z^2}=\left[\frac{\phi M_A}{RT}\cdot\frac{\mu}{K\rho_A A}\right]\frac{\partial P_A}{\partial t} \qquad (10)$$

where K is the permeability of the fluid, μ is the viscosity of the fluid, A is the cross- sectional area of the cleat, R is the universal gas constant, t is the absolute temperature, M is the molecular weight of methane.
Equation (9) represents the model for the methane flow in coal as porous media.

2.2 Solution Technique and Operating Parameters

Equation (9) with the respective boundary conditions P(x,0)= 7.5mpa, and P(0,t)= P_0 was solved numerically using implicit formulation of Finite Difference method. The following operating parameter obtained from literature was used for the simulation.

PARAMETERS (UNIT)	VALUE
Temperature (T)	293K
Viscosity (μ)	1.081 x 10^{-5}NS/m^2
Initial Pressure (P_0)	101.325 kPa
Porosity (Ø)	0.025
Universal Gas Constant (R)	8314J/kmol.K
Molecular Weight of methane gas(MA)	16.043
Permeability of the matrix (k)	2.47 x $10^{-15}$$m^2$
Density of matrix (ρ)	1370kg/m^3

3.0 RESULTS AND DISCUSSION

3.1 Variation of partial pressure of methane with cleat distance at permeability k =2.47e-15; porosity φ= 0.025

Figure 2 shows a plot of the methane gas pressure against the Cleat distance for a permeability of 2.47e-15 and porosity of 0.025 at different times. There is a fast decrease in pressure in all times within 28 meters of the Cleat. This amounts to the release of more methane gas within this region of the Cleat.

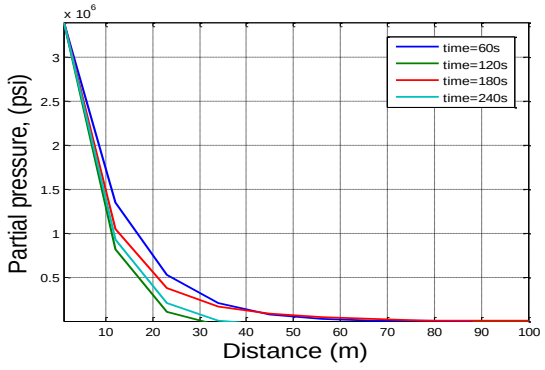

Figure 2. Methane gas pressure against Cleat Distance for Permeability k = 2.47e-15 and Porosity φ= 0.025

It was also observed that there was a very small decrease in the pressure after about 80 meters of the Cleat. This could arise due to the small amount of the methane gas occupying this region of the Cleat.

3.2 Effect of porosity on partial pressure of methane with cleat distance at permeability k =1.47e-15; porosity φ= 0.025

Figure 2 shows a graph of the partial pressure of methane for about 10% decrease in the permeability of the system. A close observation showed that, even though there was no noticeable change in the partial pressure of the gas, as compared to Figure 1, the amount of the gas released was smaller.

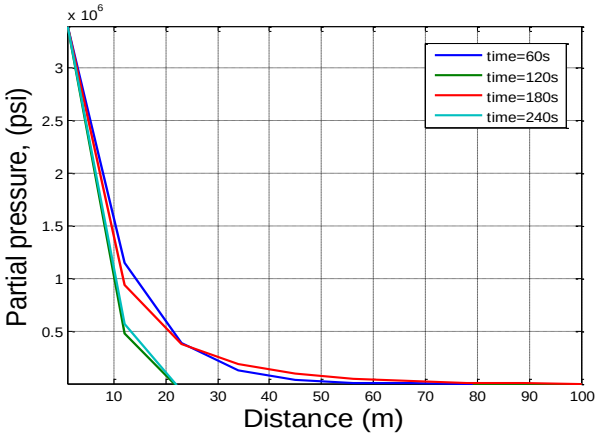

Figure 3. Gas pressure against Cleat distance for Permeability k =1.47e-15; Porosity φ= 0.025

This observation demonstrated that the permeability of the system plays important role when the flow or release of the methane gas from the Cleat was considered. High permeability allows for large extraction of the gas from the coal seams.

3.3 Effect of Porosity Partial Pressure of Methane with Cleat Distance at Permeability k =2.47e-15; Porosity φ= 0.020

For a 10% reduction in the matrix porosity, the partial pressures of the gas at different times are very distinct, as Figure 3 showed. This graph also illustrated that within 10 meters of the Cleat, the amount of the flue gas was almost the same, independent of the time in simulation. After about 12 meters, the release of the gas became a function of time.

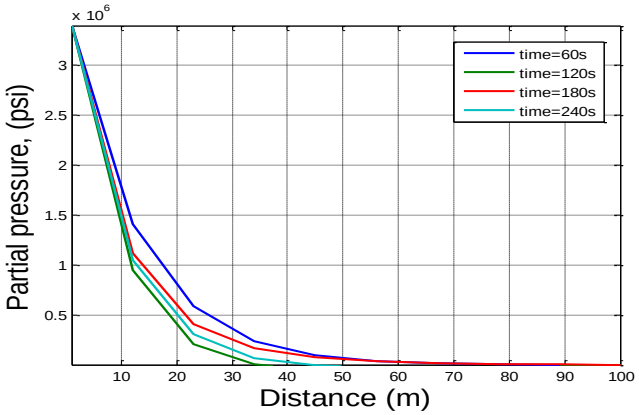

Figure 4.. Partial pressure of methane gas against Cleat distance for permeability K=2.47e-15 and Porosity φ= 0.020

That is to say that more gas was released after 240s. Furthermore, the production of methane was independent of Cleat distance after 70 meters for all the time simulated.

3.4 Effect of Viscosity on Partial Pressure of Methane with Cleat Distance at Permeability k =2.47e-15; Porosity φ= 0.020

The production of pure methane could be achieved by the decrease in the viscosity of the gas. That would mean that there was no impurity coming along with the gas.

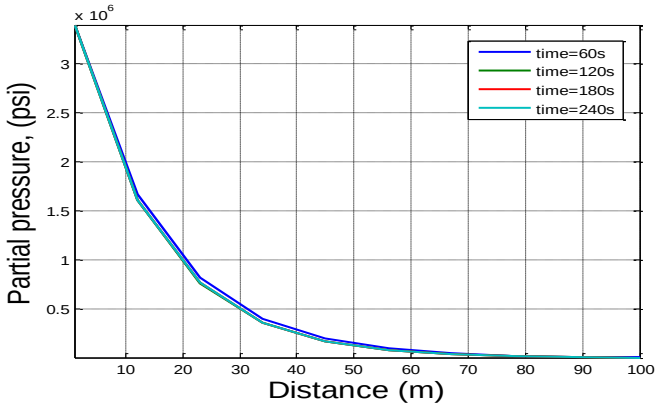

Figure 5. Methane pressure vs Cleat distance for K = 2.47e-15, φ=0.02, μ = 1.081e-6 (10% decrease)

If this assumption was considered true scientifically, then Figure 5 could be considered correct. This figure showed that the production of pure methane gas was independent of the simulation time. This illustrated that the same amount of methane was produced irrespective of the time of operation.

3.4 Effect Of Temperature on Partial Pressure of Methane With Cleat Distance at Permeability K =2.47e-15; Porosity Φ= 0.020

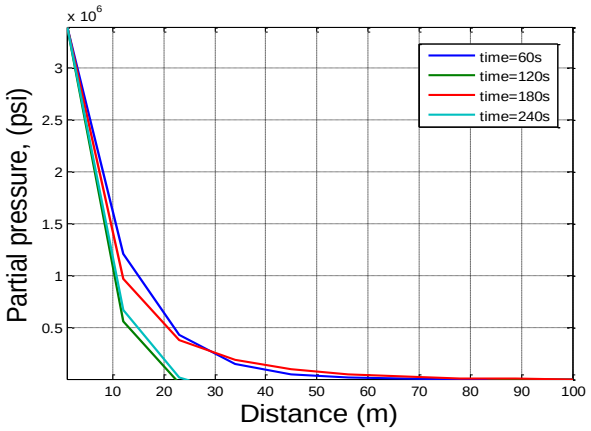

Figure 6. Methane gas pressure Vs Cleat distance for T=313K, k=2.47e-15, μ= 1.081e-5, and φ = 0.02

An increase in temperature did not alter the behavior of the system. However, it was observed that there was a little distortion of gas flow from the Cleat if the temperature was further increased above 313K. This result is in agreement with work done in literatures (Karacan *et al.*, 2011; 2007; Wang, 2013)

4.0 CONCLUSION

This work has demonstrated that more of the methane gas was released from the Cleat base when there is an increase in the partial pressure of the gas in question. The effect of parameters such as permeability, cleat distance, temperature, permeability, porosity, viscosity and the partial pressure were investigated. The results revealed that an increase in temperature did not affect the behavior of the system but however if the temperature rises above 313K there will be changes in its behavior. It was also observed that at 10% decrease in porosity, the changes in the behavioral pattern of the partial pressure of methane gas are almost negligible. The proposed model considered only laminar flow applying Darcy's law and can be applied to the flow of methane in the macro-pores (fractures) of coal bed.

REFERENCES

Alpern, B., Lemos de Sousa, M.J. (2002) Documented international enquiry on solid sedimentary fossil fuels; coal: definitions, classifications, reserves resources, and energy potential. *Inter. J. of Caol Geology*, Vol. 50, pp. 3-41.

Andersen M.A. (2003), *Oilfield Review Schlumberger Autumn-2003*

Curl, S. J. (1978), Methane Prediction in coal mines, IEA coal Research, London, P50

Gamson P.D., Beamish B.B., Johnson D.P. (1992), Coal microstructure and micro permeability and their effects on natural gas recovery. Published In: *Fuel* Vol. 72, pp 186-193

Hargraves, A. J. (1984) particular gas problems of Australian deep coal mining. *Proceedings 3rd international mine ventilation congress, Harrogate* (U.K) Pp 127-133

Harpalani S., Schraufnagel R.A. (1990), Cleats and their relation to geologic lineaments and coal bed methane potential in Pennsylvanian coals in Indiana. Published In: International Journal of Coal *Geology*, Pp 124-132.

Harpalani S., Schraufnagel R.A. (1990), Shrinkage of coal matrix with release of gas and its impact on permeability of coal. *Journal Fuel*, Volume 69

Harpalani S., Zhao X. (1991). The effects of overburden stress on coalbed methane production. *Energy Sources*, Volume 13, Pp 204-217

Karacan, C. Ö., Esterhuizen, G. S., Schatzel, S. J. and Diamond, W. P. (2007). Reservoir simulation-based modeling for characterizing longwall methane emissions and gob gas venthole production. *International Journal of Coal Geology*, 71**,** 225-245.

Karacan, C. Ö., Ren, T. and Balusu, R. (2008). Advances in grid-based numerical modelling techniques for improving gas management in coal mines. *12th US/North American Mine Ventilation Symposium.* Sparks, Nevada, USA.

Karacan, C. Ö., Ruiz, F. A., Cotè, M. and Phipps, S. (2011). "Coal mine methane: A review of capture and utilization practices with benefits to mining safety and to greenhouse gas reduction." *International Journal of Coal Geology*, 86**,** 121-156.

Lama, R. D., and Nguyen, V. U. A. (1987) A model for determination of methane flow Parameters in coal from desorption tests, *Proceeding of the 20th international symposium on the application of computers and mathematics in mineral industries. Volume 1: mining, Johanesburg*, Pp 275-282.

Mazumder S., Herment P.V., Bruining J., Wolf K.H.A.A. (2001), A preliminary model of CO_2 sequestration in coal for improved coalbed methane production. *The 2001 Alabama Coal bed Methane Symposium*

Saulsberry, J.L., Schafer, P.S., Schraufnagel, R.A. (1996). A Guide to Coal bed Methane Reservoir Engineering. Gas Research Institute, Chicago, U.S.A.

Wang, Z. (2013) Application of computational fluid dynamics modeling in underground coal mines; *PhD Thesis, School of civil, mining and environmental Engineering, University of Wollongong, Australia.*

STATISTICAL ANALYSIS OF ZEOLITE A AND Y SYNTHESIZED FROM AHOKO KAOLIN USING TWO DIFFERENT HYDROTHERMAL METHODS AND THE STUDY OF THEIR ION EXCHANGE CAPACITIES

***Kovo, A.S., Abdulkareem, A.S. and Salami, H.**
Department of Chemical Engineering, Federal University of Technology, Minna.
kovo@futminna.edu.ng , 08094059107

ABSTRACT

Zeolite A and Y have been successfully synthesized using conventional and alkaline fusion methods from Ahoko Kaolin. The percentage crystallinity of synthesised Zeolite A ranged from 22.52 to 30.70 % for samples synthesized by conventional hydrothermal method and from 28.74 to 43.35 % for those synthesized by alkaline fusion route. Zeolite Y crystallinity ranged from 37.09 – 48.92 % and from 37.55 - 47.73 % for the conventional and alkaline fusion synthesized zeolite respectively. A replicated 2^3 factorial design was used to study the influence of three different variables (crystallization temperature, crystallization time and ageing time) on the quality of the synthesized zeolites expressed in terms of CEC. For zeolite A, the crystallization temperature is the most significant factor and the interaction between the ageing time and crystallization temperature is less significant on the CEC. While for zeolite Y, the ageing time is the most significant factor and the interaction between crystallization time and ageing time is less significant. The average CEC for Zeolite A and Y samples obtained by conventional and fusion method ranges between 264.32 – 585.75, 303.31 – 627.74, 239.32 – 585.74 and 287.31 – 600.75 meq/100 g respectively.

Keywords: *Zeolite, Alkaline fusion, Factorial design, cation exchange capacity and crystallinity.*

1.0 INTRODUCTION

Most common synthetic zeolites are types A, X, Y and ZSM-5 and are widely used in the process industries as well as many other human endeavours. Due to their exceptional properties, both natural and synthetic zeolites are commercially useful in adsorption, ion-exchange operation as well as molecular sieve and as catalyst especially in refinery operations (Breck , 1974).

Most natural zeolites are of lower Si/Al ratios, since structure-directing agents necessary for formation of siliceous zeolites are absent. Also the catalytic activity of natural zeolites is limited by their inadequate supply, non-uniform pore size, impurities and low surface areas (Kovo, 2011). As a result of these shortcomings, synthetic zeolites were developed mimicking the conditions of their natural counterparts but at lower temperature and shorter time (Auerbach, *et al* 2003; Kovo, 2011, Karami and Rohani (2009)). Zeolites are generally synthesized by hydrothermal processes using commercial or synthetic chemicals (sodium aluminate, aluminium hydroxide, silica gel, sodium metasilicate) as a source of silica and alumina and which are quite expensive generally. The use of kaolin as a combined source of silica and alumina is economical because it reduces the cost of producing zeolite from expensive chemicals (Kovo, 2011).

Many previous works on the synthesis of zeolitic material from Ahoko kaolin were carried out by conventional hydrothermal method (which is based on dissolution of metakaolin with alkaline solutions, mainly NaOH followed by hydrothermal crystallization of the aluminosilicate gel) using one-factor-at-a-time approach which fails to detect interaction among variables (Kovo, 2011). In this work, design of experiments (two-level factorial design) was used in the transformation of Nigerian Ahoko kaolin into zeolites A and Y by two different methods: (i) Conventional hydrothermal alkaline activation (ii) Alkaline fusion prior to hydrothermal treatment. The second method tends to dissolve more of the aluminosilicate and also aid in transformation of quartz and kaolinite into sodium silicate (Rios, *et al* 2008; Espejel-Ayala, *et al*, 2013). Since kaolin composition vary with location and the optimal way to learn about zeolite synthesis is by examining zeolite synthesis from different perspectives (Auerbach *et al*, 2003), it become imperative to use this method on a new deposit such as Ahoko Kaolin.

Design of experiments (DOE) has become one of the most popular statistical techniques since 1990s. When planning a test series, several experimental strategies can be used and one suitable method that is increasingly been adopted as an experimental strategy is the factorial design as it takes into consideration the interactions between factors and examine if a factor has an influence on a specific variable or not (Montgomery, 2005).

Cation exchange capacity which is a significant property of zeolites results from the presence of loosely bound cations of alkali and alkaline earths elements, often called exchangeable cations in the structure of the zeolites which are easily exchanged when zeolites come in contact with solutions of "saturating" or "indexing" ions (Konstantinos, 1999). The commonly exchangeable ions are Ca^{2+}, Mg^{2+}, K^{+}, Na^{+} and NH^{4+} and it is usually expressed as milliequivalents per gram (or per 100g) of material. The reaction between a zeolite and an ionic solution is illustrated as:

$$N_1(Z) + N_2(S) \leftrightarrow N_2(Z) + N_1(S) \quad (1)$$

N_1 is the exchangeable cation in the zeolite Z and N_2 is the saturating or index ion in solution. According to the work of Mumpton (1999), Cational Exchange capacity (CEC) increase with the aluminum content of the zeolite because more extra framework cation is needed to balance the charge.

The most widely used cation exchange process is by treating zeolites with aqueous solutions that contains the cation to be introduced. This is achieved by suspending the zeolites in the solution under the appropriate conditions (amount and concentration of the salt, temperature and pH) for ion exchange, followed by filtration and washing of the filter cake. This work therefore study the preparation of zeolite A and Y from Ahoko kaolin using different techniques and also investigate their cation exchange behavior using two level factorial design analysis for the first time.

2.1 MATERIALS AND METHODS

The starting material is Ahoko kaolin which was refined to reduce the quartz content. This is followed by drying and pulverizing using porcelain mortar and pestle. The chemicals used are: sodium hydroxide pellets (97.5%), sodium hydroxide powder (99%), sodium metasilicate (95%), ammonium acetate (98%), ethanol (99%) and deionised water.

2.2 Experimental Design

In order to reduce the total number of experiments, two level experimental designs with three factors was used. The experimental factors chosen are ageing time (hr), crystallization time (hr) and crystallization temperature in (^{o}C). The number of experiments is expressed as:

$$N = (2^k) \times R \quad (2)$$

Where N= Number of experiments, k = Number of factors and R = Number of replicate. The level of independent variable of the experiment are shown in table 1 and 2 for the two zeolites while the factorial design matrix are presented in table 3 and 4 for the zeolites synthesized

Table 1 levels of Independent Variable for Zeolite A

Levels	Low	High
Coding	-1	+1
Ageing Time (hr)	3	12
Crystallization time (hr)	3	6
Crystallization temperature (^{o}C)	70	100

Table 2 Levels of Independent Variable for Zeolite Y

Levels	Low	High
Coding	-1	+1
Ageing Time (hr)	3	6
Crystallization time (hr)	6	9
Crystallization temperature (^{o}C)	70	100

Table 3: Factorial Design Matrix for Zeolite A Synthesis Using Conventional Treatment (AC) and Alkaline Fusion (AF) Methods.

Samples AC	AF	Ageing Time (hr)	Crystallization Time (hr)	Crystallization Temperature (^{o}C)
AC1	AF1	3	3	70
AC2	AF2	12	3	70
AC3	AF3	3	6	70
AC4	AF4	12	6	70
AC5	AF5	3	3	100
AC6	AF6	12	3	100
AC7	AF7	3	6	100
AC8	AF8	12	6	100

Table 4: Factorial Design Matrix for Zeolite Y Synthesis Using Conventional Treatment (YC) and Alkaline Fusion (YF) Methods.

Samples YC	YF	Ageing Time (hr)	Crystallization Time (hr)	Crystallization Temperature (^{o}C)
YC1	YF1	3	6	70
YC2	YF2	6	6	70
YC3	YF3	3	9	70
YC4	YF4	6	9	70
YC5	YF5	3	6	100
YC6	YF6	6	6	100
YC7	YF7	3	9	100
YC8	YF8	6	9	100

2.3 Zeolites Synthesis Procedures

2.3.1 Conventional Synthesis Method for Zeolite A and Y

Synthesis of Zeolite A

The metakaolin was obtained by calcinations of refined kaolin in a muffle furnace at 600^{o}C for 1 hour using a crucible. The synthesis of zeolite A was carried out from reaction mixture with molar composition $4.25Na_2O:Al_2O_3:2SiO_2:275.4H_2O$. In order to synthesize zeolite A with the above molar composition, 2.434 g of NaOH pellets was dissolved in 35 g of distilled water in reaction beakers and subsequently 1.574 g of metakaolin was added under stirring condition.

Synthesis of Zeolite Y

Zeolite Y was synthesized from gel with molar composition of: $10Na_2O:Al_2O_3:10SiO_2:300H_2O$. 25 g of distilled water was measured and divided into two equal parts. 1.181 g of NaOH pellets and 1.332 g metakaolin was dissolved in one part and 12.953 g of sodium metasilicate was equally dissolved in the second part and both sets were mixed together. The aluminosilicate gels were aged at room temperature for different ageing time. Hydrothermal treatment of the aged mixtures was carried out in an autoclave at varying crystallization

time and temperature. At the end of which the mixture was filtered and washed with distilled water until pH of filtrate were about 9. The samples were subsequently dried in an oven at 80^{o}C for 6 hours and characterized with XRD.

2.3.2 Alkaline Fusion Method for Zeolite A and Y

Synthesis of Zeolite A

In this method, 6.2 g of kaolin (combined source of silica and alumina) was dry mixed with 7.44 g of NaOH powder (kaolin/NaOH = 1/1.2) for 30 minutes. The mixture was heated in a muffle furnace at 600^{o}C for 1 hour.

The fused product of kaolin and NaOH was ground and then 4.4 g of this was dissolved in 21.5 ml of distilled water under stirring (in ratio of 4.9 ml of water/g of fused product) under stirring condition to form the amorphous precursors followed by ageing at room temperature and hydrothermal treatment at different crystallization temperatures and times. At the end of the hydrothermal treatment, the sample was filtered, washed (to a pH of 9) and dried in an oven for 6 hours at 80^{o}C. The products obtained were characterized by XRD.

Synthesis of Zeolite Y

In order to synthesize zeolite Y from kaolin by fusion method, 6.2 g of kaolin was dry mixed with 9.3 g of NaOH powder in a ratio of 1/1.5 (kaolin/NaOH), the mixture was calcined in a muffle furnace at 750^{o}C for 3 hours.

2.5 g of the fused mass and 3.168 g of sodium metasilicate were dissolved in 37.5 ml of distilled water in a ratio of (15 ml of water/g of fused mass). The resulting gel was aged at room temperature and crystallization was carried out at desired temperatures and time. The amount of reagents used was based on previous experimental work of Xinmei *et al*. (2003) and Mu Mu (2008) who synthesized Zeolite Y with molar composition of $9Na_2O:Al_2O_3:6SiO_2:249H_2O$ using this method. At the end of the hydrothermal treatment, the sample was filtered, washed (to a pH of 9) and dried in an oven for 6 hours at 80^{o}C. The products obtained were characterized by XRD.

2.4 Determination of Cation Exchange Capacity

The cation exchange capacity (CEC) was determined using the ammonium acetate saturation method at room temperature under standard atmospheric pressure using zeolite powders. About 150 mg of the <125 µm size fraction was accurately weighed from each sample and transferred to a mechanical shaker where 10 ml of 1N solution of sodium acetate (CH_3COONa) was mixed for 5 minutes. The mixture was then centrifuged in order to obtain a clear supernatant solution which was decanted. This procedure was repeated another two times to ensure that all cations in the zeolite have been replaced with Na ion. The Na-laden zeolite was washed with 30 ml of 99% ethanol and shaken in a mechanical shaker for 5 min. The supernatant was removed, and the procedure was repeated one more time to ensure that the zeolite was clean and laden only with Na.

The Na laden zeolite was then mixed with 1N ammonium acetate solution (CH_3COONH_4) buffered at pH 7 to replace the exchanged sodium ion with ammonium ion. The suspension was well shaken, left overnight and centrifuged. The clear liquid was decanted. The same procedure was repeated with CH_3COONH_4 five times adding fresh 10ml of CH_3COONH_4 to ensure that all Na ions were replaced by NH_4 ion. After each step, the supernatant of CH_3COO^- solution was decanted to a 100 ml volumetric flask which was diluted to 100 ml with ammonium acetate solution and the sodium ion concentration in this supernatant was determined by atomic absorption emission spectroscopy. The sodium binding capacity was then calculated from:

$$q_e = \frac{(c_o - c_b) \times V}{MW \times m} \quad (3)$$

Where q_e is the exchanged Na ions per weight of zeolite (mg/100 g) or CEC value, c_o is the Na concentration (mg/L), and c_b is the Na concentration in the blank (mg/L). Both c_o and c_b were measured by AAS. V is the volume of the aqueous phase (ml), equal to 100 ml in this experiment; m is the amount of zeolite (g), equal to 150mg and MW is the molecular weight of Na (g).

3.0 CHARACTERIZATION TECHNIQUE

The nature of phase and percent purity (crystallinity) of synthesized zeolites were identified using an AXS Bruker advance-8 Diffractometer using CuKα (λ=0.1541nm) radiation at 40 kV and 40 mA and a scan speed of 0.04^{o} in the 2θ range of 5-50^{o},

4.0 RESULTS AND DISCUSSION

Figures 1 and 2 show the XRD pattern of the synthesized zeolite A using both conventional and alkaline fusion methods respectively. From the conventional method, the formation of zeolite A was observed through the peak diffraction at 2θ = 12.49, 17.69, 24.04, 35.83, 39.53, 43.61, 47.41 and 48.02 as reported by Traecy and Higgins (2001). The zig-zag peaks in the background indicates the presence of amorphous phase of metakaolinite. The peak at 2θ is 28.53 confirm the presence of sodalite. This is in accordance with Ostwald's rule of successive reaction. From the analysis of the peak area, percent crystallinity was estimated. The percent crystallinity ranged from 22.52 - 30.70 with sample AC7 having the highest percent crystallinity.

While the characteristic peak of zeolite A synthesized by alkaline fusion method was observed at 2θ between the range of 7.21, 10.19, 12.49, 20.47, 24.04 and 36.59. The peak due to quartz was observed to be present at 2θ = 26.6 (Treacy and Higgins, 2001). Although the peaks are weak, but they are quite consistent with the reference especially the AF samples. The percent crystallinity

ranged from 28.74 - 43.35 % with sample AF6 having the highest percent crystallinity.

From the analysis of the results for the two methods of synthesis, except samples AF2 and AC2, samples synthesized through alkaline fusion route possess higher percent crystallinity than the samples synthesized by conventional method. Also the first diffraction peak appeared at 2θ = 7.21 and 12.49 for AF's and AC's samples respectively. This can be attributed to the fact that the fusion aid in transformation of quartz and kaolinite into large amount of sodium silicate amorphous aluminosilicate (metakaolinite), which indicates that the fusion process was very effective in extracting the Si species in these mixture (Rios *et al*., 2008 and Espejel-Ayala *et al*., 2013).

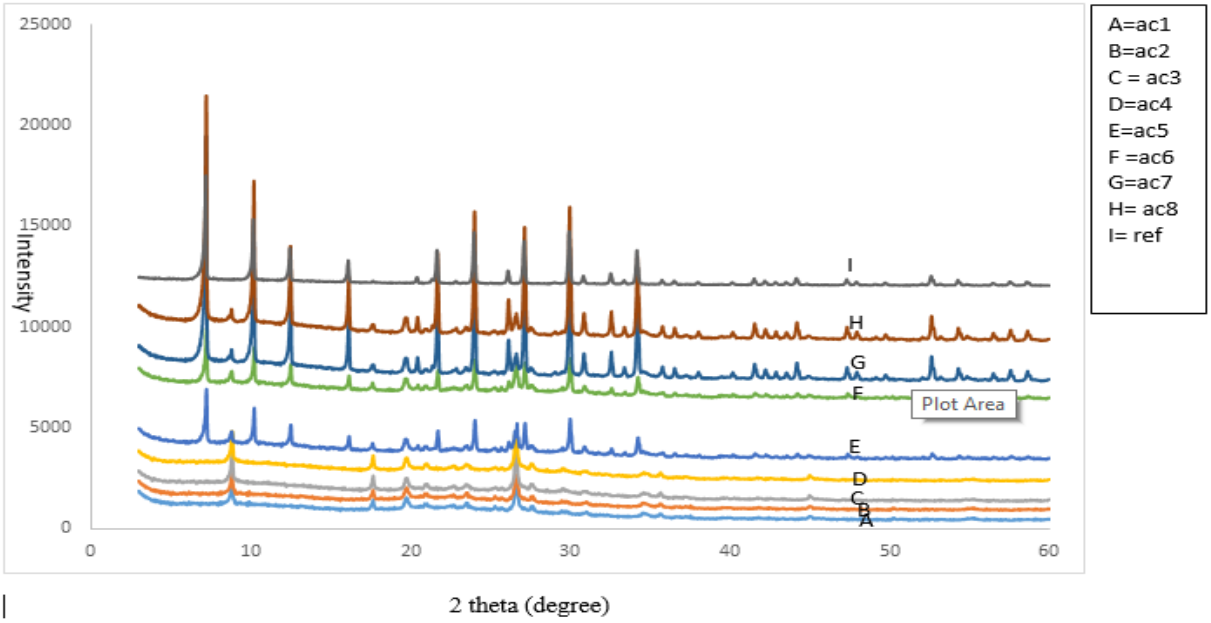

Figure 1: XRD Pattern of Synthesized Zeolite A by conventional method (AC Samples)

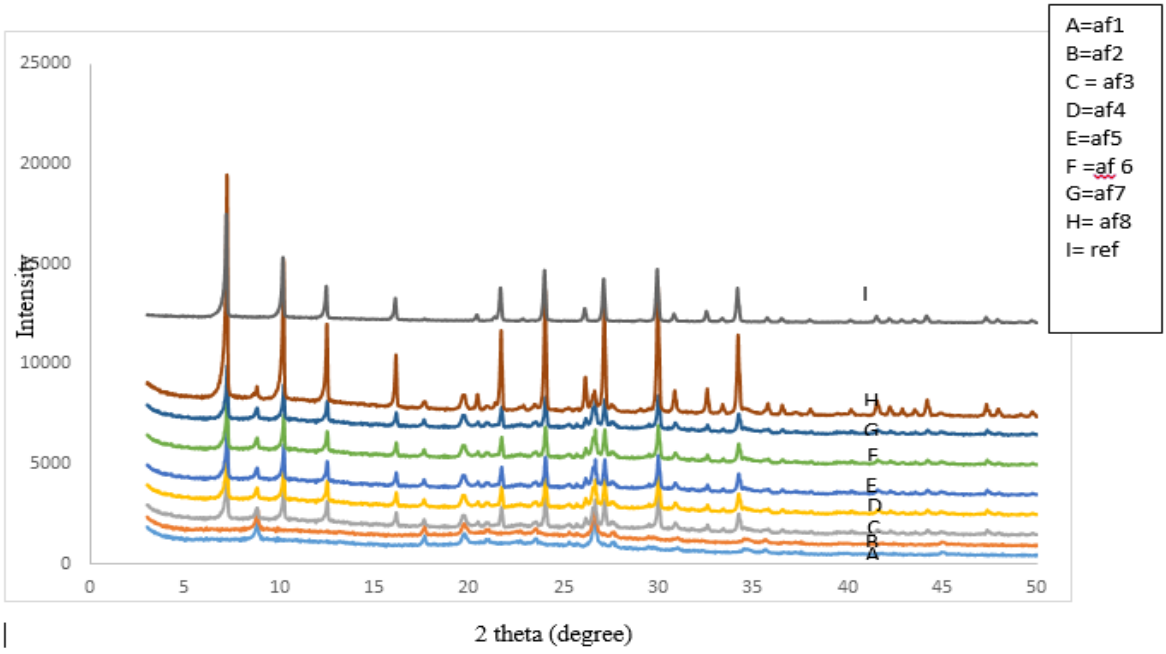

Figure 2: XRD Pattern of Synthesized Zeolite A by fusion method (AF Samples)

Figures 3 and 4 show the XRD pattern of the synthesized zeolite Y using both conventional hydrothermal and alkaline fusion prior to hydrothermal treatment methods respectively. The characteristic peak of zeolite Y prepared by conventional hydrothermal method was observed at 2θ = 11.86, 15.61, 23.58, 29.55, 35.56, 39.38, 43.11 and 47.64 as reported by Traecy and Higgins (2001). The percent crystallinity ranged from 37.09 – 48.92 % for samples YC6 and YC1 respectively. On the other hand the first diffraction peak for alkaline fused zeolite Y are observed at 2θ = 6.19 for samples YF7 and YF8, 11.86, 21.7, 23.58, 28.87, 33.19 for all samples. Other peaks appeared at 23.58 (YF7 and YF8). For samples YF5, YF6 and YF8 Zeolite Na- P1 was present at 2θ = 17.66 as reported by Treacy and Higgins (2001). Except the work of Mu Mu and Mya Mya, (2008), and Xinmei *et al*. (2003) there is limited literature on synthesis of zeolite-Y from kaolin by alkaline fusion route. Though weak, most of the peaks are quite consistent with the reference especially the YF samples.

There is the presence of quartz at 2θ = 26.6 for all the samples indicating the unreactive nature of quartz. From the peak area the percent crystallinity was calculated and it ranged from 37.55 for sample YF2 to 47.73 % for sample YF7.

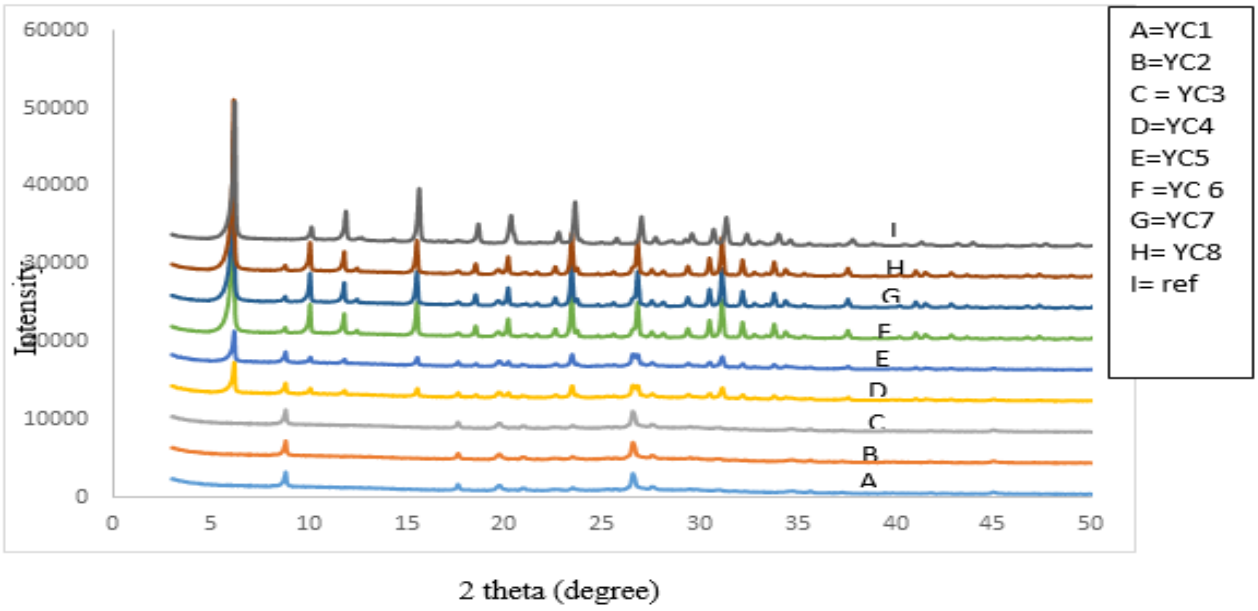

Figure 3: XRD Pattern of Synthesized Zeolite Y by conventional method (YC Samples)

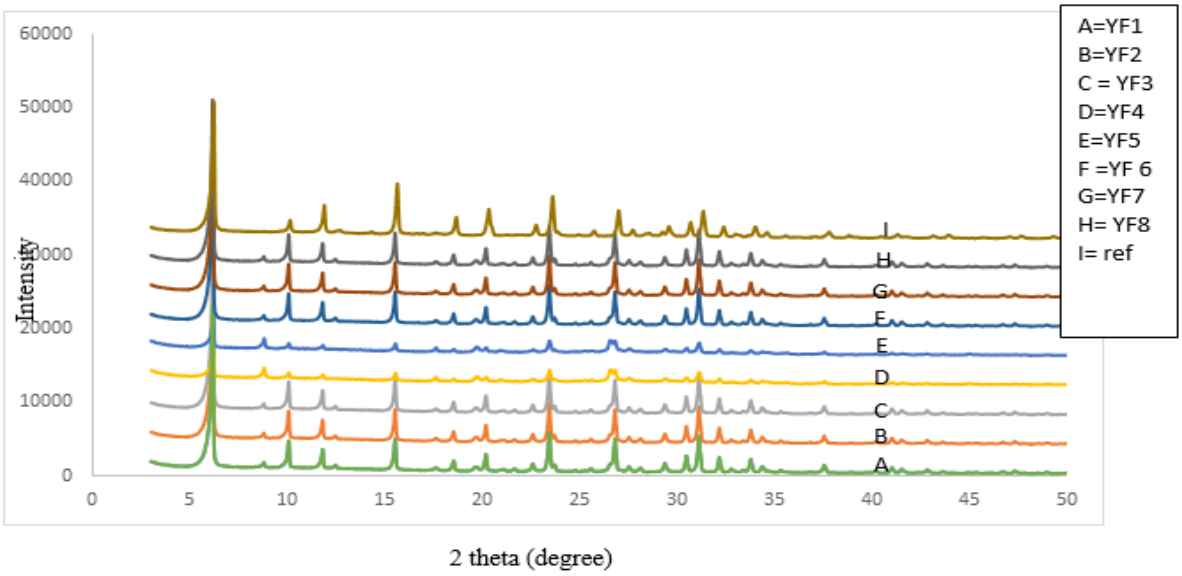

Figure 4: XRD Pattern of Synthesized Zeolite Y fusion method(YF Samples)

Comparing the two methods, unlike in zeolite-A synthesis where the alkaline fused products gave a better result in terms of percent crystallinity, at low temperature (70^{o}C) YC samples have higher percent crystallinity except YC3, while at a temperature of 100^{o}C, YF samples, the fused product gave better percent crystallinity.

Kovo, 2011 concluded that temperature is an important parameter that influences zeolite crystallization because a small change in heating temperature can cause instant transformation in the zeolite phase.

The full factorial design presented in Tables 3 and 4 and their uncoded values are shown in Figures 5 and 6.

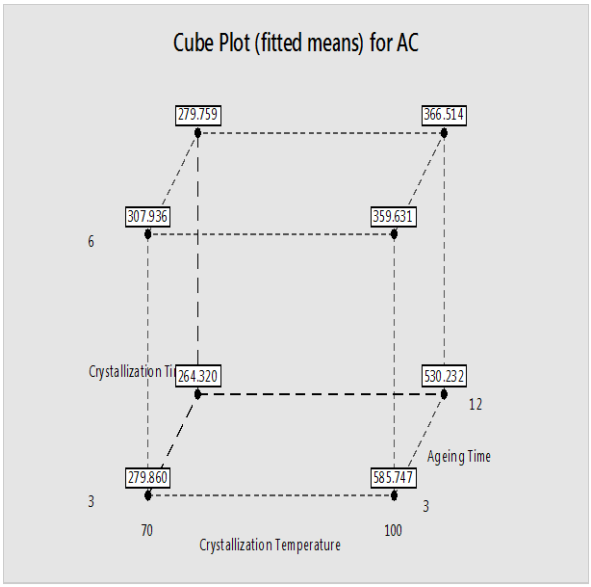

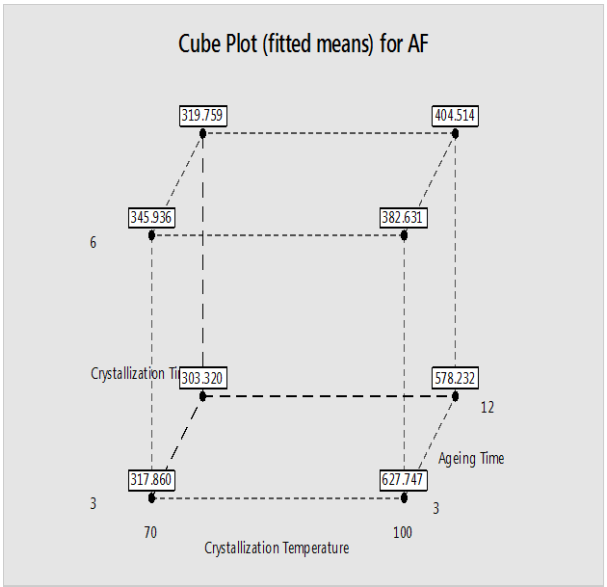

Figure 5. Cube Plots for Zeolite A CEC Response

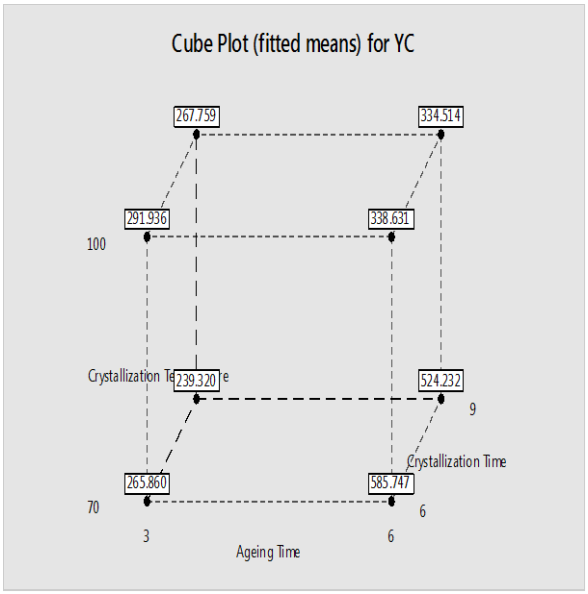

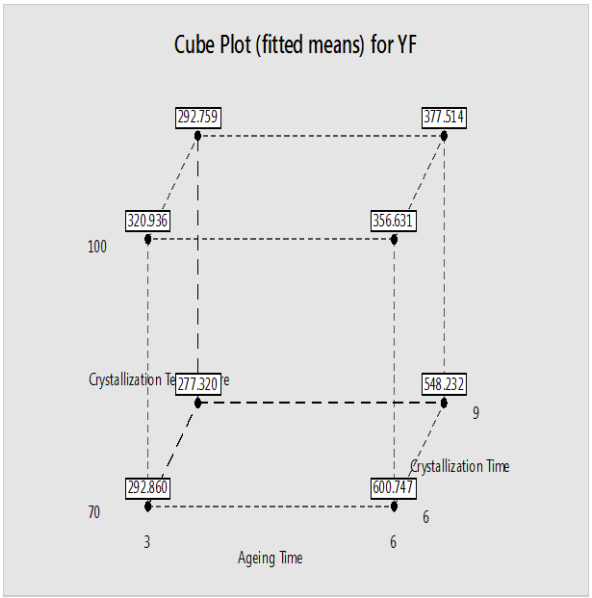

Figure 6 Cube Plots for Zeolite Y CEC Response

The cube plot was used to examine how the process variables affect the zeolite A CEC. The plots show the response surface plot of zeolite A CEC. The cube plot corner points represent a different factorial design and illustrate the average zeolite A CEC result for the synthesis based on the process variables level.

Some of the calculated CEC values are quite high compared to the theoretical values of 548 and 339 meg/100 g for zeolites A and Y respectively which may be due to presence of some unidentified/undetected phases or impurities. These values are higher than values reported by San Cristobal (2010) which is 292.8 meq/100 g for zeolite A and by George and Hara (2008) who reported a value of 330 meq/100 g for zeolite Y.

The alkaline fused samples gave better results than the conventional synthesized samples, in addition, Zeolite A has higher CEC than Zeolite Y, and this could be due to the high aluminum content of Zeolite A, since CEC

increases with the number of aluminum present in the zeolite framework (Mumpton, 1999).

4.3 Factorial Analysis Showing Effects of Crystallization Temperature, Crystallization Time and Ageing Time on Zeolite A CEC.

Tables 5 and 6 show the estimated effects and coefficients for zeolite – A CEC. The result of the estimated effects suggests that the model contains three main effects, which can be evaluated in the absence of significant interactions and three two-way interaction effects. The p-values for all three main effects are less than 0.05 (Crystallization temperature = **0.000**, Crystallization time = **0.000** and ageing time = **0.000**). Therefore, there is evidence of a significant effect. The p-value result from the Tables also indicate that there is significant interaction between crystallization temperature and crystallization time (0.000) and between crystallization time and ageing time as their terms have p-values less than 0.05 ($\alpha = 0.05$). The Tables also show that crystallization temperature has the greatest effect (177.56 and 176.56) on zeolite A CEC. In addition, the tables show that setting the crystallization temperature high produced higher zeolite A CEC than setting the crystallization temperature low. The interaction between crystallization temperature and crystallization time has the second greatest effect (-108.34 and -115.84) on zeolite A CEC. The negative sign shows the settings of the two process variables have antagonistic effect (need to be at opposite setting). The result of the main effect plots show that the crystallization temperature is set high and crystallization time is set low to produce zeolite A of high CEC.

Crystallization time has the third greatest effect (-86.58 and -93.58) on zeolite A CEC. In addition, setting the crystallization time high produced lower zeolite A CEC than setting the crystallization time low. Ageing time has the fourth greatest effect (-23.09 and -17.09) on zeolite A CEC. In addition, higher ageing time produced lower zeolite A CEC than lower ageing time. The interaction between crystallization temperature and ageing time has the smallest effect (-1.23 and 3.27) on zeolite A CEC. In addition, setting the interaction high produced lower zeolite A CEC than setting the interaction low. The values in brackets are for AC and AF respectively.

Table 5: Estimated Effects and Coefficients for Zeolite A (Samples AC) CEC

Term	Effect	Coef	SE Coef	T-Value	P-Value
Constant		-1143.	2.56	145.35	0.000
Crystallization Temperature	177.56	19.95	2.56	34.71	0.000
Crystallization Time	-86.58	227.9	2.56	-16.93	0.000
Ageing Time	-23.09	29.5	2.56	-4.51	0.002
Crystallization Temperature*Crystallization Time	-108.34	-3.102	2.56	-21.18	0.000
Crystallization Temperature*Ageing Time	-1.23	-0.426	2.56	-0.24	0.816
Crystallization Time*Ageing Time	12.44	-6.95	2.56	2.43	0.041
Crystallization Temperature*Crystallization Time*Ageing Time	18.76	0.0926	2.56	3.67	0.006

Table 6: Estimated Effects and Coefficients for Zeolite A (Samples AF) CEC

Term	Effect	Coef	SE Coef	T-Value	P-Value
Constant		-1161.	1.56	262.56	0.000
Crystallization Temperature	176.56	20.747	1.56	56.53	0.000
Crystallization Time	-93.58	244.7	1.56	-29.96	0.000
Ageing Time	-17.09	30.27	1.56	-5.47	0.001
Crystallization Temperature*Crystallization Time	-115.84	-3.343	1.56	-37.09	0.000
Crystallization Temperature*Ageing Time	3.27	-0.437	1.56	1.05	0.326
Crystallization Time*Ageing Time	14.94	-7.61	1.56	4.78	0.001
Crystallization Temperature*Crystallization Time*Ageing Time	20.76	0.1025	1.56	6.65	0.000

The earlier analysis obtained from p-values of Tables 5 and 6 show that the three main effects were significant at the 0.05 α-level. Surface plot of zeolite A CEC against crystallization time and crystallization temperature of Figure 7 shows how crystallization temperature and crystallization time are related to zeolite A CEC. To maximize zeolite A CEC, high setting of crystallization temperature of 100^{o}C and low setting of crystallization time of 3 hrs, while holding ageing time at 7.5 hrs should be chosen.

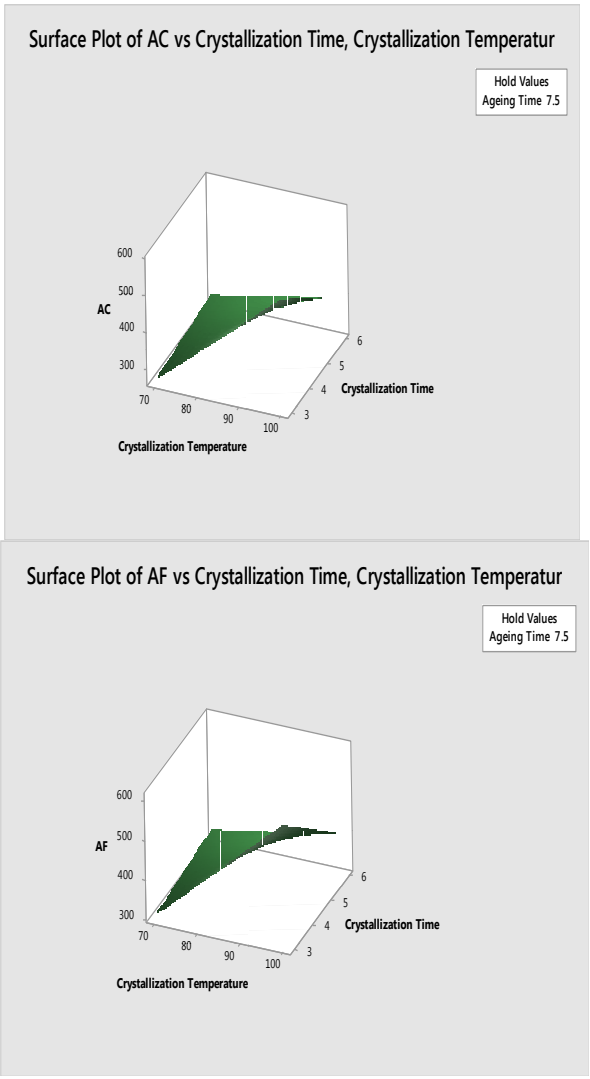

Figure 7. Surface Plots of Zeolite A CEC against Crystallization Time and Temperature

The model Equations can be built up from estimated coefficients for zeolite A CEC of Tables 5 and 6.
For conventional method,

$$Y_p = -1143.6 + 19.95x_1 + 227.9x_2 + 29.5x_3 - 3.102x_1x_2 - 0.4261x_1x_3 - 6.95x_2x_3 + 0.0926x_1x_2x_3 \quad (4.1)$$

For alkaline fusion method,

$$Y_p = -1161.6 + 20.747x_1 + 244.7x_2 + 30.27x_3 - 3.343x_1x_2 - 0.4371x_1x_3 - 7.61x_2x_3 + 0.1025x_1x_2x_3 \quad (4.2)$$

Where x_1 = Crystallization temperature x_2 = Crystallization time and x_3 = Ageing time.

(The model equations are valid if x_1, x_2 and $x_3 \neq 0$)

4.3.2 Factorial Analysis Results Showing Effects of Crystallization Temperature, Crystallization Time and Ageing Time on Zeolite Y CEC

Tables 7 and 8 show the estimated effects and coefficients for zeolite Y CEC. The result of the estimated effects suggests that the model contains three main effects, which can be evaluated in the absence of significant interactions and three two-way interaction effects. The p-values for all three main effects are less than 0.05 (ageing time= **0.000**, crystallization temperature= **0.000** and crystallization time= **0.000**). Therefore, there is evidence of a significant effect. The p-value result from Tables 4.3 and 4.4 also indicate that there is significant interaction between ageing time and crystallization temperature (0.000) and between crystallization temperature and crystallization time as their terms have p-values less than 0.05 ($\alpha = 0.05$). The Tables also show that ageing time has the greatest effect (179.56 and 174.81) on zeolite Y CEC. In addition, the tables show that setting the ageing time high produced higher zeolite Y CEC than setting the ageing time low. The interaction between ageing time and crystallization temperature has the second greatest effect (-122.84 and -114.59) on zeolite Y CEC. The negative sign shows the settings of the two process variables have antagonistic effect. The result of the main effect plot shows that the ageing time is set high and crystallization temperature is set low to produce zeolite Y of high CEC.
Crystallization temperature has the third greatest effect (-95.58 and -92.83) on zeolite Y CEC. In addition, setting the crystallization temperature high produced lower zeolite Y CEC than setting the crystallization temperature low. Crystallization time has the fourth greatest effect (-29.09 and -18.84) on zeolite Y CEC. In addition, higher crystallization time produced lower zeolite Y CEC than lower crystallization time. The interaction between ageing time and crystallization time has the smallest effect (-3.73 and 3.02) on zeolite Y CEC. The values in brackets are for YC and YF respectively.

Table 7: Estimated Effects and Coefficients for Zeolite Y (Samples YC) CEC

Term	Effect	Coef	SE Coef	T-Value	P-Value
Constant		-1015	4.10	86.79	0.000
Ageing Time	179.56	428.0	4.10	21.89	0.000
Crystallization Temperature	-95.58	13.49	4.10	-11.65	0.000
Crystallization Time	-29.09	43.80	4.10	-3.55	0.008
Ageing Time*Crystallization Temperature	-122.84	-4.258	4.10	-14.97	0.000
Ageing Time*Crystallization Time	-3.73	-18.2	4.10	-0.45	0.662
Crystallization Temperature*Crystallization Time	14.94	-0.585	4.10	1.82	0.106
Ageing Time*Crystallization Temperature*Crystallization Time	13.76	0.204	4.10	1.68	0.132

Table 8: Estimated Effects and Coefficients for Zeolite Y (Sample YF) CEC

Term	Effect	Coef	SE Coef	T-Value	P-Value
Constant		-1219	2.23	171.66	0.000
Ageing Time	174.81	472.8	2.23	39.14	0.000
Crystallization Temperature	-92.83	16.59	2.23	-20.78	0.000
Crystallization Time	-18.84	83.9	2.23	-4.22	0.003
Ageing Time*Crystallization Temperature	-114.59	-4.936	2.23	-25.65	0.000
Ageing Time*Crystallization Time	3.02	-26.41	2.23	0.68	0.518
Crystallization Temperature*Crystallization Time	15.19	-1.096	2.23	3.40	0.009
Ageing Time*Crystallization Temperature*Crystallization Time	21.51	0.3186	2.23	4.82	0.001

The earlier analysis obtained from p-values of Tables 7 and 8 show that the three main effects were significant at the 0.05 □-level. Surface plot of zeolite Y CEC against ageing time and crystallization temperature of Figure 4.6 shows how ageing time and crystallization temperature are related to zeolite Y CEC. To maximize zeolite Y CEC, high setting of ageing time of 6 hrs and low setting of crystallization temperature of 70°C, while holding crystallization time at 7.5 hrs should be chosen.

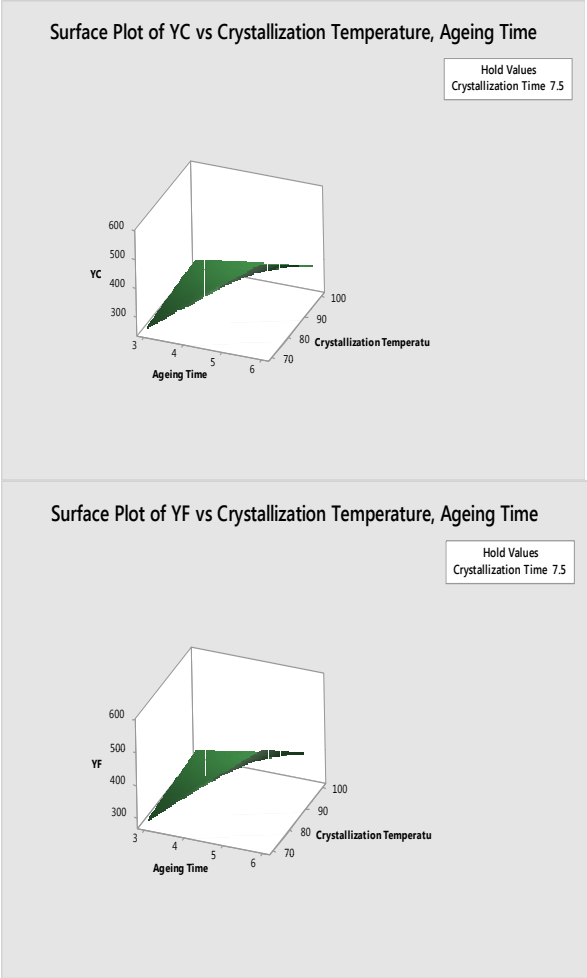

Figure 8. Surface Plots of Zeolite Y CEC against Crystallization Temperature and Ageing Time.

The model Equations can be built up from estimated coefficients for zeolite Y CEC of Tables 7 and 8.

For conventional hydrothermal method,

$$Y_p = -1015 + 428.0x_1 + 13.49x_2 + 43.8x_3 - 4.258x_1x_2 - 18.2x_1x_3 - 0.585x_2x_3 + 0.204x_1x_2x_3 \quad (4.3)$$

For alkaline fusion method,

$$Y_p = -1219 + 472.8x_1 + 16.59x_2 + 83.9x_3 - 4.936x_1x_2 - 26.41x_1x_3 - 1.096x_2x_3 + 0.3186x_1x_2x_3 \quad (4.4)$$

Where x_1 = Ageing time x_2 = Crystallization temperature and x_3 = Crystallization time.

(The model equations are valid if x_1, x_2 and $x_3 \neq 0$)

Table 9: Statistical Parameters of the Model Correlating Zeolite A and Y CEC to Crystallization temperature, Crystallization time and Ageing time

Values				
Statistical Parameters	AC	AF	YC	YF
S	10.2303	6.2462	16.4076	8.9334
R^2	99.60%	99.86%	99.08%	99.70%
R^2adjusted	99.25%	99.73%	98.27%	99.44%
R^2predicted	98.39%	99.43%	96.30%	98.81%

Table 9 shows the model proportion of the response variability that is (R^2), the predicted R^2, which is the level of prediction of the future data by the model and the adjusted R^2 useful for comparing models from the same data with different numbers of terms. The R^2 value lies between 0 and 100%. The model predicts better when R^2 value is closer to 100% (Doddapaneni, Tatineni, Potumarthi and Mangamoori, 2007). The sum of squares of the prediction errors (PRESS) for assessing model's predictive ability from Table 4.5 is 10.2303, 6.2462, 16.4076 and 8.9334 for AC, AF, YC and YF samples respectively. Low PRESS value is an indication that the model fits the data as Montgomery (2005)

reported that the model fits the data better when the PRESS is smaller.

5.1 CONCLUSIONS

Conventional and alkaline fusion methods was used successfully to synthesize zeolite-A and Y from Ahoko kaolin. This study also demonstrated the application of factorial analysis in determining the zeolite synthesis parameters that are having significant effect on zeolite CEC. For all the analysis of the samples synthesized, and using the percent crystallinity estimated from the peak area, the AF's gave better results than AC's samples while YF's has better values than YC's only at higher temperature.

The alkaline fused samples gave better results than the conventional synthesized samples, while Zeolite A has higher CEC than Zeolite Y, and this could be due to the high aluminum content of Zeolite A. The synthesized zeolites showed high CEC as compared to other commercial zeolites Based on the factorial analyses; the crystallization temperature is the most significant factor for zeolite A.

Acknowledgment

This Research was funded by the TETFund Research fund with Project code TETF/DESS/NRF/FUTM/20/14/STI/VOL.1

REFERENCES

Auerbach, S., K. A. Carrado, and P. K. Dutta (2003). *Handbook of zeolite science and technology*, New York, Marcel Decker Inc 1170.

Breck, D. W. (1974). *Zeolite Molecular Sieves*. John Wiley and Sons Ltd, New York.

Doddapaneni, K. K, Tatineni, R., Potumarthi, R., Mangamoori, L. N. (2007). Optimization of media constituents through response surface methodology for improved production of alkaline proteases by Serratia rubidaea. *J Chem Technol Biotechnology*. 82, 721–729.

Karami, D and S. Rohani (2009), Synthesis of pure zeolite Y using soluble silicate, a two-level factorial experimental design, Chemical Engineering and Processing, 48, 1288–1292.

Espejel-Ayala, F, Schouwenaars, R Dura´n-Moreno, A., Ramırez –Zamora, R.M., (2013), Use of drinking water sludge in the production process of zeolites, *Res Chem Intermed* DOI 10.1007/s11164-013-1138-8.

George E. C. and Hara P. (2008), Synthesis of FAU Type Zeolite Y from Natural Raw Materials: Hydrothermal SiO2-Sinter and Perlite Glass". *The Open Mineralogy Journal*, 2, 1-5.

KonstantinosP. K. (1999). Cation exchange capacity of zeolitic volcaniclastic materials: Applicability of the ammonium acetate saturation (AMAS) method. *Clay and clay minerals*, 47(6), 688-696.

KovoA. S. (2011). Development of zeolites and zeolite membranes from Ahoko Nigeria kaolin. PhD Thesis, *Faculty of Engineering and Physical Sciences, School of Chemical Engineering and Analytical Science, the University of Manchester.*

Montgomery, D. C. (2005). *Design and Analysis of Experiments*. New York: John Wiley & Sons.

Mu Mu, H. and Mya Mya, O. (2008). Preparation of Zeolite Y Catalyst for Petroleum Cracking, *World Academy of Science, Engineering and Technology* (48).

Mumpton, F. A. (1999). Proceedings of the National Academy Science USA. *Colloquium Paper* 96, 3463-3470.

San Cristóbal, A.G., Castelló, R., Martín Luengo, M.A., and Vizcayno, C., (2010). Zeolite prepared from calcined and mechanically modified kaolins: A comparative study. *Applied Clay Science* 49, 239–246.

Treacy, M.M.J., and Higgins J.B. (2001). Collection of Simulated XRD Powder Patterns for Zeolites 4th revised Edition Elsevier, New York.

Rios, C. A., Williams, C. D., and Fullen M. A., (2008). Nucleation and growth history of zeolite LTA synthesized from kaolinite by two different methods. *Journal of applied clay science*, unedited manuscript.

Xinmei, L., Zifeng, Y., Huaiping, W., Yantuo, L. (2003). In-situ Synthesis of NaY Zeolite with Coal-Based Kaolin, *Journal of Natural Gas Chemistry* (12), 63-70.

EFFECTS OF DEALUMINATION ON THE PHYSIO-CHEMICAL PROPERTIES OF CLAY FOR INDUSTRIAL APPLICATIONS

[*]Eterigho, E. J.[1], Farrow, T. S.[2]. Uthman, H.[3] and Faruq, A.[4]

[1,3 &4]Chemical Engineering Department,
Federal University of Technology, Minna, Niger State, Nigeria
[2]Chemical and Petroleum Engineering Department,
Niger Delta University Wilberforce Island, Bayelsa State, Nigeria
e-mail: jummyeterighoj@gmail.com; Mobile number: +2348028648808
**Corresponding author*

ABSTRACT

The physiochemical properties of natural clay and its modified form were investigated for use as catalyst. The clay samples were from Ukpor, in Nnewi in Anambra state, south eastern Nigeria. The particle size of 2mm was used. A known weight of the natural clay was mixed with a 36 N sulphuric acid at a molar ratio of 1: 5. The mixture was heated in a furnace at 500^oC, ramped at 5^oC/min for one hour. The resulted clay was calcined at 600^oC for 6 hours. Both samples were characterized using X-ray fluorescence equipment (XRF), X-ray diffraction (XRDP) powder patterns, Scanning Electron Microscopy (SEM), X-ray photoelectron spectroscopy (XPS), Energy Dispersive X-ray (EDX). The results of the treated clay revealed it's amorphous, 67% increase of silicon. The EDX revealed 36.5% Si, 2.4% Al. No significant change in the O_2 of both samples. Surface area was 500 m^2/g. The Si/Al ratio was raised to 15.0 for the treated clay. De-alumination method used showed greater influence on the physiochemical properties compared to aqueous HCl, $NaHSO_4$ and H_2SO_4. This opens up higher possibility of controlling the degree of alumina and silica by choice for different industrial applications.

Keywords: *Clay; Beneficiation; Dealuminated clay; Dissolution; Sulphuric acid*

INTRODUCTION

The creation of powerful new materials for innovative applications is one of the big technical and scientific challenges in our day. Clay, an aluminisilicate, material can be a good source of silica. High purity silica is used in a variety of industrial applications. It is used as a filler, a catalytic support, in optical glasses, in fused silica wares, and as a waveguide. Also, clays are solid minerals that can function as both Bronsted and Lewis acids in their natural and ion exchanged form. Ion exchange is the property of clays to adsorb certain anions and cations as well as their capacity to retain them in exchangeable state. In other words, the adsorbed ions are exchanged for other anions and cations in an aqueous solution, however, such exchange reaction can also take place in non-aqueous medium. The exchangeable ions are held around the outside of the silica-alumina clay structural units, and the exchange reaction generally does not affect the structure of the silica-alumina packet (Carlson, 2004). A well-known example of the ion exchange reaction is the softening of water by the use of zeolites. Clay minerals are the most important chemical weathering products of aluminium rich rocks. Generally, clay is crystalline, the atoms are arranged in a regular order. The character of the clay mineral found in a given soil depends on the nature of the parent material, climate, topography, vegetation and time during which these factors have operated (Grim, 1992). Aluminosilicates is a three dimensional framework structure of silicate mineral in which the silicon atoms are replaced by aluminium atoms in a negatively charged framework with other cations uniformly distributed through it (Obaje *et al*., 2013).

Treatments of clay involve subjecting clay to various treatments so as to modify the properties for the intended purpose. Such treatments include doping, desilication, dealumination, etc. Modifying the properties of clay can lead to variety of catalysts that are useful in effecting more different reactions and higher selectivity in product structure and yield. Their chemical composition and crystal structure are the basis on which clay is divided into groups, such as Kaolinite, Ulite,

Smectite and Chlorite. Among these, the most useful as a catalyst is a sub-group of the Smectite clay called Montmorillonite which is the main constituent of bentonites and Fuller's earth. (Arata and Hino 2011). Clay is important in the construction industry both as a building material and as a foundation for structures. An important industrial application of clays can be found in petroleum and petrochemical processing. Others include ceramic, electrical, pharmaceutical, paint, paper, nuclear energy and textile industries, respectively, etc. Pillared clays which are more stable at higher temperatures (>200°C) are used in petroleum cracking, catalytic reforming and isomerisation of n-alkanes to branched chain alkanes. Many synthetic aluminosilicate can be made and several are manufactured industrially for use: as an ion exchanger and molecular 'sieves, examples are feldspars and zeolites (Fernando and Joan, 2007). The authors studied the dealumination of kaolin using sodium potassium hydroxide during gel formation for the synthesis of zeolite X. A variety of organic reaction that are catalysed by Bronsted acids or Lewis acids have been shown to take place in clays especially montmorillonite, more efficiently under milder conditions, with greater selectivity, better yield, and shorter reaction times.

EXPERIMENTAL PROCEDURE

The clay sample was pre-treated and sieved to 2mm. Dealumination of kaolin was carried out according to Iyakwari *et al*. (2016). A known weight of the natural clay was mixed with a standard analytical-grade 36 N sulphuric acid (H_2SO_4) solution at a molar at a ratio of 1: 5. Aliquot of the mixture was placed in open quartz crucible. It was heated in a furnace at 500^oC, ramped at 5^oC/min for one hour. Once the reaction time and temperature was reached the crucible was left in the furnace for 6 h. The physio-chemical properties of the resulted material were analysed. The catalytic surface areas of the catalysts were obtained from N_2 adsorption isotherms determined at 77K using the Coulter^{TM} (SA 3100^{TM} series). The samples were outgassed under high vacuum for 2 h at 200°C prior to the analysis. The pore size was determined using ImageJ software with SEM images. The crystallite size of the modified sample was calculated using data from X-ray diffractogram and X'pert data viewer software in the Scherrer's formula.

RESULTS AND DISCUSSION

The textural properties and elemental analysis of the natural and the dealuminated clay are given in Table 1. For convenience clay is designated as 'C' and its modified form as 'DC'.

Table 1: Result of Physical Analysis

Parameter	Natural clay (C)	Dealuminated clay (DC)
Specific surface area, m^2/g	100	500
Particle size, µm	250	250
Particle density, kg/m^3	1120	850
Pore-volume, m^3/g	0.25	0.40
Porosity	0.34	0.45

The XRPD pattern of the clay was crystalline with three mineral phases identified (kaolinite, quartz and mica) however, the quartz and mica were minor. In the X-ray diffraction pattern of dealuminated clay, there were no kaolinite crystalline peaks. The disappearance of these major peaks gave way to amorphous material with a very broad band within the low-range angle 15-35^o 2θ as in shown in Figure 1Figure. Rosenberg and Anderson (2012) described the broad band as an amorphous phase of silica (SiO_2).

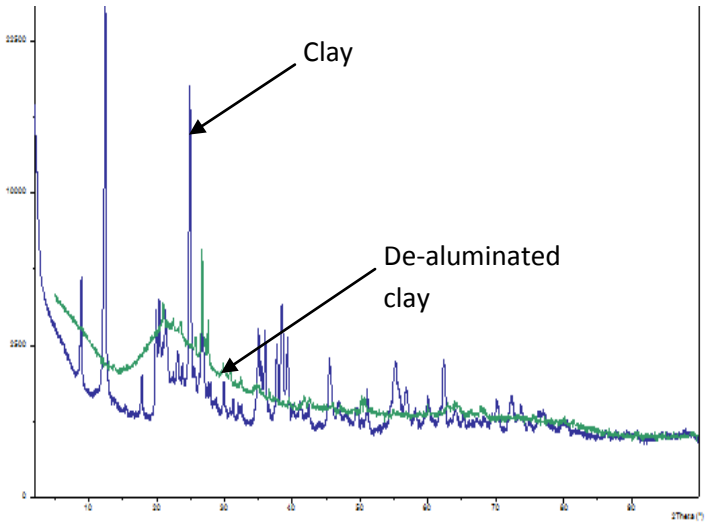

Figure 1: XRPD patterns of both clay and its de-aluminated form

The elemental analysis shows that the aluminium content was reduced by 86% and the silicon increased by 69% (Table 2). However, the level of oxygen remained relatively constant. The presence of 0.9 wt% sulphur in the dealuminated clay is due to the sulphuric acid that was used during the dealumination of the clay.

Table 2: Textural and Elemental Composition of clay and dealuminated samples

Catalyst	Crystallite size (nm)	Elemental analysis (EDX) (wt%)					
		O	Si	Al	P	Fe	S
C (clay)	42.06	57.8	21.5	18.0	1.9	0.9	-
DC (dealuminated clay)	-	57.3	36.5	2.4	2.9	-	0.9

The dealumination was clearly successful, as the SiO_2/Al_2O_3 ratio of the clay, which was initially 1:2 increased to 15.0 (EDX analysis in Table 3). The modified clay has more silica and less alumina than the natural clay.

Table: 3 Elemental Analysis and Textural Properties of Support

Sample	Si/Al (wt%)	XRD pattern
C (clay)	1.2	Crystalline
DC (dealuminated clay)	15.0	Amorphous

The effect of dealumination on percentage composition of the Si and Al was also shown by XPS analysis. The Al 2p spectra for clay and its dealuminated form at the same binding energy of 74.5eV (**Error! Reference source not found.**2), correspond to aluminium (III) oxide (Moulder *et al*., 1995; Wagner *et al*., 2000) .

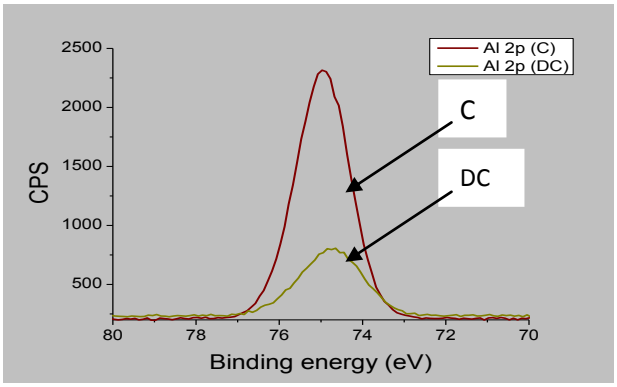

Figure2: XPS Spectra of Al 2p of clay and the dealuminated samples

The silicon (Si 2p) spectra of both samples were very similar around 103.3eV (the binding energy of silicon), as shown in **Error! Reference source not found.**3, which is a confirmation Si^{4+} in silicon oxide.

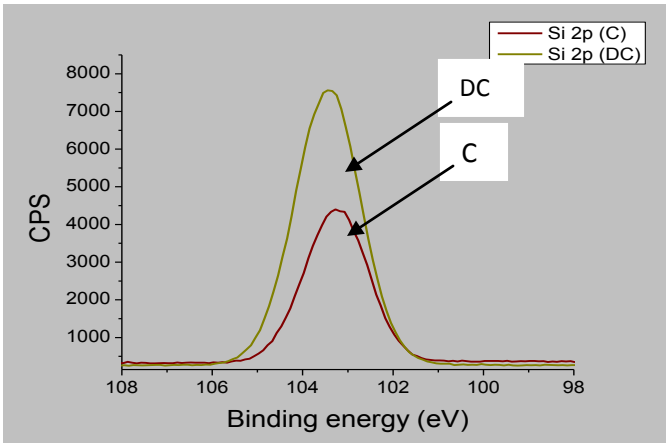

Figure 3: XPS Spectra of Si 2p of both clay and the dealuminated samples

CONCLUSION.

The process of dealumination showed noticeable change in the properties of the clay. The result showed that the dealuminated clay had increased surface area; generally, it revealed improved physical properties of the treated clay sample. From the results obtained, it was deduced that the chemical composition of the dealuminated clay sample was different from the natural sample. However, the chemical composition was not relatively altered, but the percentages were altered. This research has successfully reduced the Al^{3+} and increase the Si^{4+} of clay via a very simple process. Thereby, increasing the clay's ability for Bronsted acid characteristics if used as catalysts or doped with metals for various industrial applications. The resulted aluminium sulphate is also an industrial chemical.

REFERENCES

Arata, K. and Hino, M. (2011) 'Preparation of superacids by metal oxides and their catalytic action', *Materials Chemistry and Physics*, 26, (3-4), pp. 213-237.

Carlson, L., 2004. Bentonite Mineralogy, *Finland Geological Survey Working Report* 2004-02, pp 108.

Fernando G. C. and Joan Llorens (2007) 'Study of the dissolution of dealuminated kaolin in sodium–potassium hydroxide during the gel formation step in zeolite X synthesis', *Microporous and Mesoporous Materials*, 100, pp. 302–311

Grim, R.E., 1992. *Applied clay mineralogy*, McGraw-Hill Book Co., New York.

Iyakwari, J., Agbajelola, D. O., S. Farrow, T. S. and Eterigho, E. J. (2016) Assessment of Heavy Metal Contamination on Dumpsite in Kuyi Village, Niger State, Nigeria, *Int'l Journal of Research in Chemical, Metallurgical and Civil Engineering.* (IJRCMCE) Vol. 3, Issue 1 pp 42-44

Moulder, J. F., Chastain, J., Stickle, W. F., Sobol, P. E. and Bomben, K. D. (1995) *Handbook of x-ray photoelectron spectroscopy: a reference book of standard spectra for identification and interpretation of XPS data.* Physical Electronics.

Obaje, S. O., Omada, J. I. and U. A. Dambatta (2013) Clays and their Industrial Applications: Synoptic Review, *International Journal of Science and Technology*, pp264-270

Rosenberg, D. J. and Anderson, J. A. (2002) 'On determination of acid site densities on sulphated oxides', *Catalysis Letters*, 83, (1-2), pp. 59-63.

Wagner, C. D., Naumkin, A. V., Kraut-Vass, A., Allison, J. W., Powell, C. J. and Rumble, J. R. (2000) *NIST X-ray Photoelectron Spectroscopy Database* Available at: http://srdata.nist.gov/xps/Default.aspx (Accessed: 02/02/13).

DEVELOPMENT OF NIGERIA'S BITUMEN FOR NATIONAL ECONOMIC GROWTH: OPPORTUNITIES FOR MEMBRANE SEPARATION TECHNOLOGY

***Muritala, K. B.[1] and Adewole, J. K.[2]**

[1]Chemical and Polymer Engineering, Lagos State University, Lagos, Nigeria

[2]Center for Integrative Petroleum Research, College of Petroleum Engineering & Geosciences, King Fahd University of Petroleum & Minerals, Dhahran 31261, Saudi Arabia

kabirmuritala@gmail.com

ABSTRACT

Nigeria is richly endowed with a variety of solid minerals ranging from precious metals to precious stones and industrial minerals. The Nigeria Extractive Industry and Transparent Initiative (NEITI) reported that there are forty (40) different kinds of solid minerals and precious metals buried in Nigeria soil waiting to be exploited and processed. One of such minerals is Bitumen. Processed bitumen plays an important role in many everyday applications. It is one of the most used solid mineral resources. The massive investment in infrastructure that will be required to cater for this exploitation presents a research opportunity into how solid minerals are explored and processed in Nigeria. Membrane separation (MS) technique is an essential separation and purification technology that can be used for a sustainable solid mineral processing and purification. This is due to its simplicity, lower capital and operating costs, and energy efficiency. It is a commercially successful competitor to other conventional separation techniques that are currently employed for solid mineral production, purification and treatment. The essence of this paper is to acquaint the readers with the immense benefits of membrane separation techniques in the extraction of Nigeria Bitumen and possibly see necessity of investing into its development.

Keywords: *membrane filtration, energy consumption, solid minerals treatment, produced water.*

1.0 INTRODUCTION

Minerals are naturally occurring inorganic substances with a definite and predictable chemical composition and physical properties(Mohammed, et al., 2013, Vancleave, 2010). They can be in the form of solid, liquid or gas (such as metallic ores, crude oil and natural gas). Solid minerals are said to be mined in solid form before undergoing processing. And there are various forms of solid minerals; these include ores of metals (iron ore, gold), limestone, bitumen, coal and so on (Ajaka, 2009).

Bitumen is a sticky, black and highly viscous liquid or semiliquid form of petroleum. It may be found in natural deposits or may be refined product; it is a substance classed as a pitch (Muhammad, 1992). Its viscosity ranges between 8 and 10 API degrees. Its density (kg/m^3) lies between 1.0 and 1.18 and it is insoluble in water. It has a boiling point greater than 300^0C with melting point ranging from 54 - 173^0C and flash point greater than 200^0C. Bitumen is around 95% hydrogen and up to 5% sulfur, 1% nitrogen and 1% Oxygen and 200ppm metals (www.aboutcivil.org).

Processed bitumen plays an important role in many everyday applications. It is one of the most used solid mineral resources. It is said to be useful in Roofing, Sports, Environmental protection, pipe coating, Land slip containment, walkways, sound proofing, electrical insulation, cosmetics, medicine and textiles. Bitumen's waterproofing and adhesive properties, durability and resistance to heavy loads make it the ideal material for use in all-weather environments. It is also a prime material in applications where strength and weather proofing are essential requirements. Moreover, bitumen membranes are extensively used as sound-deny panels in the automobile markets. It is also used as bituminous paints and disinfectants on a number of different surfaces, bitumen-based lubricants, preservative to plastic, sealants, and as asphalt for road construction and maintenance (Jacques, 2009, Kristjandottir, 2006).

The total estimate of natural occurring bitumen deposit reserve in the World was in the range of 600 and 21,000 billion metric tons (3,000 and 6,100 billion bbl) (Adewusi, 1992) and about 88 countries have been identified having known deposit of heavy oil and oil sands. The largest deposits are in Athabasca area in the north eastern part of the province of Alberta Canada,

this reserve contains ore 700 billion bbl. Other deposits, each containing 15 million bbl of bitumen are identified and are located in USA, Venezuela, Albania, Rumania, Malagasy and USSR (Ademodi et al., 1987, Adewusi, 1992).

Bitumen is found in large amounts worldwide but in exceptionally large quantities in Canada and Venezuela. Nigeria is also reported to have the second largest deposit of tar sand in the world containing about 41 billion barrels of oil found in cretaceous ferruginous sediments extending over about120km from Ogun state, across Ondo state to the margin of Edo state. When fully developed, the industry will no doubt meet local requirements for road construction, farming improvement and also become a source of foreign exchange for the country (Milos, 2015, Enu, 1985).

Bitumen is used primarily for paving roads and for the production of water proofing products, such as roofing felts and for sealing flat roofs. As a result of the increase in oil price since 2003, upgrading of bitumen to synthetic crude has become economical. Considering the scarcity of prime coking coals, bitumen extract has also been used as additive to upgrade medium coking coals to cokeable grade for coke making. The Nigerian market for bitumen has been estimated at about 150,000 per annum (Sepulveda et.al, 2010, Weskamp et.al, 1987). Thus, incorporating energy efficient and cost effective separation technology such as membrane into exploration, processing and purification of bitumen in Nigeria cannot be over emphasized. Specific roles of membrane separation processes in the bitumen industry include separation of bitumen from sand, water and minerals, treatment or removing residual water and upgrading various fractions.

2.0 OVERVIEW OF MEMBRANE SEPARATION TECHNOLOGY

In several processing industries, separation technology is widely used for separation and purification of mixtures. In the industry, separation process consumes 40% of industrial energy needs which is equivalent to 13.2% of total energy consumption. Separations take advantage of differences in physical or chemical properties of the mixture components. Out of the several separation techniques that are presently available, membrane separation technology could be used to bring about significant reduction energy consumption in solid mineral processing. There are several other advantages of using membrane separation technology when compared to other techniques (Ahmad, et al., 2013, Ahmad, et al., 2014, Koros, et al., 2009).

1. Membrane can separate components of mixtures in its native state.
2. Theoretically, all the industrial separation needs can be met by using membrane process
3. Most membrane processes generally do not require a phase change to make a separation
4. It is a modular separation system which requires relatively less energy
5. Membrane processes present basically a very simple flow sheet
6. Systems employing differing classes of membranes ranging from microfiltration to reverse osmosis allow for precise contaminant removal at the lowest cost
7. Membrane systems typically require 50-70% less space than conventional technologies
8. Membrane system have competitive life expectancy
9. Membrane processes are environmentally benign since they require the use of relatively simple module,non-harmful materials or solvent and less carbon emission.
10. Membrane system contains no moving parts.

Table 1 Comparison of Energy Consumption of Membrane with Conventional Separation Techniques used Process Industry(Blume, 2004, Collings, et al., 2004, Eykamp, 1997, Gottschlich and Jacobs, Humphrey and Keller, 1997, Koros, Kratochvil, Shu and Husain, 2009)

Processes	Energy Consumption
Suspended Particles and Macromolecular Solutes Processing	
Flash Evaporation	73kwh/m^3
Micro/ Ultra Filtration	7.6Kwh/m^3
50millions gallons/day Seawater Processing	
Thermal Distillation Plant	78.5Kwh/m^3
State-of-the-art Seawater RO	6.7Kwh/m^3
Propylene/Propane Separation	
Cryogenic Distillation	0.302Kwh/lb propylene prod
Vapor Permeation Membrane	0.050Kwh/lb propylene prod

Table 1 shows the comparison between the energy requirement for membrane and other conventional separation processes used in the process industries.

Despite the advantages of membrane over other separation processes, its use in industry is still relatively low. Some of the major reasons for this is the fear that is usually associated with the use of new technologies. Moreover, the life span of the conventional separation process plants (which may be up to 30 years) makes it difficult to immediately replace them with new ones. Thus, it is technically and economically advisable to initially inculcate the use of membrane while building new processing plants rather than replacing them in already existing plants. For existing plants, membrane can be introduced in the form of retrofit and use as hybrid along with the existing separation units.

Membrane separation processes differ based on separation mechanisms and size of the separated components. The widely used membrane process include microfiltration (MF), ultrafiltration (UF), nanofiltration(NF), reverse osmosis(RO), dialysis, electrodialysis, gas separation, pervaporation, membrane distillation, membrane crystallization and membrane contactors(Adewole, et al., 2013, Adewole, et al., 2015, Criscuoli, 2009, Eykamp, 1997, Li and Chen, 2005). All these processes differ in membrane material characteristics, membrane pore size and operating pressure to which they are exposed to. For instance, microfiltration membrane is defined as having pore size >0.1micron, ultrafiltration is as having between 0.01 and 0.1micron, while nanofiltration is defined as > 0.001 and <0.01micron (Eykamp, 1995, Meynen, et al., 2014, Petersen, 1993).

Dialysis is the transfer of solute molecules across membrane by diffusion from a concentrated solution to a dilute solution. In the electrodialysis process (such as the concentration of brine) a typical electrodialysis stack consists of a series of anion-exchange and cation-exchange membranes arranged in an alternating pattern between an anode and a cathode to form individual cells (Strathmann, 1995). A reverse osmosis membrane separates the various low molecular-weight molecules and ions from the solvent by forcing the solvent or major component to pass selectively through the membrane by applying pressure greater than the normal osmotic pressure. Separation occurs based on size, solubility, and/or charge of the various penetrant species(Strathmann, 1995). Ultrafiltration is another pressure-driven membrane process capable of separating somewhat larger solution components on the basis of molecular size and the shape under an applied pressure difference across the membrane. In this process, the smaller molecules pass through the membrane and are collected as permeate while the larger molecules are retained by the membrane (Blume, 2004, Eykamp, 1995, Li, et al., 2005). The microfiltration process is similar to the ultrafiltration process, except that its effective separating range is from 1000Å to 100000Å in molecular size whereas the ultrafiltration range is from 10Å to 1000Å (Petersen, 1993,Singh,etal.,2012). The most commonly used synthetic membrane devices (modules) are flat sheets/plates, spiral wounds, and hollow fibers.

Flat plates are usually constructed as circular thin flat membrane surfaces to be used in dead-end geometry modules. Spiral wounds are constructed from similar flat membranes but in the form of a “pocket” containing two membrane sheets separated by a highly porous support plate (Osada et al., 1992). Several such pockets are then wound around a tube (figure 1) to create tangential flow geometry and to reduce membrane fouling. Hollow fiber modules consist of an assembly of self-supporting fibers (figure 2) with dense skin separation layers, and a more open matrix helping to withstand pressure gradients and maintain structural integrity (Osada et al., 1992). The hollow fiber modules can contain up to 10,000 fibers ranging from 200 to 2500 μm in diameter. The main advantage of hollow fiber modules is very large surface area within an enclosed volume, increasing the efficiency of the separation process

.

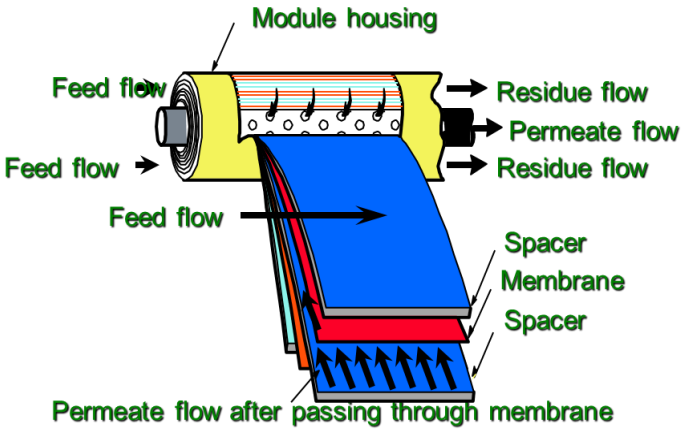

Figure 1: Spiral wound membrane module;(Source: MTR Inc, *Aquilo Gas Separation)*

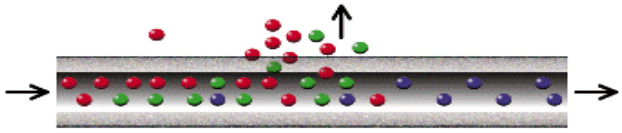

Figure 2: Cross Section representation of Hollow Fiber; (Source: MTR Inc, Aquilo Gas Separation)

3.0 SEPARATION METHODS IN BITUMEN INDUSTRY

The extraction of bitumen from oil sand mines involves the liberation and separation of bitumen from the associated sands in a form that is suitable for further processing in order to produce a marketable product. Among several processes for bitumen extraction, the Clark Hot Water Extraction (CHWE) process is a well-developed commercial recovery technique. In the CHWE process, mined oil sands are mixed with hot water to create slurry suitable for extraction. Caustic soda is added to adjust the slurry pH to a desired level in order to enhance the efficiency of the separation of the bitumen. Recent industry development has shown the feasibility of operating at lower temperatures and without caustic addition in the slurring processes. In the CHWE process, the extract typically comprises hydrocarbon predominant phase (known as tailing stream) which is made up of coarse solids, some fine solids, and water. A typical composition of bitumen froth stream is about 60wt% bitumen, 30wt% water and 10wt% mineral matter(solids). The water and mineral matter in the froth are considered as contaminants. Therefore, the froth needs to be purified to eliminate the contaminants or reduce them to a level suitable for feed into an oil refinery or an upgrading facility.

The process to reject the water and mineral matter contaminants are known as froth treatment process. Due to the high viscosity of bitumen, the first step in the treatment is usually the introduction of a solvent. There are two major commercial approaches to reject the froth contaminants, namely naphtha solvent-based froth treatment, and paraffinic solvent-based froth treatment. Solvent addition (dilution) increases the density differential between bitumen, water and mineral matter. Contaminants rejection can be carried out by a number of methods, such as centrifugation or gravity separation. The separation scheme generally results in a product effluent stream of diluted bitumen and a reject or tailings stream, commonly referred to as the froth treatment tailing (which comprises of mineral matter, water, residual solvent, and some residual bitumen). In the paraffinic froth treatment process, the solvent dilution reduces the precipitation of asphaltenes from the bitumen as an additional contaminant which results in an improvement in the efficiency of the contaminant rejection process(Milos, 2015).

An example of froth treatment (NFT) is disclosed in US Patent (Tipman and Sankey, 1993). Addition of naphtha may yield a bitumen product containing 1 to 3wt% water and <1.0wt% solids. However, such product composition does not meet pipelines specifications and renders the NFT product stream unsuitable for transportation through pipeline. Paraffinic froth treatment (PFT) was described in Canadian Patents(Sharma and Raterman, 2014, Shelfantook, et al., 2002). Addition of sufficient amount of paraffinic solvent results in asphaltene precipitation, formation of aggregates with the contaminants, and settling. Unfortunately, conventional treatments which separate water and mineral matter will not remove very fine particulate (fines) from the froth. Therefore, PFT settling vessels are sized to allow gravity settling of fines and other contaminants. This process provides a solids free bitumen product (<300ppm solids, <0.5%BS&W) suitable for transportation in a common carrier to refineries. Bitumen of such quality is termed ‘’fungible’’ because it can be processed in conventional refinery processes without fouling the refinery equipment. However, PFT is energy intensive and expensive and results in a waste stream of asphaltenes (a potentially valuable commodity).

In general, water based extraction and solvent-based extraction are the two processes that have been used to extract bitumen from mined oil sands. The CHWE process, described above, is the most commonly employed water-based extraction, water is the dominant liquid in the process and the extraction occurs by having water displace the bitumen on the surface of the solids. In the case of solvent-based extraction, the solvent is the dominant liquid and the extraction of the bitumen occurs by dissolving bitumen into the solvent.

Solvent based extraction processes for the recovery of the hydrocarbons have been proposed as an alternative to water-based extraction of mined oil sands. However, the commercial application of a solvent-based extraction process has, for various reasons, eluded the oil sand industry. A major challenge to the application of solvent-based extraction to oil sands is the tendency of fine particles within the oil sands to hamper the separation of solids from the hydrocarbon extraction. Solvent extraction with solids agglomeration is a technique that has been proposed to deal with this challenge. The original application of this technology

was coined Solvent Extraction Spherical Agglomeration (SESA). A more recent description of the SESA process can be found in (Sparks, et al., 1992).Solvent extraction bitumen has a much lower solids and water content than bitumen froth that was produced in the water-based extraction process. However, the residual amounts of water and solids content in solvent extraction bitumen may nevertheless render the bitumen unsuitable for marketing.

3.1 Bitumen Extraction and Processing in Nigeria

Nigeria's Ministry of Mines and Steel Development identified three potential methods of bitumen extraction in Nigeria:

- Small-scale surface mining
- Large-scale surface mining and
- In-situ extraction.

The depth of bitumen below the surface determines which extraction type is possible. Both in-situ and large scale surface mining operations are most likely to extract bitumen for upgrading into synthetic crude oil and/or other petroleum products. Bitumen from small scale surface mining is likely to only be economical to use for paving roads. Details of all the three types of extraction and their impact are described in literature (Grant, et al., 2013, Milos, 2015).

In Nigeria, the approximate locations of the different types of oil are perhaps best explained as a gradient running north to south, with the heaviest oils generally in the north at the surface and the lightest in the south deep underground (figure Nigeria's Bitumen Belt (Lagos, Ogun, Ondo, and Edo States. Copied from Milos (2015)).3). The region which contains bitumen spans roughly across four states, namely Lagos, Ogun, Ondo, and Edo states. Much of the areas where heavier forms of oil and bitumen can be found remain under explored. Thus, the precise locations of each resource are unknown. The most comprehensive bitumen study to date is Geotechnical Investigations of the Ondo State Bituminous Sands from 1974, and was led by Professor O.S. Adegoke's of the Geological Consultancy Unit of the University of Ife. Few significant studies have been carried out since. The extents shown on the map in Figure 3 identify the zones where surface mining and in-situ mining are most likely to occur (Adegoke, 1980). Some geologists speculate this zone extends all the way to the conventional oil blocks further south.

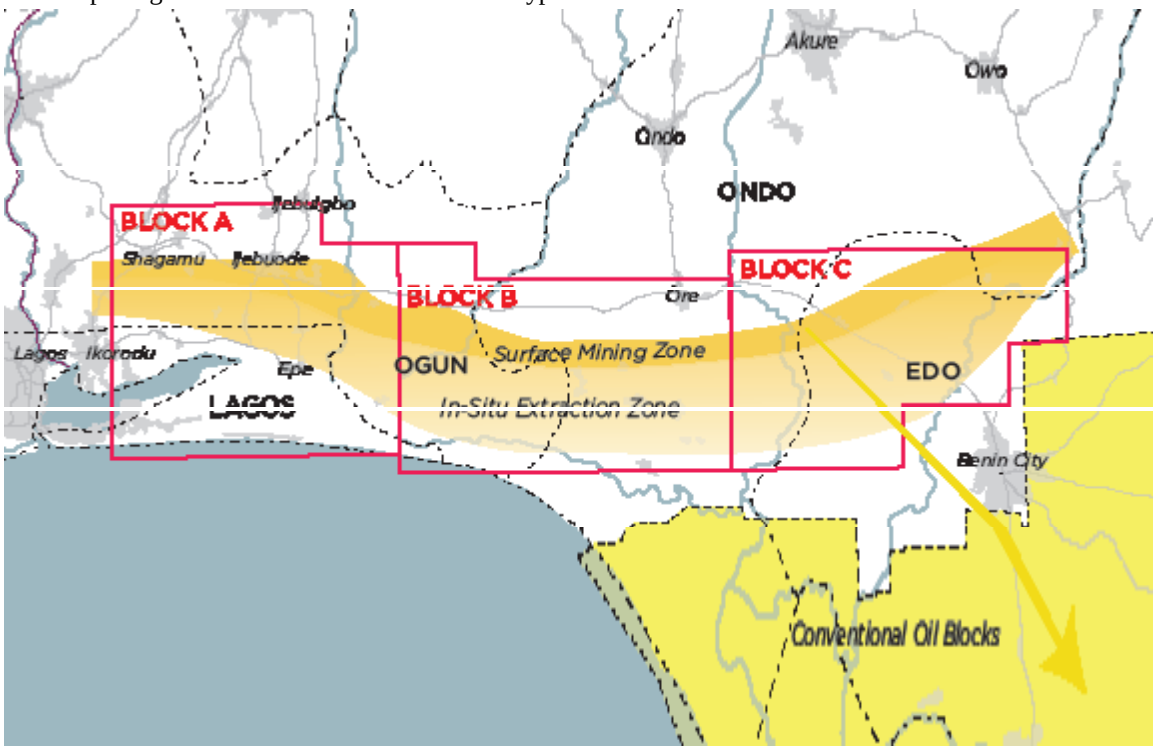

Figure 3: Nigeria's Bitumen Belt (Lagos, Ogun, Ondo, and Edo States. Copied from Milos (2015)).

4.0 ROLES OF MEMBRANE TECHNIQUES IN THE EXTRACTION OF BITUMEN

Membrane technology can be introduced into various stages of bitumen processing. This section is focused on description of some membrane separation processes that are suitable for use in bitumen processing. The U.S patent (Feimer and DesJardine, 1993)disclosed a method of ultrafiltration of heavy hydrocarbons through a multi-stage membrane system. The patent describes at least two identical and sequential ultrafiltration steps to remove metals, conradson carbon residue (CCR), and asphaltenes. Variety of membrane materials such as polymide, polysulfone, polyaryl sulfide, polycarbonate, polyamide, polyacrylonitrile, or ceramic materials can be used in the system. Another U.S Patent (Smith, 1998) demonstrated a process for the selective removal of asphaltenes and metal compounds from oil by ultra-filtration using a membrane. It emphasized the use of ceramic membrane because of its initial fouling resistance.

The invention disclosed in the U.S Patent (Koseoglu, 2014) was directed towards a process for upgrading a heavy oil feedstock. The procedure for heavy oil processing involves thermal cracking of the oil to produce a product stream which is then cooled to an intermediate temperature at which light ends and water can be volatized and removed in flash towers. Following a further cooling, the stream is mixed with an alkane solvent to facilitate asphaltenes precipitation. However, asphaltenes do not settle due to the high viscosity of the liquid. To solve this problem, the inventors suggested a two-step membrane ultrafiltration of the feed stream.

Bitumen product may be produced through a number of extraction methods known in the art. The product effluent stream may comprise bitumen, solvent, precipitated asphaltenes, water and mineral matter. The mineral matter may comprise clay, sand, particulate matter, bulkier contaminants such as coal, wood, shale or large particles, and other solids. Typically, the naphthenic froth treatment (NFT) bitumen comprises 2-3%w/w solids and/or water and does not meet pipeline specifications for transportation. All the contaminants may be removed by filtration-methods (microfiltration, ultrafiltration, or nanofiltration) (Ashtari, et al., 2012, Bakhshayeshi, et al., 2012, Eykamp, 1995, Li, Liang and Chen, 2005, Schwarze, et al., 2012, Singh, Ray, Xie and Hoang, 2012, Ullah, et al., 2012).

A method of water treatment in an in-situ recovery method of producing bitumen from oil sand comprise of separating bitumen-mixed stream so as to leave oil-containing water(which is called "produced water"). The bitumen-mixed fluid could be recovered from the oil sand well via microfiltration membrane using polytetrafluoroethylene (PTFE). Membrane configurations may include flat sheet membranes, spiral wound membranes, tubular membranes, or hollow fiber membranes. All these configurations permit separation of water, mineral matter or asphaltenes from a bitumen stream.

5.0 CONCLUSION

The potential application of membrane separation technology in bitumen processing was presented. The following conclusion can be drawn:

Academic-Industry collaborative is vital in further exploration and development of needed membrane separation techniques and subsequent application in bitumen processing.

Valuable savings could be achieved by using commercially available ready-made membrane systems while aggressively pursuing development of more novel membrane materials and modules to meet up other complex separation challenges in bitumen processing.

Developing countries such as Nigeria need to incorporate membrane units from the beginning of bitumen processing plant construction because conventional energy intensive separation units have 30-50 years useful lives. It is therefore difficult (for economic reasons) to replace them with membrane in future.

Membrane can also be incorporated into existing bitumen processing plants in the form of retrofit and hybrid separation units.

REFERENCES

Adegoke, O.S. Geotechnical investigation of Ondo State bituminous sands, *Vol 1, Geology and Reserves Estimate Report, Geological Consultancy Unit, Department of Geology, University of Ife (1980).*

Ademodi, B., Oshinowo, T., Sanni, S. A. and Olukayode, D. F. Preliminary Studies on the Recovery of Bitumen from Nigerian Tar Sands: I. Beneficiation and Solvent Extraction, *Energy Sources*, 9 (3), 173-188 (1987)

Adewole, J. K., Ahmad, A. L., Ismail, S. and Leo, C. P., "Current challenges in membrane separation of CO_2

from natural gas: A review", *Int. J. Greenh. Gas. Con.***17**, 46 (2013).

Adewole, J. K., Ahmad, A. L., Ismail, S., Leo, C. P. and Sultan, A. S., "Comparative studies on the effects of casting solvent on physico-chemical and gas transport properties of dense polysulfone membrane used for CO_2/CH_4 separation", *J. Appl. Polym. Sci.***132**, 1 (2015).

Adewusi, V.A " *Aspects of Tar sands Development in Nigeria.*

Ahmad, A. L., Adewole, J. K., Ismail, S., Peng, L. C. and Sultan, A. S., "Membrane separation of CO_2 from natural gas: A state-of-the-art review on material development", *Recent advances in mass transport in engineering materials defect and diffusion forum* Öchsner, A., Belova, I. and Murch, G., eds., Trans Tech Publications Inc., pp. 135-147 (2013).

Ahmad, A. L., Adewole, J. K., Leo, C. P., Sultan, A. S. and Ismail, S., "Preparation and gas transport properties of dual-layer polysulfone membranes for high pressure CO_2 removal from natural gas", *J. Appl. Polym. Sci.***131**, 1 (2014).

Ajaka E.O. "Recovering fine Iron minerals from Itakpe Iron Ore process tailing. *ARPN Journal of Engineering and Applied Sciences* 2009;4 (9): 17 28

Ashtari, M., Ashrafizadeh, S. N. and Bayat, M., "Asphaltene removal from crude oil by means of ceramic membranes", *Journal of Petroleum Science and Engineering* **82–83**, 44 (2012).

Bakhshayeshi, M., Teella, A., Zhou, H., Olsen, C., Yuan, W. and Zydney, A. L., "Development of an optimized dextran retention test for large pore size hollow fiber ultrafiltration membranes", *J. Membr. Sci.***421–422**, 32 (2012).

Blume, I., "Norit ultrafiltration as pretreatment for ro for wastewater reuse: The sulaibiya project", *Presentation at Advanced Membrane Technology II Conference*, , Irsee, Germany (2004).

Collings, C. W., Huff, G. A. and Bartels, J. V., USA Patent Pat. Appl. Publ. 20040004040 A1, (2004).

Criscuoli, A., "Basics in membrane contactors", *Membrane operations*, Wiley-VCH Verlag GmbH & Co. KGaA, pp. 449-461 (2009).

Enu, E.I.:"Textual Characteristics of the Nigeria Tar sands, sedimentary Geology, Vol 44, Issue 1 2,pp65 81

Eykamp, W., "Chapter 1 microfiltration and ultrafiltration", *Membrane science and technology*, Richard, D.N. and Stern, S.A., eds., Elsevier, pp. 1-43 (1995).

Eykamp, W., "Membrane separation processes", *Perry's chemical engineers' handbook*, Mc Graw-Hill, New York, NY, p. Chapter 22 (1997).

Feimer, J. L. and DesJardine, L. T., "Multi-stage ultrafiltration process (op-3711)", Google Patents (1993).

Gottschlich, D. and Jacobs, M. L., "Monomer recovery process, membrane technology and research inc., USA, p. 14.",

Grant, J., Angen, E. and Dyer, S., "Forecasting the impacts of oilsands expansion", The Pembina Institute, Calgary (2013).

Houot, R., "Beneficiation of iron ore by flotation — review of industrial and potential applications", *International Journal of Mineral Processing***10**, 183 (1983).

Humphrey, J. L. and Keller, G. E., *Energy considerations, in separation process technology*, Mc Graw-Hill, New York, NY (1997).

Jacques Van Heerden, Origins, Manufacture and Handling of Bitumen(Asphalt Cement) (2009)

Koros, W. J., Kratochvil, A., Shu, S. and Husain, S., "Energy and environmental issues and impacts of membranes in industry", *Membrane operations*, Wiley-VCH Verlag GmbH & Co. KGaA, pp. 139-165 (2009).

Koseoglu, O. R., "Process for upgrading hydrocarbon feedstocks using solid adsorbent and membrane separation of treated product stream", Google Patents (2014).

Kristjandottir, O."Warm mix Asphalt for cold weather paring" University of Washington Master thesis (2006)

Li, C. W., Liang, Y. M. and Chen, Y. M., "Combined ultrafiltration and suspended pellets for lead removal", *Separ. Purif. Technol.***45**, 213 (2005).

Li, J. L. and Chen, B. H., "Review of co2 absorption using chemical solvents in hollow fiber membrane contactors", *Separ. Purif. Technol.***41**, 109 (2005).

Meynen, V., Castricum, H. L. and Buekenhoudt, A., "Class ii hybrid organic-inorganic membranes creating new versatility in separations", *Current Organic Chemistry***18**, 2334 (2014).

Milos, C., "Bitumen in nigeria- weighing the costs of extraction", Abeysteph, Abuja, pp. 1 (2015).

Mohammed, J., Abdulsalam, S. and Ibrahim, A. R., "Hybrid technique for solid mineral processing in ajaokuta steel company (nigeria) using iron ore as case study", *International Journal of Material Science Innovations* (2013).

Osada, Y., Nakagawa, T., *Membrane Science and Technology*, New York: Marcel Dekker, Inc,1992.

Petersen, R. J., "Composite reverse osmosis and nanofiltration membranes", *J. Membr. Sci.***83**, 81 (1993).

Schwarze, M., Schmidt, M., Nguyen, L. A. T., Drews, A., Kraume, M. and Schomäcker, R., "Micellar enhanced ultrafiltration of a rhodium catalyst", *J. Membr. Sci.***421–422**, 165 (2012).

Sepulveda, J.E.,Miller,J.D. and Oblad, A.G." Hot water extraction of bitumen from Utah tar sands, *Mining Eng*., 30(9)1311(1978)

Sharma, A. K. and Raterman, M. F., "Optimizing feed mixer performance in a paraffinic froth treatment process", Google Patents (2014).

Shelfantook, W. E., Long, Y. C. and Tipman, R. N., "Solvent process for bitumen separation from oil sands froth", Google Patents (2002).

Singh, P. S., Ray, P., Xie, Z. and Hoang, M., "Synchrotron saxs to probe cross-linked network of polyamide 'reverse osmosis' and 'nanofiltration' membranes", *J. Membr. Sci.***421–422**, 51 (2012).

Smith, K. J., "Upgrading heavy oil by ultrafiltration using ceramic membrane", Google Patents (1998).

Sparks, B. D., Meadus, F. W., Kumar, A. and Woods, J. R., "The effect of asphaltene content on solvent selection for bitumen extraction by the sesa process", *Fuel***71**, 1349 (1992).

Strathmann, H., "Chapter 6 electrodialysis and related processes", *Membrane science and technology*, Richard, D.N. and Stern, S.A., eds., Elsevier, pp. 213-281 (1995).

Tipman, R. N. and Sankey, B. M., "Process for separation of hydrocarbon from tar sands froth", Google Patents (1993).

Ullah, A., Holdich, R. G., Naeem, M. and Starov, V. M., "Shear enhanced microfiltration and rejection of crude oil drops through a slotted pore membrane including migration velocities", *J. Membr. Sci.***421–422**, 69 (2012).

Vancleave, J., What are rocks?, http://scienceprojectideasforkids.com/2010/science-projects-about-rocks-and-minerals/ (accessed 28th August, 2016 2016).

Westkamp, W., Rhode, W,Stewan,W. and Habermehl,D:"Greater coke strenght through reactive and additives to coking blends proceeding II *international cokemaking congress, September 13, Germany*, section III(1987)

www.aboutcivil.org, Composition & bitumen properties, http://www.aboutcivil.org/# (accessed 28th August, 2016..n.

COMPARATIVE ASSESSMENT OF SYNTHESIS OF ZEOLITE X FROM KANKARA AND ELEFUN KAOLINITE CLAY

[*]Ajayi, O. A.[1], Maciver, V. P.[1], Arowosaiye, M. J.[1] and Adefila, S. S.[2]

[1]*Department of Chemical Engineering*
Ahmadu Bello University, Zaria-Kaduna State
[2]*Engineering and Environmental Management Services, Limited.*
Suit 5, Plot 1469, ZM Plaza, Ahmadu Bello Way, Area 11, Abuja.
Corresponding author: aoajayi@abu.edu.ng *and* segeaj@gmail.com

ABSTRACT

Zeolite NaX was successfully synthesized from both Kankara and Elefun kaolinite clay. Both clays were wet beneficiated, calcined at 850^oC for six hours, to obtain a more reactive metakaolin. The metakaolin was dealuminated using 60wt% tetraoxosulphate (VI) acid for three minutes, washed to neutrality before the introduction of calculated amount of NaOH. The resulting gels were aged for seven days at room temperature and subjected to crystallization temperature of 100^oC for reaction times of 6, 12, 24 and 36 hours, respectively. The samples and products were characterized using XRF, XRD, SEM and BET. The XRF analysis confirmed the status of the raw materials and gave a positive indication of the pretreatment and zeolitization processes. The highest intensity value from XRD was recorded for zeolite NaX at 24hrs reaction time, while the SEM and BET for products at 36hrs tends to be more desirable. The zeolite NaX from Kankara and Elefun obtained at 100^0C at 36hrs had an octahedral shape, highly crystalline in nature, having a specific surface area of about 479m^2/g and 468 m^2/g, respectively. The investigated characteristic properties tend to favorably compete with her commercial NaX (specific surface area-SSA of 423.6 m^2/g).

1. INTRODUCTION

Zeolites are a well-defined class of naturally occurring and synthetically produced crystalline aluminosilicate substances with three-dimensional structures arising from oxygen linked framework of $[SiO_4]^{4-}$ and $[AlO_4]^{5-}$ polyhedral. They are capable of facile and reversible cation exchange. The assemblages of tetrahedra create a porous matrix with regular arrays of apertures having well-defined dimensions so as to be able to selectively admit some molecules into their interiors, whilst rejecting others on the basis of molecular dimensions, giving them the important attribute of "molecular sieving." The properties of ion exchange and molecular sieving have resulted in the successful commercialization of zeolites for industry scale ammonia treatment and in detergent formulations as calcium sequestrants, and make zeolites a strong prospect for removal of heavy metals from acid mine drainage and industrial wastewaters (Breck, 1974).
Zeolite has increasingly finds a number of applications in numerous industrial processes, namely; water purification, catalyst in the petroleum refining processes, preparation of advanced materials and in nuclear reprocessing etc. Therefore, the idea of producing synthetic zeolite to continuously replace its limited natural analog cannot be overemphasized.

Zeolite X is a microporous material with a faujasite framework structure and a Si/Al molar ratio that varies from 1.0 to 1.5. Each unit cell in the three-dimensional pore system of faujasite zeolite consists of 8 supercages, 8 sodalite cages, and 16 hexagonal prisms. Zeolite X has a large pore size (7.3Å) and a high cation exchange capacity – CEC (5meq g^{-1}), which make this zeolite an interesting molecular sieve and a high-cation exchange material (Traa and Thompson, 2002). Zeolite X is receiving increased attention and currently a very attractive material for technological and environmental applications because of its prominent selective adsorption property, (Kim, 2003 and Guesmi *et al.*, 2012), high exchange capacity (Hunger *et al.*, 2000) and medium-strength basic sites. Its wide micropores make it useful for purification and separation of gases and organic components; high exchange capacity allows for adsorption of heavy cations and radionuclides (Derkowski *et al.*, 2007).

In Nigeria, many research works have been reported on the preparation and characterization of zeolites. Preliminary studies on synthesis of zeolite from local clay have been reported by Aderemi (2000), Atta (2007), Kovo (2012), Ajayi, (2012) and Ajayi (2013). Zeolites are usually synthesized from cheap silica-alumina sources in alkaline phase under hydrothermal conditions. The cheap silica-alumina sources include kaolinite. It is therefore very pertinent for researchers, engineers, to continuously investigate properties that will favour the conversion of kaolinite clay to desired zeolite, considering it application in our economy. Hence, in this research work, kaolinite clay mined from both Kankara (Katsina State) and Elefun (Ogun State) was converted using hydrothermal method into zeolite NaX while investigating the effect of crystallization time on its crystallinity.

2. METHODOLOGY AND MATERIALS

2.1 Beneficiation and Calcination of Kaolin

The clay (kaolin) samples were procured from Kankara village in Kastina State and Elefun village in Ogun State, Nigeria. Both kaolin samples were weighed and soaked in water for three days. During this period the slurries were stirred periodically (every 12 hours) after decantation of the supernatant water and addition of fresh water. The fine suspension thus obtained from each clay samples was sieved and allowed to settle. Thereafter the sediment was dried under atmospheric condition, followed by oven drying at 100^{o}C for 12 hours. The product from this stage is hereafter referred to as beneficiated Kankara kaolin (BKK) and Elefun kaolin (BEK). After drying, the beneficiated kaolin was ball milled to obtain a desired particle size. The beneficiated kaolinite clay was converted into a more reactive form - metakaolin through heating at elevated temperature of 850^{o}C in a muffle furnace for 6hours.

2.2 Dealumination

In a conical flask, 30g of metakaolin was added to 134.40ml of distilled water and 122.78ml of 96wt% H_2SO_4 (equivalent to 5-fold stoichiometric acid requirement and to form 60wt% of acid solution) to start the dealumination reaction. The reaction was driven by the thermal energy released by the acid-water mixture, with residence time set at 3 min (Ajayi *et al.,* 2010). After the set time, the reaction was quenched with 207.2ml of distilled water to bring the acid concentration to about 38wt%. The flask content was filtered through a vacuum pump filtration unit and the recovered solid was washed with deionized water in order to remove the excess acid. The de-aluminated metakaolin was dried, crushed and preserved for further application and analyses.

2.3 Gel formation and Ageing

10g of the dealuminated metakaolin (from Kankara) sample was weighed and transferred into a conical flask, where 57cm^3 of de-ionize water was introduce in batch of 35cm^3 and 22cm^3 respectively. 35cm^3 of the de-ionize water was introduce into a conical flask containing the 10g of dealuminated metakaolin sample and the mixture was agitated for about 10mins. 8.6g of the NaOH pellet was introduced under constant stirring until the mixture becomes thicker and the remaining 22cm^3 of the de-ionize water was added until a jelly like solution was noticed. The same procedure was repeated for kaolin from Elefun and the resulting gels formed were transferred into a label polypropylene bottles and aged quiescently for a period of seven days at room temperature.

2.4 Crystallization

After seven days aging, the samples in the porcelain bottles were subjected to an elevated temperature of 100^{o}C in a calibrated microwave oven. The microwave oven consumes 1,100 W AC and produces 700 W of microwave power, an efficiency of 64%, while 400 W are dissipated as heat, mostly in the magnetron tube. The reaction was made to take place at the specified temperature of 100^{o}C and time of 6hrs, 12hrs, 24hrs and 36hrs, respectively. After the synthesis, the samples were washed thoroughly with deionized water to neutrality, filtered, dried, and stored for characterization. Based on previous investigations (Ansari *et al*., 2013 and Ngoc *et al*., 2013), the crystallization temperature of 100^{0}C was chosen.

2.5 Characterization

The materials obtained at various stages were subjected to analyses, namely XRD, EDX-SEM, XRF and BET. X-Ray Fluorescence mineralogical composition of the samples was determined using a Thermo Fisher ARL9400 XP+ Sequential XRF equipped with a WinXRF software was for analyses. The samples were milled in to achieve particle sizes <75micron, dried at 100°C and roasted at 1000°C to determine Loss on Ignition (LOI) values. 1g Sample was mixed with 6g lithium tetraborate flux ($Li_2B_4O_7$) and fused at 1050°C to make a stable fused glass bead. The XRF analysis for the clay was conducted following ASTM C114 standard for oxide identification.

X-ray powder diffraction (XRD) patterns were collected on an XPERT-PRO diffractometer (PANalytical BV, Netherlands) with theta/theta geometry, operating a cobalt tube at 35 kV and 50 mA. The goniometer is equipped with automatic divergence Slit and a PW3064 spinner stage. The XRD patterns of all specimens were recorded in the 5.0°- 90° 2θ range with a step size of 0.017° and a counting time of 14 s per step. The XRD analysis was conducted following ASTM 2478, standard for clay identification, while those for zeolite NaX were conducted following ASTMD5758.

SEM and EDX analysis were recorded by using LEO S430 scanning electron microscope coupled with energy dispersive X-ray analyzer model Oxford LINK ISIS. Samples were prepared by dispersing dry powder on double sided conductive adhesive tape. Samples were coated with carbon by arc discharge method for SEM-EDX. Samples were scanned in secondary electrons (SE) for morphology and back scattered electrons (BSE) mode for compositional image.

In order to determine the specific surface area, automated gas adsorption analyzer, AUTOSORB-1 (Quanta Chrome Instruments, USA) was used with adsorption-desorption isotherms of nitrogen at -196^{0}C. For each analysis, 0.2g of sample were degassed at 300^{0}C under nitrogen for at least 3h. The specific surface areas of sample were calculated by the BET (Brunauer, Emmett, and Teller) method. The Specific surface area were determined following the standard method of ASTM C1274.

3.0 RESULTS AND DISCUSSION

3.1 Beneficiation processes-physical, thermal and chemical

The compositional analysis of the raw kaolin (Kankara and Elefun) depicted in Table 4.1 indicated that Kankara

is richer in oxides of potassium, while Elefun had a higher value for TiO_2 and both recorded similar composition for oxides of iron and magnesium. This observation was attributed to sources, location and mode of formation i.e. either potash or ferric kaolin. The effect of these inherent impurities could be noticed in the silica/alumina ratio of the starting kaolin. Theoretically, the silica/alumina ratio for pure kaolin is expected to be 2 or slightly less than 2 but not greater than 2. In this case Elefun kaolin had a relatively higher silica to alumina ratio, which might suggest level of impurities and probably incomplete formation of the kaolinite structure.

Table 2: Composition of raw, beneficiated, calcined and dealuminated kaolin

	Na_2O	MgO	Al_2O_3	SiO_2	P_2O_5	SO_3	K_2O	CaO	TiO_2	Fe_2O_3	ZnO	SrO	Si/Al
RKK	0.123	0.460	39.646	56.627	0.18	0.215	1.417	0.103	0.213	0.964	0.002	0.003	**2.42**
BKK	0.113	0.380	41.92	54.62	0.10	0.002	1.410	0.101	0.313	0.970	0.042	0.009	**2.21**
CKK	0.125	0.452	40.423	55.98	0.15	0.100	1.412	0.103	0.213	0.950	0.002	0.003	**2.35**
DKK	0.00	0.225	19.32	78.41	0.00	0.371	0.621	0.065	0.403	0.566	0.000	0.002	**6.89**
REK	0.000	0.359	30.720	60.762	0.000	0.315	0.377	0.021	4.888	1.182	0.003	0.005	**3.36**
BEK	0.103	0.480	38.92	55.62	0.00	0.301	0.360	0.001	2.313	1.170	0.022	0.003	**2.43**
CEK	0.125	0.452	40.423	54.98	0.12	0.208	0.442	0.103	0.213	0.750	0.012	0.002	**2.31**
DEK	0.00	0.199	16.91	76.30	0.00	0.363	0.363	0.077	4.958	0.828	0.000	0.002	**7.66**

Legend

RKK	Raw Kankara Kaolin	DKK	Dealuminated Kankara Kaolin	CEK	Calcined Elefun Kaolin
BKK	Beneficiated Kankara Kaolin	REK	Raw Elefun Kaolin	DEK	Dealuminated Elefun Kaolin
CKK	Calcined Kankara Kaolin	BEK	Beneficiated Elefun Kaolin		

The XRD pattern of the raw kaolin gave all the characteristic kaolinite peaks, with some peaks that can be attributed to quartz, illite, smectite, halloysite and muscovite (Figure 1). These peaks were found to conform satisfactorily to those in the open literature (Pinheiro *et al.*, 2005; Lenarda *et al.*, 2007; Panda *et al.*, 2010). The parent clay showed well defined reflections at 2Θ values of 12^0 and 30^0 (corresponding to the d values of 7.154Å; a reflection from [001]) giving typical characteristic peaks of kaolinite. The Kankara kaolin was found to contain, aside anatase, phases like potassium iron oxide and forsterite, resulting from the presence of potassium and ferric oxide in the raw kaolin. The XRD peaks were found to correlate with the XRF result as the 2Θ values of 12^0 for Elefun kaolinite clay was found to have very low intensity.

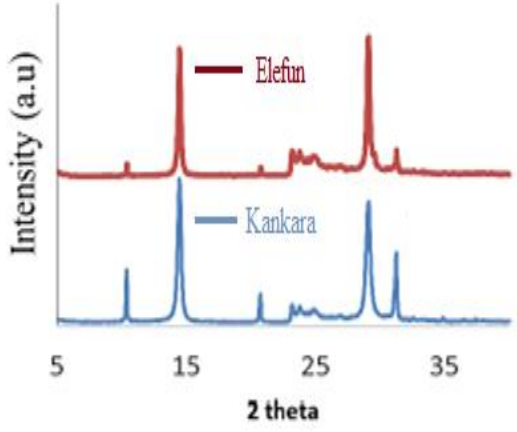

Figure 1: XRD patterns for raw Kankara and Elefun kaolinite clay.

The closely packed flaky particles are stacked together in agglomerates and seem to be predominant in both sample analyzed, as depicted in Figure 2. Noticeably small aggregate particles found in between the silica-alumina plates, under higher magnification, are indicative of inherent impurities, which are predominant in Elefun clay as shown in Figure 2 (b).

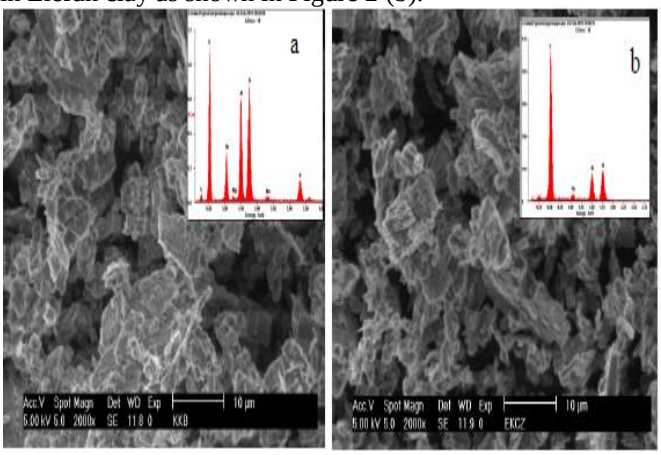

Figure 2: SEM and EDX for raw Kankara (a) and Elefun (b) kaolinite clay.

The XRD patterns of the calcined products presented in Figures 3 (a and b) are semi-amorphous in nature. The peaks for kaolinite disappeared upon thermal treatment, but it was observed that some phases were relatively passive to the thermal treatment. These observations were similar to those reported for metakaolins by other researchers (Belver *et al.*, 2002, Elimbi *et al.*, 2011). The intensity of some inherent impure phases like microcline, illite, dickite and brookite were also observed to reduce drastically with thermal treatment.

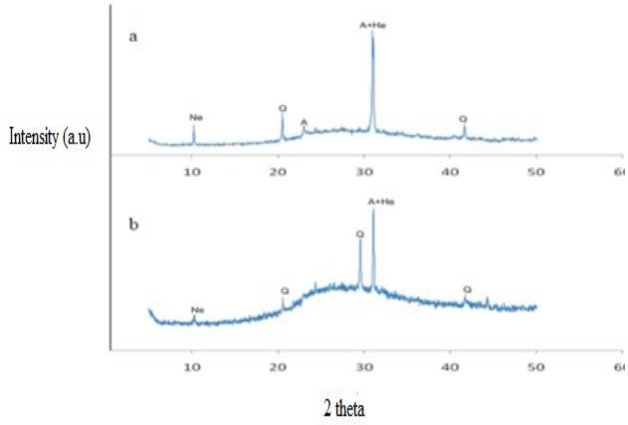

Figure 3: XRD pattern for calcined Kankara and Elefun kaolinite clay.

Figure 3b showed the XRD pattern for metakaolin obtained from Elefun kaolinite clay, with retained peaks at 2 theta around 30 and 32, attributed to the presence of quartz and hematite (Fe2O3), respectively. Those two minerals were observed to be passive to thermal treatment despite the elevated temperature of calcination, which is in agreement with the works reported by Chandrasekhar and Pramada (1999) and Lenarda *et al.*, (2007).

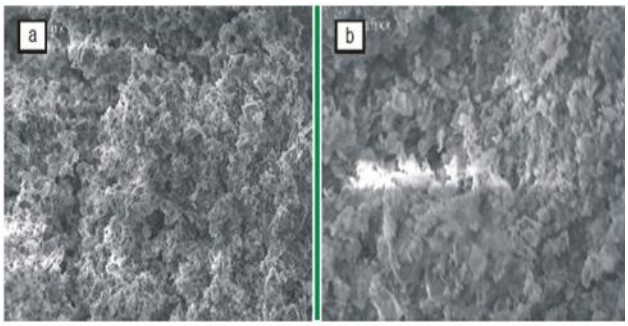

Figure 4: SEM images for calcined Kankara (a) and Elefun (b) kaolinite clay.

Figures 4(a and b) showed the SEM images for Kankara and Elefun metakaolin, respectively, obtained at calcination temperature 850^0C. The SEM images for the samples were seen to be similar, despite the source of the starting kaolin. The images gave an evidence of partial destruction of the initial kaolinite structure and formation of the semi-amorphous metakaolin, with the destruction of the noticeable card-like structure of kaolinite clay, as seen in Figure 2

The XRD patterns for the dealuminated samples pointed to the reduction of some noticeable phases after calcination and prominence of more silica rich phase with less alumina in the dealuminated sample. The intensity of these at the 2Θ around 20, 30 and 32, were more crystalline than same from the metakaolin. This tends to conforms with the chemistry of dealumination, where more silica is expected compared to alumina, for the former does not react with the acid.

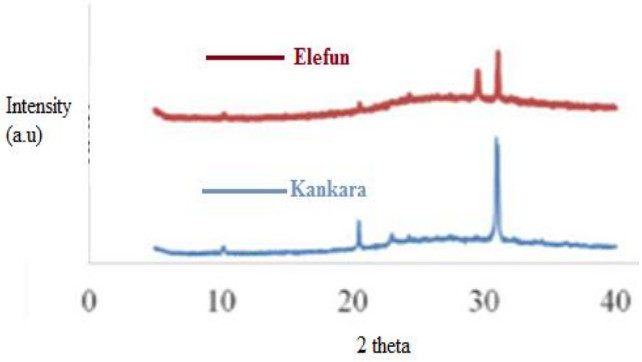

Figure 5: XRD patterns for dealuminated samples from Kankara and Elefun kaolinite clay.

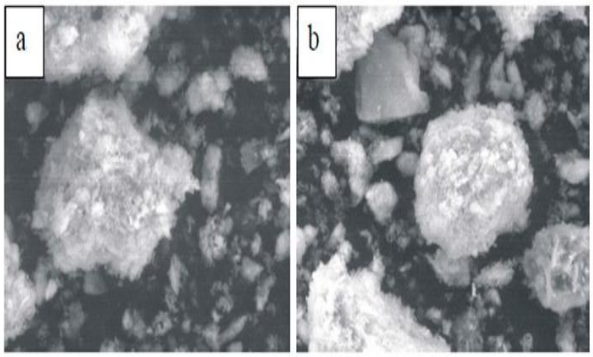

Figure 6: SEM images for dealuminated Kankara (a) and Elefun (b) kaolinite clay.

The SEM images of the dealuminated Kankara and Elefun shown in Figure 6 (a & b) indicate the disaggregation of metakaolin structure on acid treatment, resulting to surface roughness and cluster formation. The large white particles appear to be formed by several flaky particles stacked together to form well bonded agglomerates. These observations were found to favorably agree with the works reported by Lenarda *et al.*, (2007) and Panda *et al.*, (2010). Additionally, some materials remained unaffected by the acid treatment, retaining its shape from metakaolin, were noticed in the SEM for both dealuminated products.

3.2 Crystallization processes-gelation and reaction

The gels formed were observed to have closely related minerals as shown in Figure 7 (a & b), irrespective of the source of kaolinite clay used, temperature of calcination and mode of dealumination. The new phases formed namely-CIT-1, TNU-9, Go, RUB's noticed in the gels from Kankara and Elefun, testify to the action of NaOH introduced, since they are rich in sodium. The quartz peak was still noticeable in Elefun kaolinite clay. It worth mentioning, that the gel was analyzed without been subjected to aging, hence the reason for retained quartz peak in Elefun.

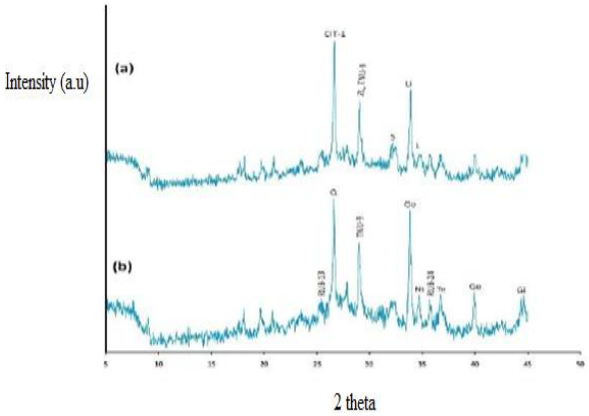

Figure 7: XRD patterns for gel produced from Kankara (a) and Elefun (b) kaolinite clay.

Conclusively, it can be inferred from the XRD patterns in Figure 7 that the gels contained disordered form of aluminosilicate in a state of higher simplexity and entropy, which is required for crystallization.

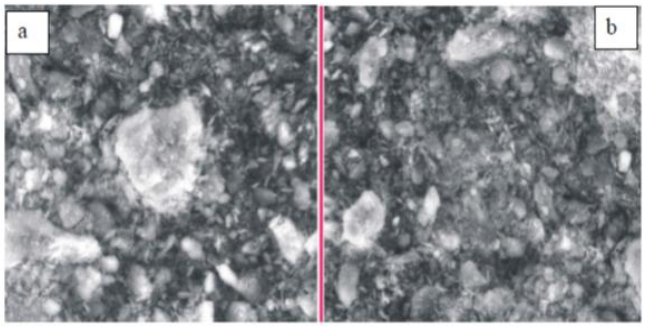

Figure 8: SEM images for gels from Kankara (a) and Elefun (b) kaolinite clay.

The SEM image actually correlates the aforementioned speculation as shown in Figures 8(a & b), where the bulky though flaky particle observed in the figures were noticed to have broken down into smaller closely packed particles. The gel obtained from Kankara was observed to retain a relatively large portion of the flaky but bulky particle, embedded in amorphous aggregates, suggesting its compositional resistance to alkaline treatment.

The XRD patterns of all the as-synthesized zeolite NaX exhibit diffraction peaks which are characteristic of NaX zeolite. It was observed from Figures 9-12, that increase in crystallization time resulted in enhanced crystallinity and crystal size of zeolites.

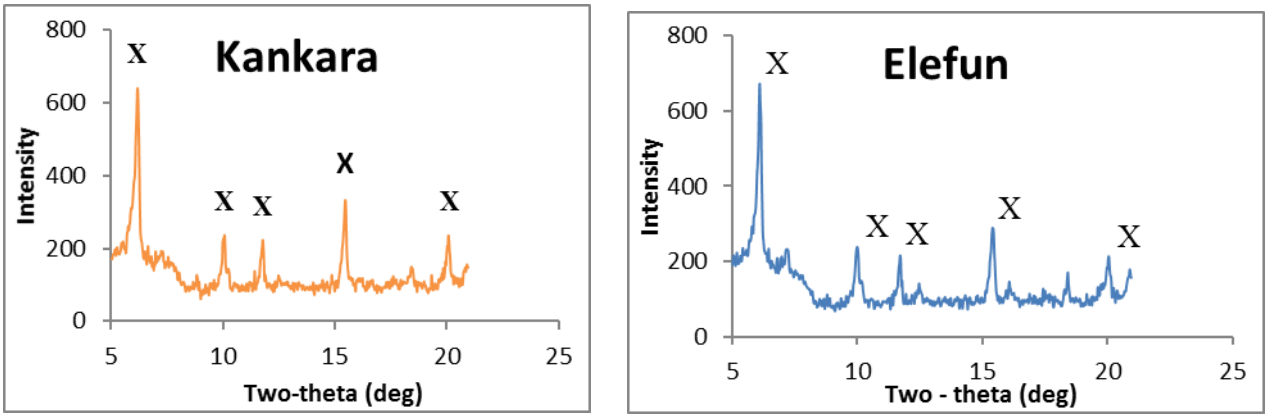

Figure 9: XRD patterns for crystallized product at 6 hours

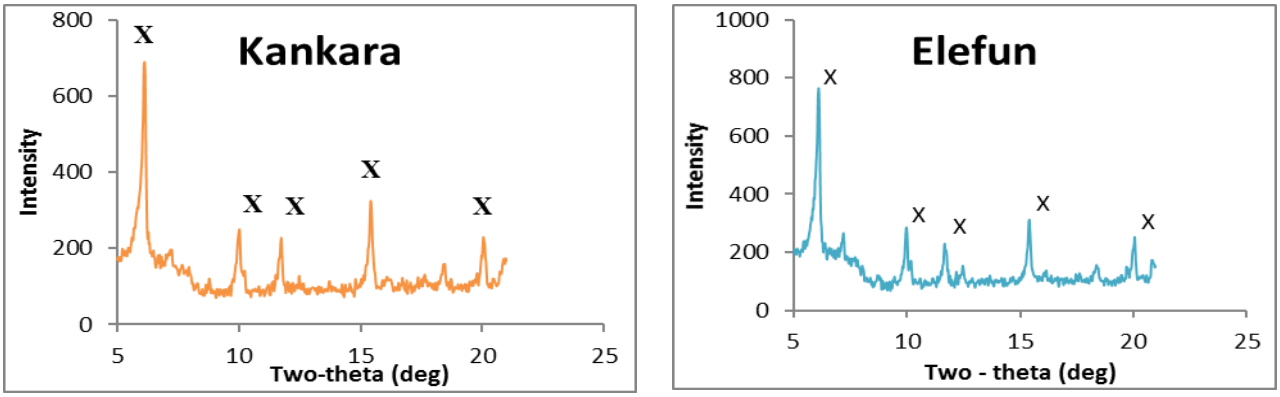

Figure 10: XRD patterns for crystallized product at 12 hours

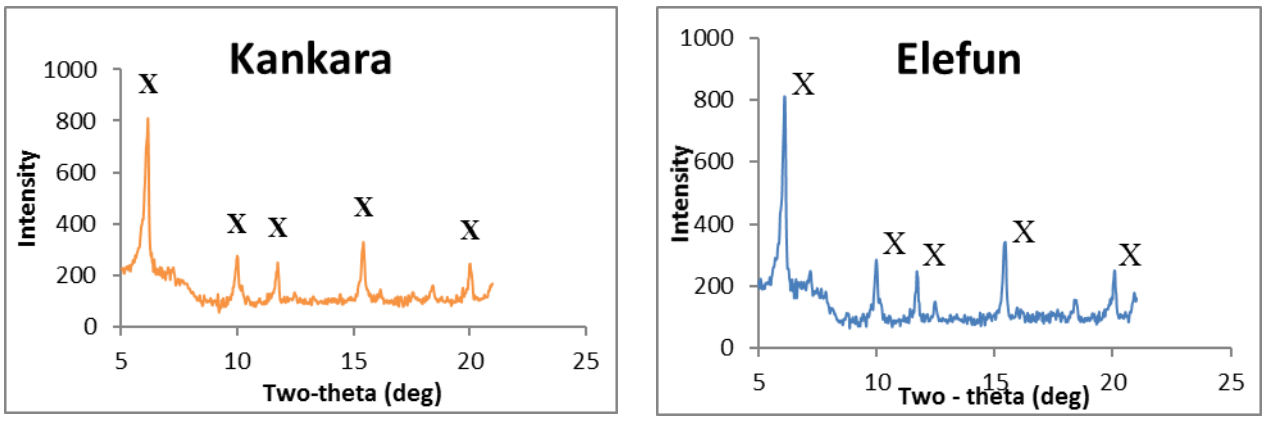

Figure 11: XRD patterns for crystallized product Sample of 24 hours

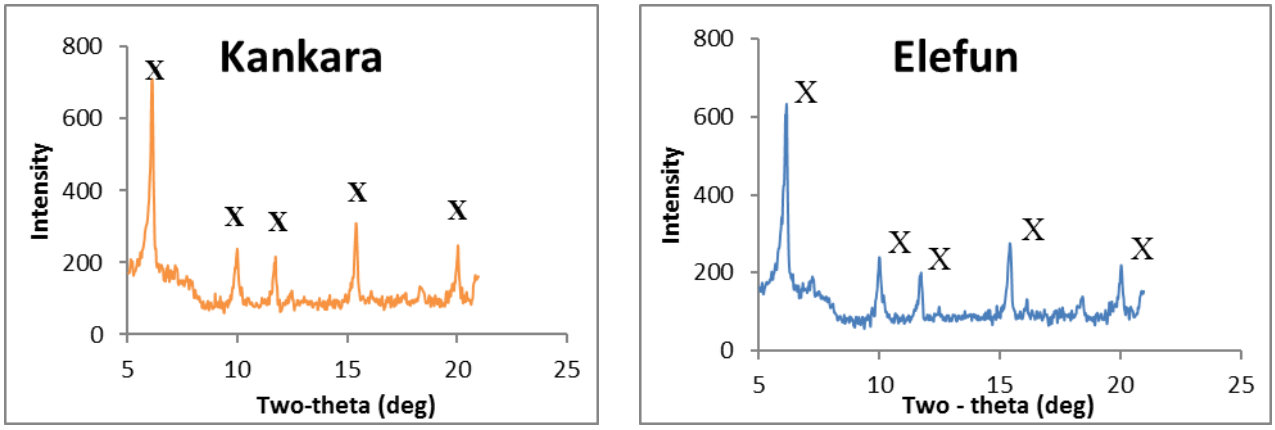

Figure 12: XRD patterns for crystallized product Sample of 36 hours

The intensity (by XRD) increased sharply with increase in crystallization time from 6 to 24hrs and then starts to decrease with time. It is speculated that the crystal phase already formed can be broken down into silica and alumina which might lead to the regrouping of the siliceous bond (formation of siloxane bridges) hence a rather more stable α-quartz phase. This can be noticed for both kaolinite clays sources, for the intensity for the major peak was observed to drop.

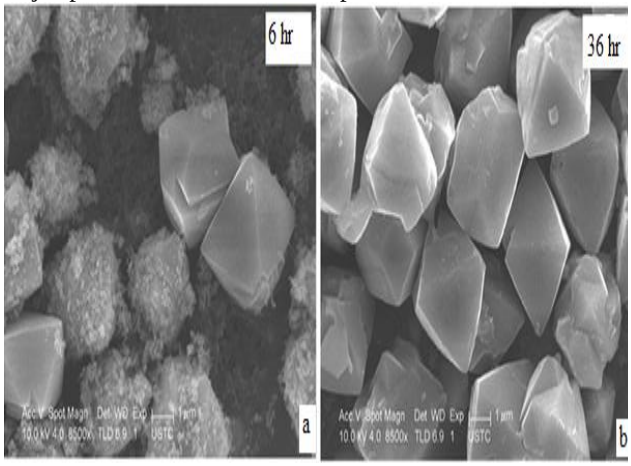

Figure 13: SEM images for Kankara based NaX zeolite crystallized for 6hr and 36hr

The SEM for NaX from kaolin and Elefun at crystallization time of 6 and 24hrs are shown in Figures 13 and 14, respectively. Figure 13a, shows the appearance of octahedron shape corresponding to NaX but with rough unsmooth edges surrounded by rather amorphous like materials, suggesting incomplete conversion/crystallization process. This observation was not seen in the better and more refined shape obtained at 36hrs (see Fig 13b). Same observation was noticed for Elefun as depicted in Figure 14 but with better morphology for NaX obtained at 6hrs and less amorphous unconverted materials.

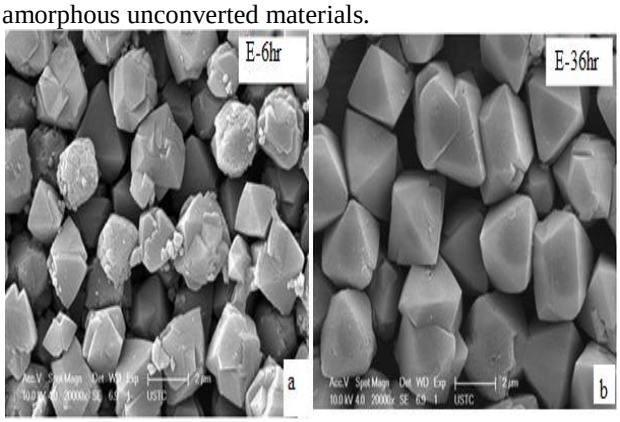

Figure 14: SEM images for Elefun based NaX zeolite crystallized for 6hr and 36hr

Figure 15 shows the values of specific surface area (SSA) for all samples and the NaX produced from it. The SSA for the raw kaolinite clays was observed to be very close in value, as well as that for the beneficiated and calcined samples. This reduction in the surface area for metakaolin is likely the result of aggregation of particles when structural water molecules were removed. The SSA for the dealuminated sample was observed to increased drastically due to the removal of alumina and enrichment of silica content, as also discussed by Belver *et al.*, (2002). The relatively high surface area observed for the dealuminated sample served as an enhancement factor for gel formation, by providing the surface area required for the gelation and subsequent crystallization. Introduction of NaOH during gel formation reduces the inherent SSA.

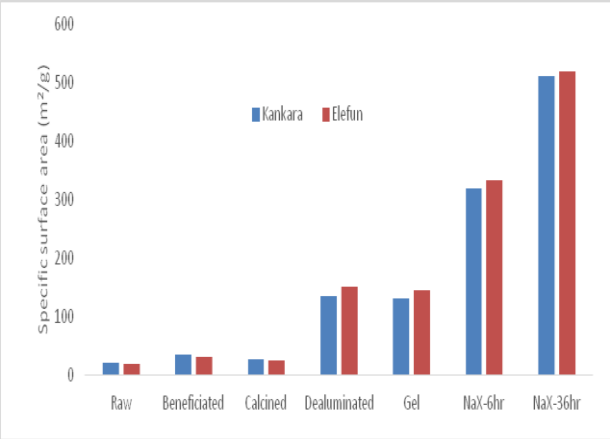

Figure 15: Specific surface area of all the samples and products

This high value of surface area is required in order to: (i) reduce the level of segregation between the reacting species and (ii) enhance the reaction rate via availability of large surface area. Also, Belver *et al*., (2002), reported that the crystalline
nature of the gel formed in their work had large particle size, responsible for the lowered surface
area. The BET surface area for the as-synthesized zeolite was recorded to be attain a value of about 310 and 330m^2/g for NaX obtained at 6hrs crystallization reaction time and over 450m^2/g for both Kankara and Elefun, respectively at crystallization time of 36hrs. This is so probably because at low crystallinity, the SSA are reduced due to amorphous aluminosilicate blockage of the external pores of zeolite crystals, which tends to be freed at increased crystallization time, hence higher SSA (Ansari *et al.*, 2013) The SSA for NaX at 36hrs conforms with the value from the literature, of 423.6m^2/g (Schimidt *et al.*, 2013).

4. CONCLUSIONS

Zeolite NaX was successfully synthesized from kaolinite clays sourced from Kankara and Elefun, despite their inherent impurities. Both clays were subjected to beneficiation processes to improve on the property of the starting material. The zeolitization processes was conducted at 1000C at varied crystallization reaction times of 6, 12, 24 and 36hrs, respectively. Zeolite NaX produced at 36hrs were observed to have closer property to their commercial counterpart despite their low intensity compared with those from 24hrs. XRD, SEM, XRF and BET analytical techniques were employed to characterized the raw materials and resulting products. It can be concluded that both clay can serve as good source for zeolite NaX synthesis, but with preference for Elefun kaolinite clay.

REFERENCES

Aderemi, B. O. (2000). Development of zeolite cracking catalyst from local raw materials, *Ph.D Thesis, ABU, Zaria*.

Atta, A.Y., Ajayi, O.A. and Adefila, S.S (2007). Synthesis of Faujasite Zeolites from Kankara Kaolin *Clay.Journal of Applied Sciences Research*, 3(10): 1017-1021.

Ajayi, O.A., A.Y Atta, B.O. Aderemi, A. S. Ahmed, M.T. Ityokumbul and S. S.Adefila (2012) Synthesis of Zeolite ZSM3 from Faujasite: Effects of Post-synthesis Ageing and *Insitu seeding*. *Chemical and Process Engineering Research* Vol 3, 29-39.

Ajayi, A.O., Atta, A.Y., Aderemi, B.O. and Adefila, S.S. (2010). Novel Method of Metakaolin Dealumination - Preliminary Investigation. *Journal of Applied Sciences Research*, 6(10): 1539-1546.

Ajayi, O. A., Adefila, S. S., Ityokumbul, M. T. (2017). Monitoring zeolite NaY formation from potassium-rich Nigerian kaolinite clay. *Ain Shams Engineering Journal.*

Ansari, M., A. Aroujalian, A. Raisi, Dabir, B. and M. Fathizadeh (2013). Preparation and characterization of nano-NaX zeolite by microwave assisted hydrothermal method. *Advanced Powder Technology*. ttp://dx.doi.org/10.1016/j.apt.2013.10.021.

Belver, C., M.A.B. Munoz and M.A. Vicente (2002). Chemical Activation of a Kaolinite under Acid and Alkaline Conditions. *Chemical Material*. 14: 2033-2043.

Breck, D. W. (1964). Crystalline molecular sieves. *Journal of Chemical Education*, 41 (12), 678-689.

Chandrasekhar, S. and P.N. Pramada (2004). Kaolin-Based Zeolite Y, a Precursor for Cordierite Ceramics, *Applied Clay Science*, 27(3): 187-198.

Derkowski, A., W. Franus, H. W-Nowicka, A. Czimerova (2007). "Textural properties vs. CEC and EGME retention of Na–X zeolite prepared from fly ash at room temperature", *Int. J. Miner. Process.*, vol. 82, 57- 68.

Elimbi, A., H.K. Tchakoute, D. Njopwouo (2011). Effects of calcination temperature of kaolinite clays on

the properties of geopolymer cements. *Construction and Building Materials*, Volume 25, Issue 6, 2805-2812

Guesmi H, Massiani P, Nouali H, Paillaud J.L.(2012). A combined experimental and theoretical study of the simultaneous occupation of SIa and SI′ sites in fully dehydrated K-LSX *Microporous and Mesoporous Materials*. 159: 87-95. DOI: 10.1016/j.micromeso.2012.04.011

Hunger, M; Schenk, U; Seiler, M; Weitkamp, J (2000). In situ MAS NMR spectroscopy of surface compounds formed from methanol and from a toluene/methanol mixture on basic zeolite X. J of Molecular Catalysis A: Chemical ISSN: *1381-1169* Vol.156 Issue 1-2 153-161

Kim, Jin-Bae (2003). Li^+- and H^+-Exchanged Low-Silica X Zeolite as Selective Nitrogen Adsorbent for Air Separation. *Bulletin of the Korean Chemical Society*, volume 24, issue 12, 2003, Pages 1814-1818. DOI : 10.5012/bkcs.2003.24.12.1814

Kovo, A.S.(2012). Effect of Temperature on The Synthesis of Zeolite X from Ahoko Nigerian Kaolin Using Novel Metakaolinization Technique. Journal of Chemical Engineering Communications, Volume 199, 2012 - Issue 6 Pages 786-797. http://dx.doi.org/10.1080/00986445.2011.625065

Ngoc, D.T., T. H. Pham and K.D. H. Nguyen (2013). Synthesis, characterization and application of nanozeolite NaX from Vietnamese kaolin. Adv. Nat. Sci.: Nanosci. Nanotechnol. 4 045018 (12pp) doi:10.1088/2043-6262/4/4/045018

Lenarda, M., L.Storaro, Talon, A., E.Moretti and Riello, P (2007). Solid acid catalysts from clays: Preparation of mesoporous catalysts by chemical activation of metakaolin under acid conditions. *Journal of Colloid and Interface Science* 311, 537-543

Panda, A. K., B.G. Mishra, D.K. Mishra, R.K. Singh (2010). Effect of sulphuric acid treatment on the physico-chemical characteristics of kaolin clay. *Colloids and Surfaces A: Physicochemical and Engineering Aspects*. Vol.363, Issues 1–3, 98–104

Pinheiro, P.G., J.D. Fabris, Mussel, W.N., E. Murad, Scovzelli, R.B. and V.K.Garg (2005). Beneficiation of a commercial kaolin from Mar de Espanha, Minas Gerais, Brazil: Chemistry and Mineralogy. *Journal of South American Earth Sciences* 20, 267-271

Schimidt, T. M. P., F. R. Soares, V. Slusarski-Santana, F. F. Brites-Nóbrega and N. R. C. Fernandes-Machado (2013). Chapter 99. Photocatalytic degradation of textile effluent using ZnO/NaX and ZnO/AC under solar radiation. Green Design, Materials and Manufacturing Processes. Edited by Telma Ferreira, CRC *Press, Taylor and Francis Group, London*. pp 563–566. https://doi.org/10.1201/b15002-109

Traa, Y. and Thompson, R.W. (2002) Controlled Co-Crystallization of Zeolites A and X. *Journal of Materials Chemistry*, 12, 496-499. http://dx.doi.org/10.1039/b108634k

JOURNAL OF THE NIGERIAN SOCIETY OF ENGINEERS
INSTRUCTION TO AUTHORS

1. TYPES OF PUBLICATION

The Journal of the Nigerian Society of Chemical Engineers will publish articles on the original research on the science and technology of Chemical Engineering. Preference will be given to articles on new processes or innovative adaptation of existing processes. Critical reviews on current topics of Chemical Engineering are encouraged and may be solicited by the Editorial Board. The following types of articles will be considered for publication:

a. Full length **articles or review papers**.
b. **Communication** – a preliminary report on research findings.
c. **Note** – a short paper describing a research finding not sufficiently completed to warrant a full article.
d. **Letter to the Editor** – comments or remarks by readers and/or authors on previously published materials.

2. MANUSCRIPT REQUIREMENTS

a. The **Manuscript** should be written in clear and concise English and typed in Microsoft Word using double spacing on A4-size paper, Times New Romans font and 12 point. A full length article or review should not exceed 15 pages.
b. The **Manuscript** must contain the full names, address and emails of the authors. In the case of multiple authorship, the person to whom correspondence should be addressed must be indicated with functional email address. As an examples, authors' names should be in this format:
Momoh, S. O., Adisa, A. A. and **Abubakar, A. S.**
If the addresses of authors are different, use the following format:
***Momoh, S. O.[1], Adisa, A. A.[2]** and **Abubakar, A. S.[3]**
Use star * to indicate the corresponding author.

c. **Symbols** should conform to America Standard Association. An abridged set of acceptable symbols is available in the fourth edition of Perry's Chemical Engineering Handbook. Greek letters, subscripts and superscripts should be carefully typed. A list of all symbols used in the paper should be included after the main text as Nomenclature.
d. All **Units** must be in the SI units (kg, m, s, N, etc).
e. The **Abstract** should be in English and should not be more than 200 words. The abstract should indicate the scope of the work and the major findings accompanying the article. Abstracts are not required for Communications, Notes or Letters.
f. **Citation** must be in the Harvard Format i.e. (Author, Date). Examples are (Smith, 1990) or (Jones et al, 2011). (Kemp, 2000) demonstrated that …..; (Mbuk, 1985; Boma, 1999; Sani, 2000) if more than two authors. (Telma, 2001a), (Telma, 2001b); etc if the citation have the same author and year of publication. For more information on Havard Referecing: Guide, visit **http://www.citethisforme.com/harvard-referencing.**
g. **References** must also be in the Harvard Format i.e. (Author, Date, Title, Publication Information) format. References are listed in alphabetical order. Examples are shown below:
Haghi, A. K. and Ghanadzadeh, H. (2005). A Study of Thermal Drying Process. *Indian Journal of Chemical Technology*, Vol. 12, November 2005, pp. 654-663
Kemp, I.C., Fyhr, C. B., Laurent, S., Roques, M. A., Groenewold, C. E., Tsotsas, E., Sereno, A. A., Bonazzi, C. B., Bimbernet, J. J. and Kind M.(2001). Methods for Processing Experimental Drying Kinetic Data. *Drying Technology*, 19: 15-34.

h. **Tables** should contain a minimum of descriptive materials. Tables should be numbered in Arabic numerals (1, 2, 3, etc). Should be places placed at the referenced point with captions (centralised) placed at the top of the table.
i. **Figures**, charts, graphs and all illustrations should be placed at the referenced point, numbered in Arabic numerals (1, 2, 3, etc) and incorporated in the text. Caption for Figures should be placed at the bottom of the Figure (centralised). Lettering set or symbols should be used for all labels on the figures, graphs, charts, photographs even when drawn in colours. (Note that figures drawn in colours may be unreadable if printed in black and white).
j. **Equations** should be typed using MS Word Equation Editor and should be centred with number (in Arabic numeral) at the right margin.
k. Wherever possible, **Fractions** should be shown using the oblique slash. E.g. x/y
l. **Footnotes** should not be incorporated in the text.
m. **Acknowledgements** should appear at the end of the paper, before the list of references.

3. SUBMISSION OF MANUSCRIPTS

Manuscripts should be submitted by sending a Microsoft Word document (A4-size, Times New Roman font, 12 point and in double spacing) to the following email address: **nschejournal@yahoo.com** and copy **stevmomoh@yahoo.com.**
All correspondences are directed to the Editor-in-Chief using the submission emails addresses: nschejournal@yahoo.com and copy stevmomoh@yahoo.com.

4. ACCEPTED PAPERS

On acceptance, authors will be required to submit a copy of their manuscripts using Microsoft Word by emails to **nschejournal@yahoo.com** and copy **stevmomoh@yahoo.com**.

5. PUBLICATION

Full NSChE Journal edition in hard copy will be published twice annually.

6. REPRINT

Reprints are available on request at a moderate fee per page. Orders must be placed before the paper appears in Print.

7. READER'S INFORMATION

The papers are wholly the view of their author(s) and therefore the publishers and the editors bear no responsibility for such views.

8. SUBSCRIPTION INFORMATION

The subscription price per volume is as follows:

a.	Individual Reader	-	N1,500.00
b.	Institutions, Libraries, etc.	-	N2,500.00
c.	Overseas Subscription	-	$30.00

Request for information or subscription should be sent to the Editor-in-Chief through the following emails addresses: nschejournal@yahoo.com and copy stevmomoh@yahoo.com.